

Identification of Drug(s) Selectively Targeting Colorectal Cancer Stem-like Cells for Differentiation (Differentiation Therapy)

Mehreen Ahmed

B.Pharm (Hons), MSc. Pharmacology

Thesis submitted to the University of Nottingham in fulfilment for the degree of Doctor of Philosophy

September 2019

Declaration

I hereby declare that this thesis, except where specifically acknowledged, is the result of my own work undertaken in Cancer Genetics and Stem Cell Group, under the supervision of Dr. Abdolrahman Shams Nateri at the School of Medicine, Faculty of Medicine and Health Sciences, University of Nottingham.

Mehreen Ahmed

Student ID: 4253937

Date: 30/09/2019

Abstract

Increasing evidence suggests that cancer cell populations contain a small proportion of cells that have the unique self-renewal, tumour-initiating and limited differentiation ability that allow them to resist the therapies and promote cancer recurrence. Therefore, undifferentiated cancer stem-like cells are of major therapeutic interest specially to devise novel diagnostic and therapeutic agents. Herein, the aim of this study is to identify compound(s) that are able to target colorectal cancer stem-like cells by inducing differentiation.

In this study, a 3D colonosphere platform was utilised that selects CSC-like population *in vitro* and incorporated it to an NCC (NIH Clinical Collection) compound library. Using CDy1 dye, Vorinostat and deficient FBXW7 cells, the stemness properties of the treated colonospheres were initially compared and evaluated, as detailed in chapter 3. This study suggested the use of CDy1 dye represents a fast and simple method to stain live colonospheres.

Next, we identified potential candidate drugs altering live colonospheres with a stem-like characteristics. Selected compounds were then validated in both *in vitro* organoids and *ex vivo* colon explant models for their differentiation induction, impediment in neoplastic cell growth, and to elucidate the mechanism of their anticancer activity (Chapters 4-6). Interestingly, three compounds with antibacterial and anti-inflammatory properties were identified; AM404, rifabutin and idarubicin for their antineoplastic ability on CRC.

Tumour-promoting inflammation is involved in CRC development and therapeutic resistance, which accounts for about 20% of cases in CRC. However, the inflammatory mediators and signalling that regulate the potency of anticancer treatment upon CSC differentiation are still not fully defined. This study revealed that anandamide uptake inhibitor

AM404 and broad-spectrum antibiotic rifabutin have high potential in preventing CRC stem-like cells features, such as stemness and de-differentiation, migration and drug-resistance. Herein, we also report that, oncogenic *FBXL5* (F-box and leucine-rich repeat protein 5) plays a vital role in CRC metastasis and might be a key target for both AM404 and rifabutin to exert their anticancer effects. In addition, AM404 showed sensitivity toward chemo-resistance and caused differentiation in CRC cells, without necessarily inducing cell death. Rifabutin, on the other hand, induced apoptosis and inhibited cell migration independent of the *FBXL5* status. Subsequently, our results suggest potential antitumor effect of cytotoxic antibiotic idarubicin, though interestingly, while showing reduction in tumour growth and proliferation, idarubicin also showed possible enrichment of CRC-SCs. Altogether, this study uncovers three new potential compounds for CRC and suggests *FBXL5* as a key target for CRC.

In future, further studies of how these drugs affect cancer progression and survival *in vivo* via exploring the stemness properties unique to the adult SCs, CSCs and their niches can be carried out using novel research strategies such as, single-cell sequencing and functional analyses including the patients derived xenograft models. Such studies will shed light on the origin of CSCs and their progenitors in the inflammation and cancer. The combination of our findings and these techniques will contribute to the elucidation of the essential mechanisms not only for the maintenance of cancer stemness, but also in the repurposing of defined small-molecule candidate compounds in CRC therapeutics.

Acknowledgements

First, I would like to thank my supervisors, Dr. Abdolrahman Shams Nateri and Dr. Roya Babaei Jadidi, for their continuous advice, challenges, and guidance throughout this PhD. For this, I'll always be grateful to them.

A very special thanks to my wonderful colleagues in the Cancer Genetics and Stem Cell group and Tumour and Vascular Biology Laboratory for their technical help and support every single day in the lab, and in those much-needed tea breaks in between. I would also like to thank all the amazing friends I had the pleasure to meet during these four years, for making this whole PhD experience significantly unforgettable ($P<0.001$).

At different stages of the PhD, I had the opportunity to collaborate with people in different labs who helped me with various techniques and provided constant supplies of materials. I must mention Nicholas Jinks, Hossein Kashfi and Marcos Castellanos Uribe for their support on the tools used in this study.

Lastly, love and thanks to the Almighty God and the most important people in my life, my parents, Khaleda Akhter Khan and Shah Jalal Uddin Ahmed, my brother Raafi, who have been nothing less than 100% supportive, all the way from Bangladesh. I could never have made it this far without their patience and confidence on me.

Table of Contents

Declaration i

Abstract ii

Acknowledgements iv

Table of Contents v

Abbreviations xi

List of Figures xiii

List of Tables xx

CHAPTER 1 1

General Introduction 1

1.1 Introduction of colorectal cancer 2

1.2 Multistep development of CRC 2

1.2.1 Genome instability 2

1.2.2 DNA damage and DNA damage response 4

1.2.3 CRC mutations 4

1.3 CRC classification 8

1.3.1 Consensus Molecular Subtypes (CMS) 8

1.3.2 TNM staging 10

1.4 Inflammation as a critical factor in CRC 11

1.5 Epithelial-mesenchymal transition (EMT) 17

1.6 Drug resistance 19

1.7 Intestinal self-renewal and loss of differentiation 21

1.8 Cancer stem-like cells (CSC) 25

1.8.1 Targeting cancer stem-like cells 27

1.9 CRC treatment 32

1.9.1 Conventional therapy in CRC 32

1.9.2 Targeting CRC-SCs 35

1.9.3 Colorectal carcinogenesis models 37

1.10 Rationale and objectives 38

CHAPTER 2 41

Materials and Methods 41

2.1 Materials 42

2.1.1 Cell lines 42

2.1.2 Human tissue specimen 43

2.1.3 NCC (NIH Clinical Collection) library 46

2.1.4 Oligonucleotides (oligos) 46

2.1.5 Antibodies 48

2.2 Methods 49

2.2.1 General cell culture techniques 49

2.2.2 Colonosphere formation assay 51

2.2.3 Patient derived tumour organoid culture 53

2.2.4 Tissue explant culture 54

2.2.5 NCC (NIH Clinical Collection) library screening on colonospheres 57

2.2.6 Cytotoxicity assay 60

2.2.7 Colony formation assay 61

2.2.8 Growth curve analysis 62

2.2.9 Propidium iodide (PI) staining 62

2.2.10 Protein expression assays 63

2.2.11 Histologic techniques and quantification (IHC) 65

2.2.12 RNA isolation and analysis 66

2.2.13 Statistical analysis 68

CHAPTER 3 70

A CDy1-Based 3D-Colonsphere Screening System for the Rapid Evaluation of Drugs Inducing-Differentiation in Cancer Stem-like Cells 70

3.1 Introduction 71

3.2 Result 72

3.2.1 Loss of FBXW7 induces the *in vitro* colonosphere formation and CDy1 intensity 72

3.2.2 Vorinostat induced differentiation in 3D colonosphere 78

3.2.3 CDy1-based drug screening of an NCC compounds library … 84

3.3. Discussion …… 98

3.3.1 CDy1-based drug screening system …… 98

CHAPTER 4 …… 101

Antibacterial Drug AM404 with Antineoplastic Properties Targets FBXL5 E3-ligase in CRC Cells. …… 101

4.1 Introduction …… 102

4.2 Results …… 103

4.2.1 3D screening revealed the anti-cancer activity of AM404 … 103

4.2.2 Inhibition of de-differentiation and stem-like properties by AM404 …… 119

4.2.3 AM404 induced growth impairment in patient derived *ex vivo* tumour organoids …… 128

4.2.4 *Ex vivo* treatment of CRC patient biopsies evaluates AM404 response as an anticancer drug …… 136

4.2.5. FBXL5 mediated AM404-induced anticancer activity …… 141

4.3 Discussion …… 152

CHAPTER 5 …… 158

Antibacterial Rifabutin Functions as an Anti-CRC drug …… 158

5.1 Introduction …… 159

5.2 Result …… 160

5.2.1 Re-validation of the anti-cancer activity of rifabutin in colonospheres 160

5.2.2 Rifabutin inhibits de-differentiation and acquisition of stem-like properties 173

5.2.3 Rifabutin impedes the growth of *ex vivo* tumour organoids 180

5.2.4. *Ex vivo* treatment of CRC patient biopsies evaluates rifabutin response as an anticancer drug 186

5.2.5. FBXL5 attenuates rifabutin-induced anticancer activity in targeting CRC 191

5.3 Discussion 200

CHAPTER 6 207

Idarubicin Exhibits Antitumor Activity in CRC 207

6.1 Introduction 208

6.2 Result 210

6.2.1 Validation of the candidate drugs determined the anti-cancer activity of idarubicin 210

6.2.2 Idarubicin induces acquisition of stem-like properties 221

6.2.3 Idarubicin induced apoptosis and growth arrest in patient derived *ex vivo* tumour organoids 226

6.2.4. *Ex vivo* treatment of CRC patient biopsies evaluates idarubicin as an anticancer drug with capacity to enrich CSCs 232

6.3 Discussion 236

CHAPTER 7 239

General Discussion 239

7.1 Overview 240

7.2 Anti-inflammatory drug AM404 targets FBXL5-E3 ligase in CRC 241

7.3 Antimicrobial rifabutin confers antineoplastic activity in CRC .. 242

7.4 Possible CRC enrichment with idarubicin 244

7.5 FBXL5 is associated in CRC metastasis 245

7.6 Experimental limitations 246

7.7 Concluding remarks and future perspectives 248

References 250

Appendices 277

Appendix 1 278

Appendix 2 302

Appendix 3 304

Appendix 4 306

Appendix 5 317

Publications 324

Abbreviations

5-FU	5-fluorouracil
°C	Degrees Celsius
cDNA	Complementary DNA
CRC	Colorectal Cancer
CSC	Cancer Stem Cell
CRC-SCs	Colorectal Cancer Stem Cells
DAPI	4′,6-diamidino-2-phenylindole
DMEM	Dulbecco's Modified Eagle Medium
DMSO	Dimethyl Sulfoxide
DNA	Deoxyribonucleic Acid
EDTA	Ethylenediaminetetraacetic Acid
EMT	Epithelial-Mesenchymal Transition
ESC	Embryonic Stem Cell
FBS	Fetal Bovine Serum
FGF	Fibroblast Growth Factor
FBXL5	F-box and Leucine Rich Repeat Protein 5
FBXW7	F-box and WD Repeat Domain-Containing 7
HDAC	Histone Deacetylases
IF	Immunofluorescence
IHC	Immunohistochemistry
Lgr5	Leucine Rich Repeat-Containing G-protein Coupled Receptor 5
mRNA	Messenger RNA
NBF	Neutral Buffered Formalin
NCC	NIH Clinical Collection

NIH	National Institute of Health
NSAID	Nonsteroidal Anti-inflammatory Drug
PBS	Phosphate Buffered Saline
PCR	Polymerase Chain Reaction
PDT	Population Doubling Time
PDTO	Patient Derived Tumour Organoid
PDX	Patient Derived Xenograft
PFA	Paraformaldehyde
PI	Propidium Iodide
qPCR	Quantitative PCR
RNA	Ribonucleic Acid
RPMI	Roswell Park Memorial Institute
SD	Standard Deviation
w/v	Weight by Volume
ZEB2	Zinc finger E-box-Binding Homeobox 2

List of Figures

Figure 1-1: Genetic changes associated with CRC ……..…..06

Figure 1-2: Multistep model of CRC progression ……..08

Figure 1-3: The inflammatory spectrum underlying the development of CRC ……..…… 13

Figure 1-4: The structure of human colonic epithelium ……..……22

Figure 1-5: Different approaches in cancer treatment ……..……..29

Figure 2-1: Preparation of colonosphere using conditioned stem cell medium ……..…… 52

Figure 2-2: Preparation of CRC patient derived tissue explants ……..…….. 56

Figure 2-3: Primary screening of NCC compounds screening on HCT116 cell derived colonospheres ……..…….. 59

Figure 3-1: FBXW7 deletion confers to increased efficiency in colonosphere formation in human colon cancer HCT116 and DLD-1 cells ……..…….. 73

Figure 3-2: CD44/MUC2 expression in HCT116$^{FBXW7+/+}$ and HCT116$^{FBXW7-/-}$ derived colonospheres ……..……75

Figure 3-3: Increased CD44 and decreased MUC2 expression in HCT116$^{FBXW7-/-}$ derived colonospheres ……..……76

Figure 3-4: CDy1 confers greater intensity in HCT116$^{FBXW7-/-}$ cell derived colonospheres ……..……77

Figure 3-5: FBXW7 deletion confers resistance to SAHA in HCT116$^{FBXW7-/-}$ cells ……..…… 79

Figure 3-6: Vorinostat treatment showing morphological alteration in colonosphere ……..…… 80

Figure 3-7: Vorinostat treatment did not cause any significant change in colonosphere formation assay 81

Figure 3-8: Vorinostat induces differentiation in CRC-SC 82

Figure 3-9: Primary screening of NIH clinical collection Plate 1 and 2 based on fluorescence intensity influenced by small molecules on colonospheres derived from HCT116 cells 86

Figure 3-10: Primary screening of NIH clinical collection Plate 3 and 4 based on fluorescence intensity influenced by small molecules on colonospheres derived from HCT116 cells 87

Figure 3-11: Primary screening of NIH clinical collection Plate 5 and 6 based on fluorescence intensity influenced by small molecules on colonospheres derived from HCT116 cells 88

Figure 3-12: Primary screening of NIH clinical collection Plate 7 and 8 based on fluorescence intensity influenced by small molecules on colonospheres derived from HCT116 cells 89

Figure 3-13: Primary screening of NIH clinical collection Plate 9 based on fluorescence intensity influenced by small molecules on colonospheres derived from HCT116 cells 90

Figure 3-14: Primary screening of NIH clinical collection on colonospheres derived from HCT116 cells 92

Figure 3-15: Re-screening of 50 compounds initially identified from the primary screening 94

Figure 3-16: Summary of NIH clinical collection screening 99

Figure 4-1: Schematic representation of the structural formula of AM404 102

Figure 4-2: AM404 mediated reduction in CDy1 fluorescence intensity 104

Figure 4-3: Cytotoxicity assay of AM404 using Sulforhodamine B (SRB) on human colorectal cancer cell lines 107

Figure 4-4: Reduction in colony formation efficiency upon AM404 treatment 110

Figure 4-5: Phalloidin staining of AM404 treated colonies..... 111

Figure 4-6: AM404 reduces the tumorigenic ability of HCT116 cells 113

Figure 4-7: AM404 reduces the tumorigenic ability of DLD-1 cells 114

Figure 4-8: Reduction of the size of colonies upon treatment with AM404 115

Figure 4-9: Growth curve of AM404-treated and vehicle-treated HCT116, DLD-1 and SW480 cells 117

Figure 4-10: AM404 induced sensitivity in CRC drug treatment 119

Figure 4-11: AM404 treatment did not cause any significant change in colonosphere formation assay 121

Figure 4-12: Induction of morphological alteration in colonospheres treated with AM404 122

Figure 4-13: Immunofluorescence assay of AM404 treated colonospheres using stemness and differentiation markers 124

Figure 4-14: qPCR analysis of AM404 treated colonospheres derived from DLD-1 cells 127

Figure 4-15: AM404 treatment presents enteroid-like structures and induces apoptosis in organoids 131

Figure 4-16: Organoid growth retardation and morphology change induced by AM404 132

Figure 4-17: AM404 treatment hindered the growth in in tumour organoid 133

Figure 4-18: Hoechst/PI staining on AM404 treated organoids 135

Figure 4-19: Effects of AM404 treatment on proliferation, apoptosis, stemness and differentiation level in the tissue explants obtained from CRC patients 139

Figure 4-20: PCA analysis of variant genes for AM404-treated and control (DMSO) colonospheres 142

Figure 4-21: Differentially expressed genes on DLD-1 derived colonospheres treated with AM404 143

Figure 4-22: Gene ontology showing the biological processes affected by the top sixteen differentially expressed genes 144

Figure 4-23: Heat-map representation of unsupervised clustering of the 16 differentially expressed genes (≥3-fold change) by AM404 in DLD-1 derived colonospheres 146

Figure 4-24: mRNA expression levels of seven differentially expressed genes in AM404 treated colonospheres 147

Figure 4-25: Cytotoxicity assay of AM404 in DLD-1 and FBXL5-knockout DLD-1 cell lines using sulforhodamine B (SRB) 149

Figure 4-26: Inhibition of migration by AM404 in DLD-1 and FBOXL5-KO cells in vitro 151

Figure 4-27: AM404 inhibits cell migration in DLD-1 and FBOXL5-KO cells 152

Figure 5-1: Schematic representation of the structural formula of rifabutin 160

Figure 5-2: 3D drug screening revealed rifabutin is inducing differentiation in colonosphere 161

Figure 5-3: Cytotoxicity assay of rifabutin using Sulforhodamine B (SRB) on human colorectal cancer cell lines 164

Figure 5-4: Rifabutin caused reduced colony formation and morphological changes in CRC cells 166

Figure 5-5: Rifabutin treatment on DLD-1 obtained cultured colonies and Phalloidin staining at the end of the treatment period 167

Figure 5-6: Rifabutin reduces the tumorigenic ability of HCT116 cells 169

Figure 5-7: Rifabutin reduces the tumorigenic ability of DLD-1 cells 170

Figure 5-8: Rifabutin reduced the size of colonies in HCT116 and DLD-1 cells 171

Figure 5-9: Growth curve of rifabutin treated and untreated colorectal cancer HCT116, DLD-1 and SW480 cells 172

Figure 5-10: Rifabutin treatment did not cause any significant change in colonosphere formation assay 174

Figure 5-11: Rifabutin showing morphological alteration in colonosphere 175

Figure 5-12: Immunofluorescence assay of rifabutin treated colonospheres using stemness and differentiation markers 177

Figure 5-13: qPCR analysis of rifabutin treated colonospheres derived from DLD-1 cells 179

Figure 5-14: Rifabutin treatment presents enteroid-like structures and induces apoptosis in organoids 182

Figure 5-15: Organoid growth retardation and morphology change induced by rifabutin 183

Figure 5-16: Rifabutin treatment hindered the growth in in tumour organoid 184

Figure 5-17: Hoechst/PI staining on rifabutin treated organoids 186

Figure 5-18: Effects of rifabutin treatment on proliferation, apoptosis, differentiation and stemness level in the tissue explants obtained from CRC patients 189

Figure 5-19: PCA analysis of variant genes for rifabutin treated and control (DMSO) colonospheres 192

Figure 5-20: Differentially expressed genes on DLD-1 derived colonospheres treated with rifabutin 193

Figure 5-21: Gene ontology biological processes revealing the top biological processes affected by the top thirty-two differentially expressed genes 195

Figure 5-22: Heat-map representation of unsupervised clustering of the 32 differentially expressed genes (≥3-fold change) by Rifabutin in DLD-1 derived colonospheres 196

Figure 5-23: Cytotoxicity assay of rifabutin in DLD-1 and FBXL5-knockout DLD-1 cell line using sulforhodamine B (SRB) 198

Figure 5-24: Rifabutin induced inhibition of migration in DLD-1 and FBOXL5-KO cells in vitro 199

Figure 5-25: Significant inhibition of migration in DLD-1 and FBOXL5-KO cells by rifabutin 200

Figure 5-26: Gene array revealed potential pathways regulating rifabutin's effects in CRC 204

Figure 6-1: Schematic representation of the structural formula of idarubicin 209

Figure 6-2: 3D drug screening revealed idarubicin inducing the stem-like characteristics in colonospheres 211

Figure 6-3: Cytotoxicity assay of idarubicin using sulforhodamine B (SRB) on human colorectal cancer cell lines 213

Figure 6-4: Reduction of colony formation efficiency by idarubicin in DLD-1 cells 215

Figure 6-5: Idarubicin treatment on DLD-1 obtained cultured colonies and Phalloidin staining at the end of the treatment period 216

Figure 6-6: Idarubicin reduces the clonogenic activity of DLD-1 cells 217

Figure 6-7: Idarubicin reduced the size of colonies in DLD-1 cells 218

Figure 6-8: Growth curve of idarubicin treated and untreated colorectal cancer DLD-1 and SW480 cells 220

Figure 6-9: Idarubicin showing extensive irregular structures in colonosphere 222

Figure 6-10: Idarubicin significantly reduced colonosphere formation efficiency in SW480 cells derived colonospheres 223

Figure 6-11: qPCR analysis of colonospheres upon idarubicin treatment 225

Figure 6-12: Idarubicin treatment induced cell death in tumour organoids 228

Figure 6-13: Organoid growth arrest and cell death induced by idarubicin 229

Figure 6-14: Idarubicin treatment hindered the growth in in tumour organoid 230

Figure 6-15: Hoechst/PI staining on idarubicin treated organoids 231

Figure 6-16: Effects of idarubicin on proliferation, apoptosis, stemness and differentiation level in the tissue explants obtained from CRC patients 234

Figure 7-1: AM404 sensitivity demonstrating silencing of FBXL5 242

List of Tables

Table 1-1: Consensus Molecular Subtypes of Colorectal Cancer ……..… 09

Table 1-2: Intervention strategies for targeting cancer-associated inflammatory responses ……..…… 16

Table 1-3: Drugs and novel compounds identified for selective CSC targeting ……..…… 30

Table 2-1: Colon cancer cell line origins ……..…… 43

Table 2-2: List of patient tumour tissues used in this study …… 44

Table 2-3: List of primers and their sequences used in this study …… 47

Table 2-4: List of primary antibodies used in this study ……..…… 48

Table 2-5: List of secondary antibodies used in this study ……..… 49

Table 3-1: List of compounds identified from re-screening of colonospheres derived from three CRC cell lines ……..…… 95

CHAPTER 1

General Introduction

1.1 Introduction of colorectal cancer

Colorectal cancer (CRC) is the third most commonly diagnosed malignancy and the second leading cause of cancer deaths worldwide (Bray et al., 2018, Arnold et al., 2017). This accounts for over 1.2 million new cases and 608,700 deaths per year. The most significant part of CRC patients shows sporadic cancer, whereas, about 5-10% of CRCs are autosomally inherited, and 20% CRC develops because of familial risk (Sancho et al., 2004, Kuipers et al., 2015). The most common tumour location is the proximal colon (41%), followed by the rectum (28%) (Siegel et al., 2017). Over the last 40 years, the dramatic rise in CRC incidence, particularly in developed countries has been attributed to the increasingly ageing population, high fat dietary habits and an increase in risk factors including smoking, low physical exercise and obesity (Kuipers et al., 2015). Although in recent years, improved treatment strategies and early diagnosis have increased the overall survival, according to the bowel cancer survival statistics, Cancer Research UK, the 5 year survival is still about 59%, which is in fact, 25% in patients with distant metastasis, https://www.cancerresearchuk.org/health-professional/cancer-statistics/statistics-by-cancer-type/bowel-cancer/survival/heading-three, accessed on January 2020.

1.2 Multistep development of CRC

CRC is a multistep process in which several genetic and epigenetic alterations and DNA damage mechanisms accumulate in sequential order for the transformation of the normal epithelium into a carcinoma. This progression usually requires a long time to develop.

1.2.1 Genome instability

Genomic instability accelerates the rate of new mutations and, thus, facilitates the activation of oncogenes and the repression of tumour suppressor genes. Until 1971, cancer was only thought to be caused by the activation of oncogenes. The 'two-hit' hypothesis by Alfred G.

Knudson led to the realization of tumour-suppressor genes that can suppress cancer cell growth and explained the relationship between the hereditary and non-hereditary forms (Knudson, 1971). According to this hypothesis, loss of tumour suppressor gene function occurs via the deletion or inactivation of two alleles. Because their cancer-preventive effects usually require a single functional gene, prototypic tumour suppressor genes are recessive, requiring inactivation of both alleles. This hypothesis defines three key properties of tumour suppressor genes: (a) they are recessive and undergo biallellic inactivation; (b) inheritance of a single mutant allele accelerates tumour susceptibility, because only one additional mutation is required for complete loss of gene function; and (c) the same gene is frequently inactivated in sporadic cancers (Sherr, 2004, Krug et al., 2002).

Although it is well agreed that genomic instability significantly influences CRC initiation and progression, the exact position and mechanism of its occurrence are yet to be clarified (Grady and Carethers, 2008). One of the most important illustrations of Knudson's 'two-hit' hypothesis is the Vogelstein model of familial colon cancer progression. According to this model, mutations in the familial adenomatous polyposis (FAP) gene (APC, on chromosome 5q21) is inherited as the first hit, and somatic mutations (usually deletions) in the APC gene represent the second hit, which eventually initiate colon carcinogenesis (Kinzler and Vogelstein, 1996, Fearon and Vogelstein, 1990).

Till date, three different pathways have been characterised for the development of tumours (1) chromosomal instability (CIN); (2) microsatellite instability (MSI); and (3) CpG island methylator phenotype (CIMP). The CIN pathway involves mutations in *APC, KRAS, DCC/SMAD4, TP53,* amongst others and represents the tendency to acquire or lose a part or whole chromosome resulting in different karyotype for the daughter cells. It is mostly associated with the inherited pathologic condition, such as familial adenomatous polyposis

(FAP), and the majority of sporadic CRCs (80-85%) (Grady and Carethers, 2008, Pancione et al., 2012). MSI, on the other hand, is responsible for the Lynch syndrome and sporadic tumours and is mainly caused by inactivation of the DNA mismatch repair genes such as hMLH1, hMSH2, hMSH6, and hPMS2. The third pathway, CpG island methylator phenotype (CIMP), refers to the widespread hypermethylation of CpG at several loci. Methylation of cytosines in these sequences induces gene silencing (Pino and Chung, 2010). Even though these pathways hardly overlap, oftentimes, they are correlated, and one pathway can occur as a result of another (Pancione et al., 2012).

1.2.2 DNA damage and DNA damage response

DNA damages are alterations in the DNA structure that may promote the mutations regulating in tumour development. In parallel, pathways detect DNA damage, promote their repair and maintain genomic integrity are known as DNA damage response (DDR).

Inactivation of DDR genes not only causes the loss of genomic integrity and affects tumour predisposition, but also alters the sensitivity of tumours to chemotherapy (Bouwman and Jonkers, 2012). The major DDR signalling components are ataxia telangiectasia mutated (ATM) and ataxia- telangiectasia Rad-3 related protein (ATR) kinases. ATM and ATR signalling enhances DNA repair either by inducing transcription or by modulating post-transcriptional modifications (phosphorylation, acetylation, ubiquitination, glycosylation, nitrosylation, methylation, lipidation and proteolysis). Upon successful repair of DNA damage repair pathways, DDR is inactivated, and the cell cycle restarts (Jackson and Bartek, 2009).

1.2.3 CRC mutations

CRC initiation and progression occur as a result of sequential aggressive gene mutations and epigenetic alterations (Grady and Carethers, 2008). It has been documented that there are approximately 80 genes with

amino acid-altering mutations which encounter in individual colorectal cancers. However, some of these mutations may possess harmless nature; and according to the following reviewers, only around 15 of them contributes to CRC pathogenesis and unregulated growth of the tumour cells (Sjoeblom et al., 2006, Wood et al., 2007, Kuipers et al., 2015). However, many mutations occur in a low proportion of the tumour cells that they are generally undetectable. Typically, mutations need to comprise at least 10% of the tumour to be detected using standard molecular techniques (Tomlinson et al., 2002).

The vast majority of CRC arises from a polyp beginning with an aberrant crypt, which evolves into an early adenoma (<1cm, with tubular or tubule-villous histology), progresses to advanced adenoma (>1cm, villous histology) and finally turns into colorectal cancer. The pioneer work by Vogelstein and Fearon introduced the multistep theory of carcinogenesis, which then was extensively studied for colorectal carcinogenesis, predicts that the cumulative effect of the loss of key tumour suppressor genes and overexpression of important oncogenes in an individual cell will cause a normal cell to become a cancer cell (Fearon and Vogelstein, 1990) **(Figure 1-1)**. In CRC, this process is driven by the accumulation of mutations and epigenetic alterations and takes over a long period of about 10-15 years (Kuipers et al., 2015). However, the cells in a carcinoma quickly acquire the potential to metastasise; for example, liver metastases occur approximately 2 years following the diagnosis of advanced CRC (Quail and Joyce, 2013).

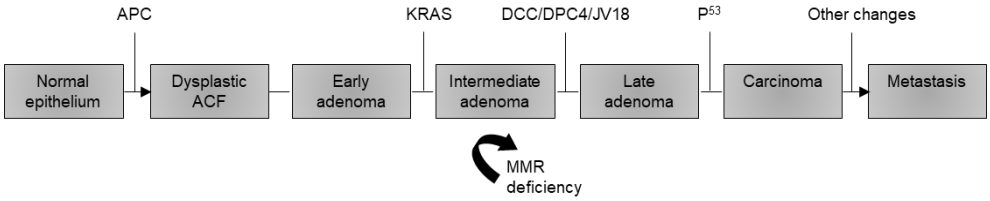


Figure 1-1: Genetic changes associated with CRC. APC mutations initiate the tumorigenesis process which then proceeds through a series of genetic alterations including oncogenes (RAS) and tumour suppressor genes (particularly on chromosomes 5q, 17p, and 16q). In patients with FAP, mutation in APC is inherited and develop dysplastic aberrant crypt foci (ACF). Tumours from hereditary nonpolyposis colorectal cancer (HNPCC) patients, go through similar series of mutations where MMR deficiency speeds up the process. RAS mutation (usually KRAS) occurs in one cell of a pre-existing small adenoma and through clonal expansion produces a larger and more dysplastic tumour. Chromosome 18q21 may contain several different tumour suppressor genes including DCC, DPC4, and JV18–1. Once the carcinomas are formed, tumours continue to progress and the accumulated loss of tumour suppressor genes correlates with the ability of carcinomas to metastasise. Adapted from (Kinzler and Vogelstein, 1996).

The tumour progression starts from an aberrant crypt and gradually transforms into a polyp, early adenoma, advanced adenoma, carcinoma *in situ*, and, lastly, invasive CRC. The most frequently mutated genes throughout this process comprise adenomatous polyposis coli (*APC,* 70%), Tumour protein p53 (*TP53,* 50%), Kirsten rat sarcoma viral oncogene homolog (*K-RAS*, 40%), *SMAD4* (25%), transforming growth factor-β receptor 2 (*TGFβR2*, 20%), F-box and WD repeat domain-containing protein 7 (*FBXW7*, 15-20%), phosphatidylinositol-4,5-biphosphate 3-kinase catalytic subunit-α (*PIK3CA*, 20%) (Hermsen et al., 2002, Douglas et al., 2004, Martin et al., 2007, Kuipers et al., 2015). Mutation of these genes and their respective signalling pathways result in major cellular consequence involved in apoptosis, proliferation, cell survival and differentiation that are fundamentally crucial for tumour initiation and progression (Sjoeblom et al., 2006).

Moreover, it was determined that CRC develops with various gene mutations contributing to specific stages of malignant transformation in the colon **(Figure 1-2)**. The initial transformation from normal mucosa to an adenoma is triggered by *APC* mutations, which typically does not allow the formation of β-catenin destruction complex. Late adenomas and early carcinomas acquire mutations in the *KRAS* and *TP53* (Walther et al., 2009). *KRAS* and *TP53* mutations are associated with a malignant disease progression in human CRC (O'Rourke et al., 2017). The loss of function of the tumour suppressor *TP53* gene is essential for the transition from benign to malignant tumour. Oncogenic *KRAS*, on the other hand, is an upstream member of the RAS-RAF-MAP kinase pathway, which controls cellular proliferation (Rajagopalan et al., 2003).

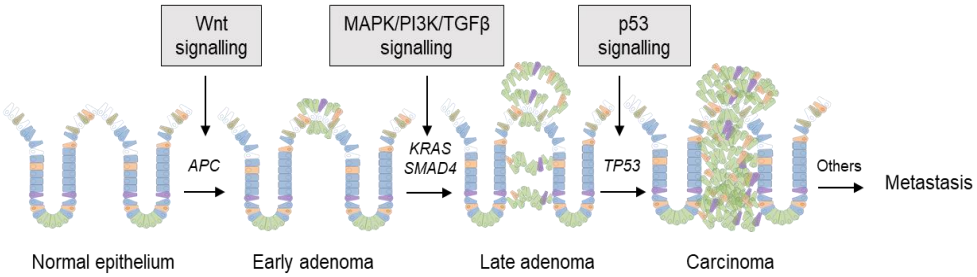


Figure 1-2: Multistep model of CRC progression. Accrual of mutations in specific genes perturbating important pathways associate with tumour development. APC mutation resulting in disregulation of Wnt signalling pathway is essential for the tumour initiation; mutations altering MAPK, PI3K and TGFβ pathways cause substantial induction of cell proliferation and drive the adenoma progression. The failure of the tumour suppressor gene TP53 triggers the transition to malignant tumour. Adapted from (Kuipers et al., 2015).

It has been reported that mutations in *APC* tumour suppressor gene followed by alterations in mitogen-activated protein kinase (MAPK), TP53, and TGF-β signalling give rise to metastatic CRC (mCRC) (Jackstadt et al., 2019, Fearon and Vogelstein, 1990). In parallel, APC-deficient tumours with compounding mutations, when propagated as *ex vivo* organoids and re-implanted into mice, give rise to CRC metastasis (Tauriello et al., 2018, de Sousa e Melo et al., 2017, O'Rourke et al., 2017).

As CRC results from the deregulation and disruption of the signalling pathways tightly maintaining tissue homeostasis, understanding their dynamics is important to study the factors underlying CRC.

1.3 CRC classification

1.3.1 Consensus Molecular Subtypes (CMS)

Comprehensive genomic analyses have demonstrated that individual CRCs are unique, with a median of 76 non-silent mutations each (Thanki et al., 2017). To resolve the inconsistencies among the reported gene

expression–based classifications and to correlate CRC phenotype with clinical behaviour, the CRC Subtyping Consortium unified six independent molecular classification systems and introduced a single consensus system known as the Consensus Molecular Subtypes (CMS). CMS has four distinct groups, that enables the categorisation of most tumours into one of four subtypes **(Table 1-1)** (Dienstmann et al., 2017). Even though CMS represents the current best description of heterogeneity at the gene-expression level, it also correlates the epigenomic, transcriptomic, microenvironmental, genetic, prognostic and clinical characteristics of CRC **(Table 1-1)** (Thanki et al., 2017, Dienstmann et al., 2017, Guinney et al., 2015).

Table 1-1: Consensus Molecular Subtypes of Colorectal Cancer. Modified from (Thanki et al., 2017).

	CMS1 (MSI phenotype)	**CMS2** (Canonical phenotype)	**CMS3** (Metabolic phenotype)	**CMS4** (Mesenchymal phenotype)
Location; incidence	Proximal; 14%	Distal; 37%	Mixed; 13%	Distal; 23%
Characteristics	Hypermutated, microsatellite unstable, strong immune activation	Epithelial, marked WNT and MYC activation	Epithelial, evident metabolic dysregulation	Marked TGF–β activation, stromal invasion and angiogenesis.
Associated mutations	MSH6, RNF43, ATM, TGFBR2, BRAF, PTEN	APC, KRAS, TP53, PIK3CA	APC, KRAS, TP53, PIK3CA	APC, KRAS, TP53, PIK3CA

	CMS1 (MSI phenotype)	**CMS2** (Canonical phenotype)	**CMS3** (Metabolic phenotype)	**CMS4** **(**Mesenchymal phenotype)
Genomic Associations	MSI, high mutation	CIN, low-moderate mutation	CIN, moderate mutation	CIN, low mutation
Epigenomic Associations	High methylation	Low methylation	Moderate methylation	Low methylation
Transcriptomic Pathways	Immune activation, JAK-STAT activation, Caspases	WNT targets, EGFR, VEFG/VEGFR, TGFB activation, cyclin upregulation	DDR, Glutaminolysis, lipidogenesis	Mesenchymal activation, immunosuppression
Stroma-Immune Micro-environment	Highly immunogenic, large immune infiltrate	Poorly immunogenic, innate immune response	Highly immunogenic	Innate immune response, EMT activation

1.3.2 TNM staging

The tumour/node/metastasis (TNM) classification is a globally recognized cancer staging system that assigns to each cancer a stage of disease by evaluating the size and extension of the primary tumour (T), regional lymph nodes involvement (N) and the presence of metastasis (M) (Freeman, 2013). While CMS classification may provide better information to the clinicians for the prognosis and therapeutic response, TNM staging may help directing the potential therapeutic strategies and interventions.

CRC gets worsen from stage 0 (carcinoma *in situ,* with tumour growing into the mucosa) to stage IV (tumour growing through the membrane covering peritoneum), with 0 (N0) to >4 lymph node (N2) involvement, and with no metastasis (M0) to cancer being spread to distant organs such as liver or lungs (M1). In terms of staging in general, stage 0, 1, 2, 3 and 4 represents Tis N0 M0, T1 N0 M0 or T2 N0 M0, T3 N0 M0 or T4 N0 M0, any T N1 MO or Any T N2 M0, and Any T Any N M1, respectively (Freeman, 2013).

1.4 Inflammation as a critical factor in CRC

Inflammation is recognised as one of the emerging hallmark features of cancer and is associated with about 20% of all cancers (Greten and Grivennikov, 2019). The hallmarks of cancer were initially introduced by Hanahan and Weinberg in 2000, where inflammation was added to the list later in 2011 (Hanahan and Weinberg, 2000, Hanahan and Weinberg, 2011). Even though the percentage of inflammation associated in CRC is relatively lower (1-2%), approximately 5–10% of inflammatory bowel disease (IBD) patients develop CRC (Munkholm, 2003). Moreover, it has been reported that a close relationship exists between the CRC risk in ulcerative colitis and inflammation-related risk factors including duration of colitis and severity of inflammation (Choi et al., 2019). The other important hallmarks include self-sufficiency in proliferative signalling, evading growth suppressors, eluding cell death, enabling replicative immortality, inducing angiogenesis, genome instability and activating invasion and metastasis (Hanahan and Weinberg, 2011, Hanahan and Weinberg, 2000, Mantovani, 2009, Colotta et al., 2009).

The first association of inflammation and cancer was reported in the 19th century by Rudolf Virchow following his observation of white blood cells or leukocytes presence in neoplastic tissues (Greten and Grivennikov, 2019). Chronic inflammation can result in conditions that promote proliferation, angiogenesis, as well as, enhance the production of free radicals that can damage DNA. In CRC, inflammation is associated

with the earliest stage of CRC development. Prolonged inflammation in the intestine, such as IBD, Crohn's disease or ulcerative colitis, leads to poor differentiation of the hyperproliferating cells and fails to form protective adherens junctions and mucus layer, which ultimately causes deterioration of intestinal barrier. Typically, the intestinal tract is populated by numerous microbial strains and any substantial shift in the bacterial population can have a significant effect on the inflammatory responses and contribute to tumour development (Lasry et al., 2016). Moreover, the formation of ectopic lymphoid structures (ELS) and parainflammation contribute to the tumour formation (**Figure 1-3**) (Greten and Grivennikov, 2019). ELS has been identified as a positive prognostic marker in CRC. Although, its mechanism in CRC is not defined yet, it acts as a niche for the tumour cells and has a tumour-promoting role in hepatocellular carcinoma (**Figure 1-3**). Parainflammation, on the other hand, is the intermediate state between chronic inflammation and basal homeostasis and has considerable effect on CRC progression. Parainflammation might contribute to the activation of p53 in tumour suppression, and therefore, following the loss of p53, parainflammation loses its tumour-suppressive nature and acquires tumour promoting nature (**Figure 1-3**). High rates of mutation might also favour loss of p53, which, when combined with parainflammation, aggravates the potent tumour-promoting mechanism (Lasry et al., 2016).

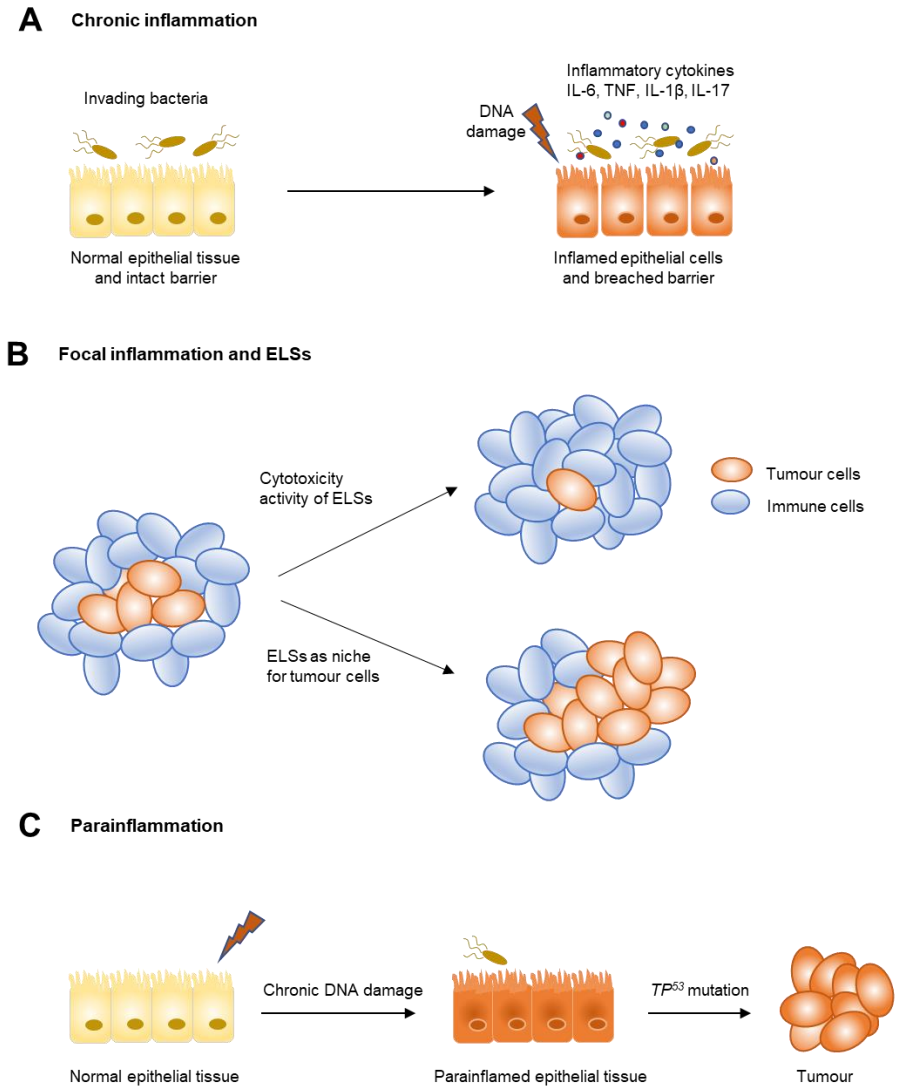


Figure 1-3: The inflammatory spectrum underlying the development of CRC. (a) Chronic inflammation, such as IBD can lead to enhanced sensitivity to bacterial invasion. The inflamed environment is susceptible toward accumulation of mutations, which can result in tumour development. **(b)** The formation of ectopic lymphoid structures (ELSs) in the intestine, act as a tumour-suppressor mechanism for the elimination of transformed cells. **(c)** DNA damage in the intestinal epithelium can activate reactions of the innate immune system via sensors of double-stranded DNA. Prolonged DNA damage in intestinal epithelium can result in parainflammation, which renders the cells more sensitive to transformation after mutation of *TP*^{53}. Adopted from (Lasry et al., 2016).

It has been reported that transcription factors, such as STAT3 and NF-κB, are implicated in the increased synthesis of key inflammatory mediators, cytokines, and chemokines (Diakos et al., 2014). NF-κB is one of the key transcription factors in inflammation that has been identified as one of the major participants in this tumour associated-inflammation transition process. One important cytokine induced by NF-κB is IL-6, which has a well-established role in the initiation and progression of colitis-associated cancer (CAC) (Lasry et al., 2016). In effect, inflammatory-driven genetic alteration and epigenetic change occur, both important aspects of tumour initiation in CRC and particularly in CAC. In CAC mouse models, constitutive activation of Wnt showed induction of TNF and leads to enhanced NF-κB activation and subsequent tumour initiation (Lasry et al., 2016).

Activation of NF-κB is also regulated via tumour necrosis factors (TNF) and inflammasome in different cancers (Diakos et al., 2014). In addition, constitutive activation of NF-κB induces reactive oxygen species (ROS) associated with DNA damage. Moreover, activation of STAT3 by IL-6 prevents apoptosis and promotes malignant cell proliferation by upregulation of anti-apoptotic or proliferative factors (Diakos et al., 2014). The role of STATs, NF-κB, and HIF1α in inflammation and angiogenesis make them potential targets for anticancer therapy.

Currently, several drugs are in the development stage for targeting the tumour associated inflammation. Some of the examples of such drugs are listed in **Table 1-2**. However, no NF-κB inhibitors are currently clinically available for the treatment of cancer, although the proteasomal inhibitor bortezomib has been shown to reduce NF-κB activity through its proteasomal degradation (Diakos et al., 2014). Non-steroidal anti-inflammatory drugs (NSAIDs), including cyclo-oxygenase-2 (COX2) inhibitors, have potential chemopreventive action in CRC, accompanied by reduced prevalence and mortality rate. NSAID mediated COX-2 inhibition has an anti-tumorigenic effect on cancers caused by prolonged

chronic inflammation. Several pathways, including Wnt–β catenin, PIK3CA/AKT/PTEN, and NF-κB, have been postulated as targets for NSAIDs (Diakos et al., 2014). However, NSAIDs are also effective in the prevention of tumours, not preceded by inflammation. For example, the cytokines released during inflammation have a role in reprogramming adult stem cells to become malignant cells. NSAIDs can block this reprogramming and thus prevent tumour development (Lasry et al., 2016).

Table 1-2: Intervention strategies for targeting cancer-associated inflammatory responses. Modified from (Diakos et al., 2014, Lasry et al., 2016).

Drug	Pathway/ mechanism of action	Application
Aspirin	COX-2, enhanced cytotoxic T-cell activity	CRC
Anakinra	Neutralisation of IL-1β and 1α	Melanoma, myeloma, and CRC
Bevacizumab	VEGF-A	Ovarian, glioblastoma multiforme and CRC
Dexamethasone	Undefined	Most solid tumours
Ipilimumab	Anti-CTL4A mAb	Metastatic melanoma, in clinical trials for other solid tumours
Infliximab, etanercept and adalimumab	TNF α	CRC (patients with IBD or CAC), ovarian, renal-cell, and breast cancer
Ipilimumab	CTLA-4	CRC
NSAIDs	Wnt–β-catenin, NF-κB, and COX-2	CRC
Nivolumab and pembrolizumab	PD-1	CRC (patients with mismatch repair defects)
Rituximab	Anti-CD20 mAb	Lymphoma
Ruxolitinib	JAK1 and 2 inhibitor	Myelofibrosis and chronic myeloid leukaemia
Siltuximab and Tocilizumab	IL-6	CRC (patients with IBD or CAC), ovarian and renal-cell cancer
Sulindac, celecoxib	Undefined	CRC (patients with FAP, Lynch syndrome or mutations involving the DNA-repair pathway)

Conversely, increasing evidence indicates a link between cancer-associated EMT and inflammatory mediators, such as soluble factors, oxidative stress, or hypoxia that can foster the acquisition of EMT-like features in cancer cells (Suarez-Carmona et al., 2017). Moreover, it has been recently reported that inflammation also drives metastasis through TGF β-dependent neutrophil recruitment (Jackstadt et al., 2019). Interestingly, they can be prevented or delayed by treatment with anti-inflammatory drugs, suggesting the involvement of inflammatory processes with tumour onset (Lasry et al., 2016, Diakos et al., 2014).

1.5 Epithelial-mesenchymal transition (EMT)

Epithelial-mesenchymal transition (EMT) is a complex biological process and one of the hallmarks of cancer, that drives the conversion of polarised and tightly bound epithelial cells into motile, invasive and migrating mesenchymal to enable cell migration to distant locations (Sato et al., 2016, Lamouille et al., 2014). This involves the epithelial cells to undergo changes in their morphology, architecture, adhesion and ultimately allows the tumour cells to migrate to ectopic sites (Gugnoni et al., 2016). Since first described in 1982 (Greenburg and Hay, 1982), EMT has been documented to be regulated by various transcription factors (TFs), small non-coding RNA, epigenetic modulators, and exogenous inducers (Chen et al., 2017).

Different pathways have been associated with the activation of EMT, including the Wnt, Hedgehog and Notch, amongst others. Transforming growth factor β (TGFβ) is considered as a master regulator, especially in solid tumours such as in CRC. As previously mentioned, this pathway also links inflammation with metastasis through neutrophil recruitment (Jackstadt et al., 2019). EMT-TFs are regulated at the transcriptional, post-transcriptional and post-translational level by mediators of these signalling pathways, hypoxia-inducible factor (HIF1), fibroblast growth factor (FGF), EGF, miR-200 family and others. The induction of EMT-TFs initiates EMT in normal or transformed cells group, which in turn leads

to the downregulation or even removal of E-cadherin from the plasma membrane (Lamouille et al., 2014, Sanchez-Tillo et al., 2012). EMT regulators form an intricate network to mediate the cellular conversion in processes of development and pathologies, among which stem cells lead an important role (Chen et al., 2017). Typically, EMT is medicated by three core groups of transcriptional regulators. The first group is the transcription factors (TFs) of the Snail zinc-finger family, including SNAI1 and SNAI2 (SLUG). The second group is the distantly related zinc-finger E-box-binding homeobox family proteins ZEB1 and ZEB2 (SIP1), and the last is the basic helix–loop–helix (bHLH) family of transcription factors, including TWIST1, TWIST2 and E12/E47 (Lamouille et al., 2014, Sanchez-Tillo et al., 2012).

However, EMT does not occur only in cancer progression, but also it occurs in other normal and pathological events, such as during embryonic development, wound healing, and organ fibrosis (Thiery et al., 2009, Cao et al., 2015a). Adhesion molecules like cadherins have a crucial role in this migratory process, such as downregulated E-cadherin expression disrupts adherens junctions, desmosomes, tight junctions and gap junctions. This ultimately results in loss of apical-basal polarity, cytoskeleton motility and invasion via membrane projections including lamellipodia, filopodia and invadopodia (Lamouille et al., 2014).

Several studies have identified the close relation of EMT to CSCs (Mani et al., 2008, Singh and Settleman, 2010). Notably, cancer stem cells (CSCs) are critical for the formation and maintenance of liver metastasis derived from CRC (de Sousa e Melo et al., 2017). Furthermore, distant metastasis is a major cause of CRC-related mortality worldwide (Mazilu et al., 2014). *In vitro* studies on CRC, ovarian cancer and breast cancer showed that EMT renders cancer cells to be invasive, migrating, drug-resistant, stem-like and, metastatic. Moreover, CSCs are suggested to be cancer cells that by undergoing EMT escape chemotherapy and migrate to another location in the body (De Craene and Berx, 2013). There is substantial

overlap in the molecular pathways that regulate both the EMT and CSC phenotypes including Wnt, Notch, Hedgehog and TGFβ. This provides a complex link between the two, where EMT cells can drive differentiated cancer cells into a CSC state. It is also suggested that cells with an active EMT programme can interact more productively with the extracellular matrix proteins, which in turn can activate more pathways conferring the CSC phenotype. Thus, CSCs and associated EMT represent a crucial therapeutic target.

It has, therefore, been reported that targeting CSCs may represent a therapeutic opportunity for managing metastatic disease (de Sousa e Melo et al., 2017). However, an anti-cancer drug may induce EMT in different tumour types. For example, in human CRC cell lines, treatment with the most commonly used chemotherapy agents, 5-fluorouracil (5-FU) or Oxaliplatin, induces EMT via increased expression of Snail, which in turn downregulates E-cadherin expression and ultimately increases chemoresistance (Yang et al., 2006).

1.6 Drug resistance

The potential of cells to repopulate a tumour despite the destruction of the chemo-sensitive cells is known as drug resistance. Drug resistance is the most common reason for the discontinuation of chemotherapy (Holohan et al., 2013).

In recent years, cancer chemotherapy has become increasingly sophisticated, yet they are not completely effective against disseminated cancer. Being one of the unique CSC characteristics, drug resistance is broadly responsible for which chemotherapeutic treatment often fails to eradicate the neoplasm completely. CSCs have some other biological properties that distinguish them from the remainder of tumour cells, including resistance to treatment (Kreso et al., 2013). Therapies targeting signalling molecules mutated in cancers can often have striking short-term effects, but the emergence of resistant cancer cells is a major barrier to full cures (Shaffer et al., 2018).

Resistance to chemotherapeutics can be divided into two broad categories: intrinsic or acquired. Intrinsic resistance indicates that before receiving chemotherapy, patients are resistant to the treatment due to inherited genetic mutations and the presence of pre-existing resistance-mediating factors in the bulk of tumour cells, which eventually makes the therapy ineffective. On the contrary, acquired drug resistance can gradually develop insensitivity during the treatment through adaptive changes such as mutations arising during treatment, individual variations in patients, as well as increased expression of the therapeutic target and activation of compensatory signalling pathways (Gottesman, 2002, Holohan et al., 2013, Shaffer et al., 2018). In most instances, such tumours initially respond well to the therapy, then become steadily resistant and lead to tumour recurrence (Scheel and Weinberg, 2012).

This is mediated by a combination of several critical features, including relative dormancy, inefficient DNA repair, high expression of multidrug-resistance-type membrane transporters and protection by a hypoxic niche environment that involved conversions between two cellular states; the epithelial and mesenchymal phenotypes (Cao et al., 2015a).

Studies on mechanisms of cancer drug resistance have yielded important information about resistance and cancer chemotherapy. At the level of the tumour, as cancer arises from the accumulation of hundreds of genetic alterations, from point mutations to entire rearrangements of chromosomes, an enormous heterogeneity is present between cancers grown in the same organ as well as among cells within the same tumour. Thus, anti-cancer therapy is aimed to select cancer cells that developed various mechanisms, such as increased drug efflux, mutations of the drug target, DNA damage repair, activation of alternative signalling pathways and evasion of cell death (Holohan et al., 2013). Simultaneously, tumours could acquire resistance to DNA damage drugs by loss of DNA mismatch repair (MMR) activity. The MMR system is required for cell cycle arrest and programmed cell death in response to certain types of DNA damage.

Cell cycle checkpoints including protein kinases CHK1 and CHK2 control cell cycle progression at the G_1-S, S and G_2-M transition. In presence of DNA damage, these checkpoints are up-regulated and by reducing the cyclin-dependent kinase (CDKs), they exert their repair function (Houtgraaf et al., 2006). Therefore, DNA repair pathway regulation in tumour cells is a critical factor in their response to chemotherapy drugs. Hence, both this pathway and DDR genes are useful targets in chemotherapy and for the resistance mechanisms acquired during chemotherapy (Bouwman and Jonkers, 2012).

1.7 Intestinal self-renewal and loss of differentiation

Intestinal stem cells (ISCs) are maintained by stemness signalling modulating self-renewal and differentiation under homeostasis (Zhu et al., 2019). The ISC niche, constituting Paneth cells together with pericryptal mesenchymal cells, immune cells, endothelial cells and neural cells, produces essential factors regulating stem cell fate and self-renewal (Sailaja et al., 2016, Barker, 2014, Clevers, 2013, Medema and Vermeulen, 2011).

The intestinal epithelium is a monolayer of cells that covers the entire lumen of the gut and is organized into crypt-villus units, constituting an important barrier against the external environment (Clevers, 2013). The crypt is occupied by adult stem cells placed at the base while the differentiating cells migrate up towards the villus accompanied by transit-amplifying (TA) cells in the middle and eventually undergo apoptosis **(Figure 1-4)** (Sancho et al., 2003, Barker, 2014).

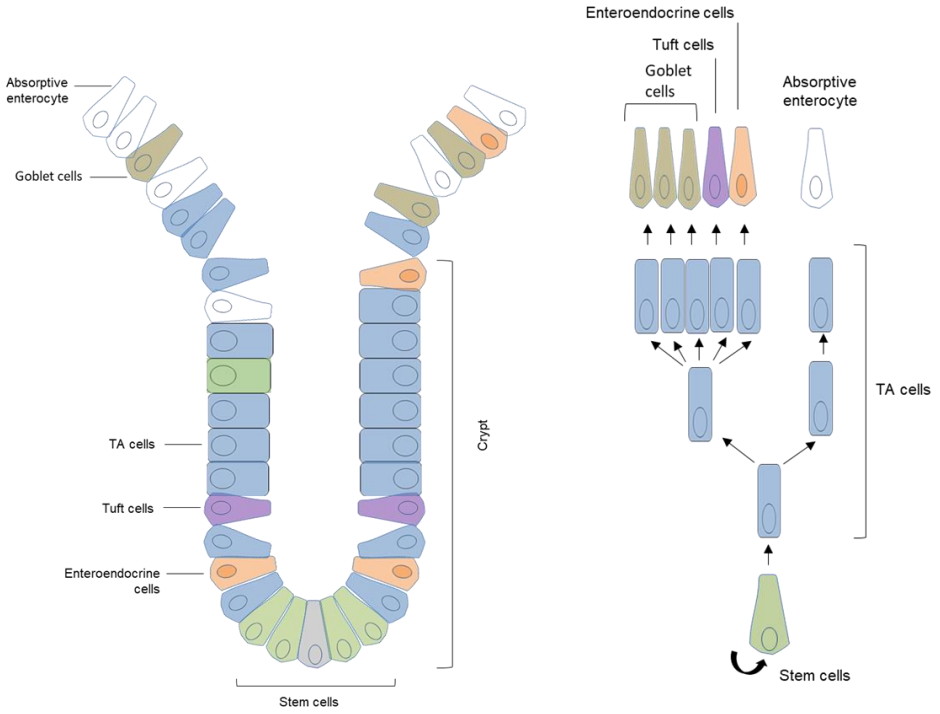


Figure 1-4: The structure of human colonic epithelium. An individual crypt is composed of stem cells in the bottom, differentiated cells toward the lumen, and transit-amplifying (TA) cells in between. TA cells subsequently differentiate into goblet cells, enterocytes, enteroendocrine cells and tuft cells. Adapted from (Barker, 2014).

Of note, intestinal epithelium is the most rapidly self-renewing tissue in the adult mammal with a turnover of every 5-7 days and is renewed from multipotent intestinal stem cells (ISCs) located at the bottom of the crypt (Zhu et al., 2019, Barker, 2014). They were first identified by Cheng and Leblond (Cheng and Leblond, 1974) and were named crypt base columnar (CBC) cells. CBCs are considered to be the functional ISCs with self-renewal ability that can differentiate to produce all other cells of the intestinal epithelium (Barker et al., 2007). Simultaneously, Potten and his collaborators also identified another population of stem cells, located at position 4 (i.e. +4) from the base of the crypt, that is thought to represent the real stem cell pool and have the ability to give rise to all epithelial lineages (Zhu et al., 2019, Potten, 1977, Potten et al., 1974).

Since then, researchers have focused on identifying population-specific markers to better elucidate the function of the putative stem cell population in the intestine.

The most distinguished marker of CBC cells is leucine-rich repeat-containing G-protein coupled receptor 5 (Lgr5), a well-known Wnt target gene that is the main source of actively cycling ISCs (Barker et al., 2007). Few more identified markers include olfactomedin-4 (olfm4) (van der Flier et al., 2009a), achaete-scute family bHLH transcription factor 2 (Ascl2) (van der Flier et al., 2009b), CD133 (Snippert et al., 2009), CD44/CD166 (Sangiorgi and Capecchi, 2008), SRY-box 9 (Sox9) (Formeister et al., 2009), ring finger protein 43 (Rnf43) and zinc and ring finger 3 (Znrf3) (Koo et al., 2012). In addition, "+4" stem cells markers are polycomb complex protein 1 (Bmi1) (Sangiorgi and Capecchi, 2008), leucine-rich repeat protein 1 (Lrig1) (Powell et al., 2012), mouse telomerase reverse transcriptase (mTert) (Montgomery et al., 2011) and Hop homeobox (Hopx) (Takeda et al., 2011). However, both CBC and +4 cells manifest self-renewal abilities, multipotency and can repopulate the intestinal epithelium in the absence of the other stem cell population (Yan et al., 2012, Takeda et al., 2011, Sato et al., 2009b, Barker et al., 2007). Moreover, Lgr5, as well as "+4" markers, are found expressed in both stem cell populations and in other cells along the crypt as secretory progenitors, which, in the absence of stem cells, dedifferentiate and reacquire multipotency (Buczacki et al., 2013, van Es et al., 2012).

Stem and progenitor cells are characterised by their ability to self-renew and produce differentiated progeny (Gómez-López et al., 2014, Lerner and Petritsch, 2014). A fine balance between these processes is achieved through controlled asymmetric cell divisions (ACD), where a stem cell generates one daughter stem cell for self-renewal and one daughter progenitor cell that undergoes further differentiation (Gómez-López et al., 2014, Bu et al., 2013).

Therefore, by balancing self-renewal with differentiation, ACD maintains the stem and progenitor cell pool and is necessary to maintain adult tissue homeostasis (Gómez-López et al., 2014).

Unlike symmetric self-renewing divisions, which amplify the stem cell compartment, ACDs balance cell proliferation with differentiation (Lerner and Petritsch, 2014, Bu et al., 2013). Therefore, disruption of asymmetric cell divisions in stem and progenitor cells are associated with tumorigenesis (Lerner and Petritsch, 2014).

Alteration in the homeostasis between self-renewal and differentiation may also alter the predisposition of CRC. For example, in *in vivo* mice model, acute genetic disruption of Apc blocks differentiation, drives hyperproliferation and expansion of undifferentiated progenitor cells. This subsequently results in the disruption of the crypt-villus axis, whereby stem and progenitor cells expand and fail to differentiate as they move up the villus (**Figure 1-4**) (Dow et al., 2015, Sansom et al., 2004). For example, in CRC patients, loss of a differentiation-promoting transcription factor, CDX2, has been associated with BRAF-driven tumour development (Kim et al., 2013, Dalerba et al., 2016, Bae et al., 2015). On the other hand, SMAD4, a differentiation-promoting transcriptional effector of the TGFβ/BMP signalling pathway, is inactivated in 10-15% of CRC (Fearon, 2011). Interestingly, both of these transcription factors have been ascribed roles antagonistic to the WNT-signalling pathway (Tong et al., 2017, Tian et al., 2012). Moreover, Bone Morphogenetic Protein, BMP2 and BMP4 have been associated with CSC differentiation and antagonizing the WNT/β-catenin signalling (Tong et al., 2017).

Therefore, such homeostasis and plasticity between self-renewal/differentiation, drug sensitivity/resistance, symmetric/asymmetric division, senescence/proliferation, epithelial-mesenchymal transition/mesenchymal-epithelial transition help

understanding the fundamental aspect of the emerging stem cell dynamics (Meacham and Morrison, 2013).

1.8 Cancer stem-like cells (CSC)

Cancer stem-like cells (CSCs) are a subpopulation of tumour cells that have the extraordinary characteristic of enhanced self-renewal and limited differentiation capacity that allow them to be resistant to anti-cancer therapies and tumour-targeted drugs, which in turn, helps them to survive treatment and initiate tumour recurrence (Batlle and Clevers, 2017, Meacham and Morrison, 2013). Experimental evidence supports the role of the therapy-resistant CSCs to generate cellular heterogeneity within a tumour, including colorectal cancer (Lytle et al., 2018, Batlle and Clevers, 2017, Shimokawa et al., 2017). According to the cancer stem cells hypothesis, only the CSCs have the capacity to generate primary tumour, recurrences and metastasis (Vermeulen et al., 2008, Visvader, 2011). Therefore, there is an ever-growing need for novel compounds to target CSCs and development of treatment strategies in combination with other cytotoxic agents and tumour-targeted drugs to prevent recurrence and regrowth of further neoplastic cell populations.

CSCs were identified for the first time in acute myeloid leukaemia as a subpopulation of tumour cells expressing CD34+/CD38- and driving tumorigenesis in recipient mice (Lapidot et al., 1994). Since then, based on the expression of cell surface markers, CSCs were identified in different types of cancers, including CRC.

With regard to CRC-SC, a variety of signals have been shown to promote self-renewal capacities. For example, Wnt, Notch, TGFβ and Hedgehog signalling pathways were found to be implicated in the regulation of CSCs (Vermeulen et al., 2010, Sato et al., 2016). Wnt and Notch signalling play a critical role in cell proliferation, and are more active at the bottom of the crypt, whereas Bone morphogenetic proteins (BMPs) and Hedgehog pathways (Hh) promote cell differentiation (Sancho et al., 2004). Furthermore, hepatocyte growth factor (HGF) has been shown to

maintain CRC-SCs in a stem-cell state and prevent differentiation (Garza-Treviño et al., 2015). It has been reported that deletion of *Apc* gene in Lgr5+ve stem cells gives rise to microadenomas within 8 days and large adenomas in 14 days in mouse small intestine (Barker et al., 2007, Vermeulen and Snippert, 2014). Whereas, *Apc* deletion in differentiated cells promotes adenomas formation with significantly lower frequency (Barker et al., 2009). These findings strongly support the hypothesis that intestinal stem cells are actively cycling, through multi-step mutations in the stem cell compartment and can initiate tumour growth. However, the exact identity of the intestinal stem cells is still debatable because of the lack of specific markers. Several markers such as CD133, ALDH, CD44, CD34, NANOG, SOX2, OCT4, CD49f, ALDH1A3, ALDH1A1 have been identified as colon CSC surface antigens (Garza-Treviño et al., 2015, Khalek et al., 2010, Ezeh et al., 2005, Toledo-Guzmán et al., 2018). However, it has also been reported that the expression of these markers is not always specific of stem-like cells only and, therefore, is not particularly sufficient to identify CSCs. Therefore, such markers are more reliable to identify CSC-rich subpopulations instead of definite isolation of all the CSCs (Chen et al., 2013b, Ahmed et al., 2017a).

In principle, CSC targeted therapy would help the tumour to eventually disappear as it will lose its self-renewal and subsequent proliferative capacity (de Sousa e Melo et al., 2017, Liu et al., 2015). Therefore, characterisation of CRC-SCs markers and the mutations which contribute to the transformation of intestinal stem cells into CSCs may help to design effective treatment strategies to target the CSCs themselves rather than the tumour bulk itself and may decrease the mortality rate.

In addition, some FDA approved commercially available drugs that are currently marketed for their antibacterial, anti-inflammatory properties, or other therapeutic indications are widely being studied for their high promise and potential in targeting CSCs. Therefore, investigating these

parameters and drugs associated with these diseases would greatly benefit the study of cancer therapeutics.

1.8.1 Targeting cancer stem-like cells

As with all cancer types, nowadays, it is believed that intratumoral heterogeneity has a significant role in the development of resistance to therapy. CSCs have a unique set of cellular characteristics which include resistance to therapy, lack of differentiation, multi- or pluripotency, and high self-renewal ability recurrence (Al-Ejeh et al., 2011, Cufí et al., 2012, Parmar et al., 2011). Interestingly, a new theory supports that CSCs are responsible for the generation of this cellular heterogeneity within a tumour. Accepting this new theory or dismissing and supporting the old theory of the Darwinian evolution of cancer is up to the individual's personal decision. Nonetheless, the evidence for the presence of CSCs and the associated therapy resistance cannot be dismissed and stress the importance of performing high standard research in the area.

Over the last three decades, treatment options including chemotherapy, surgery and radiotherapy have only made incremental improvements in term of patients survival (Sachlos et al., 2012a, Jemal et al., 2010). This is because, both chemotherapy and radiotherapy primarily target differentiated and proliferating cancer cells, whilst being less effective in targeting and eradicating the relatively undifferentiated CSCs (Yan et al., 2011, Yu et al., 2007a). Selective targeting of CSC is a huge challenge from the therapeutic point of view as strategies that are not sufficiently selective for CSCs may cause toxicity to the healthy tissues and also increase risks of recurrence among the patients (Cho et al., 2008). Many novel anticancer drugs, including tyrosine kinase inhibitors and monoclonal antibodies, also reduce tumour size but fail to eliminate CSCs, which in turn, results in cancer recurrence (Al-Ejeh et al., 2011, Bhatia et al., 2003, Bedard et al., 2009, Cufí et al., 2012, Parmar et al., 2011). Such observations on existing cancer treatments underline the need for a strategy based on selectively targeting of CSCs. Therefore,

there is an ever-growing need for novel compounds and drugs that target CSCs, preferably in combination with other cytotoxic drugs and tumour-targeted agents to prevent the regrowth of neoplastic cell populations (Reya et al., 2001). A CSCs targeted therapy would help the tumour to eventually disappear as it will lose its self-renewal and proliferative capacity (Liu et al., 2015) (**Figure 1-5**).

In recent years, several approaches have been identified including targeting specific markers or signalling pathways to eliminate the CSCs, alter their microenvironment, or reprogram CSCs for differentiation, re-sensitise to chemotherapy, apoptosis, and reversal of EMT or to reduce metastasis (Marquardt et al., 2018, Batlle and Clevers, 2017). These targets include ABC superfamily, anti-apoptotic factors, detoxifying and DNA repair enzymes and distinct oncogenic cascades such as Wnt/β-catenin, TGF-β, Hedgehog, EGFR, PTEN, BMI-1, NF-κB, Bcl-2, JAK/STAT, Notch, and PI3K/Akt/mTOR pathways (Wang et al., 2010, Liu et al., 2009, Chen et al., 2013a, Yang and Rycaj, 2015a, Naujokat and Steinhart, 2012, Boman and Wicha, 2008, Singh and Settleman, 2010). However, bringing these approaches from bench to the clinic and evaluating them in clinical settings remains as a huge challenge.

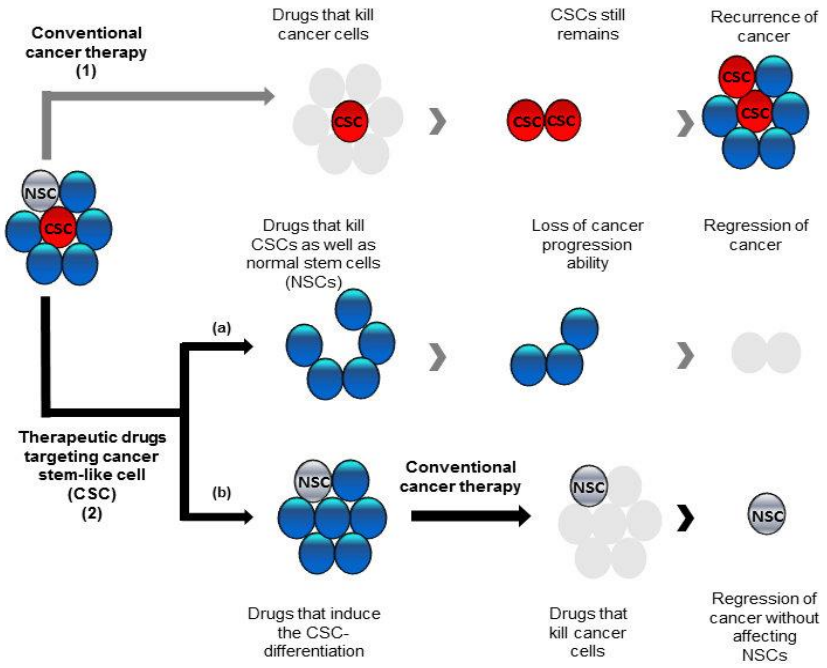


Figure 1-5: Different approaches in cancer treatment. (1) Recurrence of cancer by the remaining CSCs after conventional cancer treatment. **(2)** CSC-targeted therapies will **(a)** eliminate all types of cancer cells including CSCs and also normal stem cells (NSCs) which cause tumour collapse and tissue degeneration, and **(b)** induce CSCs-differentiation and make them susceptible to conventional cancer therapy, without affecting the NSCs. Adapted from (Ahmed et al., 2017a).

With more research being invested in CSCs, CSC-targeting compounds recently received more therapeutic attention. Some approaches are at a preliminary research stage where focus is given to the drug under investigation only. Whereas, for others, combination with conventional therapeutic drugs is being investigated in making the resistant cells susceptible to chemotherapy (Ahmed et al., 2017a). Recently, several compounds have been identified to target CSCs (**Table 1-3**). A combination of these agents with conventional chemotherapy drugs has been shown to significantly suppress self-renewal, induce

differentiation, inhibit tumour growth and metastasis and eventually eliminate CSCs (Wang et al., 2010, Ning et al., 2013) **(Figure 1-5). Table 1-3** shows some drugs and compounds identified for CSC targeting in different cancers.

Table 1-3: Drugs and novel compounds identified for selective CSC targeting. Updated from (Ahmed et al., 2017a).

Compound	Mode of actions	Cancer types	References
BBI608	STAT3 inhibitor	CRC-SC, pancreatic cancer SC, NSCLC-SC	(Zhou et al., 2018, MacDonagh et al., 2018, Li et al., 2015)
Berberine	Quaternary ammonium salt	Breast CSC, CRC-SC, oral squamous cell carcinomas SC	(De Francesco et al., 2019, Lin et al., 2017, Kim et al., 2008)
Cyclopamine,	Smo antagonist, Hedgehog pathway inhibitor	Glioblastoma SC, multiple myeloma SC, chronic myeloid leukemia SC, gastric CSC, breast CSC, prostate CSC, pancreatic CSC	(Balbous et al., 2014, Bar et al., 2007, Chen et al., 2002)
Curcumin, analogue GO-Y030, diflurinated curcumin (CDF)	Wnt inhibitor, STAT3 and NF-κB inhibitor, affects many CSC regulators (Hedgehog, Notch, PI3K/Akt/mTOR pathway	Glioblastoma SC, lung CSC, colon CSC, pancreatic CSC, breast CSC, oral squamous cell carcinoma SC	(Howells et al., 2019, Chung et al., 2019, Bano et al., 2018)
Epigallocatechin gallate (EGCG) and its synthetic analogues	Downregulates mTOR pathway, activates AMPK and upregulates p21	Prostate CSC, pancreatic CSC, breast CSC, colon CSC, lung CSC, advanced solid tumours, SCLC-SC	(Chan et al., 2018, Toden et al., 2016)

G244-LM	Wnt inhibitor	CRC-SC	(Leon et al., 2015, Lau et al., 2013)
Genistein	Wnt inhibitor, Hedgehog inhibitor	CRC-SC	(Li et al., 2019a, Sebio et al., 2014)
IWR-1	Wnt inhibitor	NSCLC-SC, CRC-SC, osteosarcoma SC	(Martins-Neves et al., 2018, Leon et al., 2015)
LGK974	Porcupine inhibitor	CRC-SC	(Masuda et al., 2015)
Metformin	Reduces EMT related ZEB1, TWIST1 and Slug	Breast CSC, gastric CSC, pancreatic CSC, thyroid CSC, prostate CSC	(Courtois et al., 2017, Janzer et al., 2014, Cufí et al., 2012, Hirsch et al., 2009)
OMP-21M18	Anti-DLL4 monoclonal antibody	NSCLC-SC, colon CSC, breast CSC	(Smith et al., 2014, Hoey et al., 2009)
PTC-596	BMI-1 inhibitor	Advanced solid tumour SC, AML SC	(Barbosa et al., 2019, Nishida et al., 2015)
Resminostat	HDAC inhibitor	Advanced colorectal CSC	(Mottamal et al., 2015)
Repertaxin	CXR1 and CXR2 inhibitor	Breast CSC, renal CSC	(Corro et al., 2019)
Resveratrol	Wnt inhibitor, upregulates miR622 and miR633	Medullo-blastoma SC, breast CSC, pancreatic CSC, glioblastoma SC, colon SC	(Zhou et al., 2019, Chan et al., 2018, Han et al., 2012)
Salinomycin	Inhibits ALDH, SOX2, CXCR4, β-catenin inhibitor, reduces CD133, vimentin, induces E-cadherin	Breast CSC, AML SCs, GIST SC, gastric CSC, lung CSC, colorectal CSC, prostate CSC, pancreatic CSC	(Wang et al., 2019b, Arfaoui et al., 2019, Zhang et al., 2018)
Sulforaphane	Wnt inhibitor	Pancreatic CSC, breast CSC, prostate CSC, CML SC	(Castro et al., 2019, Pistollato et al., 2017, Kallifatidis et al., 2009)

Vismodegib (GDC 0449)	Smo antagonist, Hedgehog inhibitor	Pancreatic CSC, lung CSC, medullo-blastoma, basal cell carcinoma, glioblastoma, chondro-sarcoma, gastric carcinoma, colon, ovarian, breast CSC	(Valenti et al., 2017, Singh et al., 2011)
WIKI4	Wnt inhibitor	Colon CSC	(Leon et al., 2015)
XAV939	Tankyrase inhibitor, β-catenin inhibitor	Colon CSC, liver cancer SC	(Huo et al., 2019, Wu et al., 2016, Sebio et al., 2014)

1.9 CRC treatment

1.9.1 Conventional therapy in CRC

At present, conventional chemotherapy of CRC is primarily based on 5-fluorouracil, oxaliplatin, and irinotecan (Chau and Cunningham, 2009). However, the response rates of CRC to these chemotherapies are limited to 40%–50% as in most cases CSCs can survive the treatment (Naujokat and Steinhart, 2012). The main purpose of cancer staging is the guidance for treatment. For example, in stage I and stage II patients, the surgery alone is generally sufficient to eradicate the tumour. On the other hand, the current guidelines recommend that patients with completely resected stage III colon cancer should be treated with adjuvant chemotherapy. Such treatment consists of 5-fluorouracil (5-FU) based therapy, in combination with leucovorin (LV, 5'-formyltetrahydrofolate) or oxaliplatin in a regimen known as FOLFOX or FLOX. In addition, patients with stage IV colon cancer are generally treated with FOLFOX or FOLFIRI (oxaliplatin is replaced by irinotecan) regiments and, occasionally, with also targeted therapies. The resection of secondary tumours, commonly colonising liver and/or lung, is achieved only if the metastases are isolated (Kuipers et al., 2015). Of note, 5-Fluorouracil in

the FOLFOX regimen can be replaced by capecitabine, but combination of capecitabine with irinotecan gives relatively toxic reactions.

In recent years, targeted therapies have also been developed to precisely aim and block the mediators and signalling pathways involved in CRC progression. Currently, several targeted therapies are being evaluated for their ability to inhibit Wnt signalling (Chen et al., 2009), destabilizing β-catenin (Fujii et al., 2007) or disrupting the β-catenin/TCF (Sampieri and Fodde, 2012) for the treatment of CRC. Recent advances also include the development of highly promising mAbs against the Wnt cascade, Fz receptors, or secreted Fz-related proteins for clinical use (He et al., 2005, You et al., 2004).

Such therapies are selective toward the tumour cells and spare healthy cells which ultimately reduce the adverse effects triggered by DNA damaging chemotherapy. For example, about 80% of CRC patients exhibit expression or up-regulation of EGF signalling pathway. Thus, metastatic patients resistant to conventional chemotherapy or not treated yet, negative for *K-RAS* mutations, benefit from administration of monoclonal antibodies such as cetuximab and panitumumab that are directed to EGF receptor (EGFR). Moreover, bevacizumab (antibody against vascular endothelial growth factor, VEGF) has significantly improved the progression-free survival and overall survival of metastatic patients, when administered in combination with FOLFOX or FOLFIRI (Kuipers et al., 2015).

1.8.2.1 FOLFOX and FOLFIRI mechanism of action

5-FU is an uracil analogue that binds to thymidylate synthase and inhibits the synthesis of deoxythymidine monophosphate (dTMP). Thymidylate synthase (TS) catalyses the methylation of deoxyuridine monophosphate (dUMP) by transferring the methyl group from reduced folate 5,10-methylene tetrahydrofolate (CH_2-THF) to dTMP. Subsequently, dTMP is phosphorylated to deoxythymidine triphosphate (dTTP) needed for DNA

replication and repair (Longley et al., 2003). Inside the cell, most of 5-FU is phosphorylated to 5-fluoro-dUMP (FdUMP) by thymidine phosphorylase (TYMP) and thymidine kinase-1 (TK1). FdUMP then inhibits TS, an important enzyme for nucleotide synthesis thereby compromises the DNA synthesis and repair, and causes DNA damage-induced cell death (Longley et al., 2003, Mhaidat et al., 2014, Mohelnikova-Duchonova et al., 2014). However, the spectrum of 5-FU metabolites depends on the administration schedule, as bolus treatment favours RNA damage by FUTP and continuous regimen favours DNA damage by FdUTP (Mohelnikova-Duchonova et al., 2014). Leucovorin or folinic acid enhances 5-FU toxicity by increasing the intracellular availability of reduced folate CH_2- THF (Longley et al., 2003).

Oxaliplatin belongs to the platinum-based class of drugs. The principal mechanism of oxaliplatin is inhibition of DNA synthesis in cancer cells by the formation of crosslinks in DNA (DNA intra-strand, DNA inter-strand as well as DNA-protein crosslinks). Such alterations disturb both DNA and mRNA synthesis provoking apoptosis-mediated cell death (Alcindor and Beauger, 2011). DNA damage by oxaliplatin is repaired mainly by nucleotide excision repair (NER), base excision repair (BER) and by replicative bypass. Oxaliplatin is transported mainly by the uptake transporters SLC22A1/OCT1 and SLC22A2/OCT2, which play a critical role not only in cellular uptake but also in the associated cytotoxicity (Mohelnikova-Duchonova et al., 2014).

Irinotecan is a camptothecin analogue, that is converted to an active metabolite, SN-38, by carboxylesterases CES1 and CES2. SN-38 (7-ethyl-10-hydroxycamptothecin) is transported by ABC transporters, namely by ABCC1, ABCC2, ABCB1, and ABCG2. Inside a cell, SN-38 inhibits topoisomerase I and subsequently blocks DNA replication and transcription causing DNA strand breaks and, ultimately, inducing cell death (Fujita et al., 2015, Mohelnikova-Duchonova et al., 2014).

1.9.2 Targeting CRC-SCs

Even though there is a broad range of conventional treatments for CRC, which include surgical resection, radiotherapy, chemotherapy and targeted monoclonal antibody therapies, success is limited. With a 5-year survival of about 65% and a 60% chance of recurrence in the first 2-3 years (Cao et al., 2015a), the discovery and development of new therapeutics to accompany the conventional treatments are crucial. Therefore, research now focuses on the identification of factors believed to be associated with the failure of conventional treatment and ways to tackle them.

The resistance of CRC-SCs to conventional chemotherapy may also be overcome by pre-treatment with histone deacetylase (HDAC) inhibitors such as vorinostat, romidepsin etc. (Emmink et al., 2011b). These inhibitors change the level of pro- and anti-apoptotic molecules, induce cell cycle arrest at G1/S or G2/M transition and thereby induce differentiation and apoptosis (Mottamal et al., 2015). In addition, Salinomycin inhibited a number of CSC characteristics, including colonosphere formation, migration, and invasion and also selectively reduced the CD133+ population (Ahmed et al., 2017a). Moreover, BMI-1 regulates stem-like cell behaviour and is associated with poor patient outcome and resistance in CRC (Yang and Rycaj, 2015a, Glinsky et al., 2005). Treatment of primary CRC cell line-derived xenografts with BMI-1 inhibitors like PTC-209 resulted in suppression of self-renewal and long-term irreversible impairment of tumour growth in CRC-SCs even with short term treatment (Kreso et al., 2014). CRC-SCs that are unresponsive to 5-FU treatment showed a high level of apoptosis with AP20187 treatment. Along with increased apoptosis, a strong decrease in tumour size and significant loss of CD133+ CSCs were observed in mouse models upon treatment of colorectal cancer with AP20187 (Kemper et al., 2012b).

Of note, in eliminating CRC-SCs, curcumin showed a superior effect to the widely used FOLFOX (Folinic acid, 5-fluorouracil and Oxaliplatin) regimen (Yu et al., 2009). It interferes with several CSC regulators including Wnt/β-catenin, Sonic Hedgehog, Notch and PI3K/Akt/mTOR signalling, and sensitises CSCs to further anti-cancer therapies (Ramasamy et al., 2015). When used with tyrosine kinase inhibitor dasatinib, the combination therapy showed more efficacy in eliminating FOLFOX-resistant CRC-SCs than the single agent (Nautiyal et al., 2011). Because of its low bioavailability, synthetic analogues with improved bioavailability were developed recently, such as GO-Y030, GO-YY078 and difluorinated curcumin (CDF) (Shibata et al., 2009).

1.8.3.1 Differentiation therapy

Normal and neoplastic stem cells are functionally defined by a tightly controlled balance between self-renewal versus differentiation potential. In the case of CSCs, this shifts toward enhanced self-renewal and limited differentiation capacity. Hence, targeting CSCs for differentiation offers promise for a new generation of therapeutics.

Differentiation therapy was first reported in 1987 with all-trans retinoic acid (ATRA) for the treatment of acute promyelocytic leukemia (APL), a rare subtype of acute myeloid leukemia (AML) (Breitman et al., 1980, Giguere et al., 1987). This introduced a new approach to obtain remission in malignancies which markedly improved the outcome of this disease (Brown and Hughes, 2012). The majority of cancer therapies being highly toxic and often nonspecific in nature, this indiscriminate cytotoxicity can also affect healthy progenitor cells and stem cells leading to dose restrictions which could therefore decrease effect or renders these compounds unsuitable for treatment (**Figure 1-5**). Differentiation therapy, therefore, offers the prospect of a less aggressive treatment by virtue of attenuated growth accompanied by limited damage to the normal healthy cells. By tackling the pathways that maintain stemness

characteristics, the self-renewing CSCs could be made responsive to force differentiation and produce differentiated cancerous progeny which enter the normal cell cycle. Since then, this breakthrough has gained immense therapeutic attention for its implication in solid tumours.

Fundamentally, such relatively less toxic form of cancer therapy involves the use of differentiation inducing agents, alone or in combination, that modify the state of differentiation and growth of cancer cells **(Figure 1-5)**. This approach employs the understanding that many neoplastic cell types exhibit reversible defects in differentiation, which upon an appropriate treatment, results in tumour reprogramming and therefore induces terminal differentiation or apoptosis (programmed cell death) (Leszczyniecka et al., 2001).

1.9.3 Colorectal carcinogenesis models

In recent years, several *in vitro* and *in vivo* preclinical models have been developed, including, spheroids, colonosphere, organoids, patient-derived tumour xenografts (PDX), and patient-derived tumour organoids. These models present valuable tools, not only for drug discovery but also for understanding the fundamental mechanisms of tumorigenesis, inflammation, and interactions between the host–pathogen.

The first adult stem cell-derived organoid cultures were established from Lgr5-expressing mouse intestinal stem cells, where the culture condition successfully mimicked the intestinal stem cell niche (Sato et al., 2009a). Since then, organoid cultures have been established in variety of tissues, including colon (Bleijs et al., 2019). In 2011, human tumour organoids have been generated from colon (van de Wetering et al., 2015, Sato et al., 2011). It has also been reported that human colon tissue obtained from colonoscopy biopsy samples, surgical resections, or single EphB2+ stem-like cells can be cultured as organoids (Sato et al., 2011).

Genetically engineered mouse model has shown to successfully recapitulate adenoma or carcinoma formation in the immunocompetent colon microenvironment. Since the initial discovery of the ApcMin mouse in 1990, several genetically engineered CRC models have been established. For example, CRISPR/Cas9-mediated editing of APC, followed by deletion of SMAD4, and TP53, and introduction of activating mutations in KRAS and PIK3CA demonstrated a adenoma-carcinoma organoid model in CRC (Drost et al., 2015). Additionally, loss of APC and TP53 showed to be the key drivers of chromosome instability and aneuploidy in human intestinal organoids (Bleijs et al., 2019, Drost et al., 2015).

Moreover, in the Patient Derived Xenografts (PDX), a segment of tumour tissue is obtained following surgery and implanted and subsequently passaged into immunodeficient mice (Bleijs et al., 2019, Hidalgo et al., 2011). The key driver mutations, including KRAS and PIK3CA remain consistent along the passages (Tignanelli et al., 2014). An important application of PDX is personalized cancer treatment. It has been reported that, PDX models represent the clinical response to therapy better than traditional xenografts (Golovko et al., 2015, Hidalgo et al., 2011, Voskoglou-Nomikos et al., 2003). In addition, Patient-derived organoids (PDTOs) can be expanded long term. Several studies demonstrated its use in investigating gene–drug associations and in high-throughput drug screens (Bleijs et al., 2019). In response to anticancer drugs, PDTOs have been suggested to successfully recapitulate the drug response as seen in the patient (Vlachogiannis et al., 2018).

1.10 Rationale and objectives

Due to the characteristic features of cancer and their association with other diseases, it is important to investigate the hallmarks of cancer in order to therapeutically target them. Inflammation is recognised as one of the emerging hallmark features of cancer, particularly in CRC, which has long been known as one of the best examples of tumour-promoting

inflammation. Approximately, 15% of deaths in CAC occurs due to the underlying IBD development (Lasry et al., 2016). While its association in promoting cell survival, proliferation and angiogenesis is widely established in cancer, the inflammatory mediators and signalling that regulate the potency of anticancer treatment upon CSC differentiation are still not fully defined. Moreover, several drugs are currently in the development stage for targeting the tumour associated inflammation in CRC. Even though NF-κB is one the major participant in tumour associated-inflammation transition, no NF-κB inhibitors are currently clinically available for the treatment of cancer (Diakos et al., 2014).

In this study, the aim was to explore three anti-inflammatory FDA approved drugs, identified from a compound library screening consisting of 707 NCC (NIH Clinical Collection) compounds belonging to a range therapeutic groups, including antibacterial/anti-inflammatory, antiviral, antihistamine and anticancer drugs, amongst others (Cao et al., 2015b, Sachlos et al., 2012b). Of note, all these compounds went through phase I-III clinical trials, and therefore possess established safety profile for medical use which can help guide their use as anticancer drugs. The primary aim of this screening was to identify the potential compound(s) that induce differentiation and overcome neoplastic self-renewal in CRC using 3D colonospheres (Sachlos et al., 2012b). Majority of current cancer therapies being highly toxic and often nonspecific, we focused on a potentially less toxic approach based on the concept to modify CSC differentiation, also known as 'differentiation therapy', which would eventually make the CSCs more susceptible to conventional chemotherapy treatment. Therefore, the specific objectives of this project were to:

(I) identify potential compounds that target CRC-SC for differentiation

(II) evaluate candidate compound AM404s' anticancer properties and elucidating its mechanism for possible repurposing as a novel agent in CRC

(III) evaluate candidate compound rifabutins' anticancer properties and elucidating its mechanism in CRC

(IV) evaluate candidate compound idarubicins' anticancer properties in CRC.

To understand the system and methodology in order to screen a library of small molecules-based drugs targeting differentiation/stemness properties, the first objective was to employ a drug screening using 3D colonospheres derived from CRC cell lines. Next, to evaluate the anticancer effects of the shortlisted anti-inflammatory, antibacterial drugs using *in vitro* organoids and *ex vivo* tumour explant models. Finally, carrying out a gene expression analysis, in order to identify the possible new target(s) by which the candidate drug(s) might exert their antineoplastic effects in targeting CRC.

CHAPTER 2

Materials and Methods

2.1 Materials

All common materials, reagents, drugs and chemicals for biochemical, molecular and cellular experiment purposes were purchased from Sigma-Aldrich (UK) unless otherwise stated.

2.1.1 Cell lines

Human colorectal carcinoma HCT116, DLD-1, and SW480 cell lines were used throughout the study. HCT11 and DLD-1 cell lines are characterised by microsatellite instability, whereas SW480 cells are characterised by chromosomal instability. Immortalized parenteral cell lines were originally purchased from the American Type Culture Collection (ATCC) (**Table 2-1**). HCT116 cell line harbouring *FBXW7* deletion on both alleles ($HCT116^{FBXW7-/-}$) was kindly supplied by A. Balmain (University of California, San Francisco, CA) and B. Vogelstein (Ludwig Centre, Johns Hopkins University, Baltimore, MD), and *FBXL5* knockout DLD-1 cells were generated using the CRISPR-Cas9 technology in our laboratory by Nicholas Jinks and Seyed Mohammad Hossein Kashfi. Cells were further characterised in our laboratory (Li et al., 2019b, Lorenzi et al., 2016a, Babaei-Jadidi et al., 2011b).

Table 2-1: Colon cancer cell line origins (Li et al., 2019b, Linnekamp et al., 2018, Babaei-Jadidi et al., 2011b).

Cell line	Patient	Organ	Disease	Stage	Derived from	Mutation
HCT116	48-year old male	Colon ascends	Colorectal carcinoma	Dukes' D	Primary tumour	*CTNNB1*/S45 *KRAS* *TGFβ-RII* *PIK3CA*
DLD-1	Male	Colon	Colorectal adenocarcinoma	Dukes' C	Mis-classified	*APC* *KRAS* *PIK3CA* *TP53*
SW480	50-year-old male	Colon	Colorectal adenocarcinoma	Dukes' B	Primary tumour	*APC* *KRAS* *TP53*

Cells were routinely tested and approved mycoplasma-free. All cells were propagated in complete medium and used for experiments within 5-7 passages from thawing using the following procedures.

2.1.2 Human tissue specimen

Tumour and adjacent healthy tissue samples of 14 colorectal cancer patients were collected from Nottingham Health Sciences Biobank (NHSB), Queens Medical Centre, University of Nottingham. Tissue samples were collected only from patients who provided written informed consent (Kashfi et al., 2018). All the patient materials used in this study are listed in **Table 2-2**.

Table 2-2: List of patient tumour tissues used in this study.

Background Information	Diagnosis	Staging	Medical History
Colonoscopy showed distal sigmoid polyp	Early rectal cancer	T1 N0 M0	Chronic back pain including previous spinal and gastric bypass surgery, Type 2 diabetes, COPD; regular warfarin treatment.
30 mm Polypoidal malignant lesion in the Rectosigmoid, at 14 cm from the anorectal verge.	Rectal cancer	T1 N0 M0	Hypertension
Bowel Cancer Screening Programme patient with a positive FOB test; malignant-looking mass in the proximal ascending colon (tattooed).	Ascending Colon Cancer	T2 N0 M0	Cholecystectomy, incisional hernia, hypertension, arthritis, and spinal problems.
Rectal cancer with suspicion of invasion into the bladder	Mid-to-low rectal adenocarcinoma	T4 N1 M0	Previously treated chemo-radiotherapy and 3 cycles of interval CAPOX chemotherapy.
Referred with change in bowel habit. CT colonography suggested invasive tumour in descending colon. Colonoscopy revealed impassable obstructing lesion in descending colon (tattooed) 45 cm from anal verge.	Descending colon cancer, adenocarcinoma	T3 N0 M0	Type 2 diabetes, osteoarthritis, hypertension, GORD, benign prostatic hypertrophy.
Referred with change in bowel habit and rectal bleeding; malignant-looking mass in the sigmoid	Sigmoid cancer, moderately differentiated adenocarcinoma	T3 N1 M0	No information provided.

(tattooed) at 20-30cm from anal verge.			
Stable rectal cancer with reduction in size/number of liver lesions.	Mid-to-upper rectal cancer	T3 N1 M1	Gleason 7 prostate cancer, Type 2 Diabetes; previously received 6 cycles of chemotherapy.
3 cm circumferential malignant tumour in ascending colon (tattooed).	Ascending colon cancer; moderately differentiated adenocarcinoma.	T3 N0 M0	Gleason 8 prostate cancer, ECOG 2, liver abscess, anaemia, anxiety.
Lesion at 6 cm from anal verge	Rectal cancer	T3b N2 M0	Previously treated with long-course chemo-radiotherapy followed by 3 cycles of interval CAPOX chemotherapy.
4 cm lesion at 15 cm from anal verge. Lesion invades the muscularis propria.	Rectal cancer	T3b N0 M0	Excision of basal cell carcinoma from nasolabial fold.
Soft tissue thickening of caecum. Colonoscopy revealed a large flat/polypoidal malignant-looking mass in the caecum.	Caecal cancer	T3 N1 M0.	Previously treated with radical radiotherapy for breast cancer; asthma, hypertension.
Malignant-looking ulcerated mass in the ascending colon extending over at least 50% of the circumference.	Ascending colon cancer	T3 N1 M0	Visually impaired, anaemic.
9 total polyps in the colon; 2 large polyps located in hepatic flexure and proximal sigmoid colon.	Sigmoid polyp cancer	T1 N0 M0	Post stroke seizure, right knee replacement.
20 mm laterally spreading polyp at the caecal pole.	Caecal Cancer	No information provided	Hypertension, sleep apnoea, and oesophagitis

2.1.3 NCC (NIH Clinical Collection) library

A clinical collection of 707 FDA (Food and Drug Administration) approved small molecule compounds from the US National Institute of Health (NIH) was kindly supplied by Evotec, USA (**Appendix 1**) (Cao et al., 2015b, Sachlos et al., 2012b). All compounds in NCC (NIH Clinical Collection) library belong to several different types of therapeutic groups, including antibacterial/anti-inflammatory, antiviral, antihistamine, anticancer and hormonal therapy, amongst others. This set of compounds have been in phase I-III clinical trials and have not been represented in other NIH arrayed collections. These compounds are now commercially available for a range of pharmacological indication.

2.1.4 Oligonucleotides (oligos)

Primers were designed to target two consecutive exons within the gene of interest and to amplify a region of 100-200 bp of size. Oligos were purchased from Sigma-Aldrich and upon arrival, then were spun down and resuspended in DNase/RNase-free water (Sigma-Aldrich, 4502) in the appropriate volume to yield a final concentration of 100 μM stock solution. The primers were then diluted to the desired working concentration and stored at −20°C until used. All primer sequences used in this study are listed in **Table 2-3**.

Table 2-3: List of primers and their sequences used in this study.

CD44	Forward	AGAAGGTGTGGGCAGAAGAA
	Reverse	AAATGCACCATTTCCTGAGA
NANOG	Forward	GCAGGCAACTCACTTTATCCCA
	Reverse	GGCAGCTTTAAGACTTTTCTGG
LGR5	Forward	GACAACAGCAGTATGGACG
	Reverse	GCATTACAAGTAAGTGCCAG
OCT4	Forward	AAGCTGCGGCCCTTGCTGCAG
	Reverse	AGCCCAAGCTGCTGGGCGATG
Krt20	Forward	TGAAGAGCTGCGAAGTCAGAT
	Reverse	TCCTCTCTCAGTCTCATACTTCAGTC
CDX2	Forward	AGCCAAGTGAAAACCAGGAC
	Reverse	CCAGATTTTAACCTGCCTCTCA
C-Jun	Forward	ACCCCAAGATCCTGAAACAG
	Reverse	ATCAGGCGCTCCAGCTCG
C-Myc	Forward	GGAGACACCGCCCACCA
	Reverse	GCGCTGCGTAGTTGTGCTG
CCND1	Forward	GCTGGAGGTCTGCGAGGA
	Reverse	CATCTTAGAGGCCACGAACA
CTNNB1	Forward	TATTACGACAGACTGCC
	Reverse	TGAAGTCCTAAAGCTTG
CXCR4	Forward	TTCTACCCCAATGACTTGTG
	Reverse	ATGTAGTAAGGCAGCCAACA
BMI-1	Forward	CCAGGGCTTTTCAAAAATGA
	Reverse	CCGATCCAATCTGTTCTGGT
N-Cadherin	Forward	GACAATGCCCCTCAAGTGTT

	Reverse	CCATTAAGCCGAGTGATGGT
Vimentin	Forward	GAGAACTTTGCCGTTGAAGC
	Reverse	TCCAGCAGCTTCCTGTAGGT
FBXW7	Forward	TGCAAGTGATAGAACCCCAG
	Reverse	TGTCTTCAGCCAAAATTCTCC
B-actin	Forward	GCGCGGCTACAGCTTCA
	Reverse	CTTAATGTCACGCACGATTTCC

2.1.5 Antibodies

Several primary and secondary antibodies were used in this study for both immunofluorescence and immunohistochemistry analysis. Details about their source and the dilution factors are listed in **Tables 2-4** and **2-5**.

Table 2-4: List of primary antibodies used in this study.

Primary antibody	Supplier	Source & catalogue number	Dilution factor	
			IF	IHC
CD44	DAKO, Millipore	1485, MAB2137 (Rat)	1:100	1:50
MUC2	Roche, Santa Cruz Biotechnology	760-4380, Sc-15334 (Rabbit)	1:200	Ready to use (RTU)
Ki-67	Roche	790-4286	N/A	Ready to use (RTU)
CDX2	Roche	760-4380	N/A	Ready to use (RTU)

Table 2-5: List of secondary antibodies used in this study.

Secondary antibody	Supplier	Source & catalogue number	Dilution factor (IF)
Alexa Fluor® 594 anti-rat	Life Technologies	P1379, Goat	1:500
Alexa Fluor® 488 anti-rabbit	Life Technologies	A-21206, Donkey	1:500

2.2 Methods

All procedures were performed under aseptic conditions under the guidance of strict safety regulations. Standard protocols of the techniques used throughout the project were followed from previously established templates and optimised where necessary or otherwise, developed in our laboratory.

2.2.1 General cell culture techniques

2.2.1.1 Cell line thawing, sub-culturing, freezing and cell counting

Low passage (passage 2-3) cells were recovered from liquid nitrogen and thawed at ambient temperature or placed in a water-bath at 37°C. Dimethyl sulfoxide (DMSO, Sigma, D4540) containing freezing medium was replaced by centrifuging the cells for 5mins at 400 relative centrifugal force (RCF) or G (bench-top centrifuge 5702-Eppendorf) and re-suspending with RPMI-1640 (Sigma, R0883) medium.

Cells were then propagated in 75 cm^2 flask (Cellstar, 658975) using complete medium; 500 ml RPMI1640 medium (Sigma Aldrich, R7509 or R0883), supplemented with 10% fetal bovine serum (FBS) (Sigma Aldrich, F7524), 5 ml of 2 mM L-glutamine (Sigma Aldrich, G7513) and 5 ml of 100 U/ml penicillin/streptomycin (Sigma Aldrich, P0781) in a humidified, 37°C, 5% CO_2 incubator. Cells were maintained at 70-80%

confluence and were sub-cultured every 2-3 days. After discarding the medium, adherent cells were then washed with 2 ml of sterile phosphate buffer solution (PBS, Sigma, D8537) followed by 5-10 mins incubation at 37°C with 1 ml 1x-Trypsin/ ethylenediaminetetraacetic acid (EDTA) (Sigma, T3924) solution to detach the cells. Next, the trypsin/EDTA solution was neutralized with 6 ml of complete medium. Based on the experimental protocol and future needs, cells were resuspended and passaged in 10 ml of complete fresh medium.

In order to freeze the cells, they were first trypsinized and centrifuged in an above-mentioned way. The supernatant was discarded, and the pellet was then resuspended in 1 ml freezing medium consisting of 10% DMSO and 90% FBS in Cryogenic vials on ice. These were kept overnight at -80°C before transferring to liquid nitrogen.

The number of cells in suspension was estimated by using a Neubauer hemocytometer (Marienfeld-Superior, Germany). Trypan-blue (Sigma, T8154) was used to stain and exclude the non-viable cells from the counting. Trypsinized cells were diluted in complete medium as necessary (by factor of 2 or 4) depending on their confluence to facilitate the counting procedure. 10 µl of the diluted cell suspension was stained with 10 µl of Trypan Blue for staining and, lastly, 10 µl of this final Trypan Blue-cell suspension mixture was loaded on the Neubauer counting chamber. As Trypan blue stains the dead cells in suspension, only the living transparent cells were counted within four different squares and the average number of cells was calculated. The final number of cells per ml of suspension was then determined by multiplying the average cell count by the applied dilution factors.

2.2.1.2 Cell cycle synchronization

Cell lines were synchronized in G_0 phase of the cell cycle by serum starvation prior to the wound healing assay in order to avoid any proliferation advantage. Cell culture medium was replaced with RPMI-1640 medium (Sigma Aldrich, R0883) supplemented with 2 mM L-

glutamine (Sigma Aldrich, G7513), and kept at 37°C, 5% CO_2 in a humidified incubator for 18 h.

2.2.2 Colonosphere formation assay

Colonosphere forming assay employs a three-dimensional (3D) assessment of stem-like cells based on their self-renewal and differentiation *in vitro* (Ishiguro et al., 2017, Shaheen et al., 2016c). HCT116, DLD-1 and SW480 cells were seeded in 6-well plates (in triplicate) at 1000 cell/well in the presence of serum-free stem cell medium (SCM).

Dulbecco's Modified Eagle Medium/Nutrient Mixture F-12 (DMEM/F-12, Life-Technologies 11320–074) is a basal medium used for the growth of colonospheres. DMEM/F12 was supplemented 200U/ml penicillin and 200 μg/ml streptomycin (1:100 dilution) (Sigma Aldrich, P0781), growth factors such as 10 ng/ml of human recombinant basic fibroblast growth factor (bFGF, R&D-System, 233-FB), 10 ng/ml of human recombinant epidermal growth factor (100 μg/ml) (EGF, Sigma Aldrich, E4127) both at 1:10000 dilution and 100x N-2 (Life-Technologies, 17,502–048) supplements. Cells were then carefully allowed to grow with the minimum movement for a period of 12-14 days in a 5%-CO_2 incubator at 37°C to form into three-dimensional aggregates of cells named colonospheres (Weiswald et al., 2015b, Shaheen et al., 2016c). Stem cell medium was only partially replaced (about one-third) every 3-4 days. On day 14, well defined colonospheres were subjected to drug treatment at their IC_{50} (**Figure 2-1**).

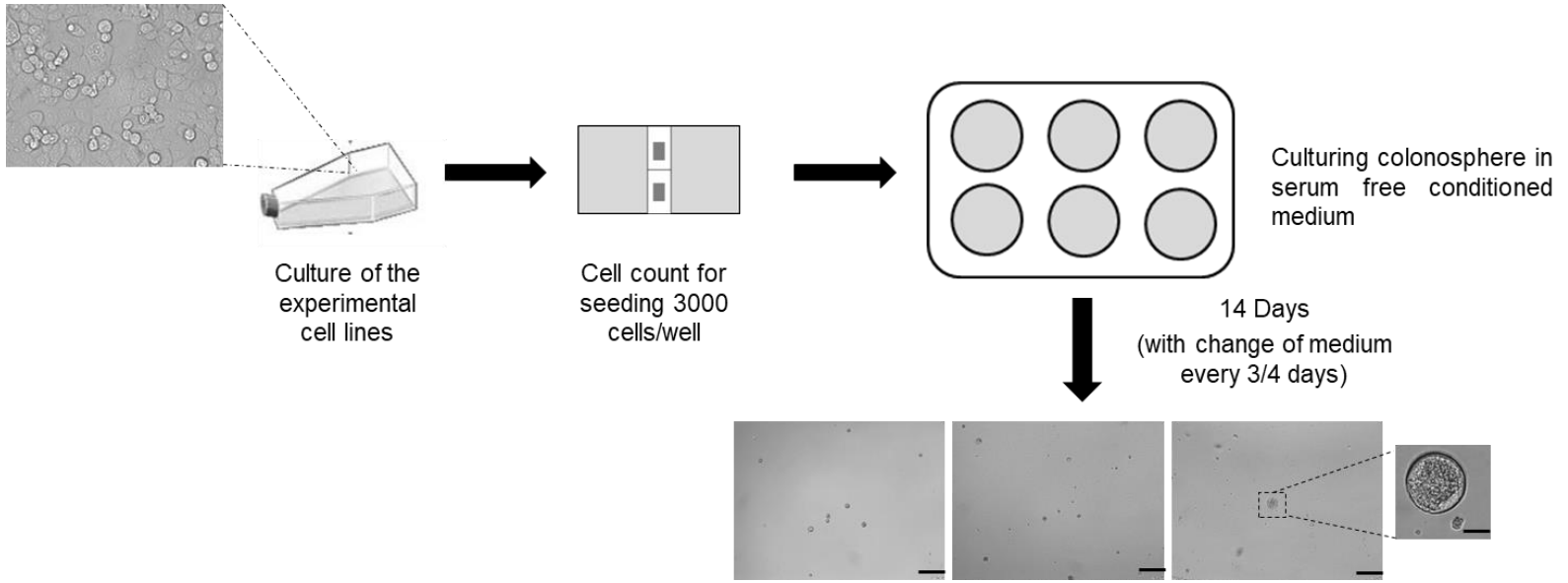


Figure 2-1: Preparation of colonosphere using conditioned stem cell medium. After 14 days, fully grown colonospheres were analysed for their colonosphere formation efficiency and stemness activity or subjected to drug treatments for subsequent drug screening and evaluating their response to drugs. Scale bar: 75 µM, 25 µM. Image was modified from (Shaheen et al., 2016c).

Following a 72-h treatment, colonopshere images were captured and the number colonospheres ranging between 50–250 μm diameter was counted using a DMI3000 B fluorescence microscope (Leica Microsystems). The percentage of colonospheres was calculated. Colonosphere forming efficiency was then analysed using Microsoft Office Excel 2007.

2.2.3 Patient derived tumour organoid culture

2.2.3.1 Tissue preparation and crypt isolation

All procedures were conducted following the Declaration of Helsinki and local ethics committee approval.

CRC patient-derived organoids were cultured as previously established and characterised in our lab (Kashfi et al., 2018, Sato et al., 2009a). Following the thawing of organoids on ice, crypts were re-suspended in Matrigel (SLS, Scientific Laboratory Supplies, 356231) at a concentration of approximately 20 crypts/25 μl Matrigel. The Crypt containing Matrigel was then added in a 48 well plate (Corning, 3548) and incubated at 37°C for 5 minutes for the Matrigel to solidify. After 5 minutes, tumour organoid medium was immediately overlaid in the crypt containing wells and placed back to the incubator.

2.2.3.2 Organoid culture and treatment

Tumour organoids were cultured in presence of tumour organoid medium. A 10 ml of medium for tumour organoid was prepared by supplementing with advanced DMEM/F12, 20% of R-spondin (2 ml), 20% of Noggin (2 ml) in-house conditioned media, 2% of B27 (200 μl) (x50, Invitrogen, 12587-010), 25 μl of 1.25 mM n-Acetyl Cysteine (Sigma, A9165), 50 μl of 10 mM Nicotinamide (Sigma, 98-92-0), 5 μl of EGF (100 μg/ml) (Sigma, E4127), 1 μl of 0.5 μM of A83-01 (TGF-β inhibitor, Tocris, 2939), 1 μl of 3 μM SB202190 (p38 inhibitor, Sigma, S7067) and 20 μl (100 μg/ml) of Primocin (InvivoGen, ant-pm-1) (Kashfi et al., 2018).

Organoids medium was carefully changed every 2 days and once they started to grow and bud (usually 4-5 days), they were subjected to subsequent drug treatment. Drug solution was freshly prepared in organoid medium for organoid treatment and follow-up re-treatment for a period or 2 weeks. Organoid growth, morphology and live/dead staining were further processed upon treatment.

2.2.3.3 Organoid imaging and microscopy

The 3D organoid images were captured using Leica DMI3000 B Manual Inverted Microscope every 2 days throughout their whole three weeks in culture. Bright-field images of organoids were used to evaluate their growths and morphology changes upon drug treatment.

2.2.4 Tissue explant culture

2.2.4.1 Tissue preparation

All procedures were conducted following the Declaration of Helsinki and local ethics committee approval.

Tissue samples obtained from 14 CRC patients (**Table 2-2**) were placed in cold PBS immediately following surgical resection and were handled on ice prior to further processing.

2.2.4.2 *Ex vivo* explant culture and drug treatment

Explant cultures of tissues were set up in the following manner: On day 1, fresh tumour tissues were first washed with cold PBS and were immediately dissected into small fragments of 2-4 mm^3 using a disposable surgical scalpel (Swann Morton, SM0508). 4-6 explants were randomly grouped and were placed 1 explant/well onto a 48 well plate (Corning, 3548) (**Figure 2-2**). Explants were then maintained in freshly made complete organoid medium supplemented with Noggin, 12-15 hours or overnight at 37 °C with 5% CO_2 for their initial recovery (Karekla et al., 2017b). A 10 ml of complete medium was prepared by supplementing with advanced DMEM/F12 (Sigma Aldrich, 12634-010), 50% of Wnt- (5 ml), 20% of R-spondin- (2 ml), 20% of Noggin- (2 ml) in-

house conditioned media, 2% of B27 (200 µl) (x50, Invitrogen, 12587-010), 25 µl of 1.25 mM n-Acetyl Cysteine (Sigma, A9165), 50 µl of 10 mM Nicotinamide (Sigma, 98-92-0), 5 µl of EGF (100 µg/ml) (Sigma, E4127), 1 µl of 0.5 µM of A83-01 (TGF-β inhibitor, Tocris, 2939), 1 µl of 3 µM SB202190 (p38 inhibitor, Sigma, S7067) and 20 µl (100 µg/ml) of Primocin (InvivoGen, ant-pm-1). On day 2, explants were subjected to drug treatments. Drug solutions were freshly prepared at their IC_{50} and explants were treated for 24 h, based on previous study (Karekla et al., 2017b). On day 3, treated explants were fixed with 10% neutral buffered formaline (NBF, 100 ml of 37% formaldehyde, 4 g sodium phosphate, 6.4 g sodium phosphate dibasic and 900 ml distilled water) at room temperature overnight. After fixation, the explants were submerged into 70% (v/v) Ethanol and placed in cold room at 4ºC prior to further processing. Fixed tissues were then processed by Leica TP1020 semi-enclosed benchtop tissue processor via automatic passages from ethanol (70%, 90% and 100%) to methanol, xylene and, lastly, paraffin. Samples were embedded in paraffin blocks to be cut in 4 µm-thick sections with a microtome and placed onto the glass slides for hemotoxylin and eosin (H&E) staining or immunohistochemistry (IHC) analysis.

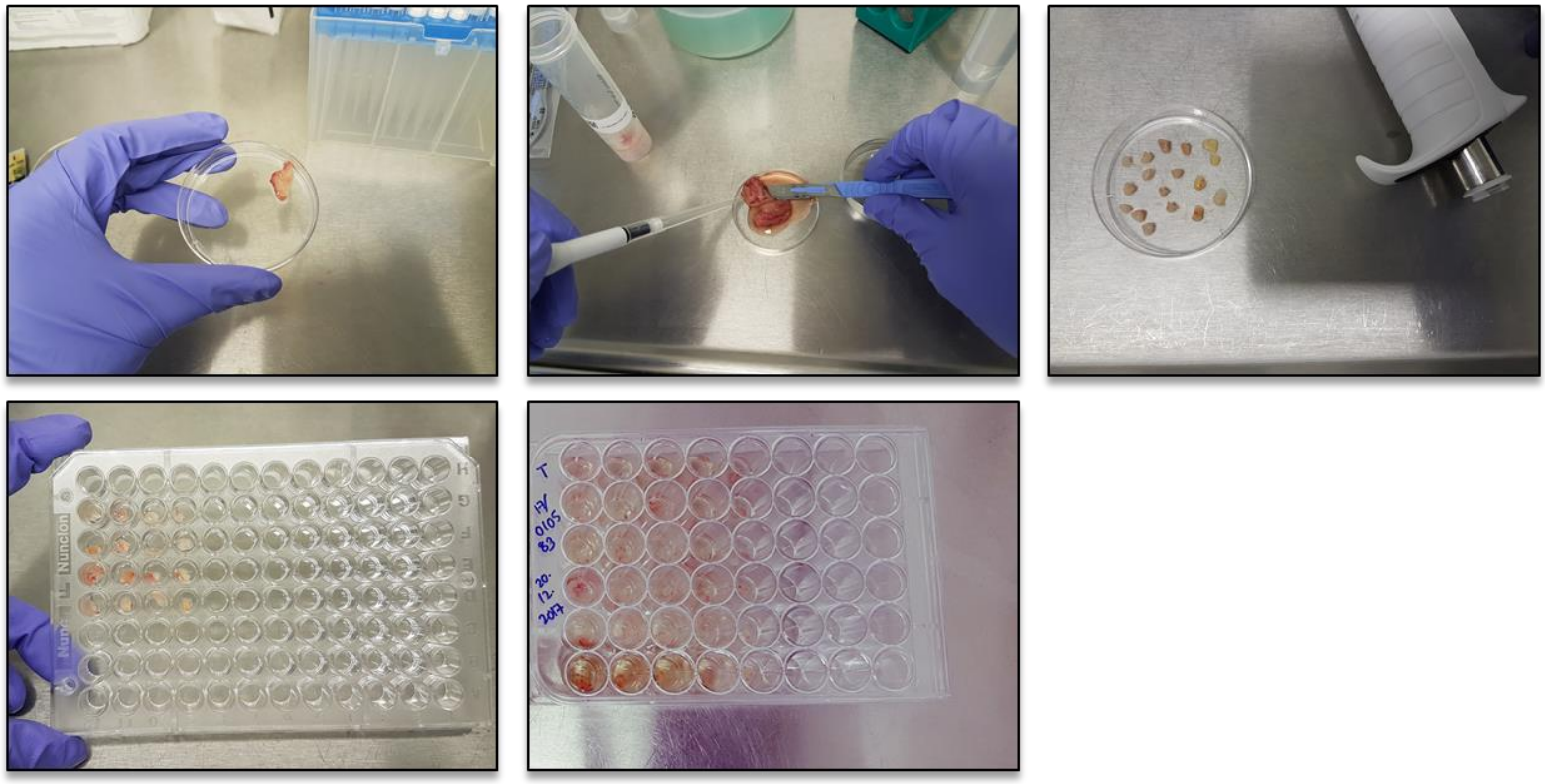


Figure 2-2: Preparation of CRC patient derived tissue explants. Tissue samples were cut into 2-4 mm^3 fragments and placed in 1 fragment/well in a 48 well plate. Explants were allowed to initially recover for 18 h in presence with complete organoid medium.

2.2.5 NCC (NIH Clinical Collection) library screening on colonospheres

2.2.5.1 NCC compounds preparation

Compounds were supplied in nine 96-well plates, each compound being dissolved in 10 µl of DMSO at a concentration of 10 mM (Cao et al., 2015b, Sachlos et al., 2012b). List of these compounds is outlined in **Appendix 1**. Compounds within the master plates were prepared by adding 90 µl of RPMI-1640 complete medium to the supplied plates at a final concentration of 1 mM.

2.2.5.2 Colonosphere preparation and drug treatment

Using the colonosphere formation efficiency in experimental cell lines, colonospheres were initially cultured in 6 well plates in order to obtain a final number of ~60 colonospheres/well in Corning® 96 well Black Polystyrene Microplate (Sigma, CLS3603-48EA), except the border wells (**Figure 2-3**). On day 14, fully grown well-defined colonospheres were carefully collected by centrifuging at 400 RCF for 5 mins and re-suspended in freshly prepared stem cell medium (Shaheen et al., 2016c). In order to obtain a final concentration of 20 µM, 3 µl of NCC compounds were transferred from the Master plates to new 96-well Working plates by careful pipetting. Following this, colonospheres were transferred to each well by ensuring equal distribution of ~60 colonospheres/150 µl of stem cell medium and were treated for 72 h (**Figure 2-3**). Control group was maintained with DMSO-stem cell medium replacement.

2.2.5.3 Stem cell dye CDy preparation and fluorescence intensity quantification

Fluorescent Stem Cell Dye CDy1 (Active Motif, 14001) was used to prepare CDy1 buffer according to manufacturer's instruction. 10 µl of CDy1 dye was diluted with 390 µl PBS to first prepare the CDy1 buffer.

Following 72 h drug treatment, 1.5 µl of CDy1 buffer was added to each well of 150 µl stem cell medium containing ~60 colonospheres (1:100

dilution) and incubated for 1.5 h in 5% CO_2, 37ºC. Colonospheres were then washed of any residual dye with 20 mM HEPES (4-(2-Hydroxyethyl)piperazine-1-ethanesulfonic acid, N-(2-Hydroxyethyl)piperazine-N′-(2-ethanesulfonic acid), Sigma Aldrich, H4034) by carefully centrifuging the 96-well plates at 400 RCF for 4 mins. Fluorescence intensity was then measured using BMG LABTECH CLARIOstar microplate reader with the optic setting for excitation and emission as 544-10 nm and 577-10 nm respectively (**Figure 2-3**) (Kang et al., 2011a). One of the unique advantages of this fluorescence reader was that it efficiently separates the excitation from the emission light, significantly reducing background noise. Moreover, using the integrated Time Resolved Fluorescence (TRF) based detection, longer period of time after excitation was carried out. This ultimately ensured high performance measurement with minimal background noise.

Average of the fluorescence intensities conferred by the solvent control (DMSO) treated colonospheres was set as 0 (n = 3). All compound treated colonosphere intensities were expressed as percentage of the fluorescence intensities conferred by the control-treated colonospheres in their respective plates. GraphPad Prism 7 software was used generate the graphs for each plate reading.

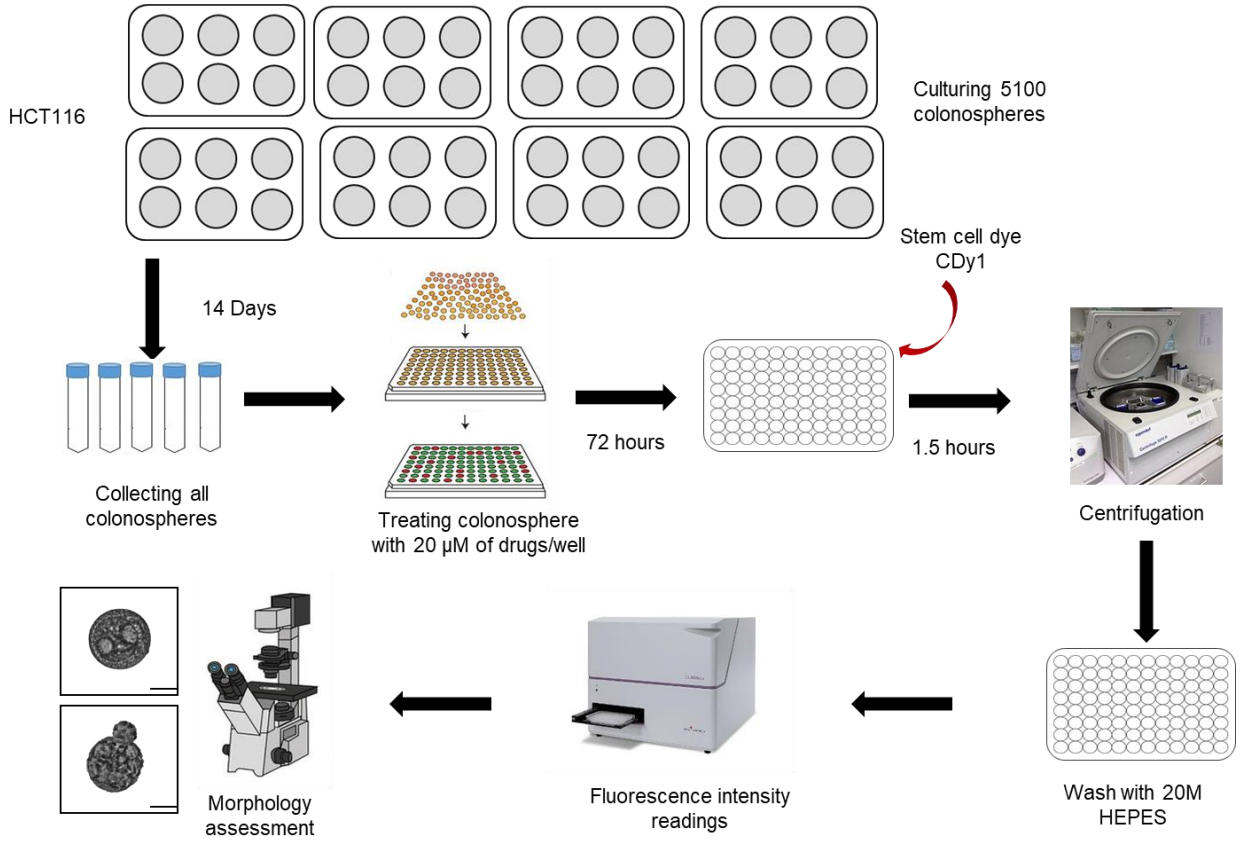


Figure 2-3: Primary screening of NCC compounds screening on HCT116 cell derived colonospheres. Treated colonospheres were subjected to CDy1 staining for 1.5 h. Fluorescence intensity of live colonospheres was measured using microplate reader.

2.2.6 Cytotoxicity assay

The sulforhodamine B (SRB) colorimetric assay was used to determine drug cytotoxicity. It is one of the most widely used methods for *in vitro* cytotoxicity screening. SRB is an anionic dye that binds electrostatically to cellular proteins. This assay relies on the ability of SRB to bind to the protein component of cells that have been fixed by trichloroacetic acid (TCA) (Vichai and Kirtikara, 2006, Lorenzi et al., 2016a).

At first, cells were seeded in 96 well plate (ThermoFisher Scientific, 167008) (3000 cells/well) except the border wells and were allowed to grow for 48 h prior to drug treatment with Vorinostat (Tocris, 4652), AM404 (Tocris, 1116/10), rifabutin (Sigma Aldrich, R3530-5MG), idarubicin (Sigma Aldrich, 000020 I1656-10MG), epirubicin (Tocris, 3260/10) and daunorubicin (Sigma Aldrich, 000010 30450-5MG). The medium was then replaced with a series of increasing concentrations of drugs, including, Vorinostat (0.1 to 300 μM), AM404 (1 to 100 μM), rifabutin (1 to 100 μM), idarubicin (1 to 80 nM), epirubicin (0.01 to 20 μM) and daunorubicin (1 to 20 μM) for 72 h (Lorenzi et al., 2016a). Treated cells were fixed by adding 50 μl of cold trichloroacetic acid (TCA, Sigma Aldrich, T4885) to each well without removing the medium and were incubated with a final concentration of 15% (w/v) for 60 mins at 4°C. The solution was discarded after an hour and plates were washed with tap water and air dried in room temperature. Fixed cells were then stained with 0.4% SRB (Sigma Aldrich, 230162) in 1% acetic acid (Sigma Aldrich, 320099) for 20 mins at RT. The plates were washed 5 times with 1% acetic acid and air dried. Subsequently, 200 μl of 10 mM Trizma base (Sigma Aldrich, T3253) were added to dissolve the SRB. This step is important to solubilise the SRB and photometrically measure the protein content at an optical density (OD) of 492 nm of wavelength by a microplate reader (Bio-Rad). The OD values correlate with the total protein content and therefore the number of cells. This assay thereby detects only the viable cells present in each well. Data were then

analysed by using Microsoft Office Excel 2007 and GraphPad Prism-7 software. The experiments were repeated in triplicate and on separate occasions.

2.2.7 Colony formation assay

Colony formation assay examines the ability of single cells to grow into colonies consisting of 50 or more cells. In addition, it also evaluates the potential of cells to resist treatments and grow into colonies (Kabakov and Gabai, 2018).

For all experimental cell lines, 200 cells were seeded in each well of 6-well plates (in triplicate) and were allowed to grow into colonies for 6-7 days in presence of complete RPMI-1640 medium. Drugs were added at their IC_{50} on the corresponding cell lines on day 8 for the treatment group, while fresh medium was replaced in the control group. Both control and treatment groups were re-treated or replaced the medium after further 72 h. On day 14, colonies were fixed with 4% paraformaldehyde (Alfa Aesar, 43368) for 20 minutes at room temperature and stained with 0.1% crystal violet (Sigma Aldrich, 32675). Air dried plates were then used for taking images and manually counting the size and number of colonies that are visible with naked eyes. Number and size of colonies were then measured using ImageJ software and colony formation efficiency was measured using Microsoft Excel 2007 software. Colony formation efficiency was determined using the following formula:

*Colony formation efficiency = (Number of colonies obtained) / (Number of cells seeded) * 100%*

2.2.8 Growth curve analysis

For this assay, cells were cultured for a period of 8 days. On day 0, 30000 cells were seeded per well in 24-well plates. Drugs were added to their IC_{50} on the next day, while control group was maintained by changing with fresh medium.

Cells were counted in triplicate for both control and drug-treated group on each day, at the same time. Results were then plotted on a log-linear scale. Population-doubling time was determined using the following formula:

$$\text{Doubling time} = \frac{duration \times \log(2)}{\log(final\ concentration) - \log(initial\ concentration)}$$

2.2.9 Propidium iodide (PI) staining

Propidium iodide (PI) is a fluorescent molecule that intercalates between DNA base pairs and, thus, can be used to measure the cell DNA content. This technique was used to assess organoid viability with aid of organoid live/dead staining (Kashfi et al., 2018).

At first, Matrigel embedding the organoids was mechanically disrupted with a pipette tip and was collected carefully. Cold PBS was used to wash the organoid containing wells in order to minimize losing of organoids. This step was followed by with three times centrifugation (at 300 RCF, 3 mins) and three chilled-PBS washes. The objective was to recover all the organoids contained within the Matrigel. The supernatant containing organoids were then fixed with 4% PFA for 30 mins at 4ºC and permeabilized with 0.5% TRITON X 100 solution (Sigma Aldrich, 93443) for 30 mins at room temperature. Following 2 washes with 0.2% TRITON X, organoids were co-stained with 1 µg/ml Hoechst 33342 (Sigma Aldrich, 62249) and 25 µg/ml propidium iodide (PI, Sigma Aldrich, 4864) with 1 µg/ml RNase A (Sigma Aldrich, 6513) for 30 mins in dark.

Then microscopy was performed using the Leica DMI3000 B fluorescent microscope at x10 or x40 magnification. Following 4 washes with 0.2% TRITON X and centrifugation at 300 RCF for 3 mins, organoids were carefully mounted on coverslips for visualization. Cell death in organoids were then assessed by live/dead staining and subsequent fluorescence microscopy the next day.

2.2.10 Protein expression assays

2.2.10.1 Immunofluorescence (IF) staining

The main objective of immunofluorescent (IF) analysis was to visualize the antigen–antibody complex, where antibodies are tagged with a fluorescent dye that is detected under ultraviolet (UV) microscopy. IF is used to visualise endogenous or overexpressed proteins and to compare their relative expression levels within cells. According to the IF protocol, a primary antibody specific to the protein of interest is applied, followed by immunostaining with a fluorescent dye–labelled secondary antibody directed against the immunoglobulins of the host species in which the primary antibody was raised. In this study, this technique was used to evaluate the stemness and differentiation marker expression in colonospheres, in response to the drug treatments (Shaheen et al., 2016c).

With regard to the colonospheres, to enhance the spheres adhesion to the glass coverslips, sterilised coverslips were coated with 0.01% poly-L-lysine solution (Sigma Aldrich, P4707) for 20 mins at room temperature. Coverslips were then washed with PBS and air dried. The treated colonospheres were transferred on the coverslips and were fixed with 4% Paraformaldehyde the following day for 20 mins. Following fixation, colonospheres were gently washed five times with PBS. With the aim to allow antibodies to pass across the cellular membranes, 0.5% TRITON X 100 solution (Sigma Aldrich, 93443) were applied for 5 mins

and washed again with PBS for 5 times. The permeabilised colonospheres were then blocked with 1% bovine serum albumin (BSA, Sigma-Aldrich, 4503) in PBS for 30 min at room temperature. Primary antibodies CD44 (Millipore, MAB2137) and MUC2 (Santa Cruz, SC-15,334) were diluted as 1:100 and were used to co-stain the colonospheres for 1 hr at room temperature. Negative control was probed with 1% BSA as blocking solution only. Fluorescent conjured secondary antibody for Rat and Rabbit were used at 1:200 dilution 1 hr in dark. Following 4 PBS washes, coverslips were gently removed from the 6-well plate and slides were mounted with Vectashield mounting medium 4',6-diamidino-2-phenylindole (DAPI, Vector Laboratories, H-1200). Slides were sealed with nail varnish and stored at 4°C overnight in dark. The day after, images were taken with Leica DMI3000 B fluorescence microscope (Leica Microsystems). ImageJ was used to quantify the fluorescence level and were compared using GraphPad Prism 7 software.

2.2.10.2 Phalloidin staining

Phalloidin is a dye commonly used to examine cell morphology because it has high affinity for actin filaments in the cell, binds F-actin and displays the shape of a cell.

For this experiment, coverslips were soaked in ethanol for 30 minutes and washed with PBS. They were then coated with poly-l-lysine and let to dry. Each coverslip was then placed within a well of six-well plates. 200 cells/well were seeded on top of the coverslip for all the experimental cell lines and were allowed to grow into colonies for 6-7 days following the protocol mentioned in colony formation assay. Drugs were added on day 8 at their respective IC_{50}. Photos of the colonies were taken on day 8 before the treatment, and then day 11 and day 14 for both control and treated groups. Next, on day 14 the colonies were fixed with 800 µl of 4% PFA for 20 minutes at room temperature, followed by 2

washes with PBS. Colonies were then permeabilized with 0.1% TRITON X-100 permeabilising solution for 30 minutes at room temperatureM. The following day, images were taken with Leica DMI3000 B fluorescence microscope.

2.2.11 Histologic techniques and quantification (IHC)

Haematoxylin and eosin (H&E) stain is a fundamental technique used to examine the structure of normal and pathological tissues. Haematoxylin is a basic compound that stains in blue-purple acidic (basophilic) molecules, such as the nucleic acids accumulated into the nucleus, whereas, eosin is acidic in nature and stains in pink to the cytoplasm enriched for basic (eosinophilic) molecules as proteins. In addition, immunohistochemistry technique allows the study of the expression pattern of specific proteins in tissues through the formation and detection of antigen (target protein)-antibody complexes. Immunohistochemical analysis was carried out on the drug treated and control tissue explants with and without (antibody control) Ki-67 (Dako), active caspase-3, CDX2, CD44 (Cell Signaling), and MUC2 (Santa Cruz) antibodies in collaboration with the Histopathology unit, Queens Medical Centre, University of Nottingham. Slides were scanned at 20x magnification. Images were analysed using ImageJ and NanoZoomer Digital Pathology software.

In order to quantify the staining, scanned images were analysed by calculating a percentage of stained cells exhibiting the protein expression within the tumour area. Moreover, the labelling index was determined using H-scoring system to calculate the sum and intensity of positively stained tumour cells. The H-score is ranged from 0 to 300, using the formula: (1 × % weakly stained nuclei) + (2 × % moderately stained nuclei) + (3 × % strongly stained nuclei). Scoring was independently verified by a pathologist from Queens Medical Centre.

2.2.12 RNA isolation and analysis

2.2.12.1 RNA isolation

Total RNA was extracted from colonospheres by using Qiagen RNeasy Mini Kit according to the manufacturer's instructions. Colonospheres were collected from all drug treated and vehicle-treated groups and centrifuged at 300 RCF for 3 mins. Next, Buffer RLT was added to the palette, mixed well and passed through a fine needle syringe (BD Microlance, 304432) in an Eppendorf tube. Following this step, 70% ethanol was added and then transferred through the column to a collection tube. All tubes were then centrifuged at ≥ 8000 RCF for 30 sec and the flow through was discarded. Next step was to add buffer RW1 into the columns and repeat the centrifugation step. Finally, RPE buffer was added to the column followed by 30 sec of ≥ 8000 RCF centrifugation. This step with RPE buffer was repeated again, the column was then placed in a new Eppendorf tube. In order to obtain the final RNA yield, 30 µl of RNAse free water was added and centrifuged for 1 min at ≥8000 RCF. RNA concentration was measured by Nanodrop and samples were stored at -80°C.

2.2.12.2 Reverse transcription (RT)

For cDNA synthesis, PrimeScript™ RT reagent Kit (Takara-Clontech Laboratories, RR037A) following the manufacturer's instructions. 1 µg of total RNA was supplemented to a master mix consisting of 2 µl 5x PrimeScript buffer, 0.5 µl PrimeScript RT enzyme mix, 0.5 µl oligo dT primers (50 µM), 0.5 µl random-six-mers (100 µM), and RNase free water a total volume of 10 µL per sample. The Veriti Thermal Cycler (Applied Biosystems) provided the precise temperature control and rapid temperature to acquire cDNA. cDNA was then synthesized by incubating this reaction mixture at 37°C for 15 mins and then at 85°C for 5 sec to inactivate the reverse transcriptase. The resulting cDNA samples were directly used for qPCR. cDNA samples were stored at -20°C.

2.2.12.3 Quantitative real-time PCR (qPCR)

Quantitative real-time PCR was performed to measure the gene expression changes at mRNA level, in response to the drug treatments (Lorenzi et al., 2016a). Primers were designed to target two consecutive exons within the gene of interest and to amplify a region of 100-200 bp of size.

Both forward and reverse primers (Sigma Aldrich) were resuspended in DNase/RNase free water (Roche, 04707516001) (1:10 dilution) and stored at -20°C until use. Master mix was composed of 2 µl of cDNA 10x diluted, 10 µl of LightCycler 480 SYBR Green I Master (Roche, 04707516001), 2 µl of primers and 6 µl of DNase/RNase free water for a final volume of 20 µl. SYBR Green I is a DNA double-strand-specific dye and was added to the master mix as the last step. Samples were handled on ice and were loaded in triplicate into LightCycler 480 Multiwell 96 well plate, (Roche, 4729892001). Next, they were centrifuged at 400 RCF for 1 min, emitted fluorescence was evaluated by LightCycler 480 II instrument (Roche) according to manufacturer's instruction. Expression of β-actin or glyceraldehyde 3-phosphate dehydrogenase (GAPDH) housekeeping genes was measured for data normalization. The primers used in this study are listed in **Table 2-3**. Threshold cycle (Ct) values were calculated by lightCycler 480 II software (Roche) and data analysis was carried out by using GraphPad Prism 7 software.

2.2.12.4 Transcriptomic microarray assay

The quality and integrity of the total RNA isolated from colonospheres were estimated using an Agilent RNA 6000 Nano Kit, 2100 Bioanalyzer, and Agilent 2100 Expert Software following the manufacturer's instructions (Agilent Technologies, Germany). All RNA samples showed RNA integrity number (RIN) ≥9.2, where >7 is the accepted value and were therefore used for subsequent transcriptomic assessment.

Whole-genome transcriptome analysis was conducted by hybridizing three biological samples of total RNA for each group to the Clariom™ S arrays (Affymetrix, 902926). All steps of sense cDNA synthesis, fragmentation and hybridization were performed according to the manufacturer's protocol (GeneChip® 3000 System, Affymetrix) at the Nottingham Arabidopsis Stock Centre (NASC), School of Biosciences, and University of Nottingham. cDNA was prepared from 200 ng of RNA and followed by *in vitro* transcription to produce cRNA. End-labelled and hybridization was carried out for 16 h at 45ºC to GeneChip™ Human Gene 2.1 ST Arrays (Thermo Fisher Scientific/ Affymetrix).

Transcriptomic data were then processed by a standardized sequence of analyses (gene ontology (GO) enrichment) using Ingenuity Pathway Analysis. Subsequent analyses were performed using Partek Genomics Suite V6.6 (PGS) software. The raw CEL files were normalized using Robust Multi-array Average (RMA) background correction by the Partek with quantile normalization, log base 2 transformation and mean probe-set summarization with adjustment for GC content. Quality Control (QC) metrics were checked by examining surface defects, hybridization, labelling, and a ratio of the 3′ probe set to the 5′ probe set (3′/5′ ratio) to provide the quality of the microarray data. Differentially expressed genes were considered significant if p-value with FDR ≤ 0.05 and fold-change of >2 or < -2.

2.2.13 Statistical analysis

GraphPad Prism 7 and Microsoft Office Excel were used to generate graphs and carry out statistical analysis. Fiji (Image-J) software was used to analyse images. Gene expression data were analysed using Partek Genomics Suite 7.0 (Partek Incorporated).

Statistical analyses were obtained by Student's *t*-test. P value < 0.05 (*) was considered statistically significant. One-way ANOVA was used for

the microarray analysis by Partek software. All experiments were performed in triplicate and repeated at least 2-3 times. Results are shown as mean ± standard deviation (SD), unless otherwise stated.

CHAPTER 3

A CDy1-Based 3D-Colonsphere Screening System for the Rapid Evaluation of Drugs Inducing-Differentiation in Cancer Stem-like Cells

3.1 Introduction

In recent years, advances in therapeutic targeting and improved diagnosis have indeed increased the overall survival in colorectal cancer patients, but in terms of cancer-related death, CRC still ranks the second (Bray et al., 2018, M et al., 2017). For patients with CRC, chemotherapy remains the most common treatment but often followed by tumour regrowth due to acquired chemotherapy-resistance. Emerging evidence supports the role of cancer stem-like cells (CSCs) endorsing its enhanced self-renewal and limited differentiation capacity in therapy resistance and tumour recurrence (Lytle et al., 2018, Batlle and Clevers, 2017). Therefore, there is an ever-growing need for novel compounds to target CSCs and developing treatment strategies to prevent recurrence the regrowth of further neoplastic cell populations.

Currently, in drug discovery, the compound screening starts with the 2D cell culture-based assays and only about 10% of the compounds progress successfully through clinical development (Edmondson et al., 2014). Many of these drugs fail during clinical trials, especially in their phase III, which is the most expensive phase in drug development. Such failure is principally due to the lack of predictive patient outcome by 2D models in response to the candidate drugs. In traditional 2D monolayer culture, unlike *in vivo* condition, predominantly the proliferating cells adhere and grow on a flat surface, allowing a homogenous amount of nutrients and growth factors. In contrast, 3D cell cultures grow cells into cell aggregates or spheroids within a scaffold or in a scaffold-free manner within the suspension. Various stages of cells comprise these 3D spheroids or aggregates, including proliferating, quiescent, apoptotic, hypoxic, and necrotic cells. Hence, they are more likely to provide tumour heterogeneity and recapitulate *in vivo* morphology and cellular processes including proliferation, differentiation, metabolism, gene expression and overall cell function (Edmondson et al., 2014).

The primary focus of this study was to optimize and exploit colonospheres culture for successful targeting of cancer stem-like cells via large drug screening. Therefore, the aim of this chapter was to;
I) validate and optimise the parameters and a 3D model for screening of the potential differentiation-inducing agents, and
II) apply the optimised conditions for an NCC (NIH Clinical Collection) compound library screening.

3.2 Result

3.2.1 Loss of FBXW7 induces the *in vitro* colonosphere formation and CDy1 intensity

FBXW7 (F-box and WD repeat domain-containing 7) protein belongs to the F-box protein family and functions as a receptor subunit for SCF (Skp1/Cullin/F-box protein) E3 ubiquitin ligases (Welcker and Clurman, 2008). Most of the FBXW7 substrates are proto-oncogenes and therefore loss of FBXW7 has broad implication in various cancers, with 15-20% of them being CRC (Welcker and Clurman, 2008). Our lab and others have previously reported tumour suppressor FBXW7 as one of the most frequently mutated genes in CRC, and have associated the loss of FBXW7 with chromosomal instability, cellular proliferation, EMT induction and overall tumorigenesis process (Sancho et al., 2010, Welcker and Clurman, 2008, Li et al., 2019b, Babaei-Jadidi et al., 2011a). More recent data from our lab also suggests its role in resistance to chemotherapy, following accumulation of ZEB2 (Li et al., 2019b). Therefore, in order to understand the system, and to employ a methodology to screen a library of small molecules-based drugs targeting differentiation/stemness properties, 3D colonospheres derived from CRC cell lines were used, with the wild type and deleted FBXW7 alleles and incorporated them to optimise and validate the use of CDy1.

Colonosphere were cultured by allowing HCT116$^{FBXW7+/+}$, HCT116$^{FBXW7-/-}$, DLD-1$^{FBXW7+/+}$ and DLD-1$^{FBXW7(-/-)}$ cells to grow into 3D cluster of cells

using a suspension stem cell medium. On day 14, fully grown colonospheres were manually counted, and their formation efficiency was determined. Loss of FBXW7 showed induction of 3D colonosphere generation in both HCT116 and DLD-1 cells as observed by the induction of number and size, stemness marker and CDy1 intensity.

The colonosphere formation efficiency assay showed an increase in colonosphere formation in *FBXW7* deleted cells compared to their parental HCT116 (2.5% vs 5.6%) and DLD-1 cells (4% vs 15%) (**Figure 3-1**) (Li et al., 2019b).

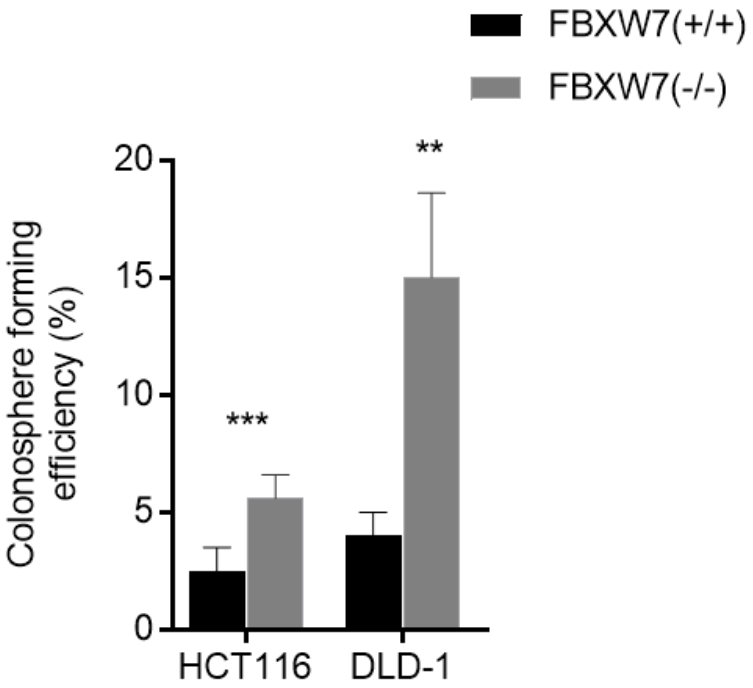


Figure 3-1: FBXW7 deletion confers to increased efficiency in colonosphere formation in human colon cancer HCT116 and DLD-1 cells. Colonospheres that are bigger than 50 μm were counted for the analysis. FBXW7(-/-) cells formed a greater number of colonospheres in comparison to FBXW7(+/+) cells. **, $P < 0.01$; ***, $P < 0.001$.

To evaluate potential changes on stemness and differentiation level, an immunofluorescence assay was performed on colonospheres derived

from both HCT116$^{FBXW7+/+}$ and HCT116$^{FBXW7-/-}$ cells. Stemness marker CD44 and differentiation marker MUC2 were used to evaluate the expression of these two markers in the cultured colonospheres. Our data shows upregulation of CD44 and relatively lower MUC2 expression in colonospheres derived from HCT116$^{FBXW7(-/-)}$ cells (**Figures 3-2 and 3-3**). Accumulating evidence indicates that CD44, especially its CD44v isoforms, are potent CSC markers and are very crucial for regulating CSC characteristics, including self-renewal, tumour initiation, metastasis, and resistance to chemotherapy (Yang and Rycaj, 2015b). MUC2, on the other hand, is a differentiation marker for epithelial cancer stem cells. This explains the typical cancer stem cell characteristics with more self-renewal and less differentiation ability associated with *FBXW7* deletion. In line with previous studies, this data suggests that *FBXW7* suppresses stemness activity and therefore plays a crucial role in the acquisition of malignant features in CRC (Wang et al., 2012). This explains the typical cancer stem cell characteristics with more self-renewal and less differentiation ability associated with *FBXW7* deletion. In line with previous studies, this data suggests that *FBXW7* suppresses stemness activity and therefore plays a crucial role in the acquisition of malignant features in CRC (Wang et al., 2012).

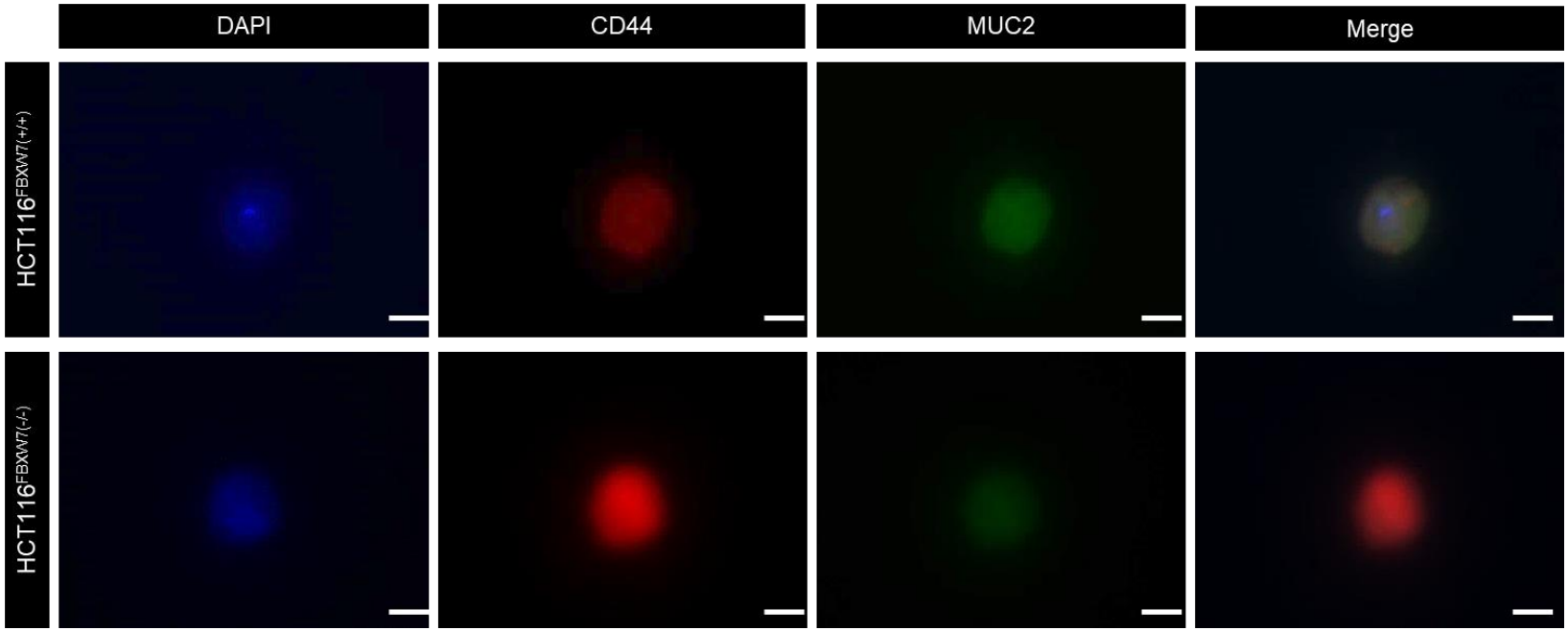


Figure 3-2: CD44/MUC2 expression in HCT116$^{FBXW7+/+}$ and HCT116$^{FBXW7-/-}$ derived colonospheres. *FBXW7* deletion confers to less differentiation and more stemness activity in colonospheres obtained from HCT116$^{FBXW7-/-}$ cells. Scale bars: 25 µm.

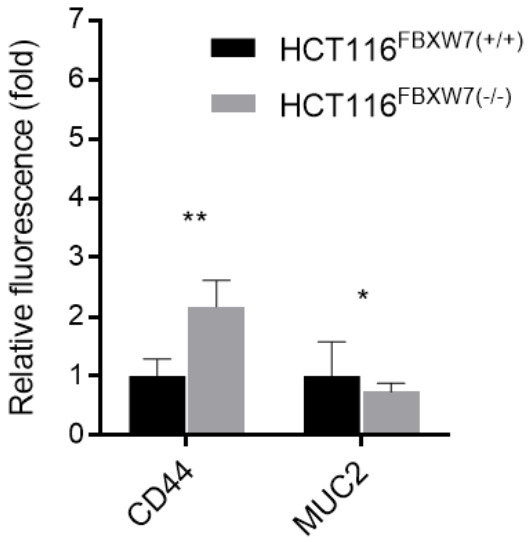
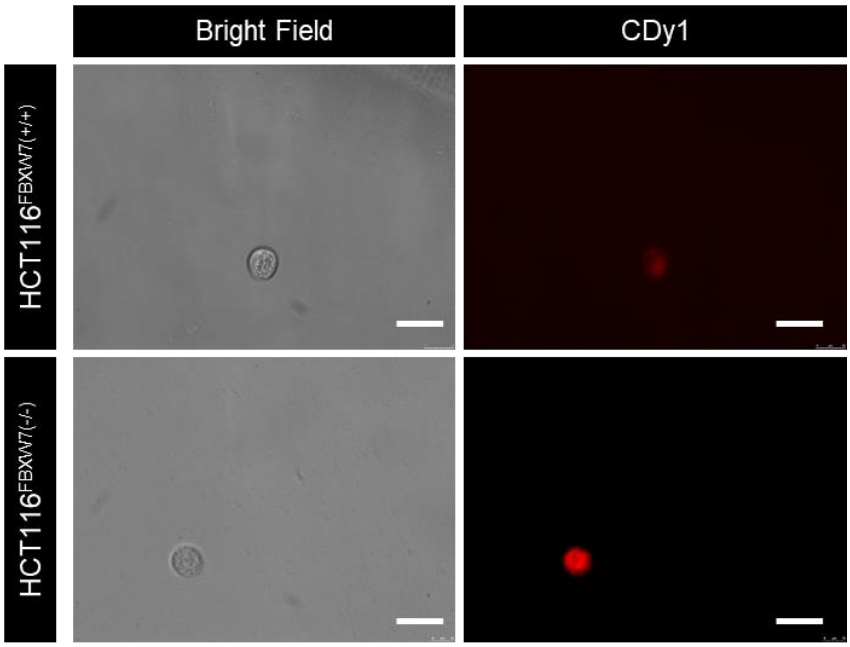


Figure 3-3: Increased CD44 and decreased MUC2 expression in HCT116$^{FBXW7-/-}$ derived colonospheres. *FBXW7* deletion confers to less differentiation and more stemness activity in colonospheres obtained from HCT116$^{FBXW7-/-}$ cells. (n = 10). *, P < 0.05; **, P < 0.01.

Next, a fluorescent Rosamine dye CDy1 was incorporated in such colonospheres derived from HCT116$^{FBXW7(-/-)}$ and subsequently measured their fluorescence intensity (**Figure 3-4**). As outlined above, CDy1 has previously been used to characterise the human embryonic cells (ESs), induced pluripotent stem cells (iPSs) and CSCs (Hawley et al., 2013, Kang et al., 2011b, Im et al., 2010). In this study, CDy1 was used to label colonospheres as an indication for induced differentiation. The main objective was to find out whether this dye can be applied to identify induced differentiation characteristics using drug library. Our results showed that the CDy1 fluorescence intensity is more than 2-fold greater in HCT116$^{FBXW7(-/-)}$ cells (**Figure 3-4**). This further confirms CDy1's reliable use to test differentiated-mediated changes in colonospheres to lose their CRC-SCs activity by a drug.



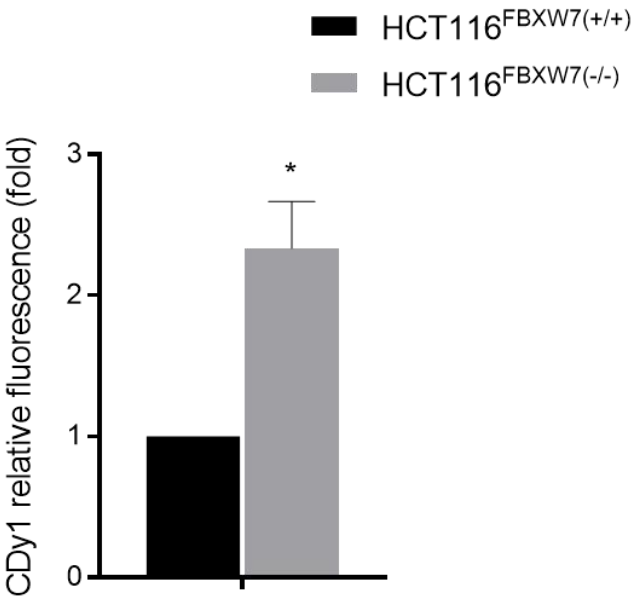


Figure 3-4: CDy1 confers greater intensity in HCT116$^{FBXW7-/-}$ cell derived colonospheres. *FBXW7* deletion indicates attainment of more stemness activity as observed by CDy1 staining. (n = 15). Scale bars: 25 µm. $P < 0.05$.

3.2.2 Vorinostat induced differentiation in 3D colonosphere

Vorinostat (Suberoylanilide hydroxamic acid, SAHA) is a potent histone deacetylase (HDAC) inhibitor that has been reported to induce differentiation and has undergone Phase I and II clinical trials (Richon, 2006, Finnin et al., 1999, Richon et al., 1998). Mechanistically, HDAC inhibitors change the level of pro and anti-apoptotic molecules, induce cell cycle arrest, apoptosis and strongly induce differentiation (Mottamal et al., 2015, Emmink et al., 2011a). Vorinostat has a broad of HDAC activity and acts by inhibiting both classes I and class II enzymes while having no effect on class III. It typically binds to the zinc atom of the catalytic site of the HDAC enzyme and accumulates acetylated proteins, including histones, which in turn manifests in multiple cellular effects (Bubna, 2015). It has also been reported that vorinostat selectively blocks cancer cell proliferation both *in vitro* and *in vivo* with little or no toxicity to normal cells (Richon, 2006).

In this study, Vorinostat treatment was used to induce differentiation in colonospheres prior to employing it within the CDy1 based screening system. First, a cytotoxicity assay was carried out on both HCT116$^{FBXW7+/+}$ and HCT116$^{FBXW7-/-}$ cells were treated with increasing concentration of SAHA (from 0.1 to 300 μM) for 72 hours. The SRB assays were performed as outlined in **Chapter 2** (**2.2.6**), and IC_{50} values were then calculated. *FBXW7*-deleted cells showed to confer resistance to Vorinostat by 2.5-fold comparing to the wild-type HCT116 cells (0.7 μM vs 1.8 μM) (**Figure 3-5**). As the main objective of this study was to evaluate Vorinostat induced differentiation and to incorporate it in the compound library screening, we then focused on HCT116 parenteral cells and evaluated the level of differentiation induced in it.

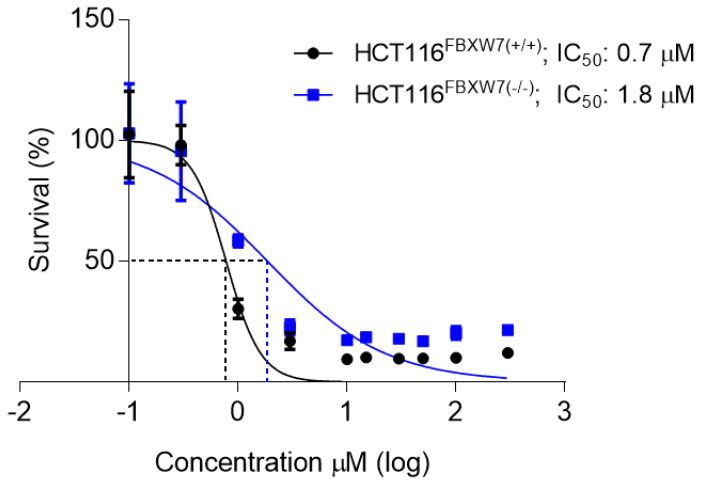


Figure 3-5: FBXW7 deletion confers resistance to SAHA in HCT116$^{FBXW7-/-}$ cells. IC_{50} of FBXW7-deleted cells were significantly higher than the wild type cell line. Nonlinear regression was used to plot the data. (n = 6; P < 0.05).

Next, colonosphere formation assay was carried out in Vorinostat treated colonospheres. Colonospheres were cultured as previously mentioned in **Section 3.2.1.**, prior to their treatment with Vorinostat for 72 h. After 72 hours, colonospheres were manually counted for evaluating colonosphere viability. No changes were observed in colonosphere numbers; however, images were captured to compare any changes in colonosphere morphology after drug treatment compared to their untreated status (**Figure 3-6**). Vorinostat significantly altered the morphology in the treated colonospheres (15% vs 30%) without affecting their viability (**Figures 3-6, and 3-7**). This result further shows 3D models being more resistance than 2D models and suggests that, Vorinostat might affect the morphology in such a way which can potentially induce differentiation. In consistence with the previous reports, such changes can be explained by Vorinostat induced differentiation (Richon, 2006, Finnin et al., 1999, Richon et al., 1998).

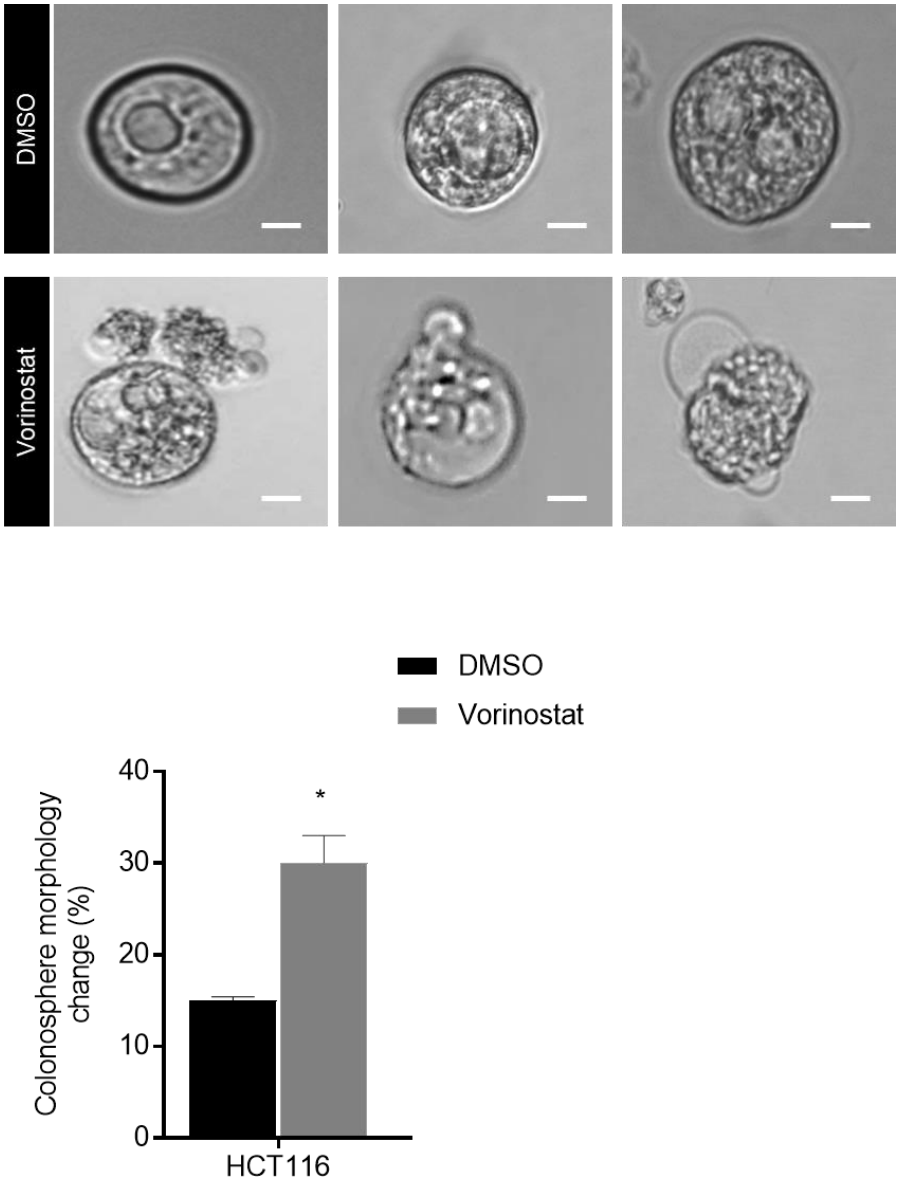


Figure 3-6: Vorinostat treatment showing morphological alteration in colonosphere. Images were taken after Vorinostat treatment. Untreated colonospheres maintained their distinct structural network of cells whereas the treated colonospheres showed more budding-like structures and loss of their structural integrity. Scale bar: 25 μm. Error bars represent mean ± S.D. n = 15.

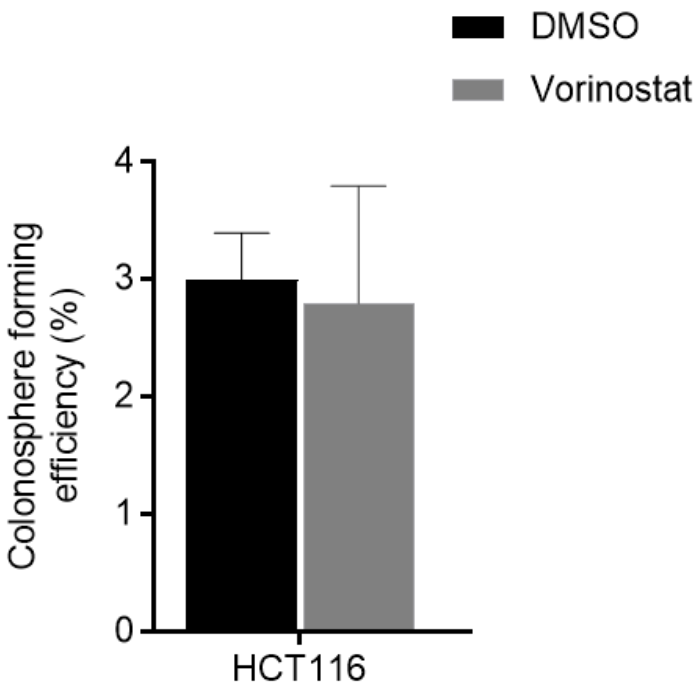


Figure 3-7: Vorinostat treatment did not cause any significant change in colonosphere formation assay. Colonospheres were derived from HCT116 and were treated with Vorinostat for 72 h. No significant changes were observed for colonosphere formation in the treated group. Error bars represent mean ± S.D. (n = 30).

However, in order to evaluate the level of induced differentiation, CDy1 staining was further carried out on Vorinostat treated and DMSO-treated control colonospheres. CDy1 dye stained only the stem-like cells and their images were used to compare the level of differentiation as exerted by control and Vorinostat treated colonospheres (**Figure 3-8**). Of note, as evident in **Figure 3-8**, CDy1 itself did not confer any change in colonosphere morphology.

In summary, this study provided valuable data and materials to explore using of colonospheres (with and without FBXW7 mutation, and, with and without Vorinostat treatment) as an effective tool to evaluate stemness and/or differentiation in *in vitro* colonospheres. Incorporating

this provision with CDy1 dye as a live indicator of stemness vs differentiation properties, we, therefore carried out a screening of a small molecules library to identify the anti-cancer compound(s) based on their capacity of inducing CRC-SC differentiation.

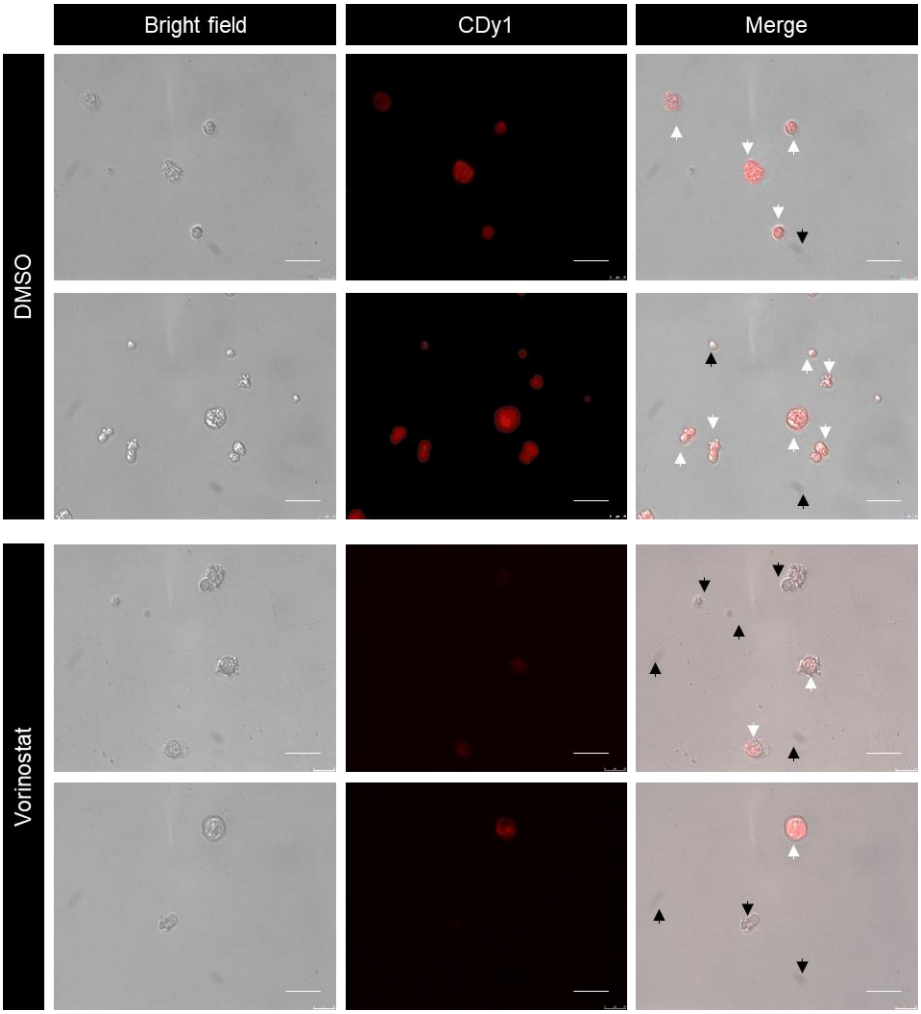


Figure 3-8: Vorinostat induces differentiation in CRC-SC. CDy1 dye marks the stem-like activity of formed colonospheres. Colonospheres were treated with vehicle control and Vorinostat for 72 hours. Black arrows show the colonospheres that were not stained with CDy1, indicating loss of their stem-like activity. Whereas, white arrows show the colonospheres with stem-like characteristics. Vorinostat treated colonospheres shows more unstained

colonospheres indicating them to reduce/lose the stem-like activity, possibly by the drug-inducing differentiation.

3.2.3 CDy1-based drug screening of an NCC compounds library

Using initial pre-screening study with CDy1 with a previously reported differentiation- inducing drug Vorinostat as a screening platform, we extended our tests to compound libraries using colonospheres derived from three colon cancer cell lines HCT116, DLD-1 and SW480. One of the particular advantages of this screening was that it has been carried out on live colonospheres without any fixation step involved. Moreover, this screening was carried out on compounds that have previously been FDA approved and therefore they possess established side effects and safety profiles in human.

We have used a library of 707 FDA approved NCC compounds from the US National Institute of Health (NIH) supplied in 9 of the 96-well plates that are prepared in DMSO at 10 mM with an aliquot of 10 µL of each compound (Cao et al., 2015b, Sachlos et al., 2012b). List of these compounds is outlined **Appendix 1**. Prior to the screening, 90 µl of complete RPMI medium was first transferred to each well of the 96-well plates to yield a final concentration of 1 mM as a master solution. In addition, stem cell dye CDy1 working buffer was also prepared with PBS according to manufacturer instruction and was used as a 1:100 dilution in the screening. The primary objective of this screening was to identify small molecules that induce differentiation and overcome neoplastic self-renewal in CRC-SCs.

3.2.3.1. Primary screening of the NCC compound library

At first, the colonospheres obtained from HCT116 cell line were used for the primary screening (Hwang et al., 2014). Well defined round shaped cultured colonospheres derived from HCT116 cells were collected carefully with mild agitation and ensured of uniform transfer (~60 colonospheres/well) in 96 well plates. Colonospheres were then treated with 707 compounds (at final concentration of 20 µM) for 72 h before selectively stain the live stem cells for 1.5 h, as a magnitude of drug-

induced stemness and/or differentiation level represented by high and low CDy1 fluorescence intensity respectively. HCT116 cells were primarily chosen for the initial screening based on their highly aggressive, resistant and non-differentiating nature (Yeung et al., 2010). The concentration of compounds was selected based on previous studies being carried out at 10 μM in monolayer cells, in line with our results and previously established data showing higher resistance with 3D colonospheres than 2D cells (**Figure 3-5**) (Sachlos et al., 2012b, Li et al., 2019b). Fluorescence intensity was measured using BMG LABTECH CLARIOstar microplate reader with the optic setting for excitation and emission as 544-10 and 577-10 nm respectively. Average of the fluorescence intensities conferred by the solvent control (DMSO) treated colonospheres was set as 0 (n = 3). All compound treated colonosphere intensities were expressed as percentage (%) of the fluorescence intensities conferred by the control (DMSO) treated colonospheres in their respective plates (**Figures 3-9 - 3-13**). To identify the compounds with the highest potential of inducing stemness/differentiation in CRC, a cut-off was set according to the BMG LABTECH CLARIOstar integrated software settings for about -30% to 40% of reduced or induced fluorescence intensities respectively (**Figures 3-9 - 3-13**; square zone). Compounds outside the square area were considered to induce stemness/differentiation in the colonospheres. All these compounds treated colonospheres were then manually checked for changes in their morphologies. The initial screening identified 50 compounds based on distinct morphology changes, colonosphere sizes and CDy1 intensity.

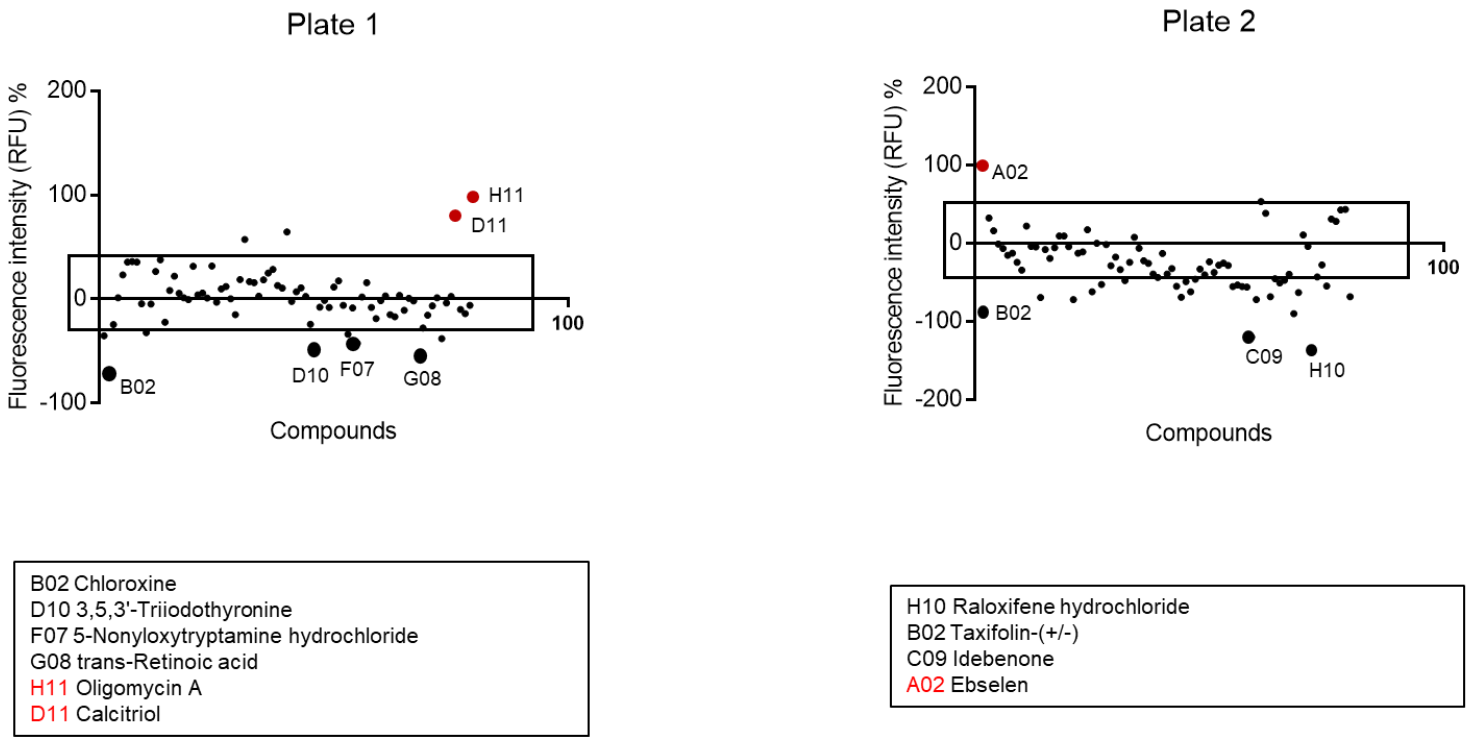


Figure 3-9: Primary screening of NIH clinical collection Plate 1 and 2 based on fluorescence intensity influenced by small molecules on colonospheres derived from HCT116 cells. Each dot represents one compound (n = 2). Compounds outside the square-zone highlighted with big circles were selected for a rescreening. Intensities were considered as an indication of induced (red) or reduced (black) stemness. Selected compounds from each plate are represented in the boxes (bottom).

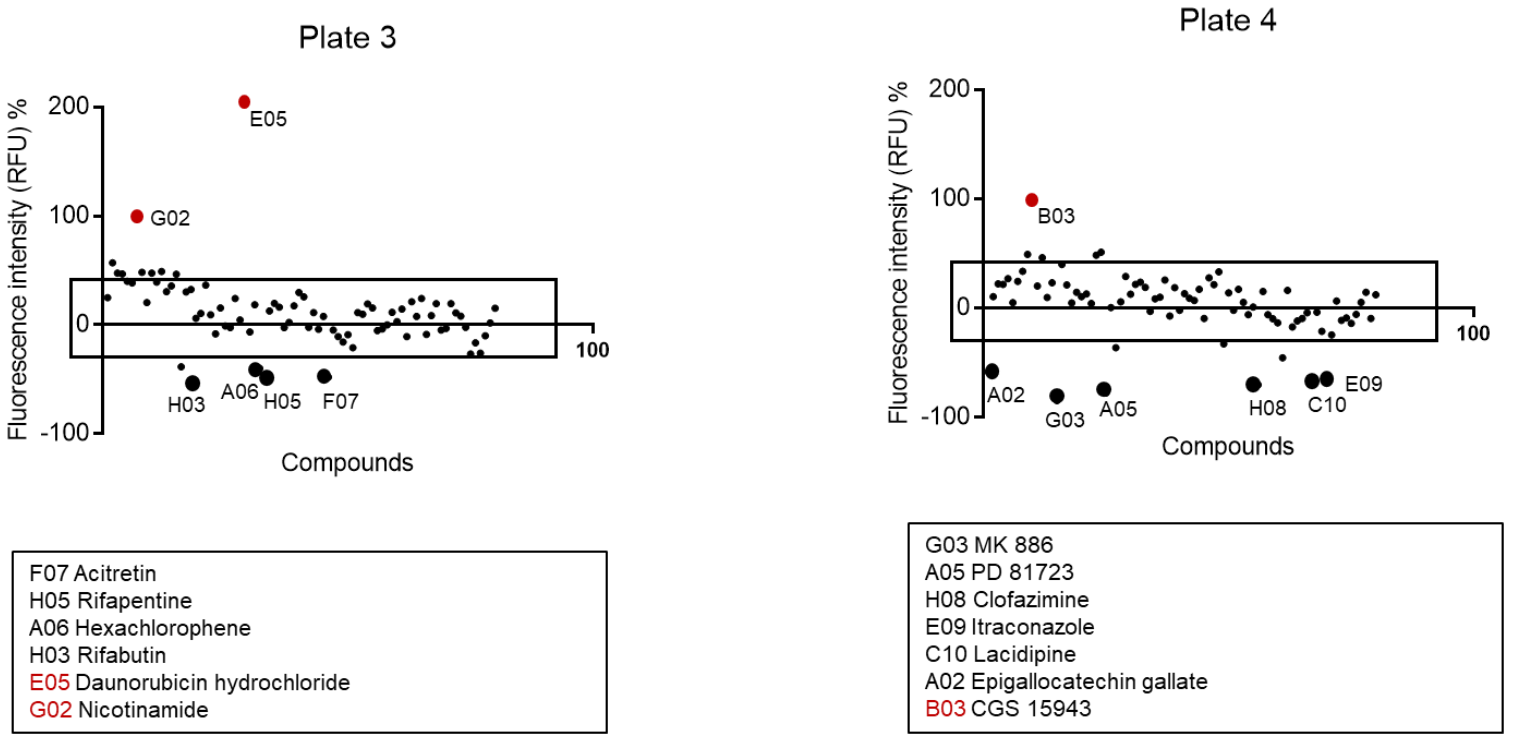


Figure 3-10: Primary screening of NIH clinical collection Plate 3 and 4 based on fluorescence intensity influenced by small molecules on colonospheres derived from HCT116 cells. Each dot represents one compound (n = 2). Compounds outside the square-zone highlighted with big circles were selected for a rescreening. Intensities were considered as an indication of induced (red) or reduced (black) stemness. Selected compounds from each plate are represented in the boxes (bottom).

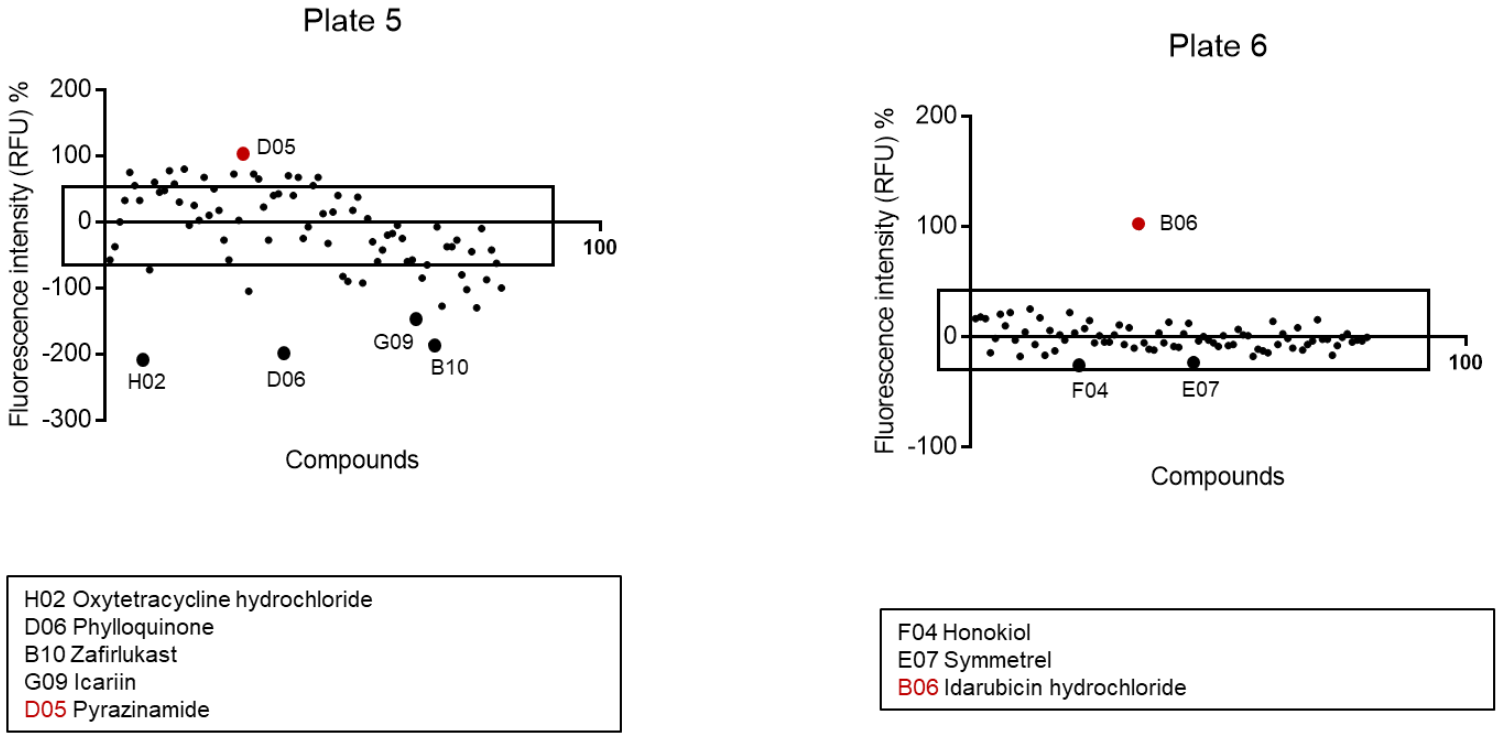


Figure 3-11: Primary screening of NIH clinical collection Plate 5 and 6 based on fluorescence intensity influenced by small molecules on colonospheres derived from HCT116 cells. Each dot represents one compound (n = 2). Compounds outside the square-zone highlighted with big circles were selected for a rescreening. Intensities were considered as an indication of induced (red) or reduced (black) stemness. Selected compounds from each plate are represented in the boxes (bottom).

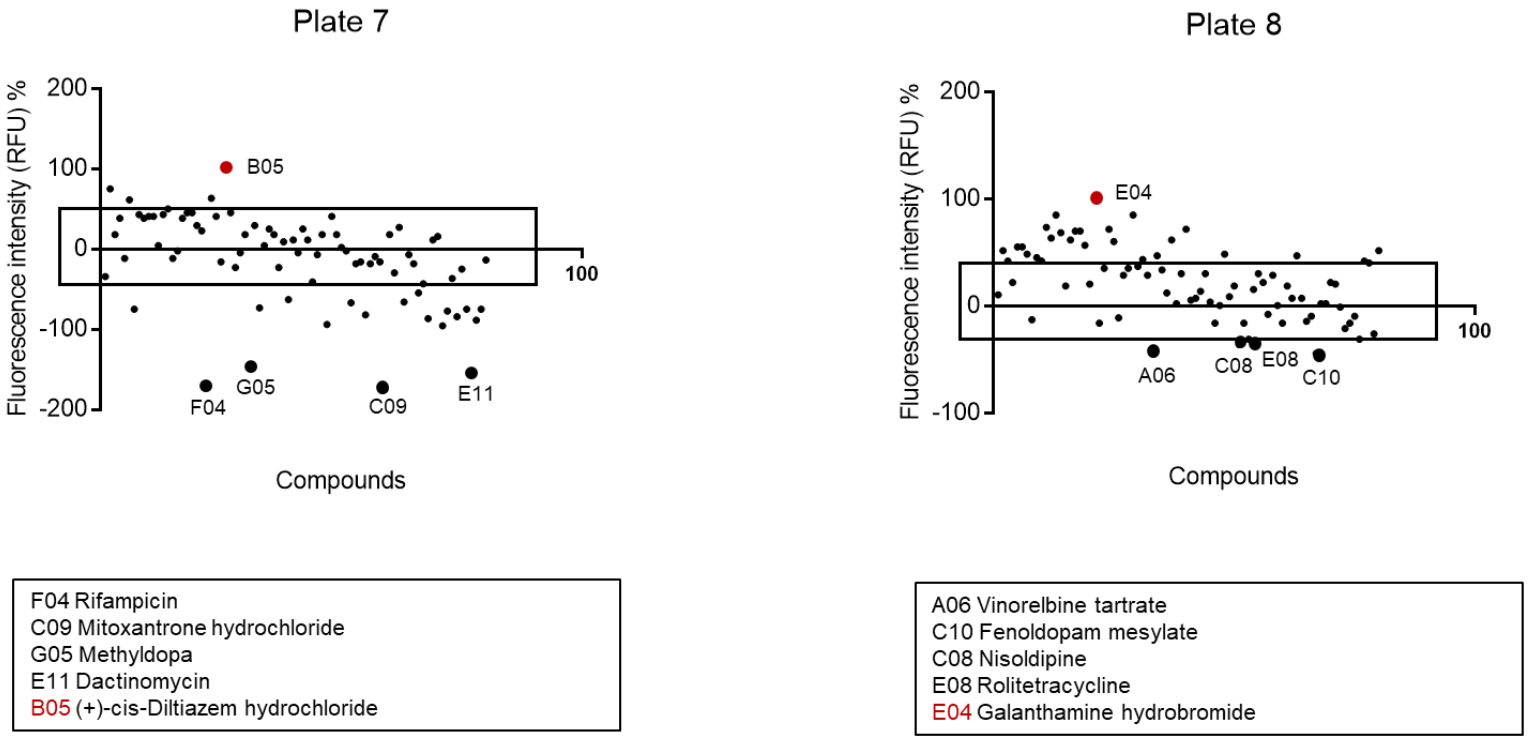


Figure 3-12: Primary screening of NIH clinical collection Plate 7 and 8 based on fluorescence intensity influenced by small molecules on colonospheres derived from HCT116 cells. Each dot represents one compound (n = 2). Compounds outside the square-zone highlighted with big circles were selected for a rescreening. Intensities were considered as an indication of induced (red) or reduced (black) stemness. Selected compounds from each plate are represented in the boxes (bottom).

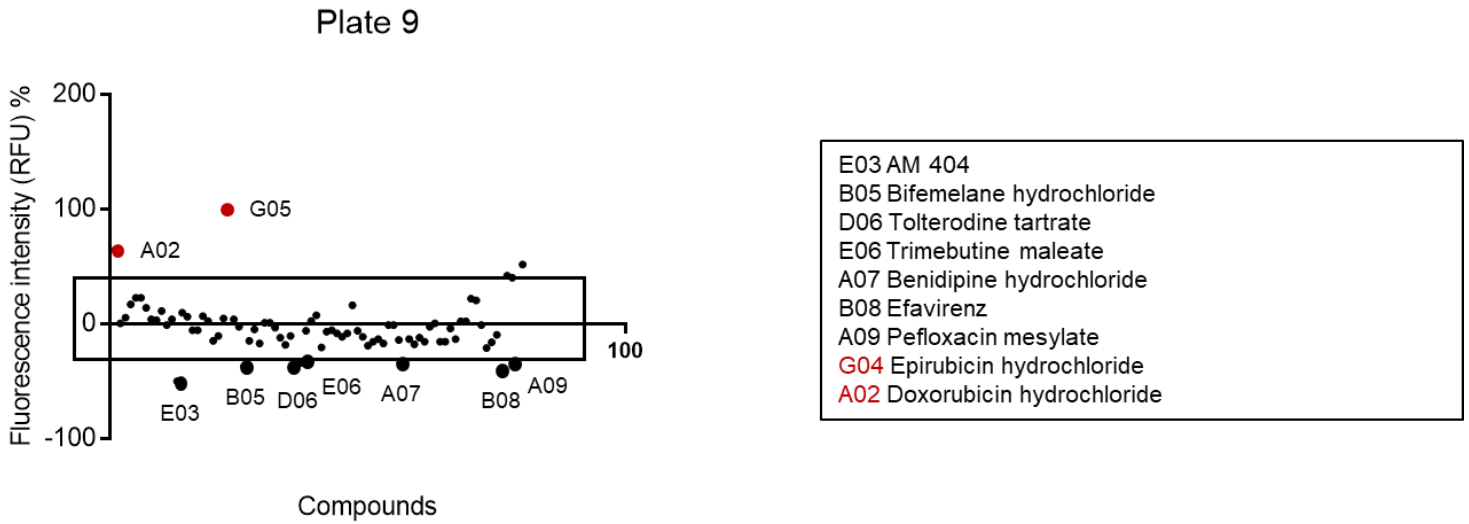


Figure 3-13: Primary screening of NIH clinical collection Plate 9 based on fluorescence intensity influenced by small molecules on colonospheres derived from HCT116 cells. Each dot represents one compound (n = 2). Compounds outside the square-zone highlighted with big circles were selected for a rescreening. Intensities were considered as an indication of induced (red) or reduced (black) stemness. Selected compounds are represented in the box (right).

At the end of the initial screening, therefore, 5.3% of compounds showed to reduce the stemness characteristics whereas, interestingly, 1.7% compounds showed an increase in fluorescence intensities conferred by CDy1 (**Figure 3-14**). This was characterised by the compounds within the square-zones causing a 30% reduction and 40% induction of fluorescence intensities compared to the controls, as represented in **Figure 3-8, 3-9, 3-10, 3-11** and **3-12.** 40 compounds were categorised as inducing a moderate level of differentiation (less than 40% reduction in fluorescence intensity), and 617 compounds within the square zone were categorised for having no/little effect as compared to controls (**Figure 3-14**). As the primary objective of this study was to identify compounds inducing differentiation, in addition to our major focus being the differentiation inducing compounds, compounds inducing stemness in CRC were also investigated. Therefore, from the primary screening, 50 compounds were selected for both their differentiation/stemness induction potential for a re-screen using colonospheres from addition cell lines (**Figure 3-15**).

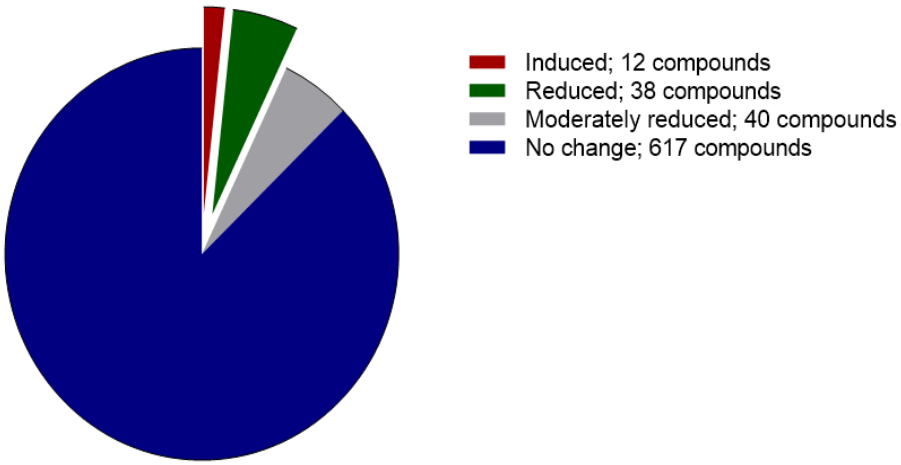


Figure 3-14: Primary screening of NIH clinical collection on colonospheres derived from HCT116 cells. Red indicates the compounds inducing stemness (12 compounds), while Green indicates compounds that reduced the stemness characteristics (38 compounds). Grey and Blue indicate compounds that showed a moderate reduction of no change in the stemness levels, respectively.

3.2.3.2 Re-Screening of selected compounds using 3D colonospheres obtained from HCT116, DLD-1 and SW480 cell lines

The initial screening revealed 50 compounds inducing or reducing CRC-SC associated stemness as exerted by stem cell dye CDy1 staining. With the primary screening conducted on colonospheres obtained from only HCT116 cells, next, a re-screening was carried out to narrow down compound numbers using other colorectal cancer cell lines (SW480 and DLD-1), in addition to HCT116 cells (**Figure 3-15**). At the end of re-screening (n = 3), 11 common compounds from 3 cell lines were selected based on their potential on CDy1 intensity induction and/or reduction (**Table 3-1**). Among of these, more recent work showed that antifungal drug itraconazole targets cell cycle heterogeneity, and epirubicin targets

metastasis and DNA-damage induced-drugs resistance in CRC (Buczacki et al., 2018, Tarpgaard et al., 2016). Since some of these compounds have previously been studied for CRC, we then focused on the compounds that had not been previously studied for the treatment of CRC.

Therefore, based on previous data and literature review, five of these compounds (AM404, epirubicin, rifabutin, daunorubicin, and idarubicin) were selected and later characterised as candidate compounds by their effects on cell viability, colony formation, neoplastic cell growth, and immunofluorescence assays. However, further clonogenic assays and assessment of organoids growth and morphology did not endorse daunorubicin and epirubicin and hence, both these drugs were excluded from further study (**Appendix 2 and 3**). The following three chapters focus on these three potential drugs that might act as anti-cancer drugs and potentially targeting CRC-SCs.

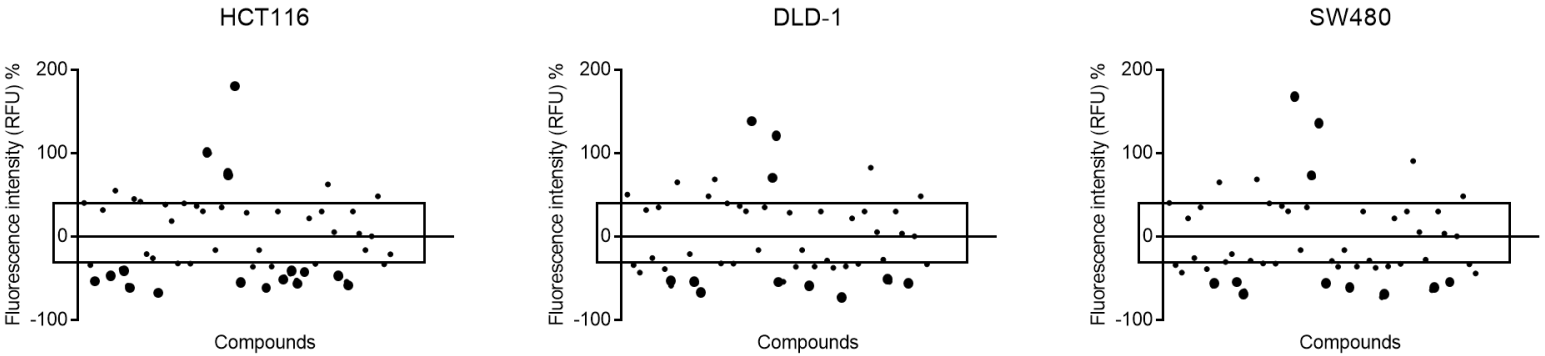
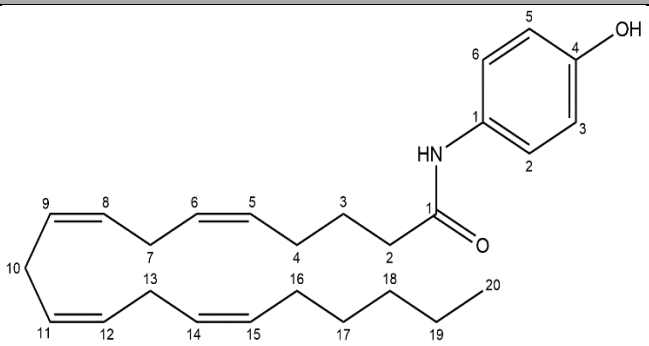
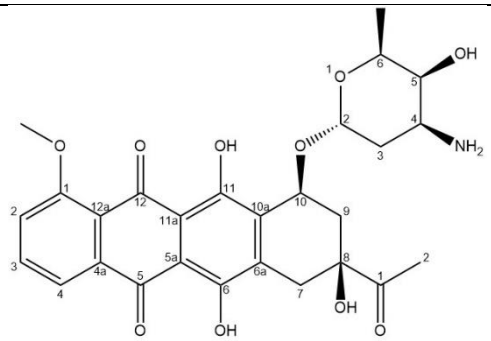
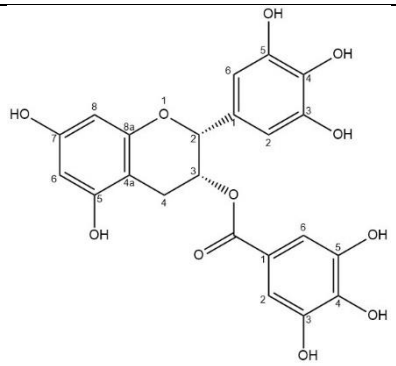
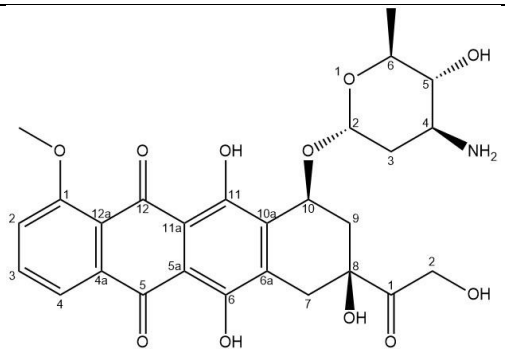
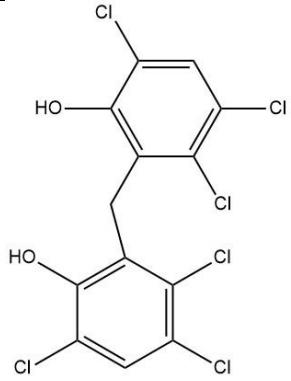
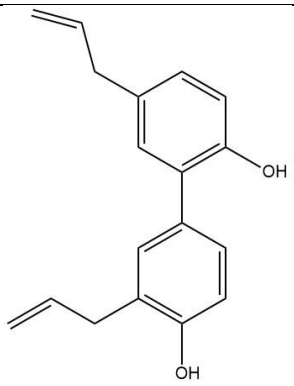
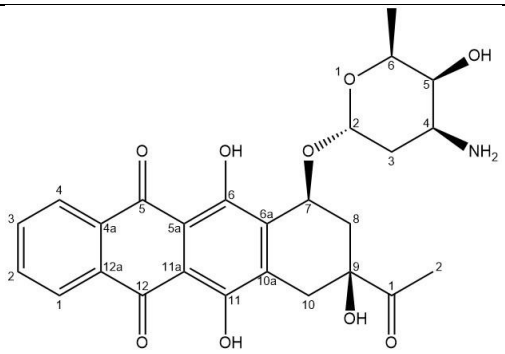
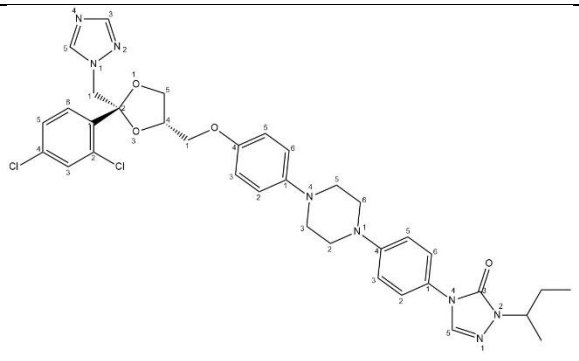
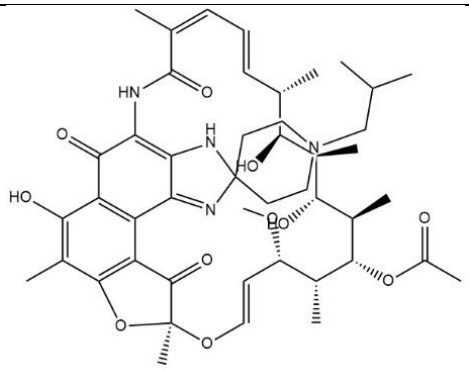
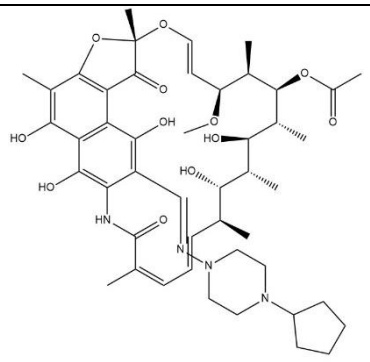
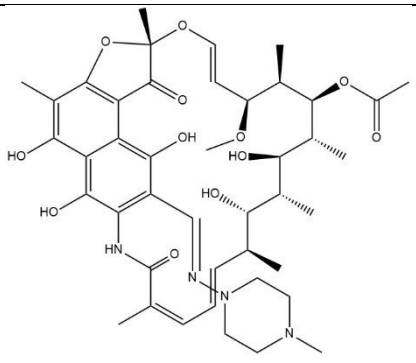


Figure 3-15: Re-screening of 50 compounds initially identified from the primary screening. Re-screening was carried out on colonospheres obtained from HCT116, DLD-1 and SW480 cell lines. N =3.

Table 3-1: List of compounds identified from re-screening of colonospheres derived from three CRC cell lines.

Compound	Molecular structure
AM 404 (PubChem CID: 6604822) (Caballero et al., 2015, Chang et al., 2008)	
Daunorubicin HCl (PubChem CID: 62770) (Wang et al., 2019a)	
Epigallocatechin Gallate (PubChem CID: 65064) (Fujiki et al., 2017)	

Epirubicin HCl (PubChem CID: 65348) (Shang et al., 2018)	
Hexachlorophene (PubChem CID: 3598) (Min et al., 2009)	
Honokiol (PubChem CID: 72303) (Pan et al., 2017a)	
Idarubicin HCl (PubChem CID: 636362) (Gunduz et al., 2014a)	

Itraconazole (PubChem CID: 3793) (Buczacki et al., 2018)	
Rifabutin (PubChem CID: 135398743) (Li et al., 2016a)	
Rifapentine (PubChem CID: 135403821) (Alfarisi et al., 2017)	
Rifampicin (PubChem CID: 135398735) (Shichiri and Tanaka, 2010)	

3.3. Discussion

3.3.1 CDy1-based drug screening system

This study demonstrates the application of colonospheres in drug screening and presents its potential in the identification of differentiation inducing drugs. **Figure 3-16** depicts a summary of the screening process. This study also reports the use of stem cell dye CDy1 in identifying CRC cells enriched with stem-like characteristics. CDy1 (compound of designation yellow 1) has been developed in 2011 as a fluorescent probe that selectively stains live embryonic stem cells (ESCs) and induced pluripotent stem cells (iPSCs) (Kang et al., 2011a). However, the exact mechanism of CDy1 is still not defined. Previously, it has been reported to selectively identify the fibroblasts undergoing reprogramming to induced pluripotent stem cells (Im et al., 2010). In this study, CDy1 stained CRC population exhibited low CD44 expression and relatively higher MUC2 expression, suggesting its association in staining the stem-like properties. Although this screening system successfully provide a reliable and robust platform to screen live colonospheres, its application is limited to the colonospheres derived from cell lines only. Colonospheres derived from primary cells were not validated using the platform. Moreover, the heterogeneity among patients might confer to variation in outcomes. Although, in this study, multiple cell lines were used with different genetic background, the candidate compounds are yet to be validated using primary cells.

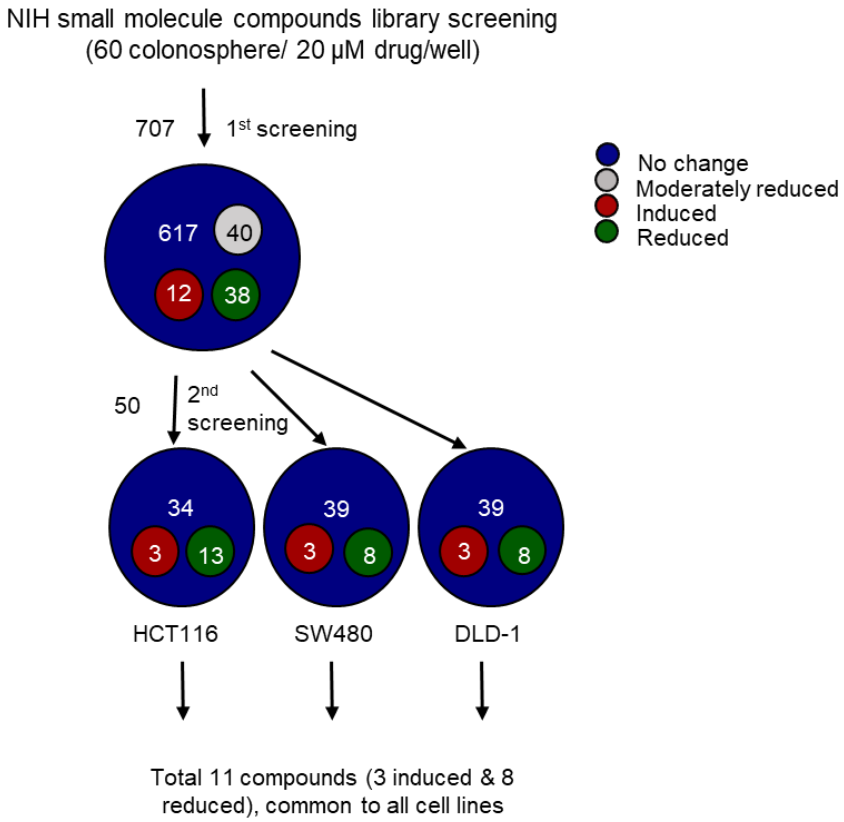


Figure 3-16: Summary of NIH clinical collection screening. Primary screening using HCT116 derived colonospheres revealed 50 compounds which underwent a re-screen using HCT116, DLD-1 and SW480 derived colonospheres. Rescreen revealed 11 common compounds affecting CRC-SC in the similar manner.

The initial screening using colonospheres derived from HCT116 cells revealed 50 compounds that might have the potential in altering CRC cells. Amongst them, 38 compounds showed to reduce the stem-like activity, as evident from the CDy1 staining, while 12 of them caused subsequent induction. Following a re-screening with two additional cell lines DLD-1 and SW480, 11 compounds were shortlisted (**Figure 3-16**). Since some of these compounds have previously been studied for CRC, based on previous data and literature review, 5 compounds were selected for further validations The shortlisted compounds were

evaluated and 3 of them showed significant potential in targeting CRC, as outlined in next 3 chapters.

CHAPTER 4

Antibacterial Drug AM404 with Antineoplastic Properties Targets FBXL5 E3-ligase in CRC Cells.

4.1 Introduction

Typically, inflammation is recognised as one of the major hallmarks of cancer as evident at the earliest stages of cancer progression (Hanahan and Weinberg, 2011), and is capable of fostering the growth of small tumours into metastatic cancers (Greten and Grivennikov, 2019, Elinav et al., 2013). Interestingly, as outlined in **Chapter 3**, the 3D colonosphere screening (Shaheen et al., 2016c, Weiswald et al., 2015a) obtained from three different colorectal cancer cell lines (HCT116, DLD-1 and SW480) initially revealed the anti-inflammatory, antibacterial drug AM404 showing high potential in targeting colonospheres.

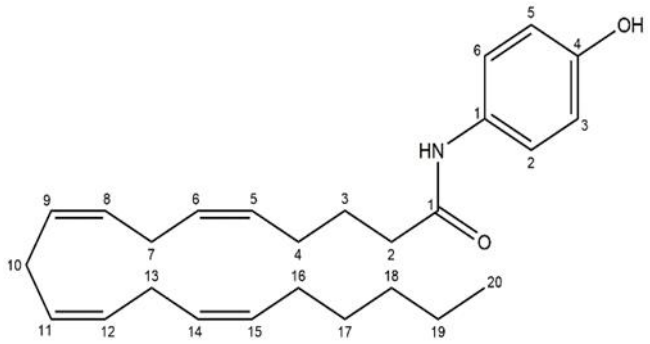


Figure 4-1: Schematic representation of the structural formula of AM404 (PubChem CID: 6604822).

AM404, also known as N-arachidonoylphenolamine is an active paracetamol metabolite with a chemical formula of $C_{26}H_{37}NO_2$ (**Figure 4-1**) (Saliba et al., 2017). Paracetamol is one of the most commonly prescribed drugs for its analgesic and antipyretic properties (Mazaleuskaya et al., 2015). Paracetamol undergoes de-acetylation to p-aminophenol in both liver, and the nervous system and p-aminophenol

is conjugated with arachidonic acid to produce AM404 in the nervous system. It has been suggested that AM404 may be responsible for the analgesic mechanism of paracetamol (Saliba et al., 2017). Some studies have demonstrated AM404s antibacterial and anti-inflammatory effects in reducing oxidative stress are associated with the presence of the phenolic group in its structure (**Figure 4-1**) (Saliba et al., 2017, Costa et al., 2006, Gerits et al., 2017). AM404 acts as a potent activator of transient receptor potential vanilloid type 1 (TRPV1), as a ligand at cannabinoid receptor 1 (CB1), or as an inhibitor of anandamide uptake, which is an endogenous agonist for both TRPV1 and CB1 receptors (Muramatsu et al., 2016). Currently, there is no established data available for AM404 in colorectal cancer.

Therefore, using *in vitro* 3D colonosphere, patient derived organoids, and *ex vivo* tumour explants, the specific objectives of this study were to:

(I) evaluate AM404s' potential in inhibiting de-differentiation and stemness properties of CRC stem-like cells.

(II) evaluate AM404s' effect on CRC growth impairment and cell morphology alteration.

(III) investigate AM04s' effect in 5FU induced chemoresistance

(IV) explore FBXL5s' effect in CRC migration

(V) identify FBXL5 as one of the targets by which AM404 exerts its anticancer effect on CRC

4.2 Results

4.2.1 3D screening revealed the anti-cancer activity of AM404

As a representative of CRC-SC (Hwang et al., 2014), the 3D colonospheres obtained from human colorectal cancer cell lines were employed into the compound library screening, as explained in **Chapter 3**. The magnitude of drug-induced stemness and/or differentiation level was determined

by high and low CDy-1 fluorescence intensity, respectively. Of the 707 compounds screened, AM404 was characterised as one of the potential compounds for reducing the stem-like characteristics in CRC-SC (**Figure 4-2**). Several *in vitro* experiments were carried out to validate AM404's effects on targeting CRC-SC.

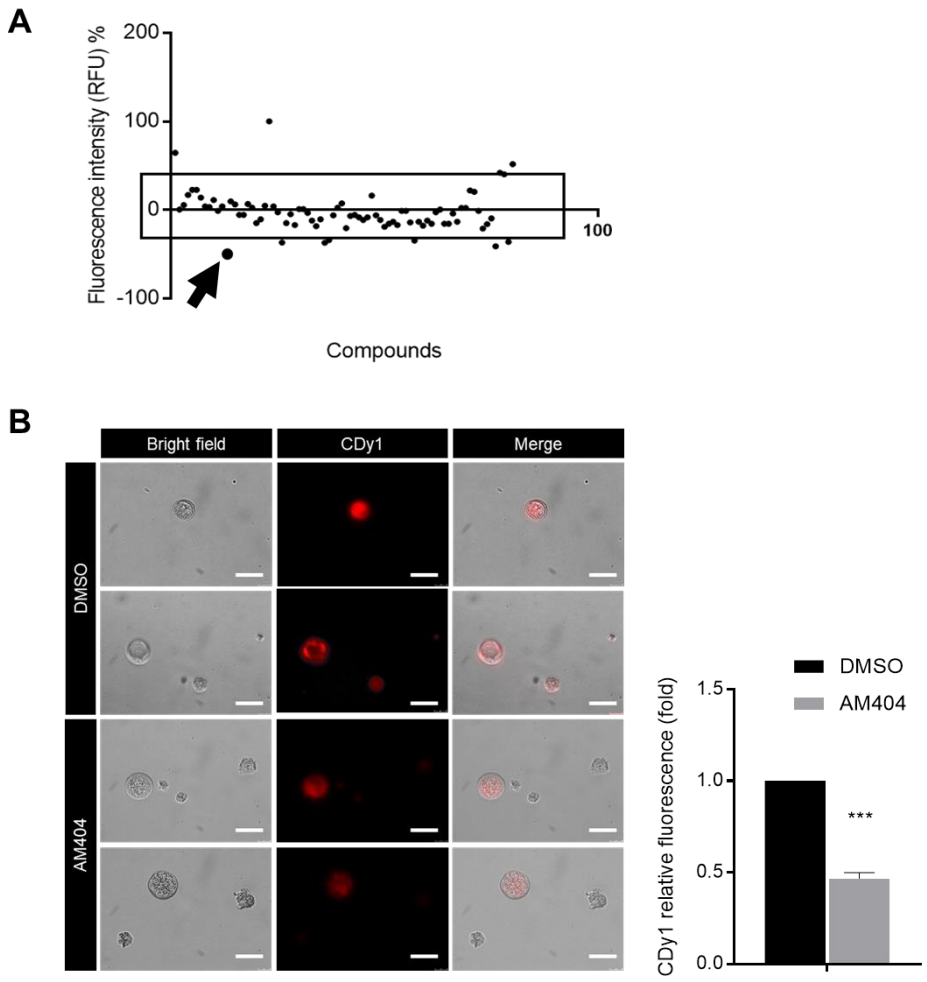


Figure 4-2: AM404 mediated reduction in CDy1 fluorescence intensity. (A) AM404 (arrowhead) caused a reduction in the relative fluorescence presented by CDy1 Rosamine dye. CDy1 has been used as a measure of

stem-like activity. Fluorescence intensity DMSO-treated (control) colonosphere was set as 0. Intensities exerted by all compounds were presented as a percentage of their induction or reduction of stem-like activity. Image was reproduced from the primary screening of NIH clinical collection Plate 9 carried out on colonospheres derived from HCT116 cells (Figure 3-13). **(B)** Representative images of CDy1 stained DMSO-treated (control) and AM404 treated colonospheres. Scale bar: 25 µm. AM404 caused more than 50% reduction in the CDy1 intensity in treated colonospheres.

4.2.1.1 AM404 induces cytotoxicity in CRC cell lines

To evaluate the effects of AM404 in CRC, Sulforhodamine B (SRB)-based colorimetric assay was first performed on HCT116, DLD-1 and SW480 cell lines as described in **Chapter 2**; Materials and Methods (Li et al., 2019b).

A wide range of doses (1 to 100 μM) was used to calculate the half-maximal inhibitory concentration (IC_{50}) which defined AM404 as an ideal candidate for further in-depth evaluations with IC_{50} that is lower than the initial target threshold in screening (20 μM) (Sachlos et al., 2012b). This result was backed by the previous studies reporting AM404 to be well tolerated in animal models and was less toxic on mammalian cells up to the 4× of the MIC, indicating its relatively safe profile (Gerits et al., 2017, Costa et al., 2006). Our results were highly comparable between the DLD-1 and HCT116 cell lines, with IC_{50} of 15.3 and 15.2 μM respectively, whereas, AM404 shows slightly more sensitivity towards SW480 with an IC_{50} of 12.3 μM (**Figure 4-3**). The measured dose was then used throughout the experiments to carry out its in-depth evaluations on CRC, including treatments on patient derived organoids and tissue explant models.

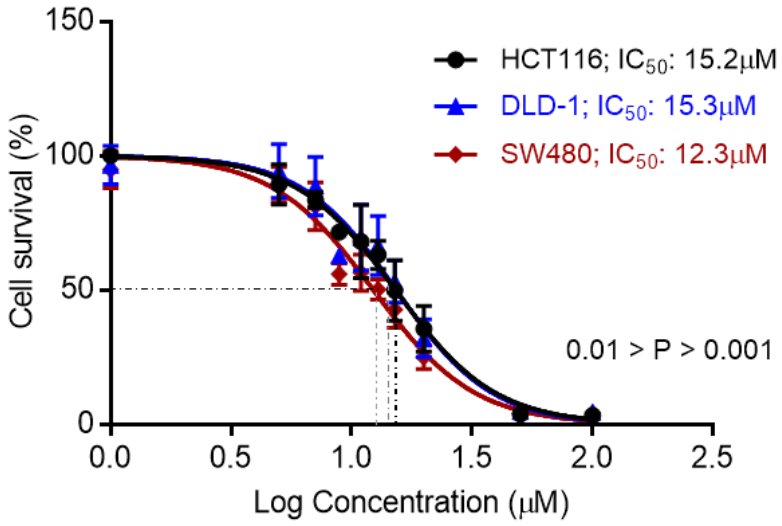


Figure 4-3: Cytotoxicity assay of AM404 using Sulforhodamine B (SRB) on human colorectal cancer cell lines. Survival curves were denoted by HCT116 (black), DLD-1 (blue) and SW480 cells (red) treated with AM404. The dotted line represents half maximal inhibitory concentration (IC_{50}). Error bars represent mean ± S.D. Nonlinear regression was used to plot the data. **, P < 0.01; ***, P < 0.001. Experiments were performed at least three independent occasions (n = 6).

4.2.1.2 AM404 reduces the tumorigenic activity in CRC cells

AM404 showed significant reduction in CRC colony formation, size, growth, morphology alteration, while inducing differentiation and reducing the well-established stemness associated markers.

Colony formation assay is an *in vitro* cell survival assay based on the ability of a single cell to grow into a colony consisting of 50 or more cells. Generally, it is a two-dimensional approach that applies a good correlation with tumour response *in vivo* (Kabakov and Gabai, 2018, Franken et al., 2006). One of the advantages of this assay is that it enables assessment on the proliferation and the ability to undergo unlimited division for every cell in the population (Franken et al., 2006, Kabakov and Gabai, 2018). Typically, a clonogenic assay also evaluates the

potential of a single cell to resist treatments and grow into a colony. This assay is independent of the way that cells have died, as such, by apoptosis, necrosis, autophagy, or other mechanisms and measures the ability of a single cell to divide, attach and form colony (Kabakov and Gabai, 2018). Therefore, in order to investigate AM404's effect on the tumorigenic property, following the cytotoxicity analysis, we next performed colony formation and cell growth curve analysis. Both these assays strongly suggested morphological alteration and reduction in colony formation, size, as well as cell growth retardation by AM404 in all CRC experimental cell lines (**Figures 4-5, and 4-9**).

A limited number of HCT116, DLD-1 and SW480 cells were allowed to grow into colonies as described in **Chapter 2**; Materials and Methods for 6-7 days. On day 8, AM404 was added to its IC_{50} and were maintained for one more week with re-treating the treated colonies every 72 h or replacing the medium, for treatment and control groups respectively. Traditionally clonogenic assay is performed by counting the size and number of colonies or foci of cells (Guzman et al., 2014). At the end of the treatment period, colonies were stained with crystal violet for counting and analyses (**Figure 4-4; A**).

Our results showed a significant reduction in the number of colonies during the treatment along with their morphological alteration upon AM404 treatment (38% vs 26% on HCT116, and 44% vs 27% on DLD-1 cells; $P < 0.01$), with no colonies being formed on SW480 cell line (**Figure 4-4; B**). This might be because of the plating efficiency in SW480 cells were not sufficient to form into colonies. We initially optimized our seeding efficiency for this assay in HCT116 and DLD-1 cell lines with 500 cells/well in a 6-well plate. Since cancer cells are heterogeneous, the plating efficiency might also differ from each cell lines. However, since cancer cells typically rely on paracrine signalling for their growth, if the cell number is large compared to the surface area, cells might not get sufficient paracrine growth factors or cytokines for their growth and

therefore might not form into colonies. Moreover, some proliferating cell lines also have been reported to have a poor colony-forming ability (less than 5–10%), and are less convenient for this assay (Kabakov and Gabai, 2018).

To distinguish differences between morphological structures and possible alterations conferred by AM404, colonies were grown on sterile coverslips as descried on **Chapter 2**; Materials and Methods and were stained with Phalloidin. Phalloidin binds on F-actin and thereby evaluates the cytoskeletal organization within colonies whereas DAPI binds directly onto the DNA. Phalloidin staining significantly distinguished the morphological differences, including the sizes of colonies conferred by AM404 in DLD-1, treated colonies (**Figure 4-5**). Generally, cancer entities tend to show more compact and round structure. As speculated, our results show a dense connective network within the vehicle-treated colonies; as evident by Phalloidin and DAPI staining (**Figure 4-5**).

On the other hand, AM404-treated colonies showed a vast difference in their size while retaining the structural integrity. Interestingly, the nuclear density of treated colonies was also found to be dense throughout the colonies. This could indicate AM404's suppressing effect on colony growth and proliferation, without necessarily inducing any cell death (**Figure 4-5**).

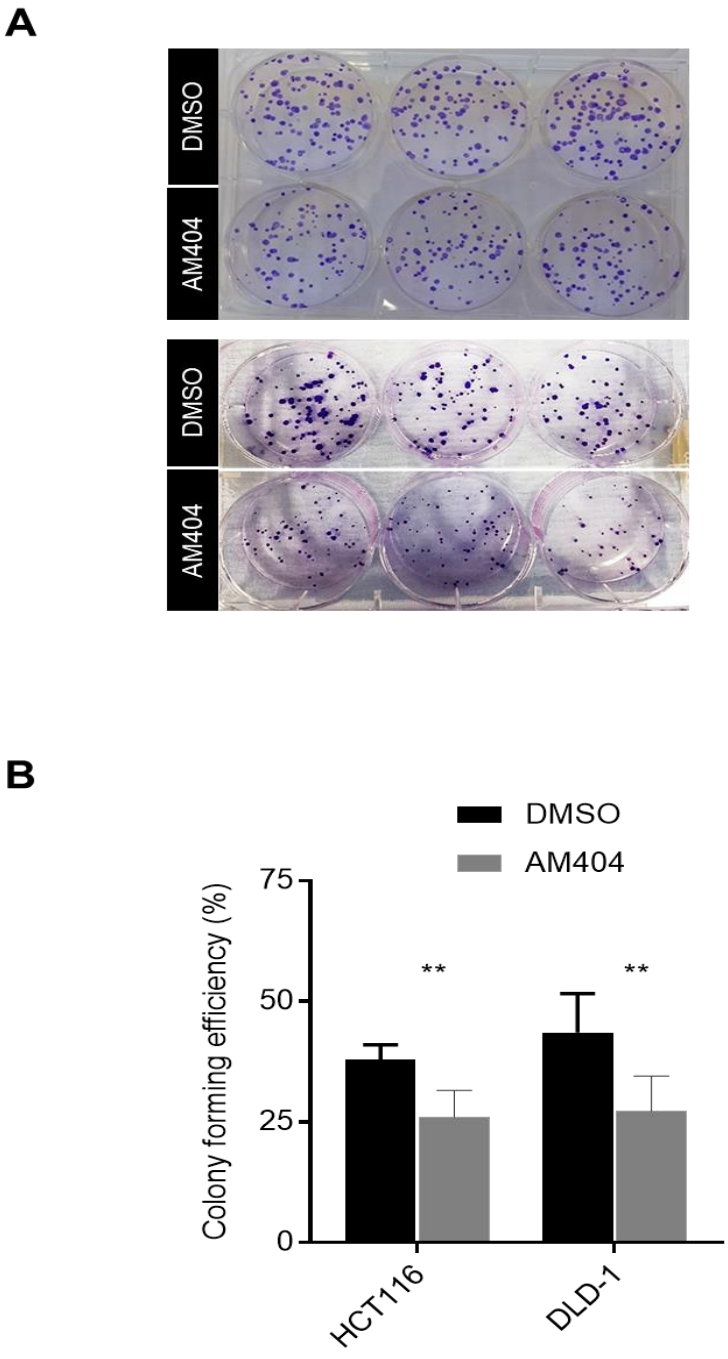


Figure 4-4: Reduction in colony formation efficiency upon AM404 treatment. (A) Representative images of colony formation assay on HCT116 (top) and DLD-1 (bottom) cells. **(B)** AM404 showing significant reduction in colony formation assay in HCT116 and DLD-1 cells. $P \leq 0.01$. Experiments were performed three independent occasions (n = 3).

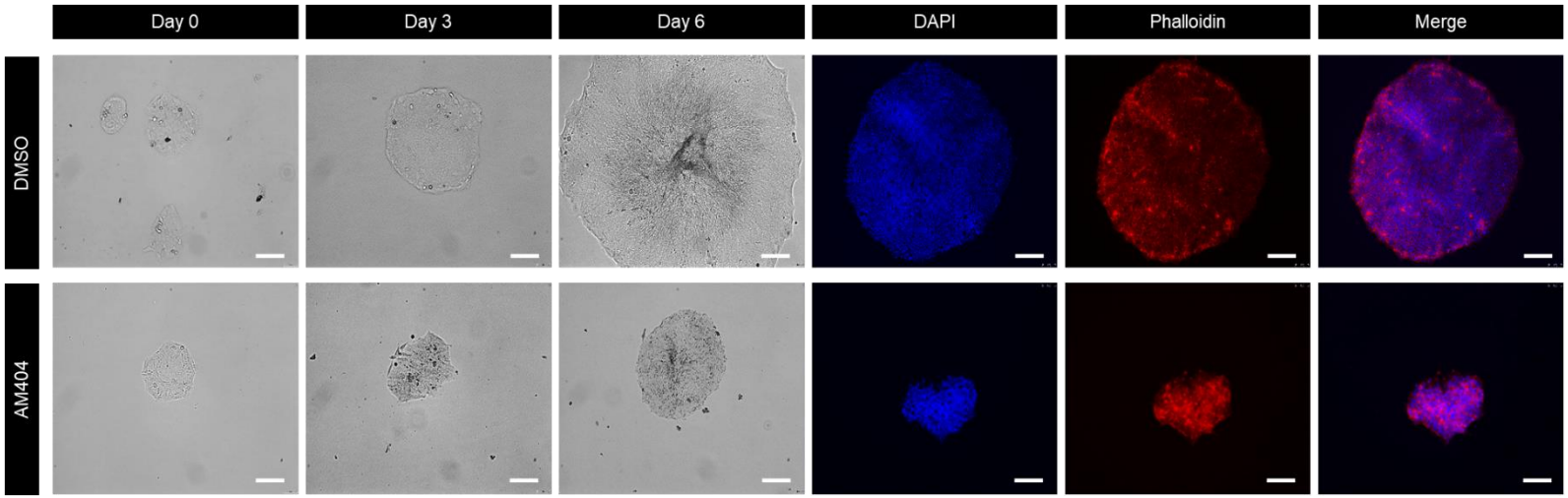


Figure 4-5: Phalloidin staining of AM404 treated colonies. Nuclei were detected with DAPI-blue fluorescent stain. Scale bar: 75µm.

In addition to the colony numbers, a significant reduction in colony size was strongly evident in both HCT116, and DLD-1 cell-derived colonies within the first three days of treatment (**Figures 4-6, 4-7, and 4-8**). This effect was also seen in the growth curve analysis where AM404 started to exert its effects on cell growth within the first three days of treatment (**Figure 4-9**). Colony sizes were greater on day 14 compared to day 8 for vehicle-treated groups, which was in contrast to the strong impediment observed in the AM404-treated groups throughout the treatment period (**Figures 4-6, and 4-7**). At the end of the treatment, for both HCT116 and DLD-1 cell lines, colony sizes were significantly reduced in the AM404-treated groups (1396 μm vs 852 μm for HCT116, and 1192 μm vs 379 μm for DLD-1 cells; $0.05 > p > 0.01$) (**Figure 4-8**). The differences in size were also evident in the microscope photographs in **Figure 4-6** and **Figure 4-7**.

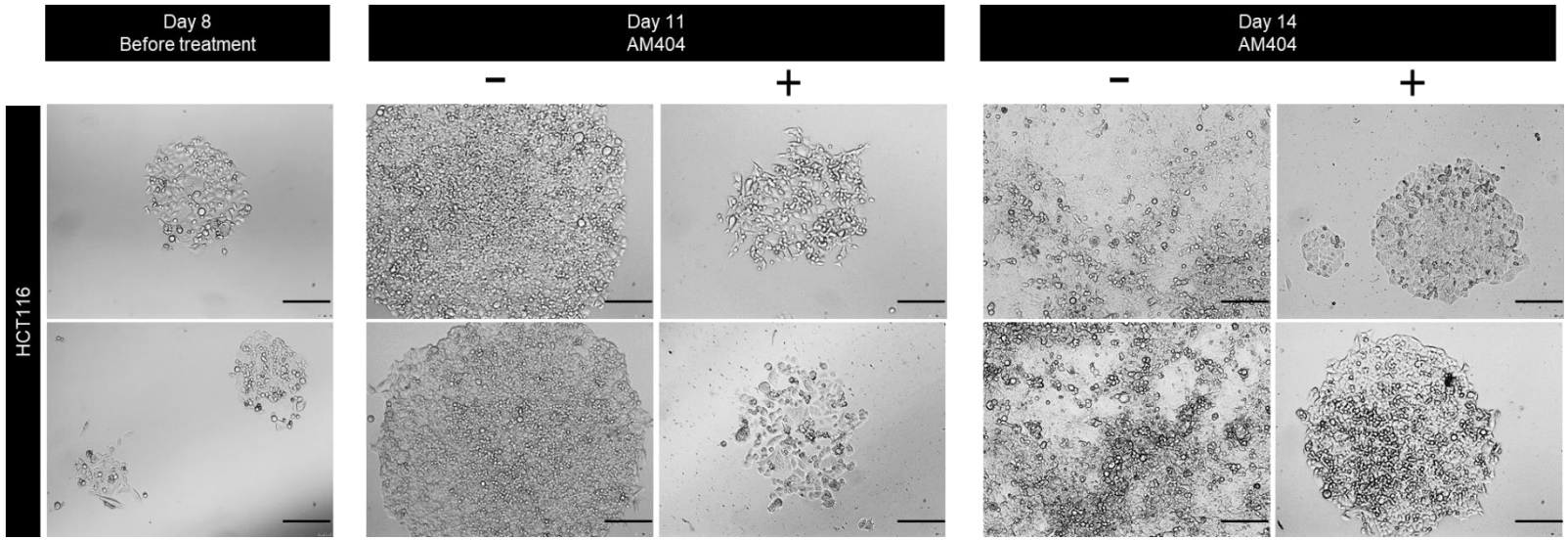


Figure 4-6: AM404 reduces the tumorigenic ability of HCT116 cells. Images were taken before treatment on day 8, after 72 h on day 11 and at the end of treatment period on day 14. AM404 treatment showed a reduction in colony size on day 14 as compared to the vehicle-treated colonies. Scale bar: 75 µm.

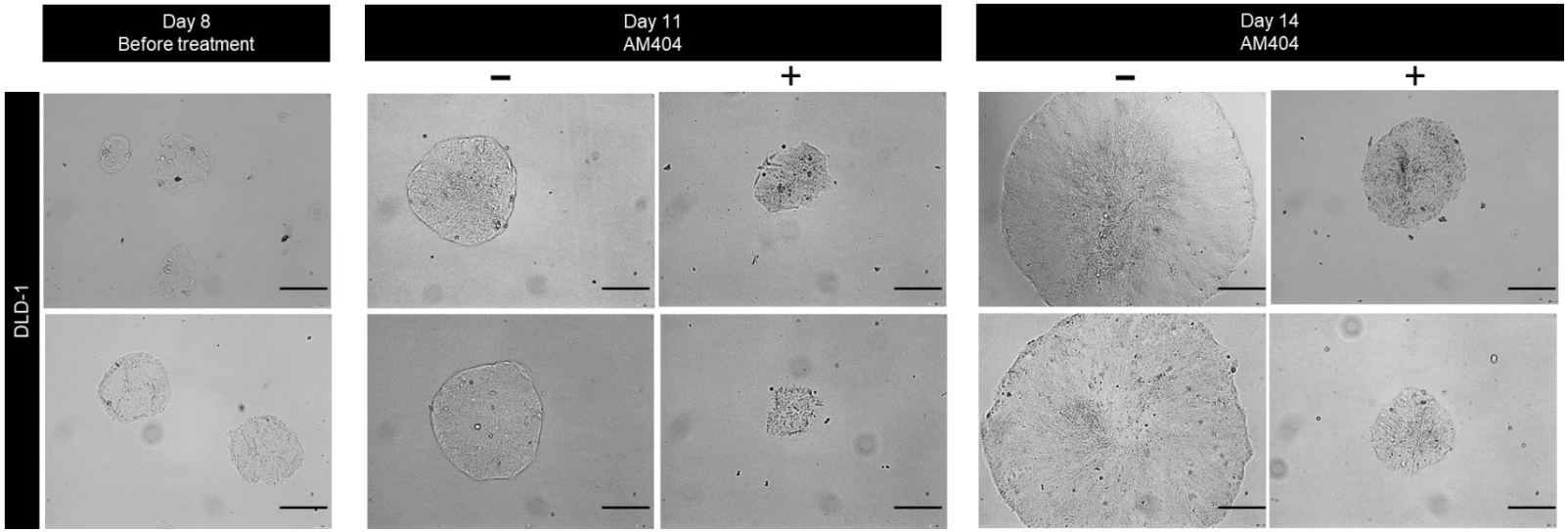


Figure 4-7: AM404 reduces the tumorigenic ability of DLD-1 cells. Images were taken before treatment on day 8, after 72 h on day 11 and at the end of treatment period on day 14. AM404 treatment showed a reduction in colony size on day 14 as compared to the vehicle-treated colonies. Scale bar: 75 µm.

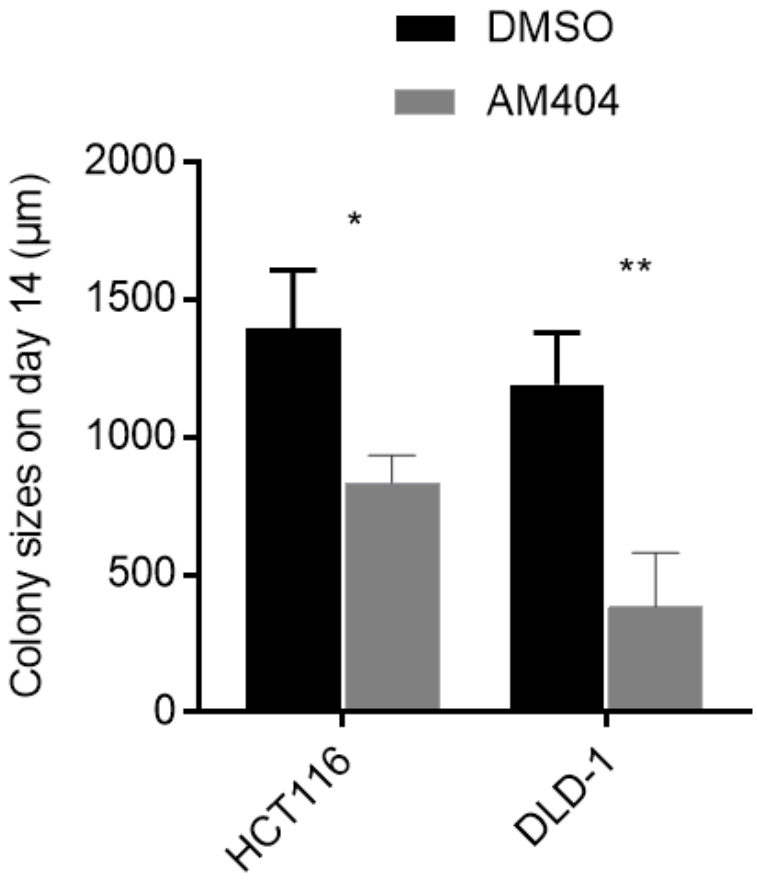


Figure 4-8: Reduction of the size of colonies upon treatment with AM404. Significant decrease in colony size were observed in both cell lines upon AM404 treatment. Error bars represent mean ± S.D. Experiments were performed at least three independent occasions (n = 25); 0.05 > p > 0.01.

Next, cell growth curve analysis was carried out on HCT116, DLD-1 and SW480 cell lines. Reduction in growth and an increase in cell doubling time was evident in all three cell lines upon AM404 treatment. Tumour cells typically show sigmoid pattern in their growth. Their growth kinetics can therefore be characterised by three well-defined stages: first stage being the tumour formation stage that is also known as lag phase, second is the log phase that portrays rapid tumour growth, and lastly, the stationary

phase, where tumour growth slows down and eventually converges to a final volume (González et al., 2017).

Cells were treated with the IC_{50} of AM404 (**Figure 4-3**) on day one and were counted every day for a period of 8 days at the same time. A distinct lag phase was absent between day 0-1 in all cell lines, while in log phase cell growth showed an exponential fashion reaching the plateau on day 6 for HCT116 and SW480 cells and day 5 for DLD-1 cells. AM404 treatment, on the other hand, caused a shift in the population doubling time (PDT) from 21 h to 29 h, 22 h to 25 h, and, 33 h to 35 h in HCT116, DLD-1 and SW480 cells respectively. These shifts suggest lag in the doubling time, indicating steady impedance in the exponential cell growth (**Figure 4-9**). From day 2 of treatment, cell numbers were significantly less in the treated groups throughout the whole experimental period (day 2-8).

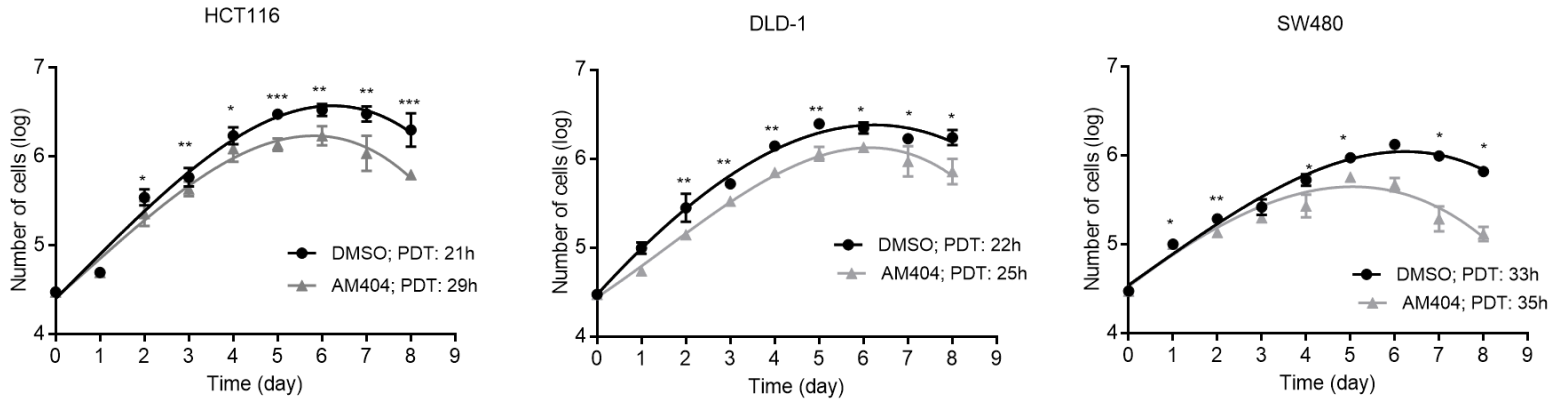


Figure 4-9: Growth curve of AM404-treated and vehicle-treated HCT116, DLD-1 and SW480 cells. AM404 was added at its IC_{50} on day 1. Cells were cultured for 8 days and were counted each day at the same time. Error bars represent mean ± S.D. (n = 6). Since day 2, the number of cells in the treated groups were significantly lower. Experiments were performed at least three independent occasions (n = 6; 0.05 < P < 0.001).

4.2.1.3 AM404 induced sensitivity in CRC treatment

To study AM404's effect in conventional chemotherapy, we examined the effect of AM404 on the sensitivity to 5-fluorouracil (5FUra), one of the most widely used anticancer drugs used for the treatment of several types of cancer, particularly for CRC (DB et al., 2003). This experiment was carried out in collaboration with one of my co-supervisors, Dr. Roya Babaei-Jadidi. Cytotoxicity assay was carried out on HCT116 cells, deleted for *FBXW7* for a range of concentrations used for 5FUra. Of note, our lab has previously investigated the sensitivity to 5-FUra on CRC and showed that FBXW7-deficiency-induced chemoresistance in CRC (Li et al., 2019b, Izumi et al., 2017, Lorenzi et al., 2016b). Our data showed that HCT116$^{FBXW7(-/-)}$ cells treated with AM404 in combination with 5FUra (**Figure 4-10**) was more sensitive to treatment with 5FUra alone. This result indicates that AM404 induced sensitivity in the chemoresistance and to the 5FUra treatment thereby suggests AM404 as a potential anticancer drug candidate in CRC treatment (**Figure 4-10**).

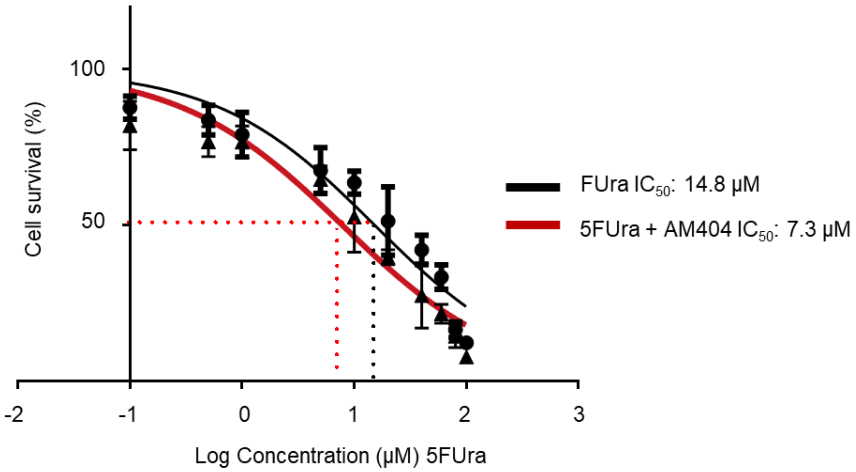


Figure 4-10: AM404 induced sensitivity in CRC drug treatment. Cytotoxicity assay of 5FUra using Sulforhodamine B (SRB) on HCT116$^{FBXW7(-/-)}$ cells. Survival curves were denoted by 5FUra treatment (black), and AM404 + 5FUra treatment (red). The dotted line represents half maximal inhibitory concentration (IC_{50}). Experiments were performed three independent occasions Error bars represent mean ± S.D. 0.05 > P > 0.001. (n = 3).

4.2.2 Inhibition of de-differentiation and stem-like properties by AM404

To study AM404's effects on cancer stem-like cells, particularly for colonosphere formation, morphology changes and acquisition of stem-like properties, 3D colonospheres were cultured from CRC cell lines for about 14 days as described in **Chapter 2;** Materials and Methods (Shaheen et al., 2016c, Weiswald et al., 2015a). On day 14, fully grown and round shaped colonospheres were treated with AM404 for a period of 72 h. At the end of the treatment, only the colonospheres with diameter >50 μm were counted under a microscope and their colonosphere formation efficiency was quantified (**Figure 4-11**). Our results showed that AM404 treatment-induced distinct morphological

alteration; however, the number of colonospheres remained the same after the treatment (**Figures 4-11, 4-12**).

Colonospheres with a defined round structure that are difficult to recognise as individual cells were classified as fully grown, "self-renewing" entities, whereas colonospheres presenting as discrete aggregated cells were considered to be "differentiating" ones (**Figure 4-12**). The AM404 treated group, while making no significant difference on the colonosphere formation, vastly presented differentiating-like morphology within the culture (**Figure 4-12**). The distinct structure of colonosphere was lost upon AM404 treatment, while presenting more anchorage-like phenotypes indicating AM404's potential in inducing differentiation on CRC-SC. This result is in line with the morphological changes observed in 2D colonies obtained from HCT116 and DLD-1, however, unlike 2D colonies, the colonosphere numbers remained the same even after the treatment.

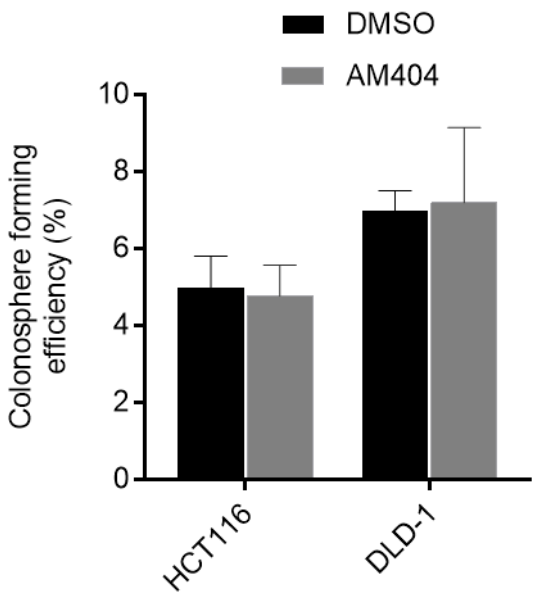


Figure 4-11: AM404 treatment did not cause any significant change in colonosphere formation assay. Colonospheres were derived from HCT116 and DLD-1 cells and were treated with AM404 for 72 h. No significant changes were observed for colonosphere formation in the treated group. Error bars represent mean ± S.D. (n = 30).

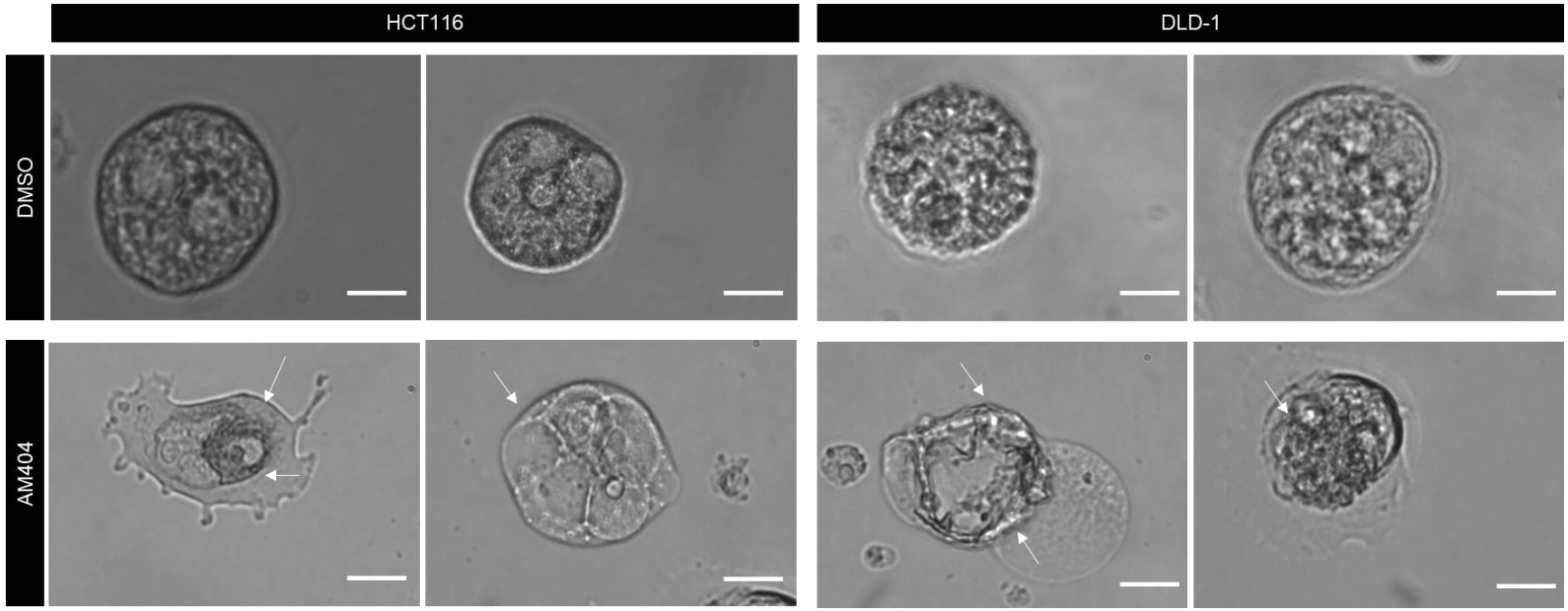
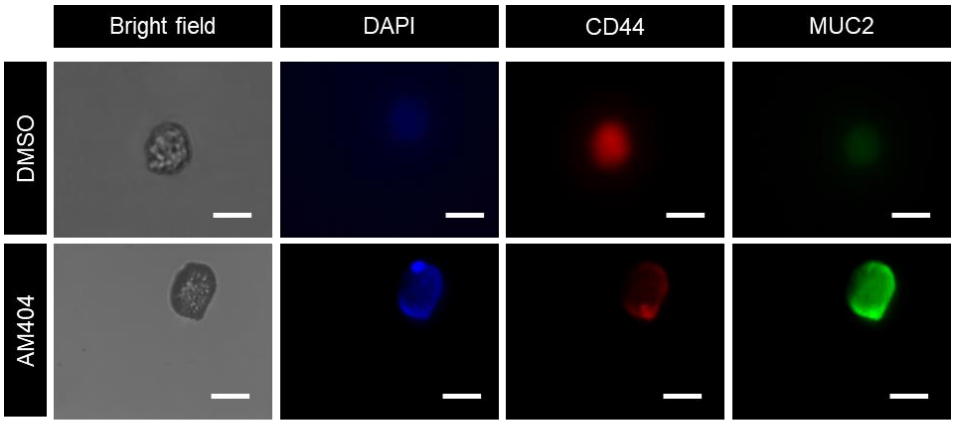


Figure 4-12: Induction of morphological alteration in colonospheres treated with AM404. Images were taken after 72 h of AM404 treatment. Untreated colonospheres maintained their distinct structural network of cells whereas the treated colonospheres showed relatively discrete structure and loss of their structural integrity. Scale bar: 25 µm.

As the screening presented in **Chapter 3** identified AM404 for its potential in inducing differentiation in CRC-SC, in order to associate this morphology change with differentiation (**Figure 4-12**), AM404 treated colonospheres were further evaluated for their expression of CD44 and Mucin2 by IF technique.

CD44, is a cell surface adhesion receptor, is highly expressed in many cancers, including CRC. It acts by binding to extracellular matrix components, including hyaluronan and osteopontin, as well as to messenger molecules, such as growth factors present in the tumour microenvironment (Morath et al., 2016, Zoller, 2011). Accumulating evidence indicates that CD44, especially its CD44v isoforms, are important for regulating CSC characteristics, including self-renewal, tumour initiation, growth, metastasis, motility and resistance to chemotherapy (Senbanjo and Chellaiah, 2017, Yan et al., 2015, Todaro et al., 2014, Zoller, 2011). Mucin2 (MUC2), on the other hand, is a secretory protein, secreted from terminally differentiated goblet cells into the intestinal lumen, and is commonly used as differentiation marker (Wang et al., 2017a, Hsu et al., 2017, Zhou et al., 2015). In addition, MUC2 plays an important role in intestinal homeostasis and suppresses the migration of colon cancer cells *in vitro*. It is the primary component of the protective mucus layer of the colon and plays an important role in CRC progression (Hsu et al., 2017).

Cultured colonospheres were carefully collected and transferred on coverslips and treated with AM404. After 72 h, colonospheres were further processed for IF analysis as described in **Chapter 2**; Materials and Methods (**Figure 4-13**). AM404 treatment significantly reduced expression of CSC marker CD44, and an upregulation of the differentiation marker MUC2. This result is also backed by qPCR data showing significant reduction in CD44 in AM404 treated colonospheres (**Figure 4-14; A**).



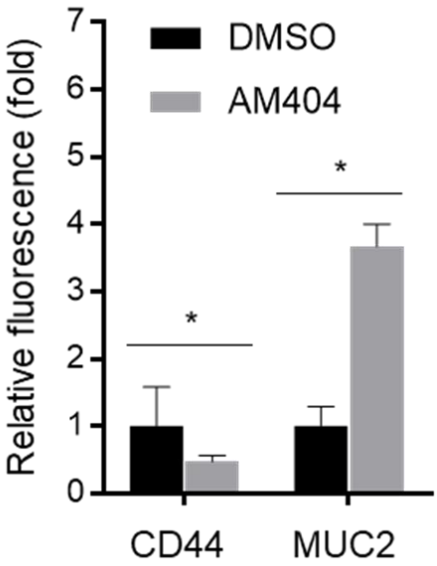


Figure 4-13: Immunofluorescence assay of AM404 treated colonospheres using stemness and differentiation markers. Scale bars: 25 µm. AM404 treatment significantly reduced CD44 expression while increasing MUC2 expression on DLD-1 derived colonospheres suggesting induction of differentiation upon drug treatment (n = 12), $P < 0.05$.

Characterisation of the inhibition pathway involved in the mechanism of action of AM404 on CSC-like properties was initially performed by gene expression analysis from mRNA isolated from colonospheres of roughly the same size using qPCR analysis. The primary objective of this experiment was to determine the expression level of established stemness and differentiation markers in the CSCs. Therefore, total RNA was extracted from AM404 treated colonospheres with RNeasy Mini Kit as described in **Chapter 2**; Materials and Methods.

In CRC, some distinct biomarkers have been identified to distinguish the CSC subpopulations, including LGR5, CD44, CD133, CD24, NANOG, among others (Kemper et al., 2012a, Ricci-Vitiani et al., 2007, Dalerba et al., 2007). As previously mentioned, CD44 is a well-established marker for CRC-SCs. It is a multifunctional transmembrane glycoprotein located on the cytomembrane and is encoded by the highly conserved CD44 gene on chromosome 11 in humans (Yan et al., 2015, Zeilstra et al., 2013). However, amongst the other important biomarkers, the Leucine-rich repeat-containing G-protein-coupled receptor 5 (LGR5) is a well-established epithelial stem cell marker in the small intestine and colon. At the base of the crypt, the self-renewing LGR5+ stem cells are capable of producing progenitor cells which in turn form the mature crypt cells of the intestinal epithelium (Yip et al., 2018). Another well-established stemness marker NANOG has been reported to be aberrantly expressed during malignancy in cancer cells, with NANOG positive cells being extensively exhibited the CSC and EMT traits in CRC (Pan et al., 2017b, Yao et al., 2016). Both NANOG and OCT-4 are well established embryonic transcriptional factors and are linked to the pluripotency and self-renewal characteristics of CSCs (Radwan et al., 2016). It is also speculated that OCT4+ CSC subpopulation within a primary colon tumour undergoes EMT process (Humphries et al., 2018). OCT44, NANOG, BMI-1 are typically characterised as stem cell markers and are significantly expressed in cancer cell lines and cancer tissues. In addition,

BMI-1 is a transcriptional repressor, widely expressed in diverse tumours and belongs to the polycomb-group of proteins that regulate proliferation and senescence (Amini et al., 2014). Notably, our results showed a significant reduction in expression level for all these stemness markers *CD44*, *NANOG*, *OCT4* and *BMI-1*, whereas, differentiation markers *KRT20* and *CDX2* were significantly increased upon AM404 treatment in colonospheres (**Figure 4-14; A, B**). Moreover, in support with the previous studies, while significantly reducing *NANOG* and *OCT-4* expression, AM404 herein indicated its association with EMT process (Humphries et al., 2018, Yao et al., 2018). In line with this and recently published findings from our lab, AM404 significantly reduced N-cadherin (*NCAD*) and induced E-cadherin (*ECAD*) expression while increasing the expression of tumour suppressor *FBXW7* (**Figure 4-14; C, D**) further suggests its possible affiliation on EMT (Li et al., 2019b). Of note, as previously reported and showed in **Chapter 4**, deletion of *FBXW7* has been associated with high tumorigenesis in CRC. AM404, while increasing *FBXW7* expression in colonospheres, also caused a subsequent reduction in the WNT target genes, including Cyclin D and c-JUN and thereby reduced the stem-cell signatures (**Figure 4-14; D**). These results for stem cell markers, prognostic factors, differentiation and the EMT markers have revealed the potential of AM404 in targeting stem-like cells in CRC.

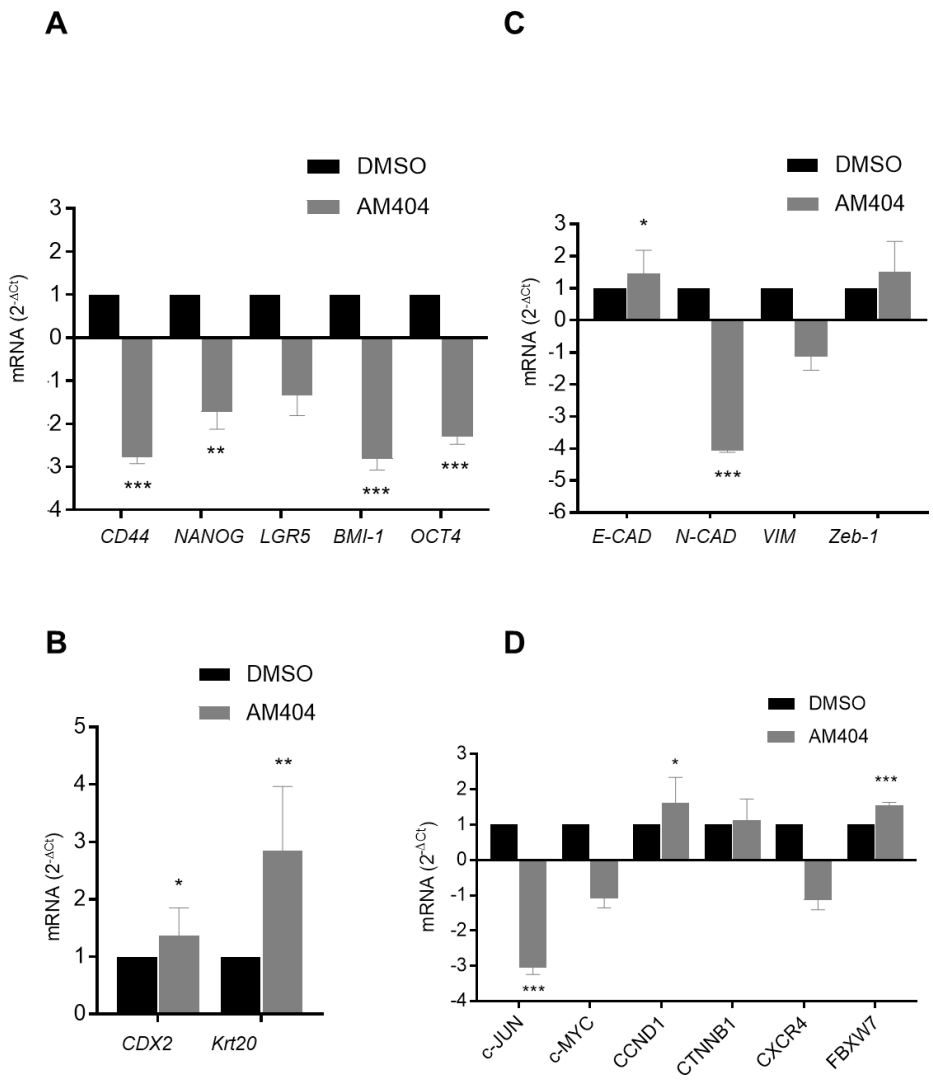


Figure 4-14: qPCR analysis of AM404 treated colonospheres derived from DLD-1 cells. Expression of **(A)** Stemness, **(B)** differentiation, **(C)**, EMT, and **(D)** transcription factor for recurrence, poor survival, metastasis and tumour suppressor, in colonospheres treated with AM404. Results were normalized to those obtained with β-actin, and all assays were performed in triplicate. (n = 3; *, P < 0.05; **, P ≤ 0.01; ***, P ≤ 0.001.

4.2.3 AM404 induced growth impairment in patient derived *ex vivo* tumour organoids

As a first step towards mimicking the patient tumour tissues, CRC patients' derived organoids were used, to study their response to AM404 (Ahmed et al., 2019). Organoids were cultured from previously characterised organoid line in our lab, as described in **Chapter 2**; Materials and Methods (Kashfi et al., 2018). This culture is largely dependent on three essential factors: R-spondin1, a Wnt agonist and ligand for LGR5 that induces crypt hyperplasia; EGF induces intestinal proliferation; and Noggin, a BMP agonist that induces a marked increase of crypt numbers. Combination of these components in basement membrane extract (BME) are essential to sustain the growth of small intestine organoids, their cell-cell interaction, cell architecture and composition to the original tissue (Testa et al., 2018).

Once the organoids started to grow (usually day 4-5), they were treated with AM404 and/or complete organoid medium as vehicle-control for their morphology and growth evaluation as well as live/dead staining. Re-treatment and/or organoid medium replacement was carried out every two days, for the whole 2 weeks experimental period. The 2 weeks treatment period was chosen based on the majority of control-treated organoids starting to exhibit large cystic structure at the end of the total period of 3 weeks. However, throughout the entire culture, organoids display different morphologies, ranging from cystic to solid structures (Ahmed et al., 2019). For example, enterospheres are characterised as spherical structures composed of several types of small intestinal epithelial cells. They can be formed from isolated single cells or small intestinal crypts. Enteroids can develop from enterospheres by forming one or more budding crypts. Such structures appear as spheroids with crypt-like projections. Cysts, on the other hand, can appear as large enterosphere with transparent pseudolumen and thin lining of epithelial cells (Li et al., 2019b, Yip et al., 2018, Stelzner et al., 2012). Changes in

organoid phenotypes can therefore be measured and assessed for their morphology changes.

When compared to control-treated tumour organoids, AM404 appeared to induce distinct morphological changes such as branching formation (which may indicate of AM404-induced differentiation), in addition to delaying the growth rate (**Figure 4-16**, arrowheads). However, the morphology change was highly variable in appearance. On day three, most of the organoids in control group were formed by enterospheres (~90%) with a few of cystic organoids. For over a period of fourteen days, they eventually turned into large defined cystic organoids. In contrast, in the treatment group, at day three of AM404 treatment, even though the majority of the organoids were also enterospheres, as treatment progressed, more of significantly smaller enteroid-like irregular structures appeared which may suggest of AM404 induced differentiation (**Figures 4-15, 4-16** arrowheads).

Therefore, AM404 treatment caused significant growth impairment in tumour organoid (**Figures 4-16**, **4-17**). Considering the 3D structure, volume of organoids was measured by taking 3-4 separate diameters for each organoid. Half of the average of this diameter was then considered as radius (r), and therefore, organoid volume was measured using the following formula:

$$V = \frac{4}{3}\pi r^3$$

In the AM404 treated group, volume was significantly smaller (1.99×10^8 μm^3 vs 0.85×10^8 μm^3; $P < 0.05$, $P < 0.01$). In addition, at the end of the treatment, only 10% of organoids were measured to be as more than 700 µm in the treated group, as compared to the 30% of total organoids in control group. Similarly, in reference to all the organoids being larger than 300 µm in control group, 20% organoids were still within the range of 100-300 µm in AM404 treated group (**Figure 4-17**). This result shows

a high population of AM404-treated organoids being in smaller diameter range, suggesting its inhibitory effect on organoid growth.

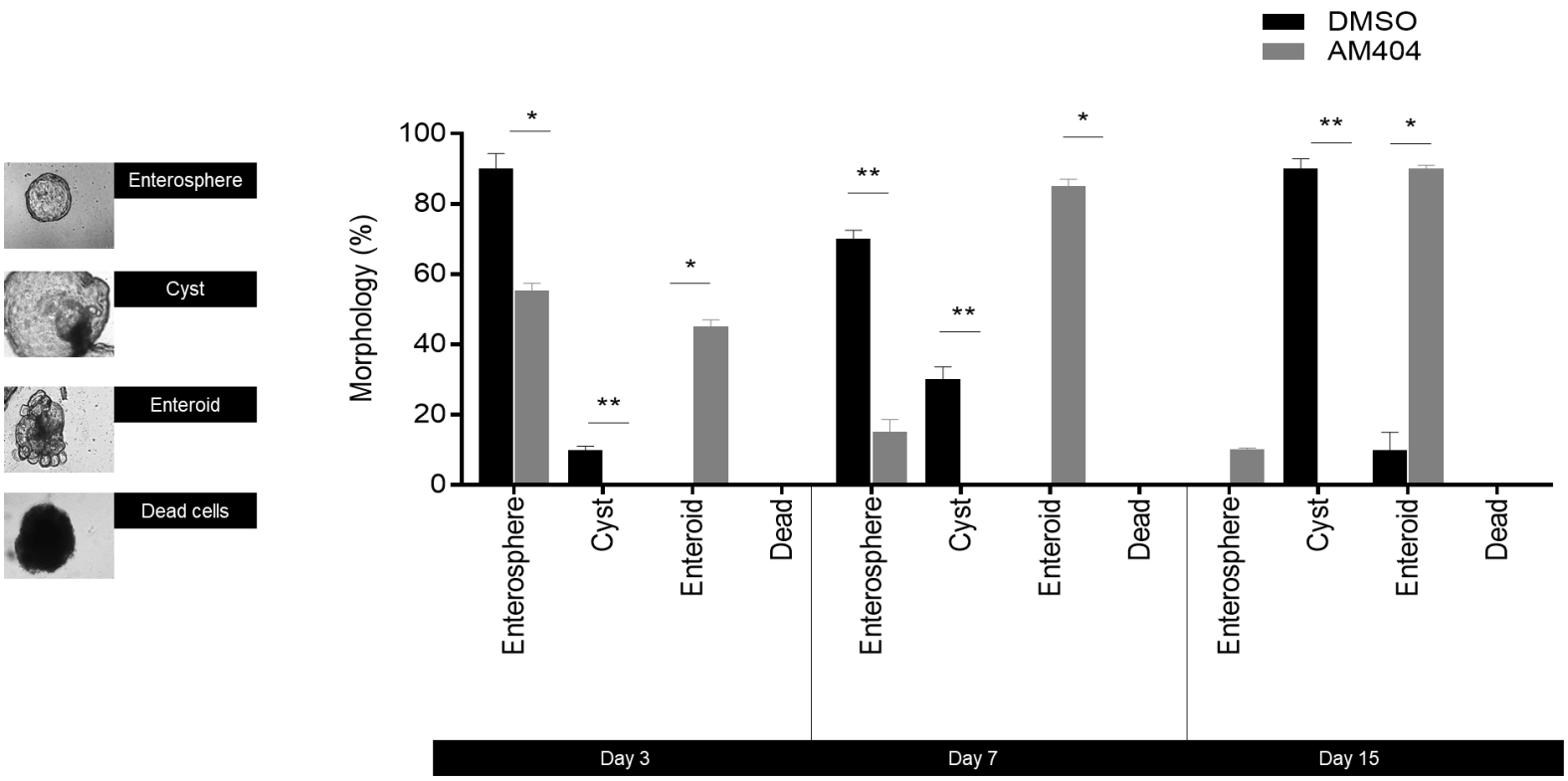


Figure 4-15: AM404 treatment presents enteroid-like structures and induces apoptosis in organoids. Percentage of enterosphere, cyst, enteroids and dead cells at day 3, 6 and 15 days of treatment. Organoids were counted by microscopy (n = 20; *, P < 0.05; **, P < 0.01).

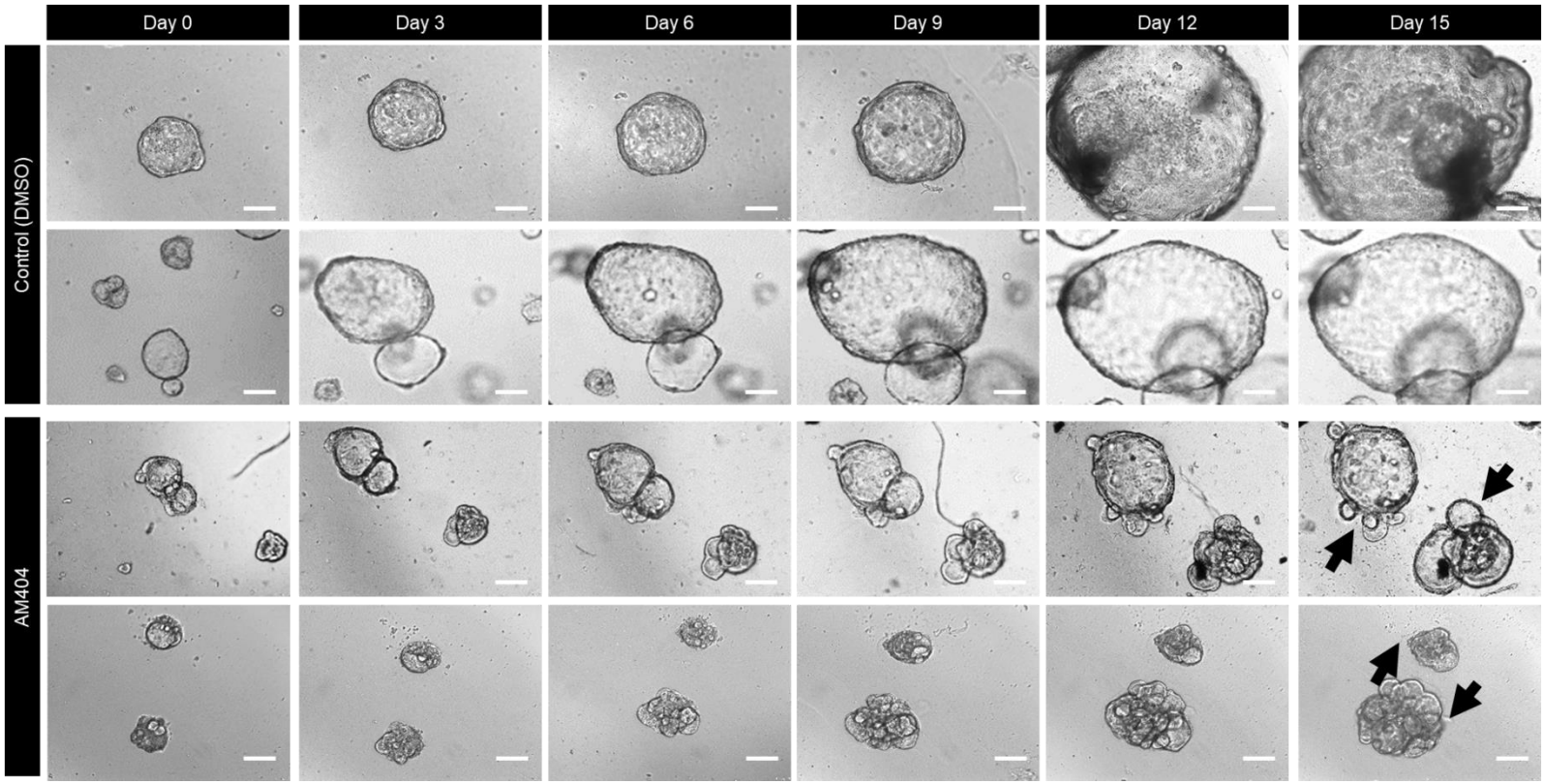


Figure 4-16: Organoid growth retardation and morphology change induced by AM404. Representative images of tumour organoids treated with AM404 for a period of 2 weeks. Morphological alteration and variation in growth were observed throughout the treatment period. AM404 treated group showed distinct morphological changes and smaller enteroid-like irregular structures indicating AM404 induced differentiation (arrowheads). Images were taken using Leica microscope. Scale bar: 75 µm.

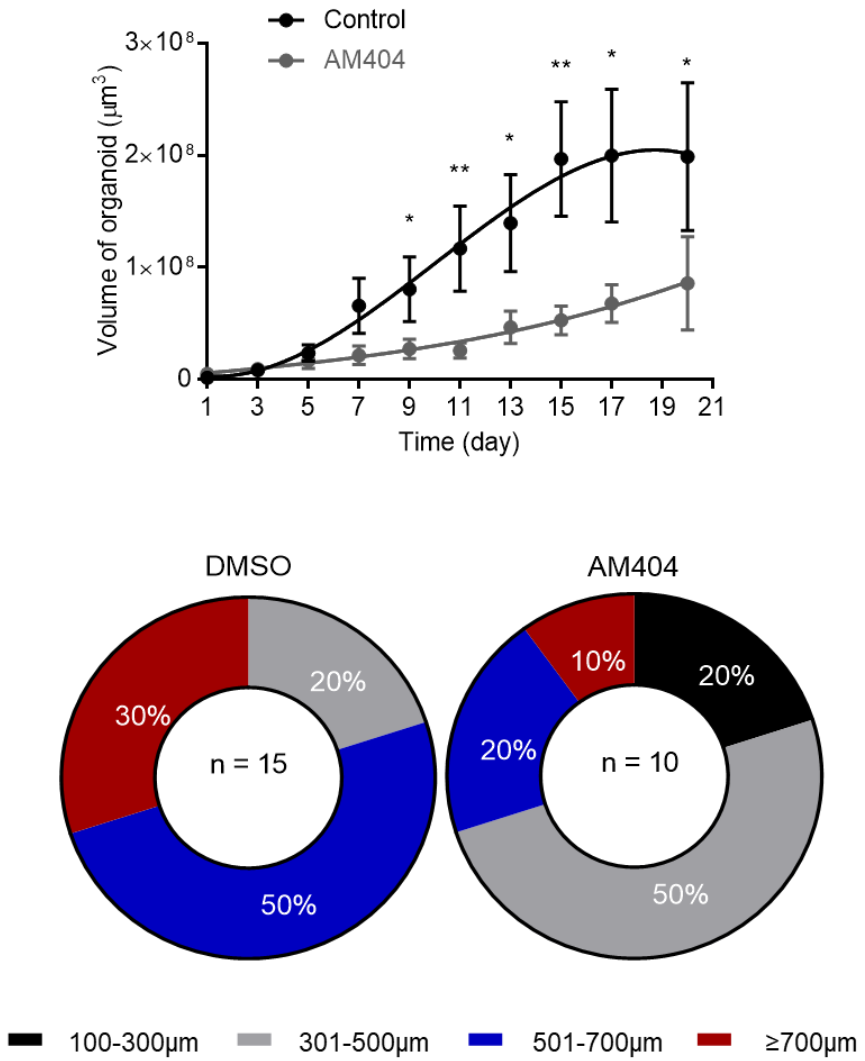
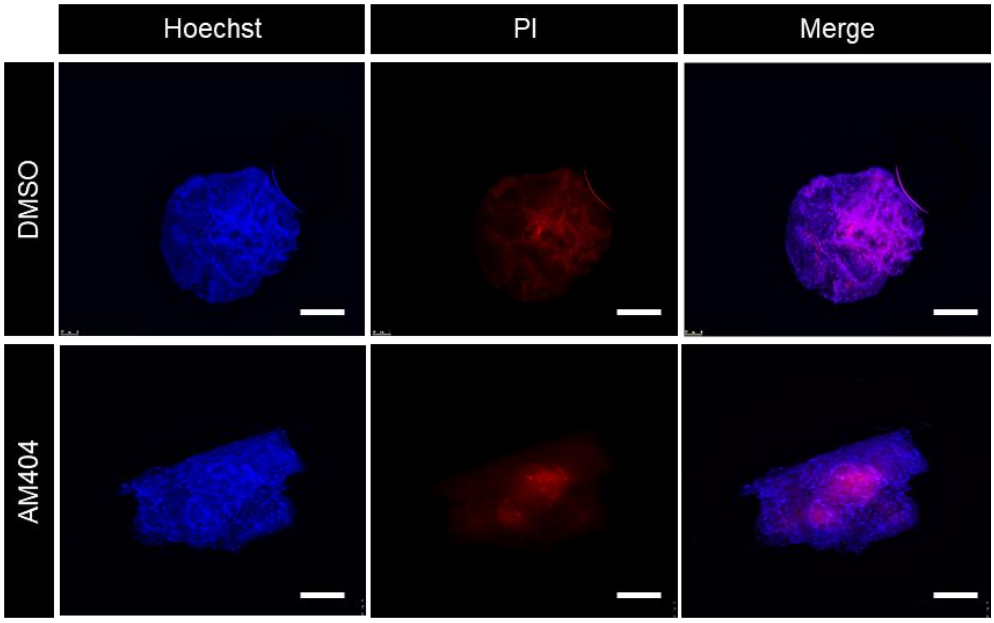


Figure 4-17: AM404 treatment hindered the growth in in tumour organoid. Volumes of organoids were measured every 2 days for the whole treatment period. Number of organoids in different size groups (diameter) at the end of the treatment shows significant inhibition to the tumour growth in the treated group. Numbers in each size group are expressed as percentage of the total. Error bars represent mean ± S.D. (n = 15; control, n = 10, AM404). *, $P < 0.05$; **, $P < 0.01$.

Cell dead/alive status was identified by PI/Hoechst staining. AM404 treatment showed slight/no reduction in PI staining followed by 6 days treatment period in tumour organoids (**Figure 4-18**). This result suggests minimal/no changes in cell death caused by AM404 on tumour organoids. These results are consistent with previously reported evidence that AM404 is well tolerated on mammalian cells and in animal models (Costa et al., 2006, Gerits et al., 2017). Moreover, AM404 treatment did not cause any difference in the organoid viability as compared to the DMSO-treated organoids (**Figure 4-18**). Taken together, these results may indicate that AM404 induces differentiation, without necessarily killing the cells and thereby influencing the sensitivity to chemotherapeutic drugs.



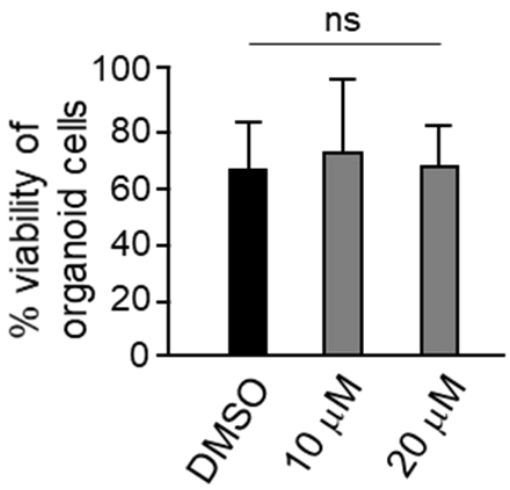


Figure 4-18: Hoechst/PI staining on AM404 treated organoids. The similar pattern in PI staining indicates no changes in cell death upon AM404 treatment. (n = 10). Scale bar: 25 μm.

4.2.4 *Ex vivo* treatment of CRC patient biopsies evaluates AM404 response as an anticancer drug

The data from monolayer cells, 3D colonospheres, and patient-derived organoids have shown that AM404 impedes the growth and can induce morphology change while reducing the stem-like properties. However, it has been repeatedly reported that tumour microenvironment and heterogeneity can limit the predictive response of existing biomarker-based therapeutic strategies (Yamada and Cukierman, 2007, Majumder et al., 2015). In this regard, in recent years, in recent years, an *ex vivo* culture of human tumours shows that they can reliably manifest the tumour growth in vivo (Karekla et al., 2017a). Though *ex vivo* explants have been reported to be more viable in the short-term culture method (Karekla et al., 2017a, Majumder et al., 2015), they can also grow at high frequency for long period and still present many of their *in vivo* properties, including tissue organization and architecture, retention of differentiated function; tumorigenicity; and the three-dimensional growth of different types of cells from a single tumour (Freeman and Hoffman, 1986).

In order to obtain patient relevant predictability of CRC response to AM404 while maintaining the original tumour architecture, we have exploited the *ex vivo* tumour explant model derived from CRC patients. Fresh tumour tissues from 7 patients were obtained following the surgery and processed immediately for culturing explants as outlined in **Chapter 2**; Materials and Methods (Karekla et al., 2017a, Majumder et al., 2015). Primary tumour tissue samples were cut in 2-4 mm segments and were maintained in complete organoid medium supplemented with Noggin 12-15 hours or overnight. Explant samples were then treated with the AM404 for 24h. The initial tissue recovery period of 15-17 hours was selected based on previously published data (Karekla et al., 2017a, Majumder et al., 2015). Tissues were fixed overnight in 10% neutral-buffered formalin (NBF) and processed for hemotoxylin and eosin (H&E)

staining or immunohistochemistry (IHC). Quantification of staining was carried out as outlines in **Chapter 2;** Materials and Methods.

Our result showed a trend of decreasing cell proliferation and stemness marker with increasing differentiation marker in AM404 treated tissue explants. In addition, no change in their apoptosis level was also observed (**Figure 4-19**). This was found to be consistent for tumour explants generated from all the CRC patients, with 5-6 images analysed per tumour sample.

The nuclear and nucleolar protein Ki-67 is an established prognostic and predictive indicator for the assessment of biopsies from patients with cancer. Ki-67, being expressed in proliferating cells from G1 to M phase of the cell cycle with exception of the resting phase G0 (Jing et al., 2019), makes it an excellent marker for determining the growth fraction of a cell population. Ki-67 negative cells, however, represent the cells temporarily withdrawn from the cycle (Darzynkiewicz et al., 2015). Our results showed that levels of Ki-67 staining and number of proliferating cells were significantly reduced (20%) by 24 h AM404 treatment as compared to the control-treated group on explant model (**Figure 4-19**, A). In line with the colonosphere data, AM404 treatment on explant model also showed no significant change in the cell death, as evident with Caspase-3 staining (**Figure 4-19; B**). Generally, Caspases are ubiquitously expressed intracellular cysteine proteases mediating cell death and inflammation (Choudhary et al., 2015). Amongst them, Caspase-3 has long been regarded as the hallmark of apoptosis and expression of active caspase-3 in cells and tissues represents cell death induced by a wide variety of apoptotic signals. (Wang et al., 2017b, Galluzzi et al., 2011). Of note, within the organoid culture, cell death was observed at the end of 2 weeks treatment period, however, this result was also observed in the similar fashion for the vehicle-treated organoids. This may further suggest the cell death in organoids being independent of AM404 treatment. Therefore, to associate the candidate

compound with cellular differentiation and stem-like activity, CDX2 and CD44 were also used as markers for differentiation and 'stemness' in tumour explants (**Figure 4-19; C and D**). Overexpression of CDX2 has been strongly implicated in various cancer, as previously shown to induce differentiation and inhibit proliferation in CRC (Yu et al., 2019, Qualtrough et al., 2002). Our result showed a significant increase in CDX2 expression in tumour explants treated with AM404 suggesting induction of differentiation in the AM404 treated tissue explants. This result also supports the 1.5-fold increase in CDX2 expression in AM404 treated colonospheres as previously shown (**Figure 4-14; B**). In line with the proliferation pattern, CD44 also showed to have a similar trend in significantly reducing the stemness level in cultured tumour explants from 7 CRC patients treated with AM404 (**Figure 4-19; D**). Thus, treating these tumour explants with AM404 shows a reduction in proliferation and stemness while also increasing the level of differentiation characteristics in CRC.

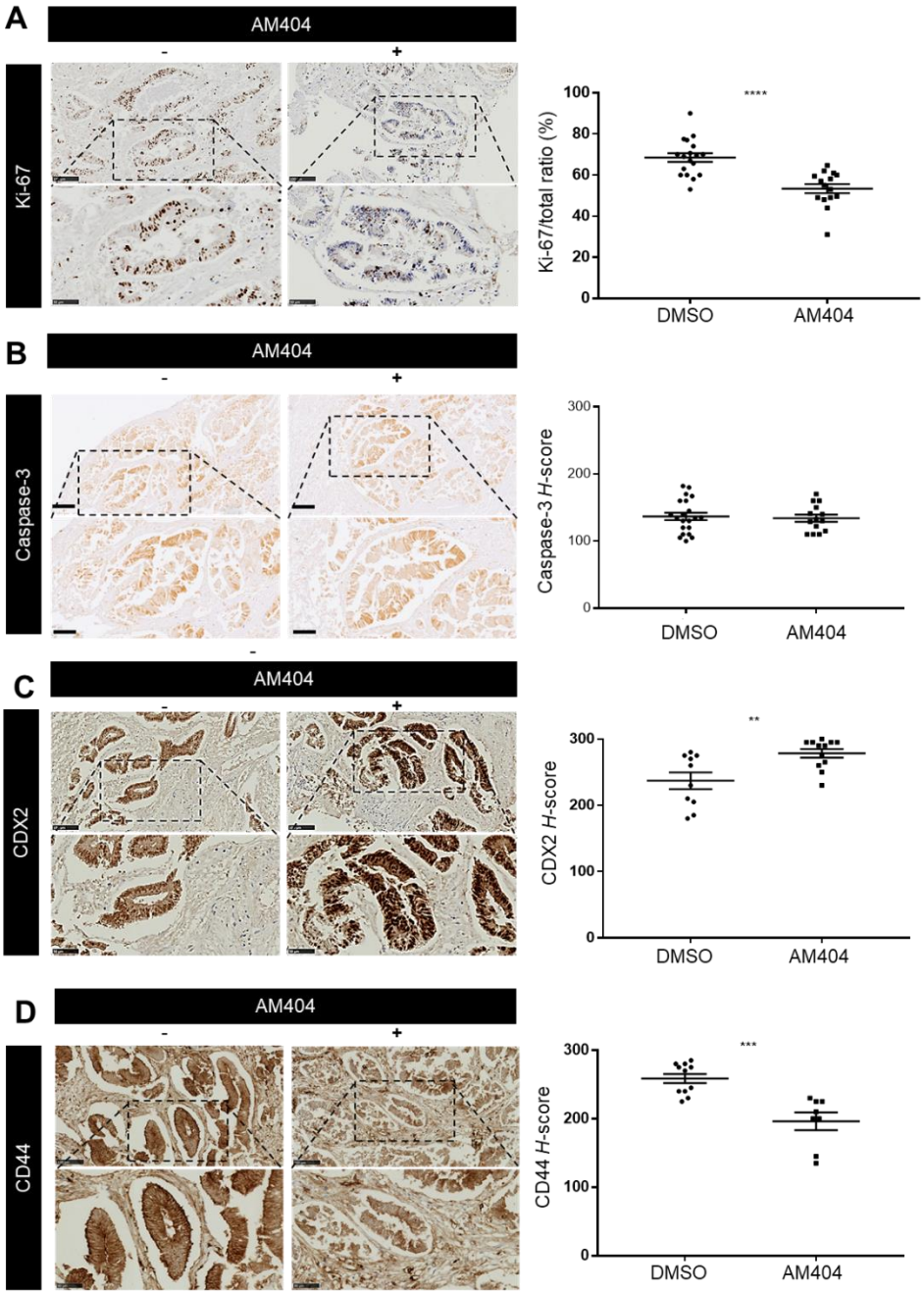


Figure 4-19: Effects of AM404 treatment on proliferation, apoptosis, stemness and differentiation level in the tissue explants obtained from CRC patients. (A-D) Proliferation was assessed by quantitating Ki-67 **(A)** IHC staining, cell survival by caspase-3 **(B)**, whereas differentiation and stemness levels were assessed by CDX2 **(C)** and CD44 **(D)** staining quantification respectively. IHC stains were counterstained with hematoxylin and eosin. Representative images (top panel) shows the images at 20x magnification with

a scale bar of 100 μm. Bottom panel shows the selected parts in higher 40x magnification with scale bar 50 μm. Each dot (Right panels) represents an image used for quantification. Control treated groups represents the level of intrinsic proliferation, stemness and differentiation level in tumours. For the Ki-67 staining, Ki-67 +ve cells were counted and expressed as a percentage of the total cells. In case of Caspase-3, CDX2 and CD44, H-scores were used as a measure for the quantification. Tumour tissues were obtained from 7 different patients, and 4 segments of tissue were used for each patient. **, $P < 0.01$; ***, $P < 0.001$.

4.2.5. FBXL5 mediated AM404-induced anticancer activity

To identify the expression of specific targets associated with AM404 mechanism on CRC, the transcriptome of DLD-1-colonospheres treated with AM404 and controls was compared. Total RNA was isolated from colonospheres, and transcriptomic assessment was carried out by GeneChip™ Human Gene 2.1 ST Arrays in collaboration with the Nottingham Arabidopsis Stock Centre (NASC), School of Biosciences, and University of Nottingham. One of the major advents of using the RNA isolated from colonosphere is that it enabled the specificity of AM404's effect on CSC-like properties.

The gene expression profile data were subjected to analysis by the Partek Genomics Suite and values were log2 transformed and quantile normalised using the Robust Multi-array Average (RMA). A clear separation was observed between AM404-treated and control groups, suggesting discrete transcriptome signatures for these two populations as evident in the Principal component analysis (PCA) plot (**Figure 4-20**). PCA plot shows a scatterplot with axes corresponding to the two different principal components. Microarray analysis emphasising on 2 or more-fold changes and a *p*-value of 0.001 or less revealed that AM404 caused significant changes in the regulation of 323 genes after the false discovery rate (FDR) correction (**Appendix 4**) (**Figure 4-21**). FDR was calculated by determining the ratios of expression values between replicate controls that exceeded the AM404 treated/control expression ratio and dividing by the rank order of the treated/control ratio (Bang et al., 2019).

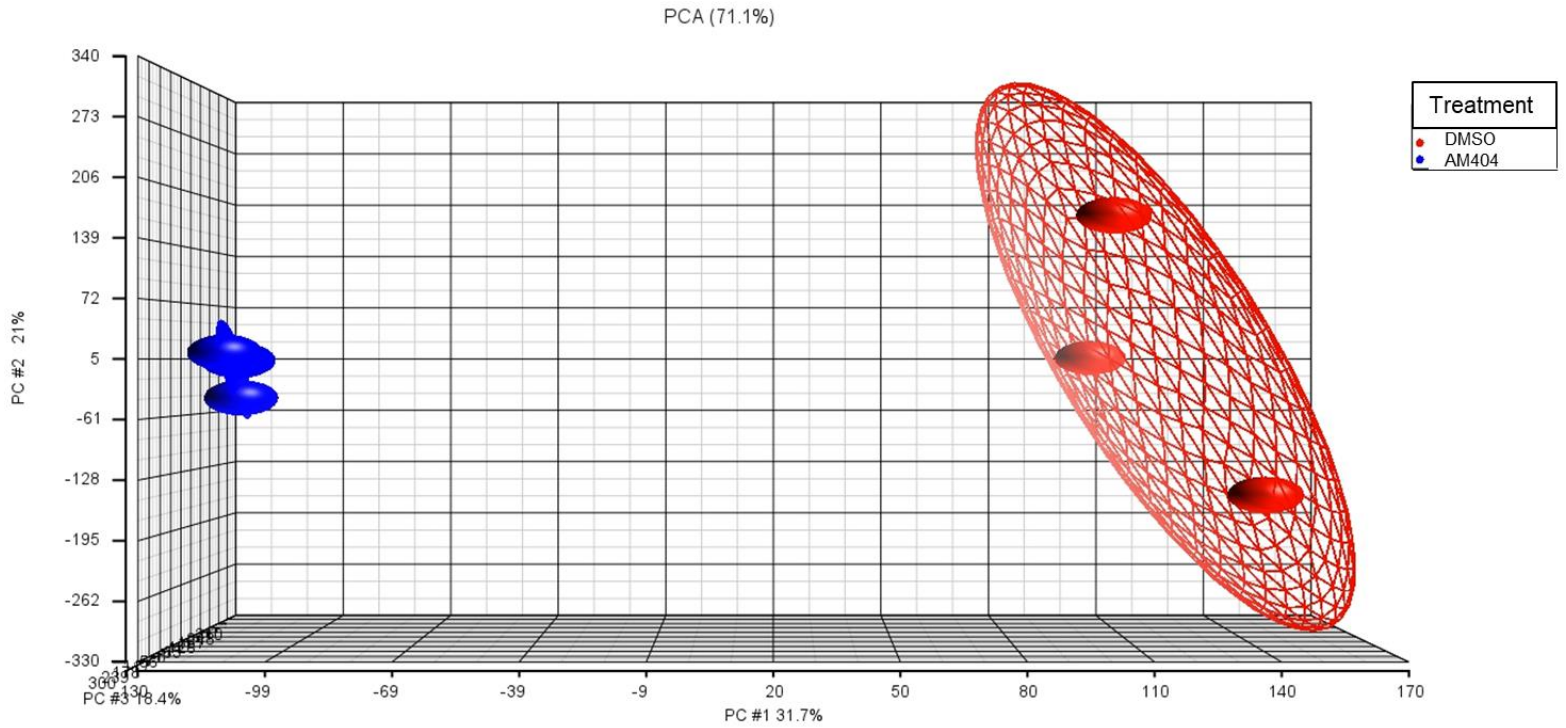


Figure 4-20: PCA analysis of variant genes for AM404-treated and control (DMSO) colonospheres. The red circles correspond the control and blue circles present AM404 treatment. PCA analysis denoted a marked distinction between these two groups.

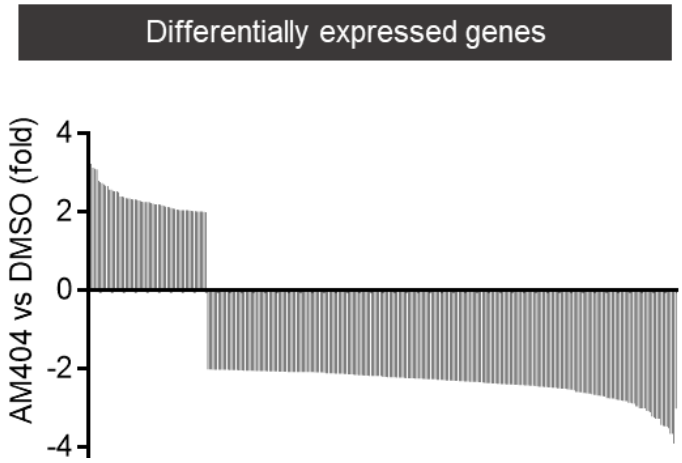


Figure 4-21: Differentially expressed genes on DLD-1 derived colonospheres treated with AM404. Each bar represents one gene that has a p-value of 0.001 or less and is 2 or higher fold increased or decreased on colonospheres following the drug treatments.

As predicted by the status of colonospheres treated with AM404, the gene ontology (GO) pathways associated with 2.5 or more-fold down-regulated and overexpressed genes in 75 genes (**Appendix 4**) were mainly associated with the cell cycle, DNA damage, and protein ubiquitination/ degradation signalling (**Figure 4-22**).

Among these top biological processes, and the 16 genes with changes of 3-fold or greater as plotted in a heatmap (**Figures 4-22 and 4-23**), protein ubiquitination is of major gene expression regulatory mechanisms of many proteins on a post-translational timescale using the ubiquitin-proteasome system. Due to the time restriction at this point of the project, validation assay using qPCR assay was carried out for 7 genes amongst these 16, in collaboration with co-supervisor Dr Roya Babaei-Jadidi (**Figure 4-24**).

The specificity of proteolysis for any particular substrate is determined by its association with a specific E3-receptor subunit. F-box proteins are the substrate-recognition components of the Skp1-Cul1-F-box-protein (SCF) E3-ubiquitin ligases. Accordingly, F-box proteins can function as oncoproteins when overexpressed (if their substrates are tumour suppressors) or as tumour suppressors (if their substrates are oncoproteins). For example, as one of the major interest of our lab, we have extensively studied FBXW7, a commonly mutated tumour suppressor gene in human tumours including 10-15% of CRC, which, was significantly increased upon AM404 treatment (**Figure 4-14, D**) (Ahmed et al., 2019, Lorenzi et al., 2016b, Babaei-Jadidi et al., 2011b, Nateri et al., 2004).

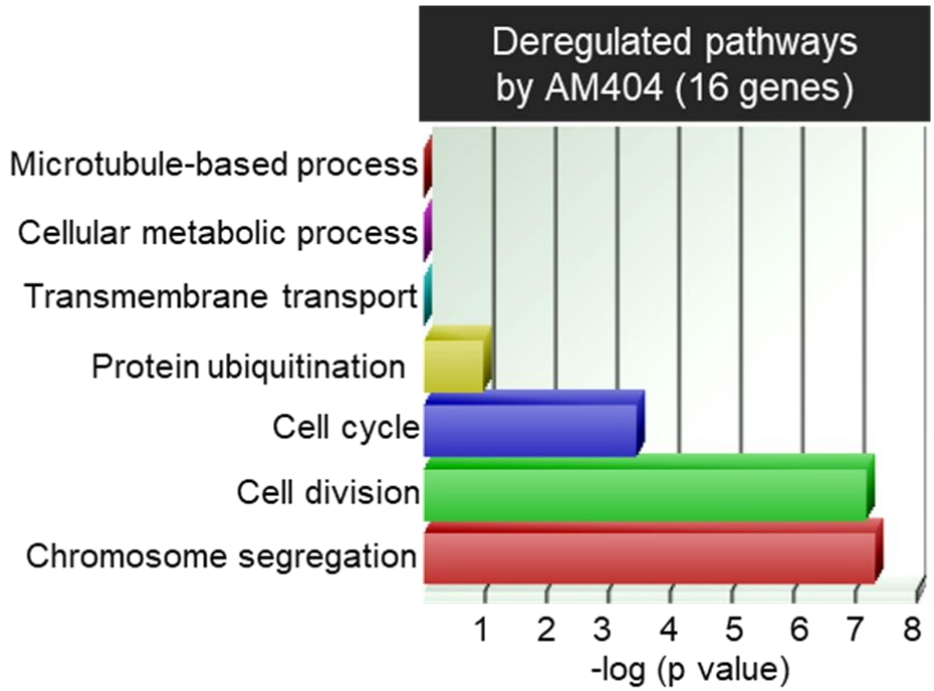


Figure 4-22: Gene ontology showing the biological processes affected by the top sixteen differentially expressed genes. Functional annotation

clustering with default settings was used; medium stringency and Benjamini–Hochberg correction was applied. Only the enriched GO terms with FDR <0.05 were selected and displayed in the bar chart.

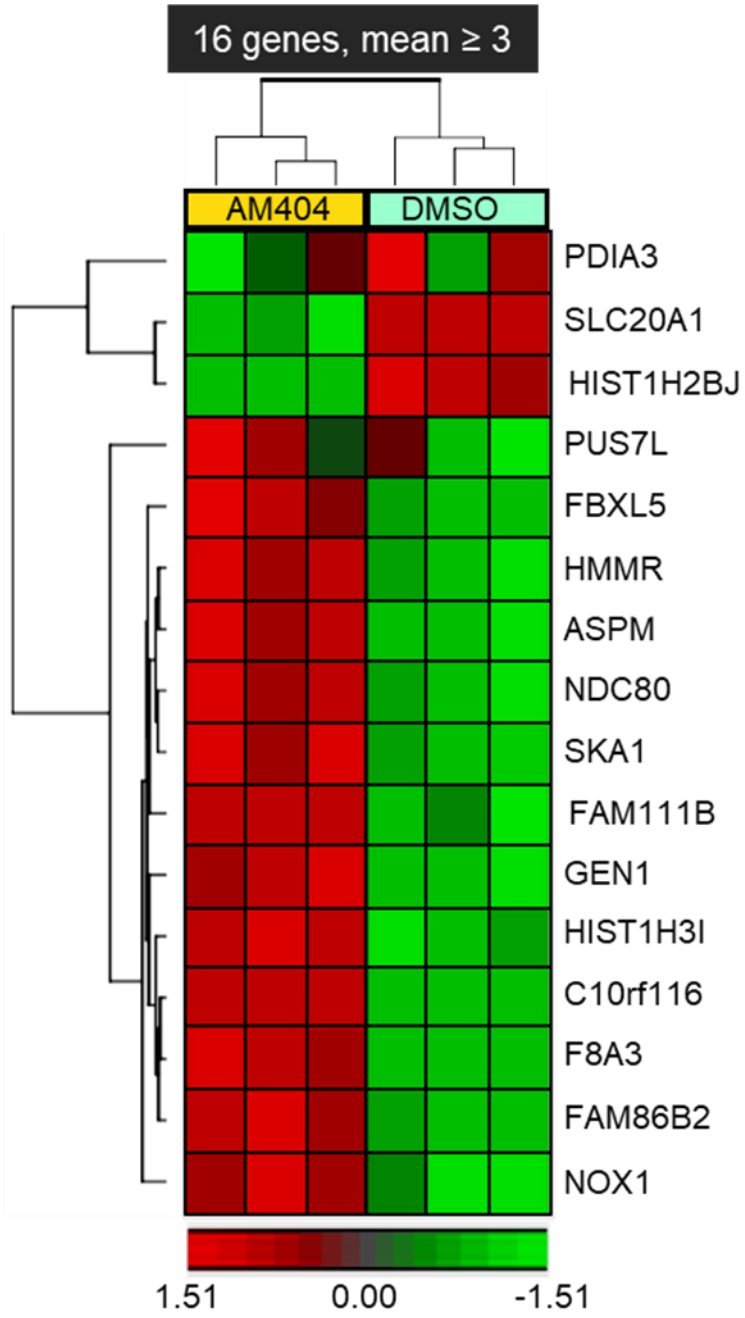


Figure 4-23: Heat-map representation of unsupervised clustering of the 16 differentially expressed genes (≥3-fold change) by AM404 in DLD-1 derived colonospheres. Each row represents a single gene. Colour code within the graph represents: green, downregulated; and red, upregulated. Horizontal and vertical clusters were created based in Euclidean distance.

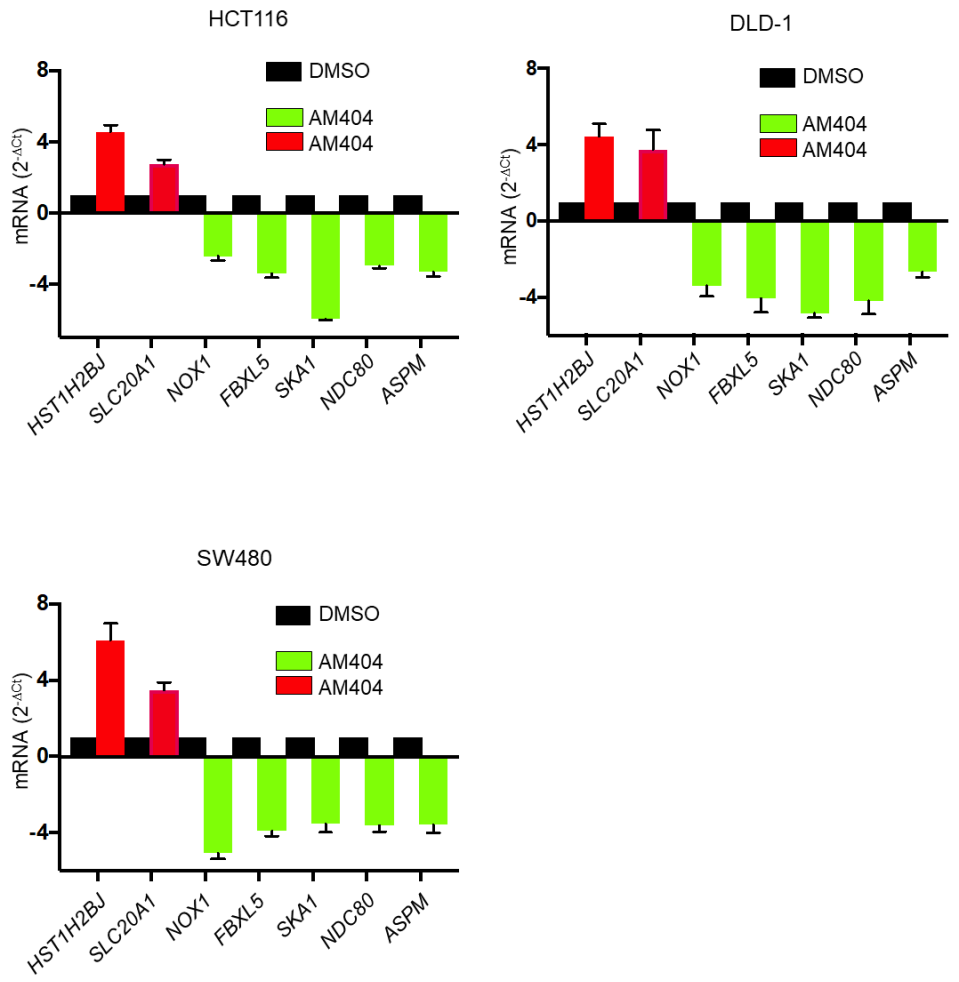


Figure 4-24: mRNA expression levels of seven differentially expressed genes in AM404 treated colonospheres. Seven different genes with differential expression including *FBXL5* obtained from the microarray analysis were confirmed by RT-qPCR analysis in colonospheres derived from HCT116, DLD-1 and SW480 cells. Error bars represent S.D. (n = 3; $P < 0.01$).

FBXL5 (F-box and leucine-rich repeat protein 5), also known as FBL4 and FBL5, is a member of the F-box protein family, characterised by an F-box motif consisting of 40 amino acids (Diaz and de Herreros, 2016, G et al., 2015, H et al., 2018). It is predominantly an iron and oxygen-regulated SCF-type E3 ubiquitin ligase containing an N-terminal hemerythrin-like

domain, α-helix-rich structure (Muto et al., 2017, Diaz and de Herreros, 2016). Based on the data suggesting AM404 changed EMT and CSC-like activity (**Figure 4-14**), and recent studies indicating FBXL5 regulating CRC metastasis, we then wanted to elucidate whether AM404 exerted its noted effects via FBXL5 in CRC cells (Machado-Oliveira et al., 2015, Yao et al., 2018, Dragoi et al., 2014).

A CRISPR-Cas9 mediated *FBXL5*-knockout DLD-1 cell line generated by my colleagues Nicholas Jinks and Seyed Mohammad Hossein Kashfi was used to evaluate AM404's effect in cell migration (**Figure 4-25**). At first, the cytotoxicity assay confirmed that loss of FBXL5 induced sensitivity to AM404 in CRC cells (11.5 μM vs 15.3 μM; $P < 0.05$, $P < 0.01$, $P < 0.001$) (**Figure 4-25**). Linking this result to the antitumorigenic effects exerted by AM404, FBXL5 may serve as a potential therapeutic target of CRC. Next, cells were synchronised by serum starvation, and performed scratch wound healing assays as described in **Chapter 2**; Materials and Methods (Liang et al., 2007). One of the particular advantages of this assay is that it allows live cell imaging, and mimics the cell migration by interaction with extracellular matrix (ECM) and cell–cell interactions *in vivo* (Liang et al., 2007). A cell free area was created in the confluent monolayer of DLD-1 and *FBXL5*-knockout DLD-1 cells by mechanical damage. Migration of cells within this area was measured by comparing the images taken at different intervals of 0, 12, 24, 48 and 72 h (**Figure 4-26**). The result showed that AM404 significantly reduces the migration of DLD-1 cells (**Figure 4-26, 4-27**, Black vs Red columns). AM404, being sensitive to *FBXL5*-knockout cells, showed to mimic this effect and caused further additive effect in inhibiting cell migration (**Figure 4-26, 4-27**, Blue vs Red columns). Of note, deletion of FBXL5 itself caused reduction on the migratory effect, suggesting FBXL5 as an important factor for migration. Furthermore, in between two treatment groups, AM404 treatment caused significant reduction in metastasis in *FBXL5*-knockout cells than that of WT DLD-1 cells (**Figure 4-27**). This finding

postulates FBXL5 as a potential target via which AM404 exerts its effects on CRC metastasis.

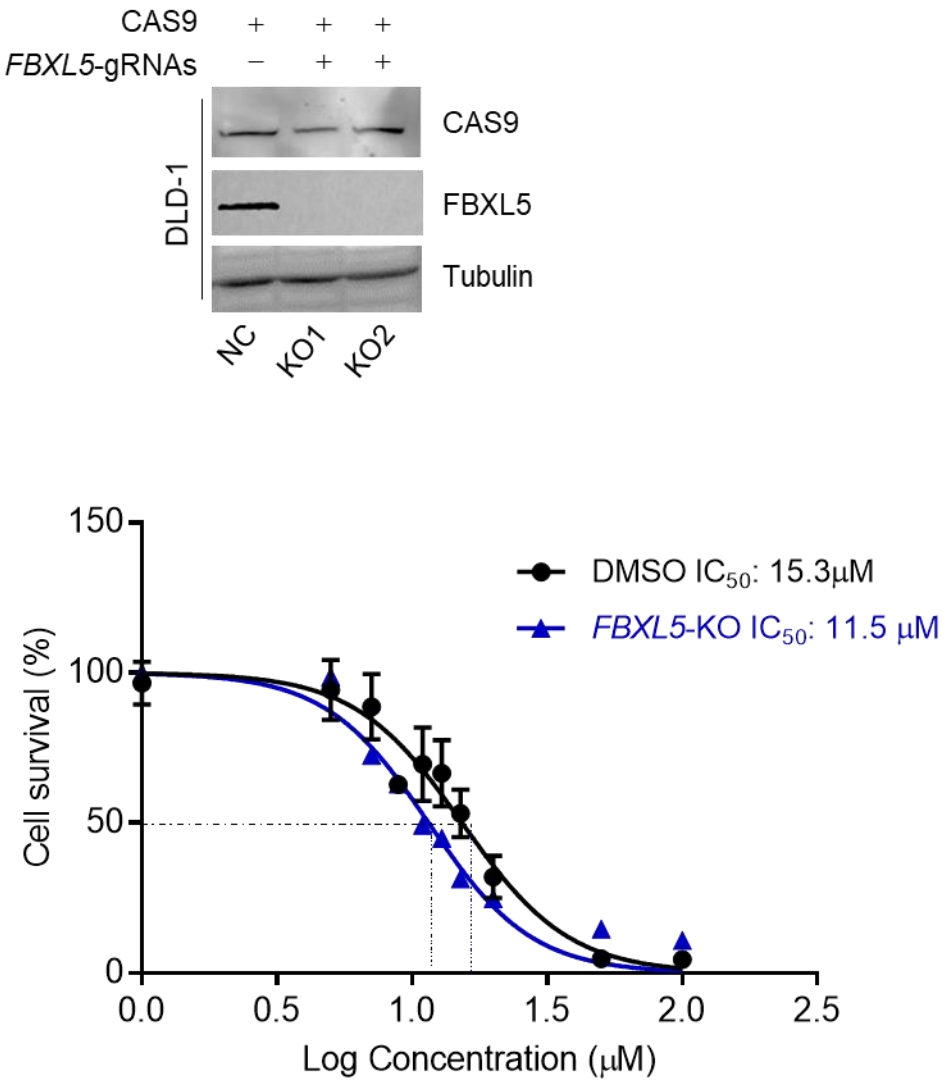


Figure 4-25: Cytotoxicity assay of AM404 in DLD-1 and *FBXL5*-knockout DLD-1 cell lines using sulforhodamine B (SRB). Survival curves were denoted by DLD-1 (black), and FBXL5-knockout DLD-1 (blue) treated with AM404. The dotted line represents half maximal inhibitory concentration

(IC_{50}). Nonlinear regression was used to plot the data. Experiments were performed at least three independent occasions (n = 6). Error bars represent mean ± S.D. (n = 6, *, P < 0.05; **, P < 0.01; ***, P < 0.001).

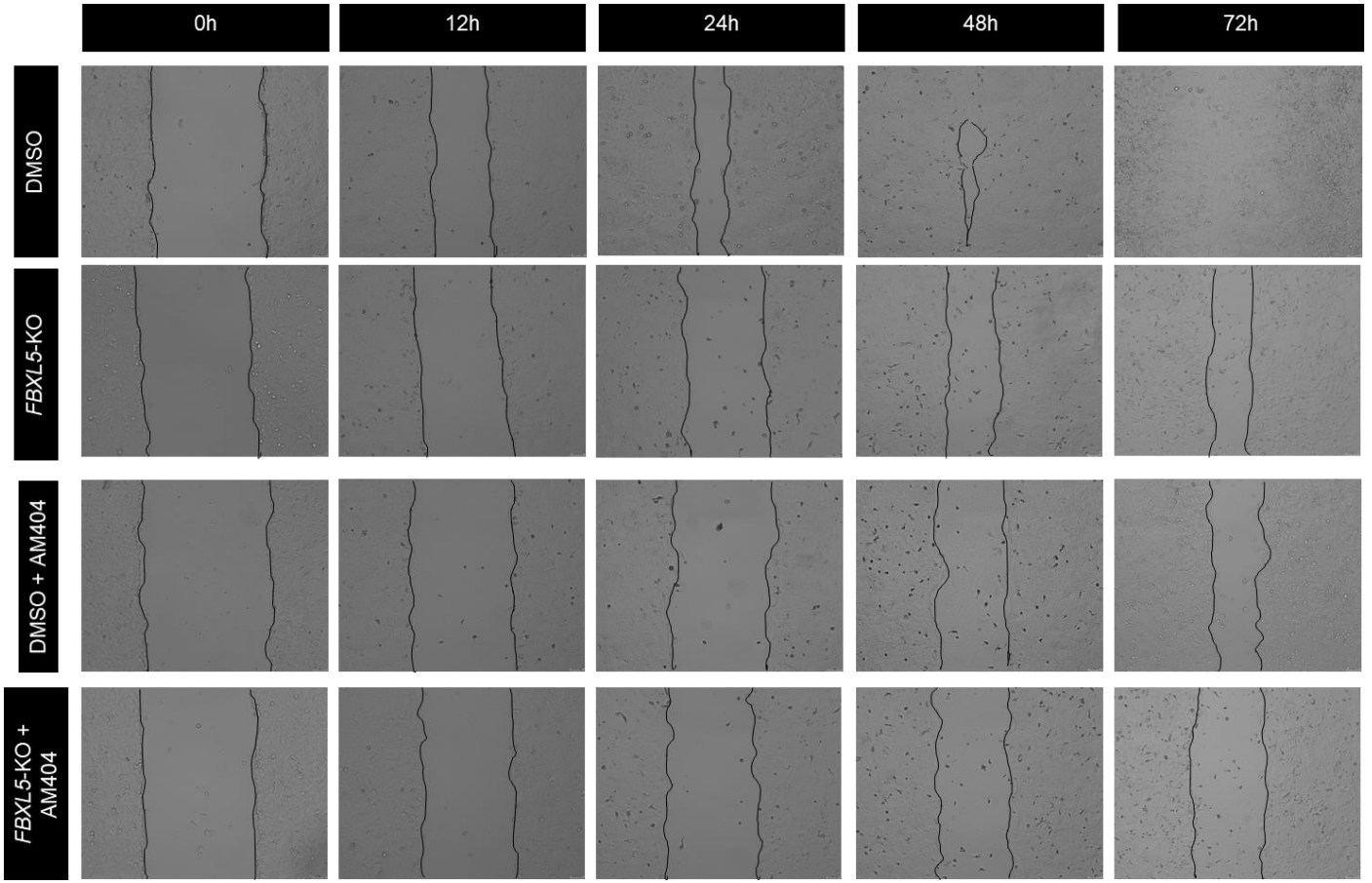


Figure 4-26: Inhibition of migration by AM404 in DLD-1 and *FBOXL5*-KO cells *in vitro*. Migration of DLD-1 and *FBOXL5*-KO cells was performed with scratch wound healing assay. Starved cells were scratch-wounded and wound width was measured to determine the healed distance at 0, 12, 24, 48 and 72 h.

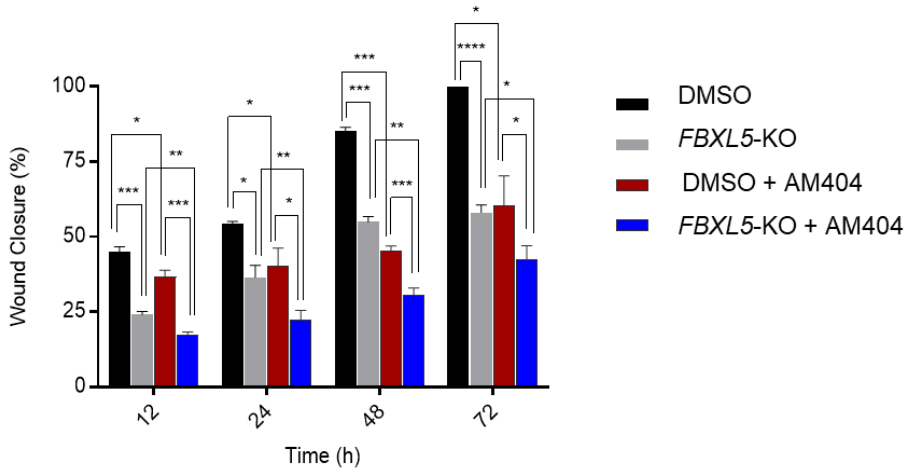


Figure 4-27: AM404 inhibits cell migration in DLD-1 and *FBOXL5*-KO cells. Significant reduction in cell migration was observed for both cell lines. Bars are expressed as mean ± S.D. (n =10). *, $p < 0.05$; **, $p < 0.01$; and ***, $P < 0.001$.

4.3 Discussion

Even though it has been well-established that tumour-promoting inflammation is involved in colorectal cancer (CRC), the inflammatory mediators and signalling that regulate the potency of anticancer treatment upon forced CSC differentiation are not fully defined. This study demonstrates the application of colonospheres, organoids and explant models to screen new antibacterial drugs for targeting CRC-SC and helps in better understanding the potential inflammatory mediators involved in CRC-related inflammation. The initial screening revealed AM404 as a potential compound to target CRC-SC, particularly for differentiation.

AM404, as an active metabolite of paracetamol, is currently being studied for its antibacterial and anti-inflammatory effects notably for reducing the production of IL-1β, IL-6 as well as decreasing oxidative stress and for their association with circulating tumour necrosis factor (TNF)-α in

murine models (Saliba et al., 2017). One of the major hallmarks of cancer highly focuses on inflammation specifically for cancer progression, development and proliferation. Due to this correlation, preclinical focuses highlighted several antibacterial, anti-inflammatory drugs for repurposing in cancer treatment.

NF-κB is one of the key transcription factors in inflammation that has been identified as one of the major contributors in cancer associated inflammation transition process. Activation of NF-κB is regulated via TNF and various cytokines including IL-6 (Diakos et al., 2014, Lasry et al., 2016). However, no NF-κB inhibitors are currently clinically available for the treatment of cancer (Diakos et al., 2014).

Previously, AM0404 has been reported to inhibit NF-κB and NFAT activation on neuroblastoma and glioma cells. In neuroblastoma cells, AM404 inhibited the NF-κB activation by targeting IKKβ phosphorylation and activation (Caballero et al., 2015) In addition, AM404 also impaired COX-2 expression, PGE2 release, migration and invasion in a cell specific manner (Caballero et al., 2015, De Lago et al., 2006). Of note, inhibition of COX-2 has an anti-tumorigenic effect in cancers that occurs due to prolonged chronic inflammation. It has been reported that AM404 inhibits COX-2 expression both at transcriptional and post-transcriptional levels (De Lago et al., 2006). Several pathways including Wnt–β catenin, PIK3CA/AKT/PTEN, and NF-κB, have been postulated as targets for NSAIDs (Diakos et al., 2014). In human T-cells, AM404 is a potent inhibitor of T-cell activation and inhibits both IL-2 and TNF-α in transcription and protein synthesis level in CD3/CD28-stimulated Jurkat T-cells regulating activation of NF-κB, NFAT, and AP-1 (Saliba et al., 2017). Moreover, AM404 associated inhibition in NFAT transcriptional activity was regulated through CB1 and TRPV1-independent mechanism (Caballero et al., 2015).

Based on the results from this study, we suggest AM404 as a new compound and FBXL5 as an associated key target gene with high therapeutic pharmacological potential to target human colorectal cancer. In our study, AM404 exhibited cytotoxic effects in 3 CRC cell lines with IC_{50} of 12-15 μM, suppressed cell growth and proliferation as well as reduced colony number and size. Data from the colonosphere study also supports this observation with extensive morphology change in AM404 treated colonospheres. Such morphology alteration was accompanied by significantly increased expression of differentiation marker MUC2 and reduced expression in stemness marker CD44. Therefore, these results indicate a correlation between AM404 induced morphology alteration and inhibition of tumorigenic activity with cellular differentiation. As the intestinal homeostasis requires a tightly controlled equilibrium between intestinal stem cell (ISC) proliferation and differentiation (Santos et al., 2018), increased level of differentiation marker highly stresses on further investigation focusing on stem-like characteristics. We showed that AM404 associated cell homeostasis caused reduction of CRC 'stemness' features, including cell proliferation and migration, as well as impeded tumour cells growth and morphology, and induction of CRC differentiation. Extending this observation to further characterisation of the inhibitory pathways, AM404 treatment showed significant reduction of the widely established stemness markers CD44, NANOG, BMI-1 and OCT4 whilst showing significant increase in differentiation marker CDX2 and KRT20 expression. This result was highly comparable when correlating with CSC-like properties, recurrence, poor survival, metastasis, and tumour suppressors. However, when interpreting CSC biomarkers, it is also to be noted that, not all CSCs will always express the same markers and some non-CSC cancer cells can also express these markers. Therefore, such markers are more reliable to identify CSC-rich subpopulations instead of definite isolation of all the CSCs (Chen et al., 2013b, Ahmed et al., 2017a). Based on this, these results were further validated in two more highly reliable patient derived 3D *in vitro* organoid

and *ex vivo* tissue explant models. Our organoid data showed clear evidence of AM404 induced growth impediment and altered morphology with more of branch formation while making no significant difference in cell death. This result was confirmed by PI staining suggesting similar pattern in cell death for both treated and untreated organoids. Additionally, the immunostaining of tissue explants also revealed no difference in apoptosis level but significant reduction in cell proliferation, stemness while increasing the differentiation status as an aftereffect of AM404 treatment. However, it has been reported that AM404 can produce an influx of calcium into cells, which might exert deleterious effects on cell proliferation (Jonsson et al., 2003).

All these results show novel promises on the principle aspects of differentiation therapy, which, in combination with conventional chemotherapy would offer an effective approach in targeting the CSCs and to treat CRC. Therefore, it is also necessary to evaluate AM404's effect in combination with other conventional CRC treatment regimens. Due to time limitation, this part yet to investigate during this study. In future, it will be interesting to look into AM404's effects in combination with currently marketed drugs for CRC treatment for subsequent pharmacokinetic and pharmacodynamic aspects.

In order to elucidate the mechanism by which AM404 exerts its effect in CRC, the gene array revealed 16 potential genes, including *FBXL5*, differentially expressed in AM404 treated colonospheres. Based on previous data and our lab interest, we have selected *FBXL5* gene, which showed over three folds decrease upon AM404 treatment, functioned as an oncogene in the progression of colon cancer through regulating PTEN/PI3K/AKT signalling (Yao et al., 2018) and HIF-1 transcriptional activity (Machado-Oliveira et al., 2015). To note, PIK3CA/AKT/PTEN signalling have been postulated as one of the potential targets of NSAIDs for tumour associated inflammation (Diakos et al., 2014). Therefore, it might be worthwhile to investigate this pathway and its association with

AM404 targeting FBXL5. Simultaneously, loss of FBXL5 caused more sensitivity to AM404 treatment. Our result showed that CRC cells with loss of FBXL5 tended to be more sensitive to the cytotoxic effects of AM404. This could therapeutically be implicated in a way that, as since FBXL5 expression in CRC correlates with tumour proliferation and malignancy, the development of AM404 as an anticancer drug would be valuable for treatment of such tumours harbouring FBXL5 deletion.

FBXL5 has previously been interpreted as oncogene whilst its association in iron regulation is required for HSC self-renewal (Muto et al., 2017). In CRC progression, FBXL5 has shown to induce cell proliferation, growth, tumorigenesis and inhibiting cell apoptosis while its overexpression resulted in high tumour formation ability (H et al., 2018, AM et al., 2014). Furthermore, they have also been reported to negatively regulate several EMT inducers, such as Notch, c-Myc and mTOR, particularly in gastric and cervical cancer (Diaz and de Herreros, 2016, H et al., 2018). It has been markedly reported that, silencing FBXL5 showed decrease in metastasis with significant increase in expression of E-cadherin at posttranscriptional level (AM et al., 2014). In line with this, AM404 showed significant reduction in the expression level of N-cadherin and Vimentin associated in EMT, and by mimicking the effect of *FBXL5* deletion, it also significantly prevented the invasion in CRC cells. Furthermore, AM404 suppressed the expression of *FBXL5* E3-ligase, where AM404 sensitivity was mimicked by *FBXL5*-knockout. However, deletion of FBXL5 itself caused an inhibitory effect in CRC migration, which showed further additive effects upon AM404 treatment. In this regard, to confirm if FBXL5 is required for cell migration process, a functional experiment would be to abolish AM404 associated effect by overexpressing FBXL5 in CRC cells. However, characterisation of other F-box proteins is also required for their roles in cancer, which could be a key breakthrough for cancer therapy and offer a potential new

biomarker(s) for early detection of epithelial tumour progression including CRC.

This study, therefore, uncovers a new molecular mechanism for AM404-targeting FBXL5 oncogene which mediates chemo-resistance and CRC invasion, thereby proposes to repurpose antibacterial AM404 as an anticancer agent (Ahmed et al., 2019).

CHAPTER 5

Antibacterial Rifabutin Functions as an Anti-CRC drug

5.1 Introduction

Interestingly, in the colonosphere screening, three rifamycin drugs including rifabutin, rifapentin and rifampicin showed the lowest CDy1 fluorescent intensity in their respective plates, indicating high level of reduction in stem-like activity induced by this group of drugs (**Chapter 3: Figures 3-10, 3-12**). Rifamycins are prokaryotic DNA-dependent RNA polymerase inhibitors that typically act by inhibiting the transcription and protein synthesis (Crabol et al., 2016, Ma et al., 2007).

Rifabutin, previously named ansamycin or LM 427, is a broad-spectrum antibiotic primarily used to treat tuberculosis. It is a semisynthetic antibiotic derived from rifamycins, and has higher intracellular penetration, tissue distribution and reduced cytochrome P450 enzyme induction than rifampicin (Crabol et al., 2016, Ma et al., 2007). Rifabutin has a chemical formula of $C_{46}H_{62}N_4O_{11}$ **(Figure 5-1)**. The four hydroxy groups located at the C-1, C-8, C-21, and C-23 positions are essential for its antibacterial activity (Ma et al., 2007). It is active against Mycobacterium tuberculosis, non-tuberculous mycobacteria (NTM), Neisseria gonorrhoeae, Neisseria meningitides, Haemophilus influenza, Campylobacter spp., Helicobacter pylori, Toxoplasma gondii, staphylococci, group A streptococci, and a variety of gram-positive and gram-negative bacteria (Kast et al., 2017, Crabol et al., 2016).

In parallel to the antibacterial activity, rifabutin has recently been proposed to repurpose for different cancer types treatment (Li et al., 2016b, Lim et al., 2013). This study focused on rifabutins' anticancer effects on CRC.

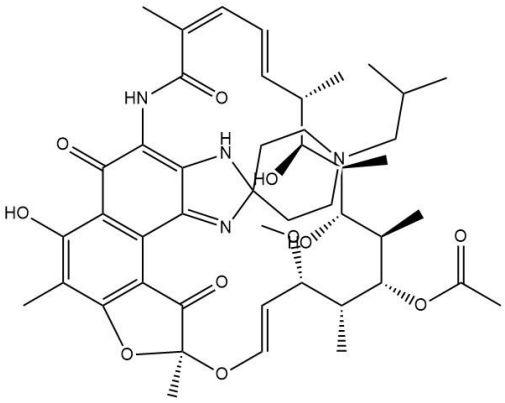


Figure 5-1: Schematic representation of the structural formula of rifabutin (PubChem CID: 135398743).

Using *in vitro* 3D colonosphere, patient derived organoids, and *ex vivo* tumour explants models, the specific objectives of this study were to:

(I) evaluate rifabutins' potential in inhibiting de-differentiation and stemness properties of CRC stem-like cells.

(II) evaluate rifabutins' effect on growth impairment and morphology alteration.

(IV) identify FBXL5 as one of the targets by which rifabutin exerts its anticancer effect on CRC

5.2 Result

5.2.1 Re-validation of the anti-cancer activity of rifabutin in colonospheres

Rifabutin was characterised as one of the candidate compounds with high potential for inducing differentiation in colonospheres (**Figure 5-2;** A **and Chapter 3**). Several *in vitro* experiments were carried out to re-validate this postulation, and therefore, our results further showed more

than 70% reduction in the stem-like activity upon treatment with rifabutin (**Figure 5-2;** B).

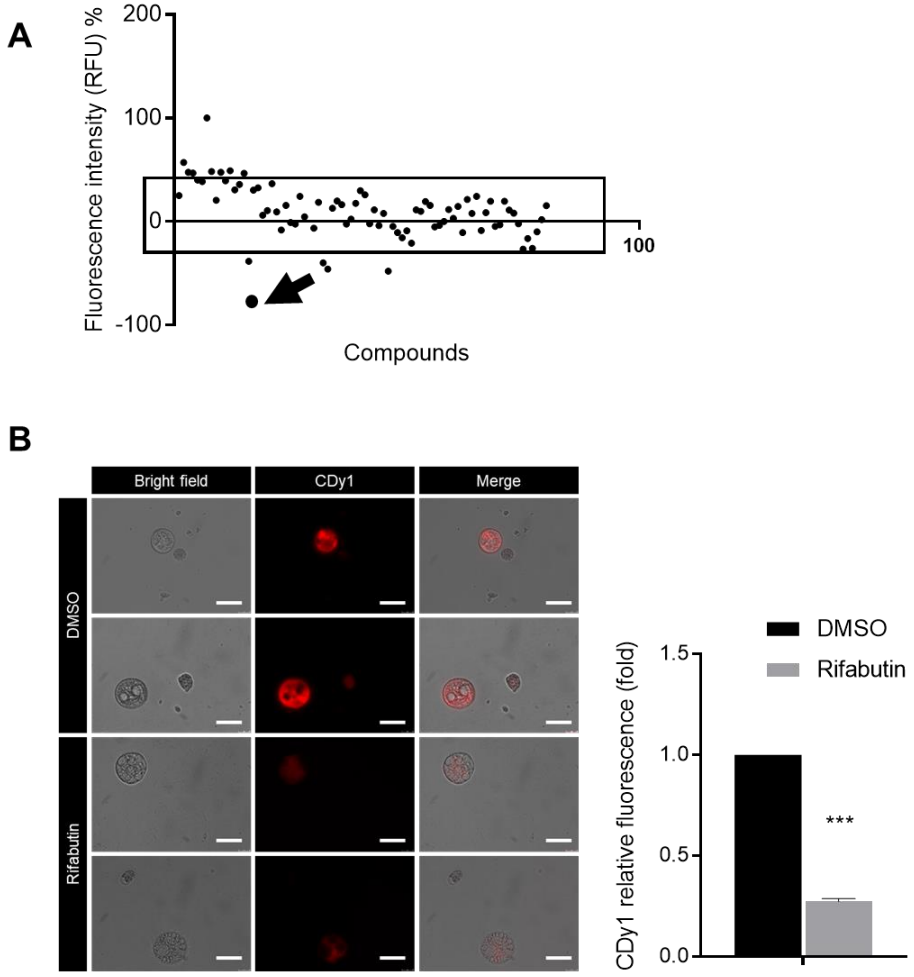


Figure 5-2: 3D drug screening revealed rifabutin is inducing differentiation in colonosphere. (A) Rifabutin (arrowhead) caused a reduction in the relative fluorescence presented by CDy1. Fluorescence intensity of DMSO-treated (control) colonosphere was set as 0. Intensities exerted by all compounds were presented as a percentage of their induction or reduction of stem-like activity. Image was reproduced from the primary screening of NIH clinical collection Plate 3 carried out on colonospheres derived from HCT116 cells (Figure 3-10). **(B)** Representative images of

CDy1 stained DMSO-treated (control) and rifabutin treated colonospheres. Scale bar: 25 µm. rifabutin showed significant reduction in the CDy1 intensity of treated colonospheres. rifabutin caused more than 70% reduction in the CDy1 intensity in treated colonospheres.

5.2.1.1 Cytotoxicity assay of rifabutin

To evaluate the effects on CRC, cytotoxicity assay was performed on HCT116, DLD-1 and SW480 cell lines with a range of increasing concentrations of rifabutin (from 1 to 100 μM) (**Figure 5-3**). Cytotoxicity assay was performed by SRB-based colorimetric assay and IC_{50} values were determined as described in **Chapter 2**; Materials and Methods (Li et al., 2019b). The IC_{50} values obtained from CRC cell lines (26-27 μM) were found to be in the range of previously reported IC_{50} (7 μM - 34 μM) in different cells (Li et al., 2016b, Parvez et al., 2016). The measured dose was then used throughout the experiments to carry out its in-depth evaluations on CRC, including treatments on patient-derived organoids and tissue explant models. Our results were highly comparable between the DLD-1 and SW480 cell lines, with their IC_{50} being 26 μM in both cell lines, whereas, rifabutin showed slightly more resistance towards HCT116 with an IC_{50} of 27 μM (**Figure 5-3**).

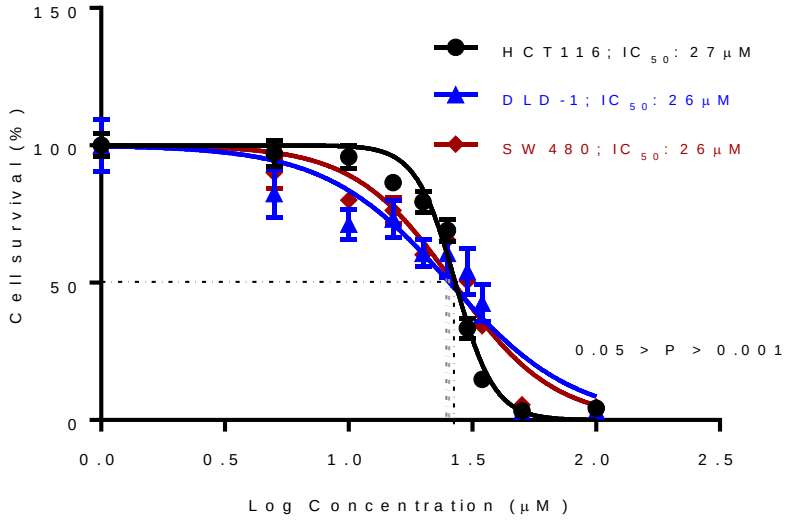


Figure 5-3: Cytotoxicity assay of rifabutin using Sulforhodamine B (SRB) on human colorectal cancer cell lines. Survival curves were denoted by HCT116 (black), DLD-1 (blue) and SW480 cells (red) treated with rifabutin. The dotted line represents half-maximal inhibitory concentration (IC_{50}). Error bars represent mean ± S.D. Nonlinear regression was used to plot the data. Experiments were performed at least three independent occasions (n = 6; *, P < 0.05; **, P < 0.01; ***, P < 0.001).

5.2.1.2 Rifabutin reduces the tumorigenic ability in CRC cell lines

Typically, the *in vitro* clonogenic ability of cells has a good correlation with the tumour responses *in vivo* (Kabakov and Gabai, 2018). In order to investigate rifabutin's effect on the tumorigenic property, following the cytotoxicity analysis, colony formation and cell growth curve analysis were then performed. Both clonogenic and cell growth assays strongly suggested morphological alteration and reduction in colony formation, size, as well as cell growth retardation by rifabutin in all CRC experimental cell lines (**Figures 5-4, 5-5**).

For all three experimental cell lines, colony formation assay was carried out as previously outlined in **Chapter 2;** Materials and Methods. At the end of 14 days, colonies were stained with crystal violet and were manually counted. The number of colonies was significantly lower in the rifabutin treated group (41% vs 29% on HCT116, and 43% vs 30% on DLD-1 cells; $P < 0.05$) (**Figure 5-4**). However, as also observed in **Chapter 3**, no colonies were formed in SW480 cell lines.

Next, to distinguish differences between morphology and possible structural alterations conferred by rifabutin, colonies were grown on coverslips and were stained with Phalloidin and DAPI. In accordance with the previous observations of 2D colonies, untreated cancer entities showed more compact and round structure (**Figure 5-5**). On the other hand, rifabutin-treated colonies lacked this integrity in their shape and formed protrusions within. Interestingly, the nuclear density of treated colonies is not only also less than the untreated ones, but also is more scattered throughout the colonies, especially at the edges. This could indicate that rifabutin induced certain level of cytotoxicity, or, since senescent cells do not form colonies, this might also indicate that, rifabutin has induced the cells to undergo senescence (Kabakov and Gabai, 2018). Another possible explanation for the morphological alterations could be induction of differentiation in the treated colonies.

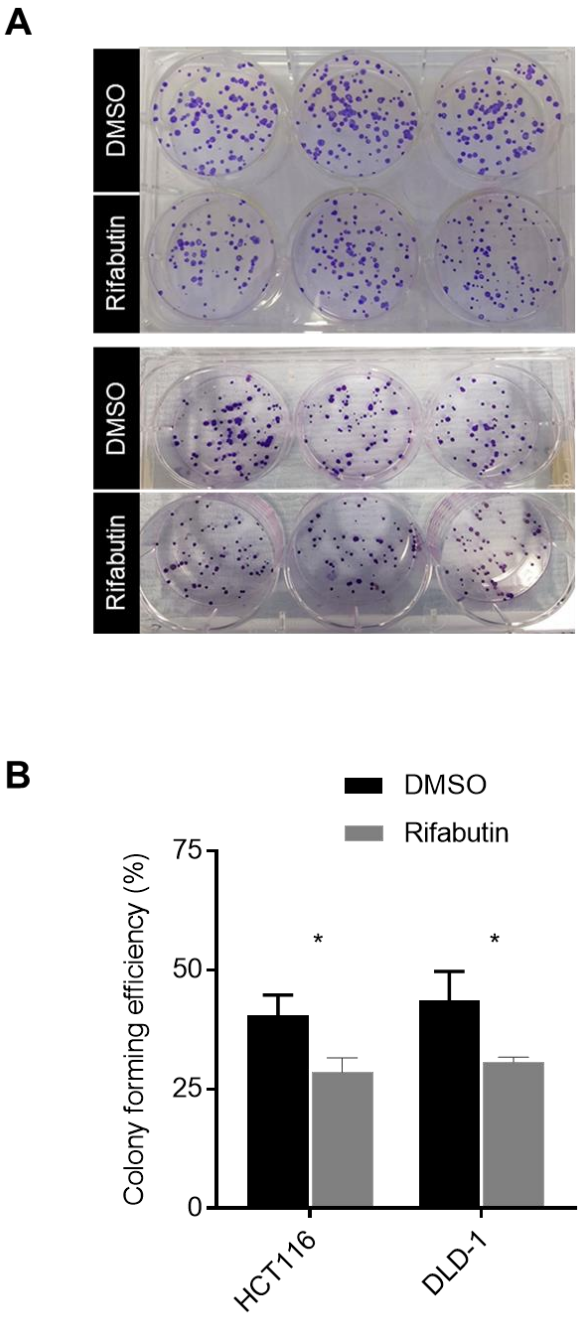


Figure 5-4: Rifabutin caused reduced colony formation and morphological changes in CRC cells. (A) Representative images of colony formation assay on HCT116 (top) and DLD-1 (bottom) cells. **(B)** Rifabutin showing significant reduction in colony formation assay in HCT116 and DLD-1 cells. $P < 0.05$. Experiments were performed three independent occasions ($n = 3$).

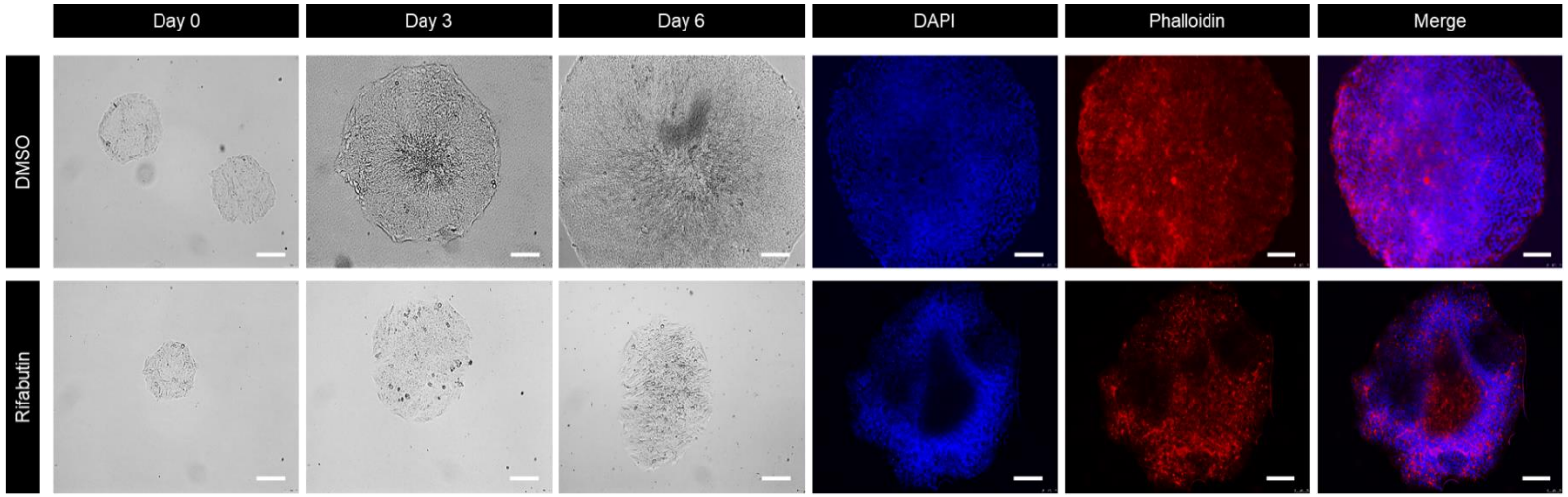


Figure 5-5: Rifabutin treatment on DLD-1 obtained cultured colonies and Phalloidin staining at the end of the treatment period. Nuclei were detected with DAPI-blue fluorescent stain. Scale bar: 75 µM.

Colony sizes were measured using ImageJ. Reduction in colony size was strongly evident within first 3 days of treatment (**Figures 5-5, 5-6, 5-7**). Sizes were greater on day 14 compared to day 8 for both rifabutin treated and DMSO-treated (control) groups. However, in both cell lines, rifabutin caused significant reduction in the colony sizes (1396 ± 211 μm vs 735 ± 100 μm for HCT116, and 1192 ± 188 μm vs 584 ± 198 μm for DLD-1 cells) (**Figure 5-8**). Moreover, DMSO-treated colonies showed a denser network between the cells, whereas, in rifabutin treated groups, scattered edges were visible throughout. The differences in size can also be speculated by comparing the microscope images in F**igure 5-6** and **Figure 5-7**.

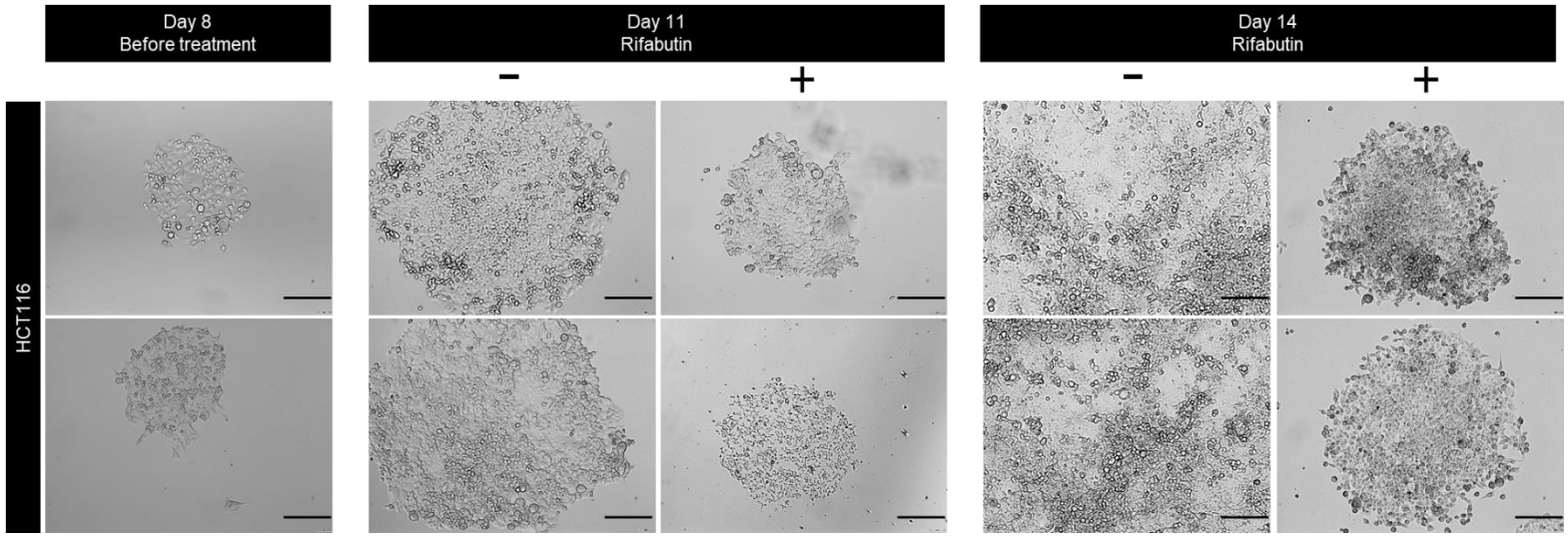


Figure 5-6: Rifabutin reduces the tumorigenic ability of HCT116 cells. Images were taken before rifabutin treatment on day 8, after 72 h on day 11 and on day 14. Day 14 control colonies showed a denser network of cells while day 14 treated colonies showed a less packed and smaller morphology with protruding edges. Scale bar: 75 μm.

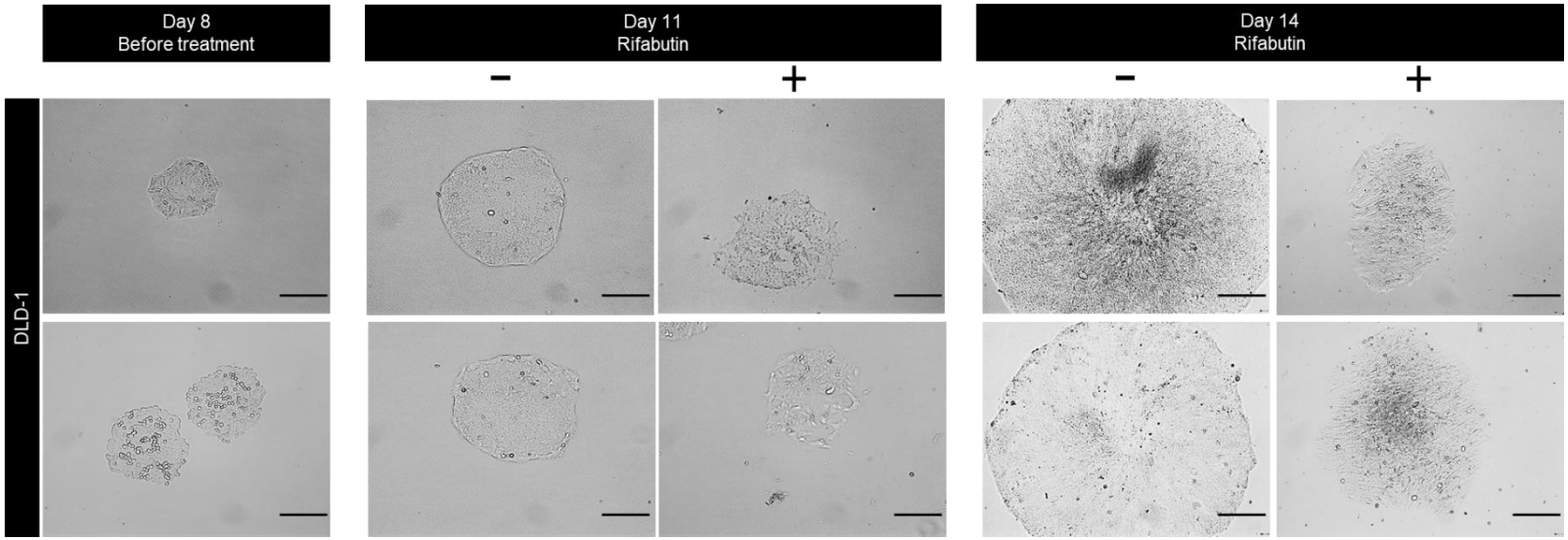


Figure 5-7: Rifabutin reduces the tumorigenic ability of DLD-1 cells. Images were taken before rifabutin treatment on day 8, after 72 h on day 11 and on day 14. Day 14 control colonies showed a denser network of cells while day 14 treated colonies showed a less packed and smaller morphology with protruding edges. Scale bar: 75 μm.

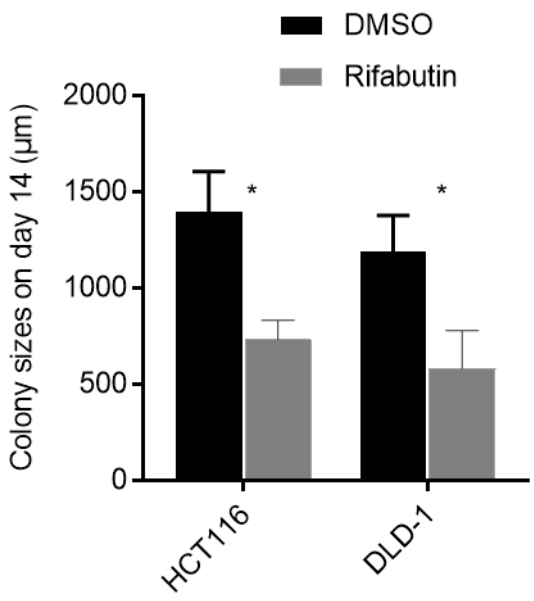


Figure 5-8: Rifabutin reduced the size of colonies in HCT116 and DLD-1 cells. Significant decrease in colony size were observed in both cell lines. Error bars represent mean ± S.D (n = 20). $P < 0.05$.

Additionally, reduction in cell growth and doubling time was strongly evident in all three cell lines upon rifabutin treatment. HCT116, DLD-1 and SW480 cells were treated with the IC_{50} of rifabutin (**Figure 5-3**) on day 1 and were counted daily at the same time for a period of 8 days (**Figure 5-9**). The number of cells in the treated groups were significantly lower throughout the experimental period (day 2-8). A distinct lag phase was absent in all cell lines, while in log phase cell growth showed an exponential fashion reaching the plateau on day 6. Rifabutin treatment, on the other hand, caused the cells to reach the plateau by day 5 (DLD-1 and SW480) and caused a shift in the population doubling time (PDT) from 21 h to 24 h, 22 h to 46 h, and, 33 h to 53 h in HCT116, DLD-1 and SW480 cells respectively. These shifts suggest a strong impedance in the exponential cell growth (**Figure 5-9**).

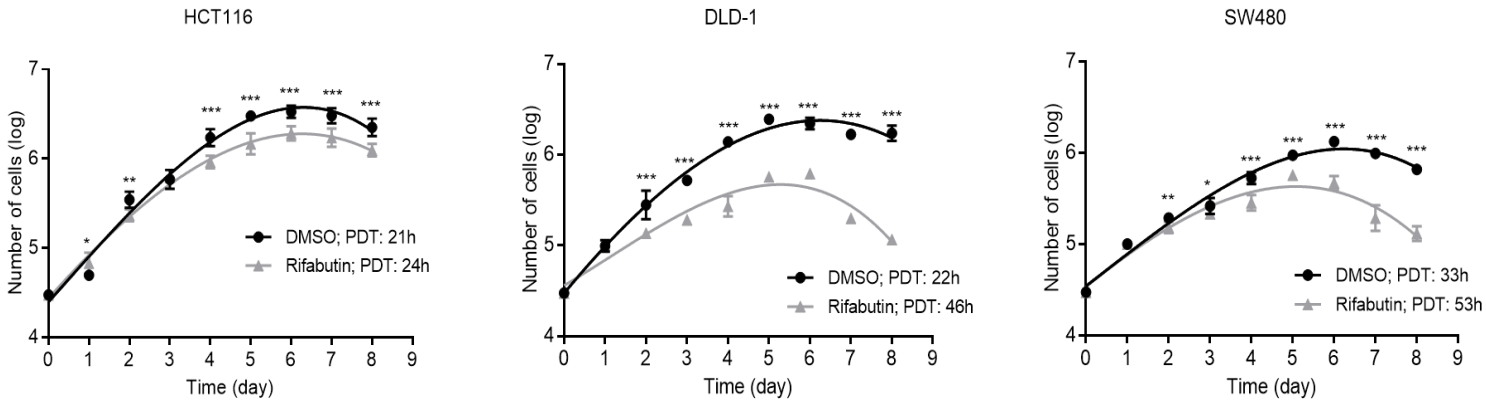


Figure 5-9: Growth curve of rifabutin treated and untreated colorectal cancer HCT116, DLD-1 and SW480 cells. Rifabutin was added at its IC_{50} of 27 μM for HCT116 and 26 μM for DLD-1 and SW480 cells on day 1. Cells were cultured for a period of 8 days and were counted daily at the same time. Error bars represent mean ± S.D. (n = 6). Since day 2, the number of cells in the treated groups were significantly lower. $0.05 < P < 0.0001$. Experiments were performed at least three independent occasions (n = 6; *, $P < 0.05$; **, $P < 0.01$; ***, $P < 0.001$).

5.2.2 Rifabutin inhibits de-differentiation and acquisition of stem-like properties

3D colonospheres were cultured in suspension and were assessed for their colonosphere formation ability, morphology changes as well as acquisition of stem-like characteristics. Of note, the sphere forming potential in a suspension culture is associated with stemness (Onuma et al., 2013).

Colonospheres were cultured from HCT116 and DLD-1 cell lines as described in **Chapter 2;** Materials and Methods (Shaheen et al., 2016a). In order to retain the putative factors secreted by CSCs, only half of the medium was replaced with a freshly made SCM, every 3-4 days. After 14 days, colonospheres were treated with rifabutin for a period of 72 h. At the end of the treatment, only the colonospheres with diameter >50 μm were counted under a microscope and colonosphere formation efficiency was quantified. Our data showed that colonosphere formation efficiency of rifabutin treated and untreated colonospheres did not make any significant differences (**Figure 5-10**).

However, even though the number of colonopsheres remained same after the treatment, rifabutin treatment showed distinct morphological alteration in colonospheres (**Figure 5-11**). Relative changes in colonospheres morphology were assessed by comparing the images of rifabutin treated and untreated colonospheres. The defined round structure and cluster of cells that are difficult to recognise as individual cells were classified as "self-renewing" colonospheres, whereas colonospheres presenting as discrete aggregated cells were considered "differentiating" colonospheres. The majority of untreated colonospheres were self-renewing, whereas almost all the rifabutin treated colonospheres showed differentiating-like morphology. The distinct structure of colonosphere was lost upon rifabutin treatment, indicating rifabutin's potential in inducing differentiation on CRC-SC. This result is in line with the morphological changes observed in 2D

colonies obtained from HCT-116 and DLD-1, however, unlike 2D colonies, there are no distinct differences between rifabutin treated colonosphere sizes.

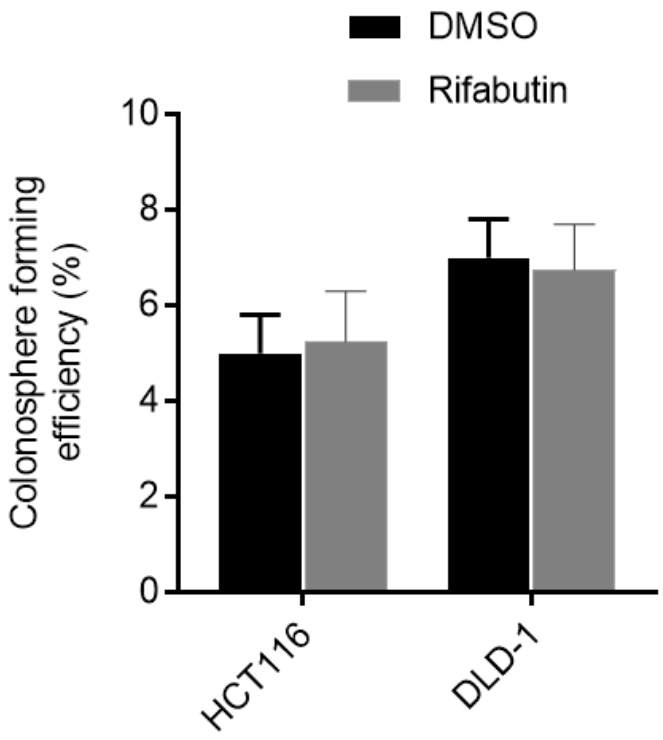


Figure 5-10: Rifabutin treatment did not cause any significant change in colonosphere formation assay. Colonospheres were derived from HCT116 and DLD-1 cells and were treated with rifabutin for 72 h. No significant changes were observed for colonosphere formation in the treated group. Error bars represent mean ± S.D. (n = 25).

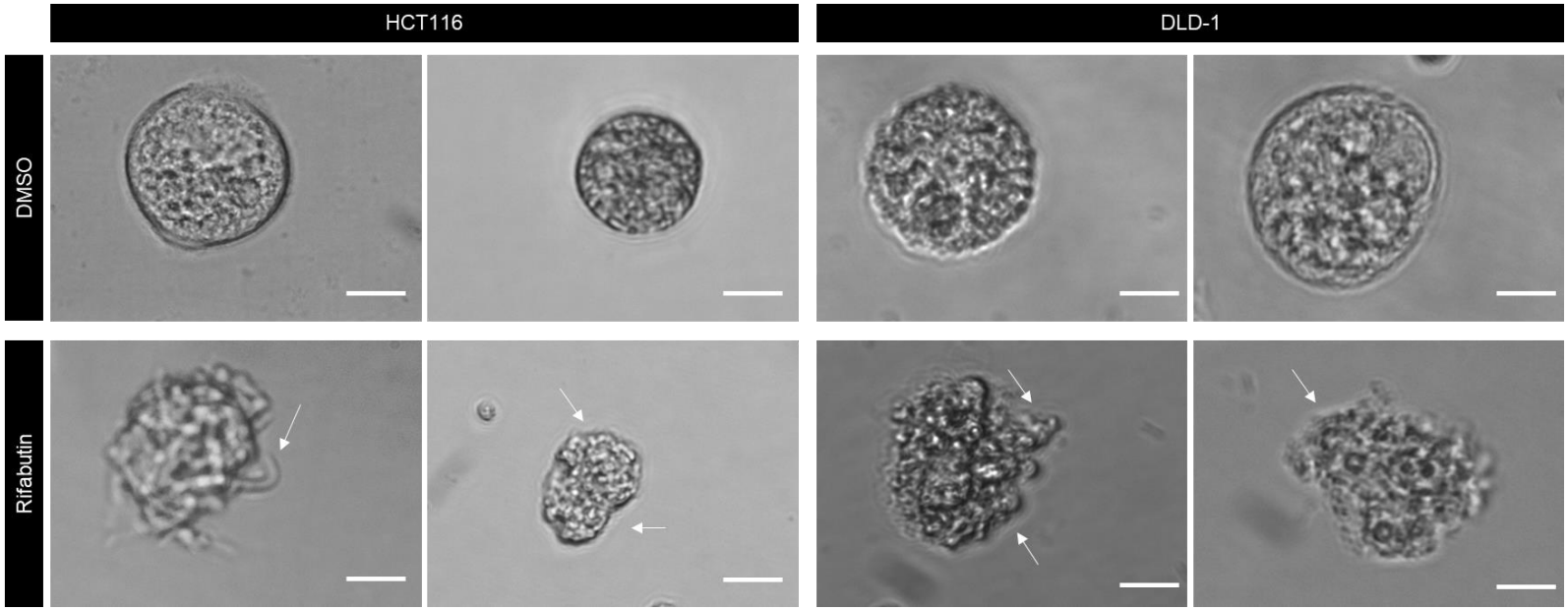
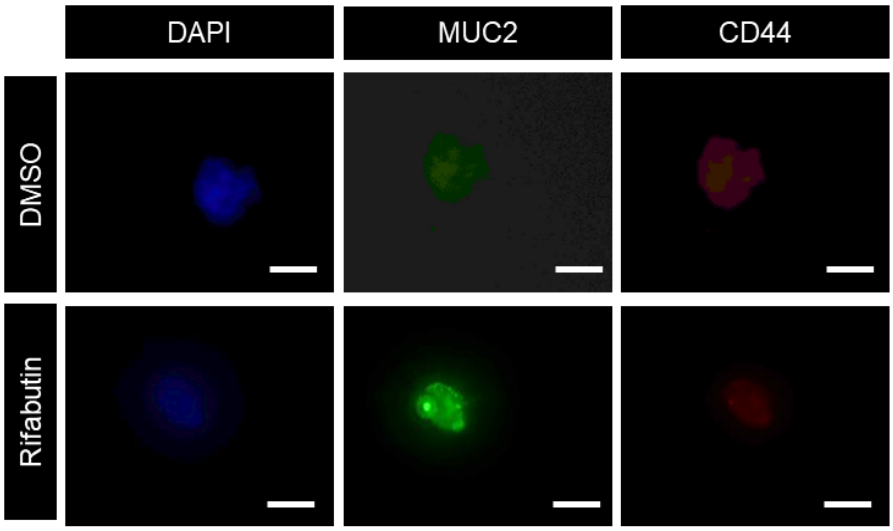


Figure 5-11: Rifabutin showing morphological alteration in colonosphere. Images were taken after rifabutin treatment. Untreated colonospheres maintained their distinct structural network of cells whereas the treated colonospheres showed loss of their structural integrity. Scale bar: 25 μM.

To further validate that rifabutin has differentiation induction potential in CRC-SC, and therefore reduces the stem-like properties, expression of CD44 and Mucin2 was analysed in DLD-1 colonospheres by IF technique.

Colonospheres were cultured as previously mentioned and were then transferred carefully on coverslips. Colonospheres were then treated with rifabutin and were further processed for IF analysis. Fluorescence intensity was measured using ImageJ software. Rifabutin treated colonospheres showed reduced expression of CSC marker CD44, and an upregulation of the differentiation marker Mucin2, compared to the untreated colonospheres (**Figure 5-12**).



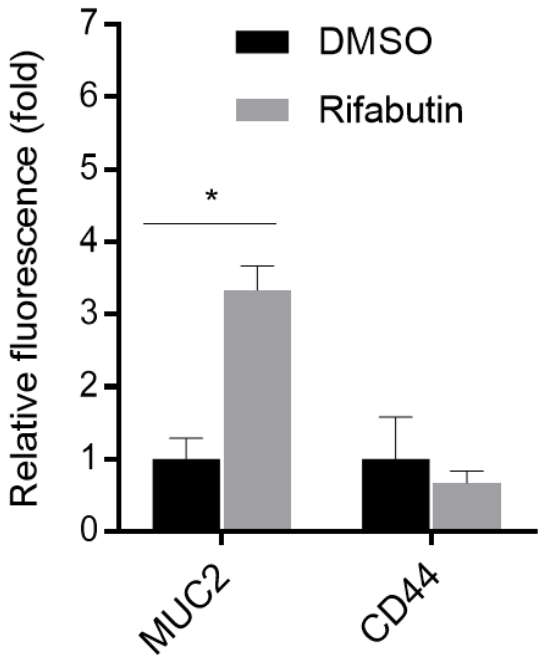


Figure 5-12: Immunofluorescence assay of Rifabutin treated colonospheres using stemness and differentiation markers. Scale bars: 25 μM. Rifabutin treatment significantly increased MUC2 expression and reduced CD44 expression on DLD-1 derived colonospheres suggesting induction of differentiation upon drug treatment (n = 10), $P < 0.05$.

To characterise of the inhibition pathway involved in the mechanism of rifabutin, a gene expression analysis was performed using qPCR from the mRNA isolated from colonospheres obtained from DLD-1 cells. Over the years, some distinct biomarkers have been identified to distinguish the CSC subpopulations form the differentiated cancer cells. Our data showed that rifabutin caused significant reduction in expression of CRC associated stemness markers including *CD44*, *NANOG*, *LGR5*, and *OCT4*, whereas, differentiation markers *KRT20* and *CDX2* were significantly increased upon rifabutin treatment (**Figure 5-13**). Interestingly, rifabutin treatment also increased tumour suppressor *FBXW7* expression and thereby significantly reduced the WNT target gene c-MYC. In addition, rifabutin also reduced both N-cadherin (*NCAD*) and Vimentin (*VIM*) expression (**Figure 5-13**) suggesting its affiliation on EMT (Li et al., 2019b). These results for several stem cell markers, CRC prognostic factors, differentiation and the EMT markers have revealed the potential of rifabutin in targeting stem-like cells in CRC.

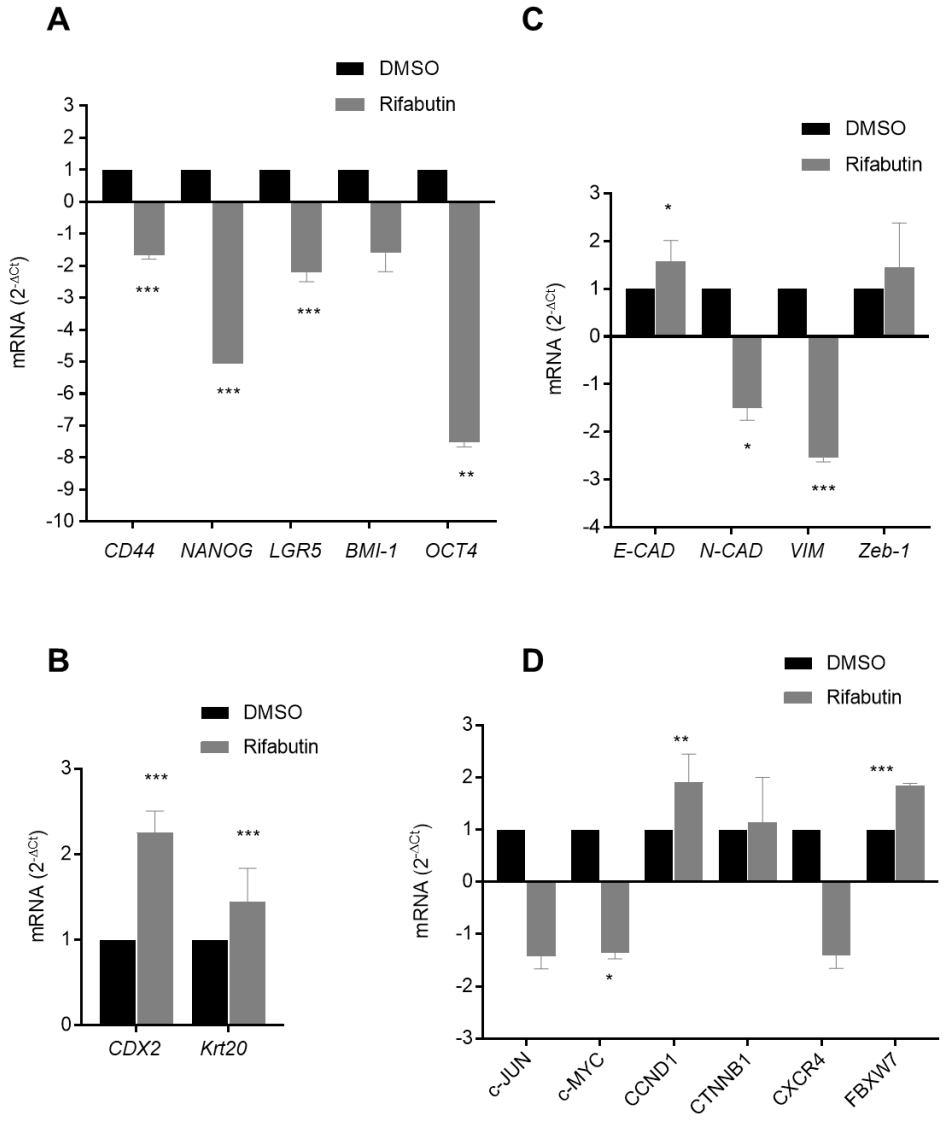


Figure 5-13: qPCR analysis of rifabutin treated colonospheres derived from DLD-1 cells. Expression of **(A)** Stemness, **(B)** differentiation, **(C)**, EMT, and **(D)** transcription factor for recurrence, poor survival, metastasis and tumour suppressor, in colonospheres treated with AM404. Results were normalized with β-actin, and all assays were performed in triplicate. (n = 3; *, $P < 0.05$; ***, $P \leq 0.001$).

5.2.3 Rifabutin impedes the growth of *ex vivo* tumour organoids

The recent advent of CRC patient derived 3D organoids revealed significant potential in disease modelling, preclinical toxicological studies, and experimental approaches in investigating drug response. Organoids serve as excellent *in vitro* model to study specific cell-type response to drugs and enable cells to grow in a more similar manner to that of living organisms (Xu et al., 2018). Typically, an intestinal organoid consists of about 20 or more cells from the bottom of the crypt (Stelzner et al., 2012). However, tumour-derived organoids display different morphologies, ranging from cystic to solid structures within an organoid culture (Li et al., 2019b, Yip et al., 2018, Stelzner et al., 2012).

In order to study rifabutin's response in a three-dimensional tissue-like model of CRC, patient derived organoids were culture and treated with rifabutin for subsequent analyses (Kashfi et al., 2018, Ahmed et al., 2019). Organoids were cultured and allowed to start budding for 5-6 days prior to treat them with drugs. Organoids were analysed across several parameters over time: integrity, morphology, survival and apoptosis. By analysing the complex phenotypical changes in organoid culture, rifabutin treatment exhibited reduced proliferative activity, hindered growth, induced morphology changes and induced apoptosis.

In healthy tissue derived organoids, an initial sphere structure appears on the first day which eventually initiates crypt budding (Yip et al., 2018). However, in tumour tissue derived organoids, a few cystic-like shapes appeared initially in the culture. In contrast to healthy organoids, these cysts fail to initiate crypt budding or branching, possibly due to the deregulation of essential signalling pathways that are required to sustain colonic crypts and their functions (Kashfi et al., 2018). Rifabutin treatment decelerated organoid growth and altered their phenotype. However, the morphology change was highly variable in appearance. By looking at the morphologies of untreated tumour organoid, on day three, most of the organoids in control group were formed by enterospheres

with a few of cystic organoids. For over a period of fourteen days, they turned into large round cystic structures. In contrast, in the treatment group, at day three of rifabutin treatment, about half of the organoids were of enterospheres, whereas, the rest was of enteroid-like irregular structures. By the end of the treatment, majority of organoids appeared to be of enteroid-like structures (~70%) which may suggest induction of differentiation. Moreover, in the treated group, about 25% of organoid population also turned into densely packed dead-cell volume, which may be suggestive of rifabutin induced apoptosis on tumour organoids (**Figures 5-14, 5-15** arrowheads).

In addition, rifabutin caused significant growth impairment in tumour organoid (**Figure 5-15**). The differences in size and volume were evident from day 3 of treatment, however, as the treatment progresses, the differences became significantly more apparent in terms of size and morphology. Previously, rifabutin has been reported to delay lung tumour growth at day 6 of initial treatment with a persistent inhibitory effect throughout the duration of treatment (Li et al., 2016b). In this study, considering the 3D structure, organoid volumes were measured by taking 3-4 separate diameters for each organoid and taking the half of their average as radius (r). The following formula was used:

$$V = \frac{4}{3}\pi r^3$$

Rifabutin treatment showed significantly smaller volume comparing to the DMSO-treated (control) group (1.99 x 10^8 μm^3 vs 0.36 x 10^8 μm^3; $P<0.05$, $P<0.01$, $P<0.001$) (**Figure 5-16**). At the end of the treatment, 20% of organoids were measured to be as more than 700 µM, as compared to the 30% of organoids in control group (**Figure 5-16**).

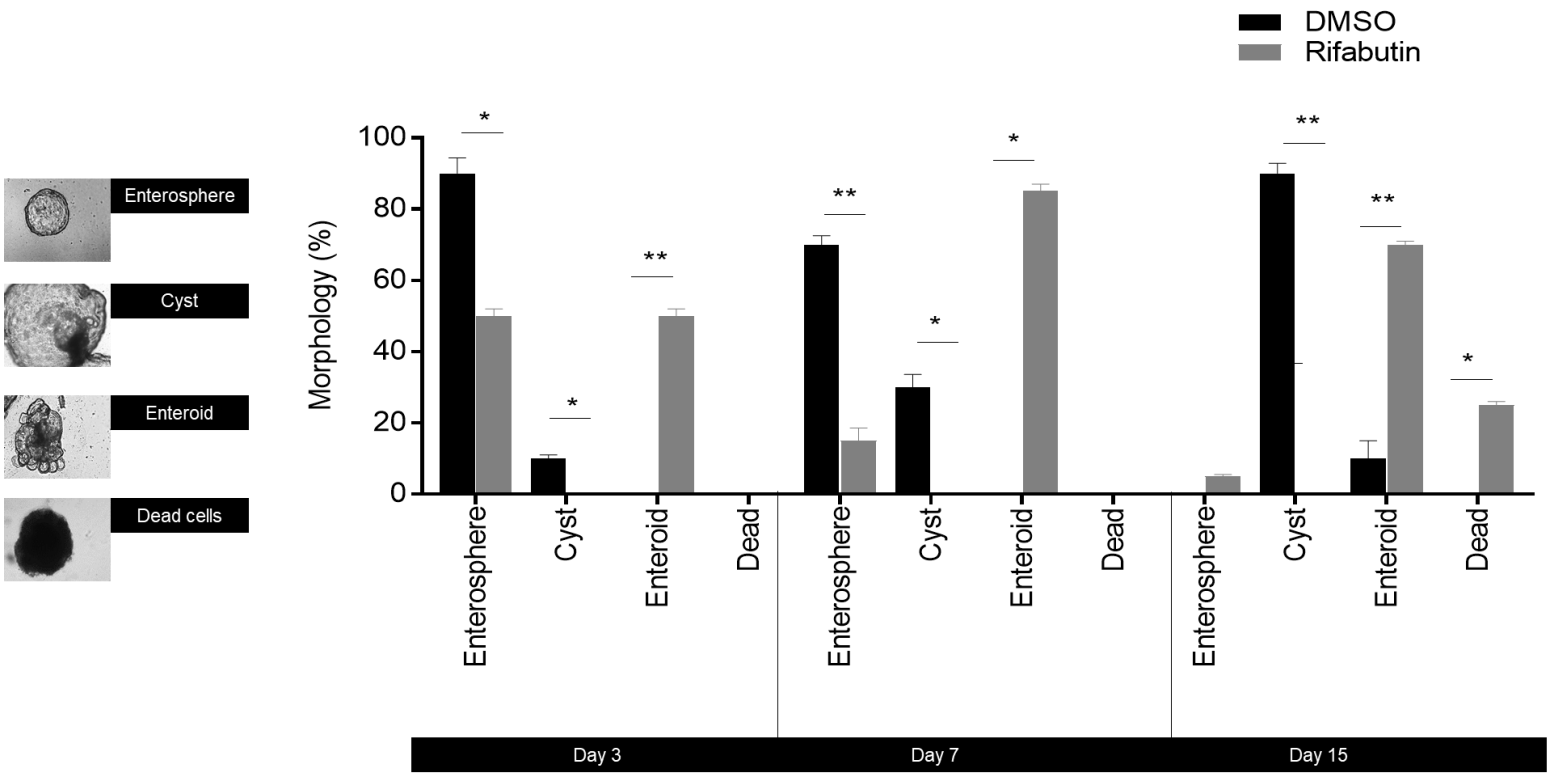


Figure 5-14: Rifabutin treatment presents enteroid-like structures and induces apoptosis in organoids. Percentage of enterosphere, cyst, enteroid and dead cells at day 3, 6 and 15 days of treatment. Organoids were counted by microscopy (n = 15; *, P < 0.05; **, P < 0.01).

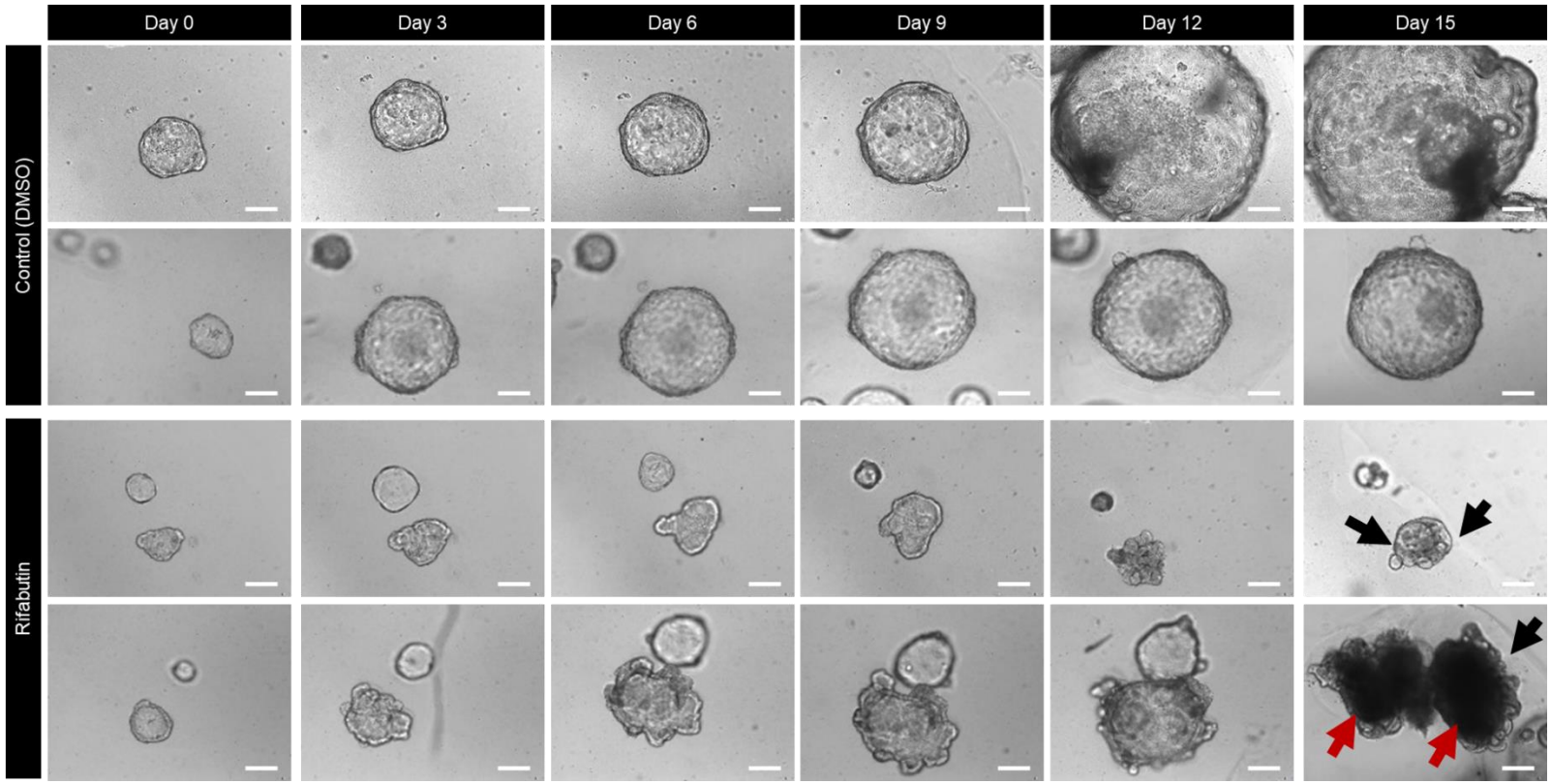


Figure 5-15: Organoid growth retardation and morphology change induced by rifabutin. Representative images of tumour organoids treated with rifabutin for a period of 2 weeks. Morphological alteration and variation in growth were observed throughout the treatment period. The treatment group showed distinct morphological changes indicating rifabutin induced differentiation (black arrowheads), as well as cell death (red arrowheads). Images were taken using Leica microscope. Scale bar: 75 µM.

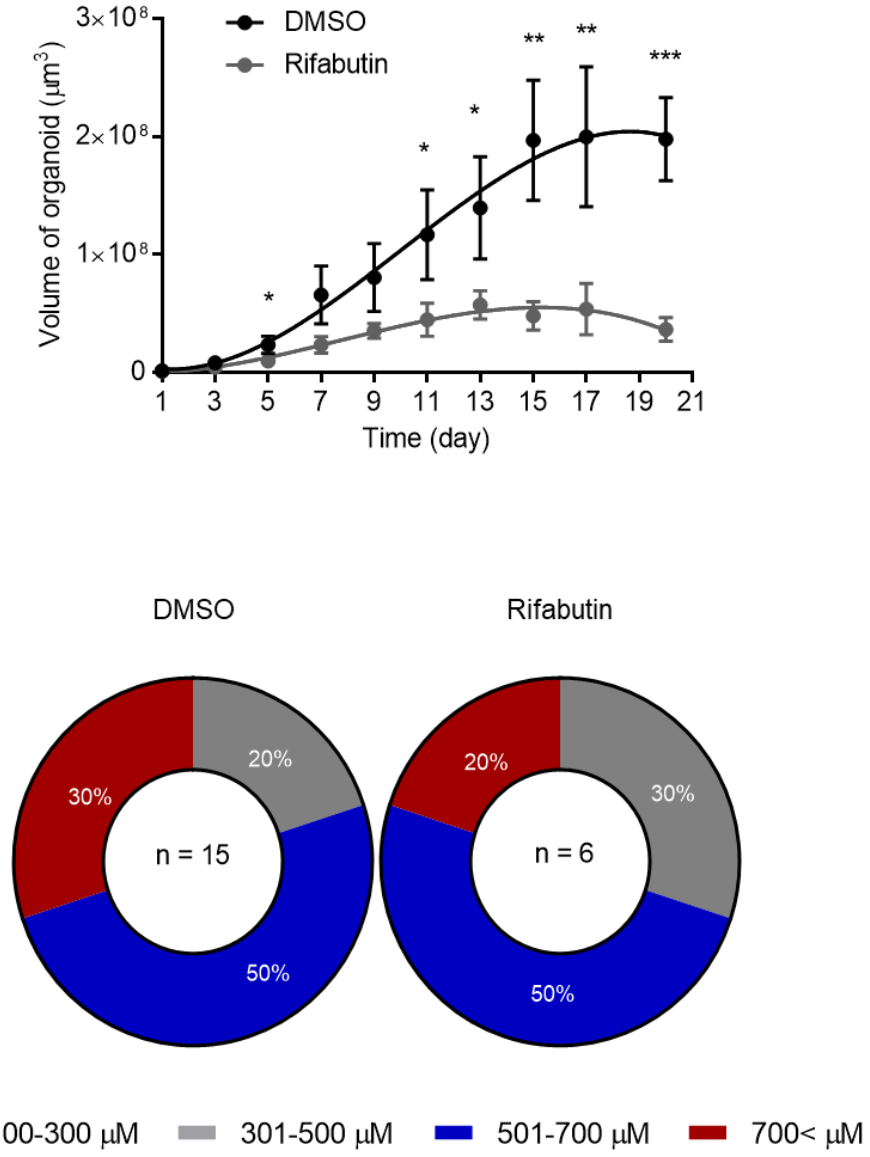


Figure 5-16: Rifabutin treatment hindered the growth in in tumour organoid. Volumes of organoids were measured every 2 days. Number of organoids in different size groups at the end of the treatment shows significant inhibition to the tumour growth in the treated group. Numbers in each size group (diameter) are expressed as percentage of the total. Error bars represent mean ± S.D. (n = 15; control, n = 10, rifabutin). *, P < 0.05; **, P < 0.01; ***, P < 0.001.

This result shows that majority of rifabutin-treated organoids being in smaller diameter range, suggesting its inhibitory effect on organoid growth. However, cell dead/alive status was also identified by PI/Hoechst staining. At the end of the treatment period, organoids were collected carefully and processed for staining. This step involved extra care to not lose the organoids, particularly during the mild agitation and washing steps. Rifabutin treatment showed slight induction/no significant change in PI staining followed by a 2 weeks treatment period in tumour organoids (**Figure 5-17**). This result suggests minimal induction of cell death particularly influenced by rifabutin on tumour organoid. Such induction, however, can further be evaluated for whether it's a consequence of cell cycle arrest or rifabutin induced senescence or death in organoid model.

Based on the organoid data, this could potentially be hypothesised that rifabutin induces significant changes in tumour size, morphology, cell death (**Figures 5-14, 5-15**), and tumour growth (**Figure 5-16**) in organoid model.

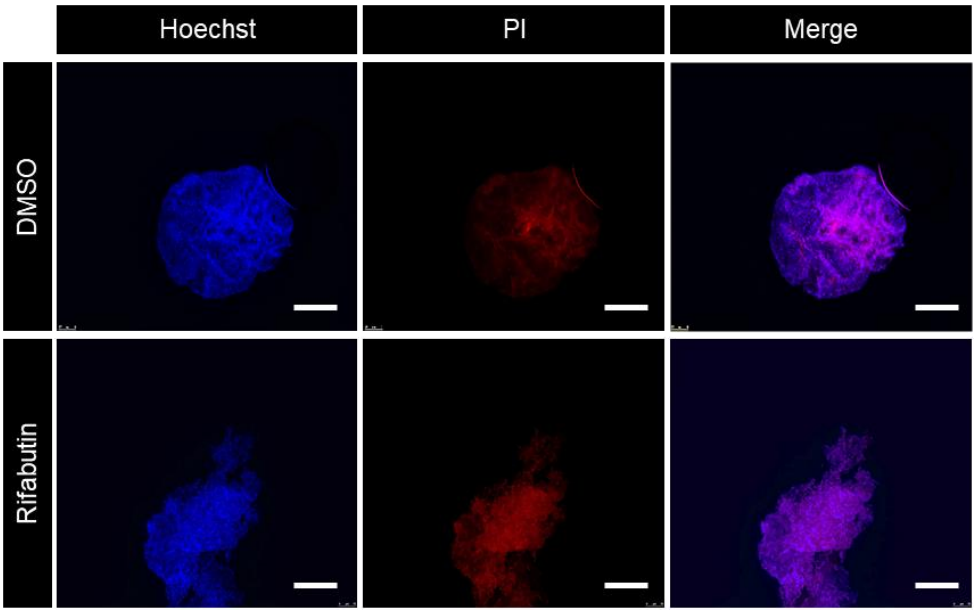


Figure 5-17: Hoechst/PI staining on rifabutin treated organoids. The similar pattern/slight increase in PI staining indicates no changes/slight increase in cell death upon rifabutin treatment. Scale bar: 25 μm.

5.2.4. *Ex vivo* treatment of CRC patient biopsies evaluates rifabutin response as an anticancer drug

Till date, the ability to predict patient tumour response to cancer therapy remains a major challenge. The spatial distribution of cancer and stromal cells within the tumour microenvironment can determine the cell-cell interaction and can influence the proliferation, differentiation, morphology and a range of cellular functions (Majumder et al., 2015, Yamada and Cukierman, 2007). Therefore, 3D colonosphere model or organoids may not completely reflect the biology of a tumour *in vivo*. Given this, to evaluate the drug response in tumour, an *ex vivo* platform recapitulating the tumour heterogeneity was employed in this study (Karekla et al., 2017a).

Fresh tumour tissues were obtained from 7 CRC patients' surgeries or biopsies and were processed immediately to recover after their initial generation. Tumour tissue explants were cultured as mentioned in

Chapter 2; Materials and Methods, and **Chapter 4**. Explants were treated for 24h, following which, Rifautin's response was evaluated using the following parameters: stemness, differentiation, proliferation and apoptosis deliberated in tumour tissue (**Figure 5-18**).

IHC analysis of rifabutin treated tumour explants showed a decreasing trend of cell proliferation and stemness marker with increasing level of differentiation (**Figure 5-18**). This was found to be consistent for tumour explants generated from all the CRC patients, with 5-6 images analysed per tumour sample using the H-score system. Levels of Ki-67 staining and number of proliferating cells were significantly affected by rifabutin as compared to the control-treated group on explant model (**Figure 5-18**). Overall, 24-hour treatment with Riabutin significantly reduced the proliferation level in tumour explants by 25% (**Figure 5-18; A,** right panel). In line with the organoid data suggesting slight induction of cell death, in the explant model, rifabutin treatment also showed a minor but insignificant increase in pro-apoptotic protein Caspase-3 staining (**Figure 5-18; B**). This stresses the importance of looking further into this by carrying out individual studies to investigate whether rifabutin induces specific cell-cycle arrest or mechanisms for cell senescence is involved herewith. Next, to associate rifabutin with cellular differentiation and stem-like activity, CDX2 and CD44 were also utilised in tumour explants (**Figures 5-18; C and D**). Overexpression of CDX2 has been shown previously to induce differentiation as well as to inhibit proliferation and is therefore, frequently downregulated during tumorigenesis (Graule et al., 2018, Qualtrough et al., 2002). Our result showed a significant increase in CDX2 expression in the treated group, suggesting significant induction of differentiation (H score 250 vs 215). In line with the proliferation pattern, CD44 also showed to have a similar trend in significantly reducing the stemness level in cultured tumour explants treated with rifabutin (H score 150 vs 262) (**Figures 5-186; D**, right panel). It has previously been reported that crypt proliferation is

strongly but reversely correlated with CRC recurrence, one major aspect of CRC-SC characteristics (Merlos-Suárez et al., 2011). Treating these tumour explants with rifabutin showed a reduction in these characteristics while also increasing the level of differentiation.

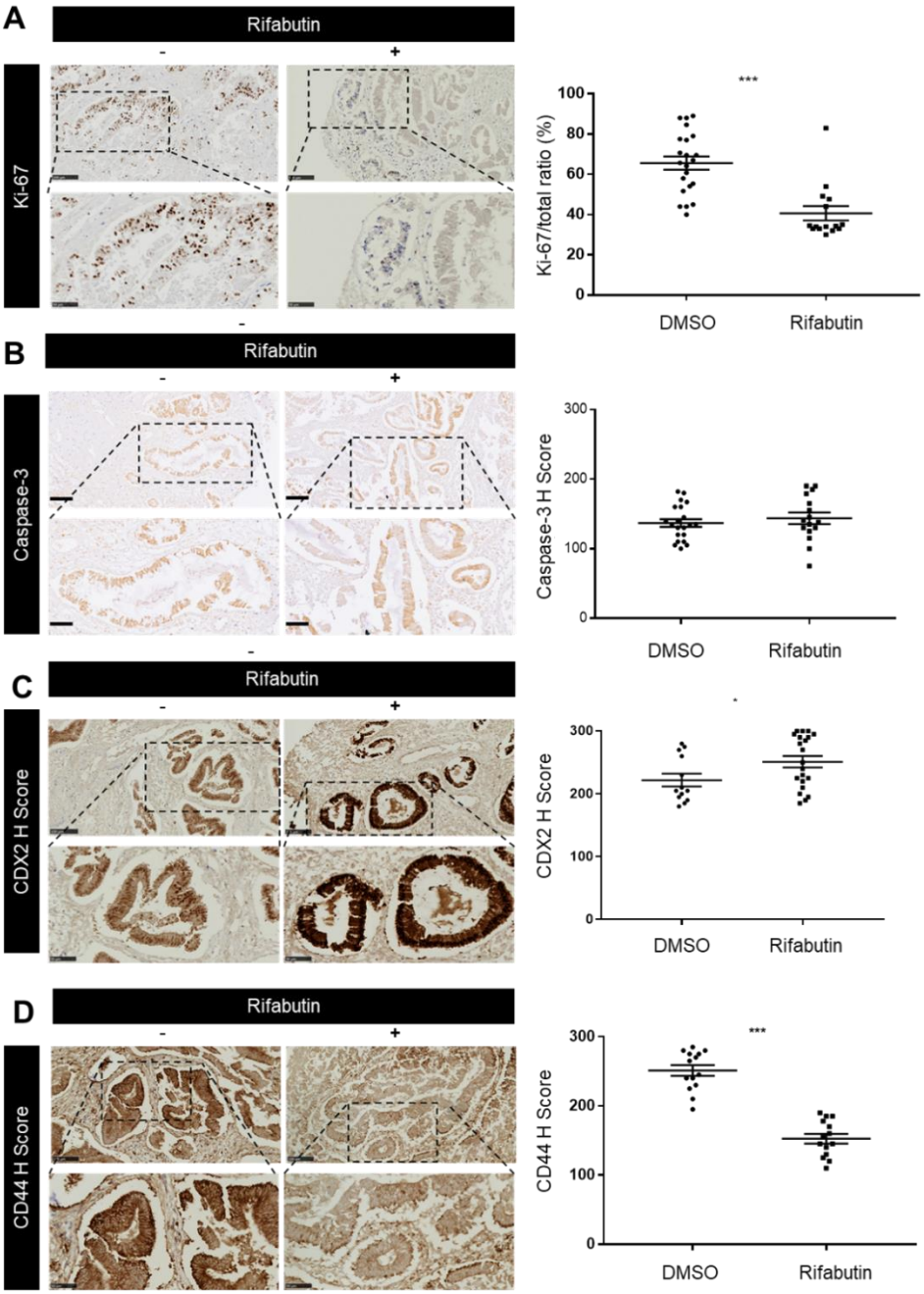


Figure 5-18: Effects of rifabutin treatment on proliferation, apoptosis, differentiation and stemness level in the tissue explants obtained from CRC patients (A-D). Proliferation was assessed by quantitating Ki-67 **(A)** IHC staining, cell survival by caspase-3 **(B)**, whereas, differentiation and stemness levels were assessed by CDX2 **(C)** and CD44 **(D)** staining quantification respectively. IHC stains were counterstained with hematoxylin and eosin. Representative images (top panel) shows the images at 20x magnification with

a scale bar of 100 μm. Bottom panel shows the selected parts in higher 40x magnification with scale bar 50 μm. Each dot (Right panels) represents an image used for quantification. Control treated groups represents the level of intrinsic proliferation, stemness and differentiation level in tumours. For the Ki-67 staining, Ki-67 +ve cells were counted and expressed as a percentage of the total cells. In case of CD44 and CDX2 and Caspase-3, H-scores were counted as a measure for the quantification. Tumour tissues were obtained from 7 different patients, and 4 segments of tissue were used for each patient. *, $P < 0.05$; ***, $P < 0.001$.

5.2.5. FBXL5 attenuates rifabutin-induced anticancer activity in targeting CRC

To identify the targets associated with rifabutin's mechanism on CRC, the whole-genome transcriptome analysis of colonospheres was carried out and compared between the rifabutin treated and control (DMSO) groups. This study was carried out in collaboration with collaboration with the Nottingham Arabidopsis Stock Centre (NASC) in University of Nottingham. A clear separation was observed between rifabutin treated and control groups, suggesting discrete transcriptome signatures for these two populations (**Figure 5-19**). Principal component analysis (PCA) of variant genes re-marked such separation between these two groups. PCA plot shows a scatterplot with axes corresponding to the two different principal components.

Microarray analysis have revealed multiple perturbations in gene expression level in rifabutin treated group. We focused on the identification and characterisation of significant changes emphasising on the 2 or more-fold changes and a p value of 0.001 or less, which revealed 267 genes with differential expression after the false discovery rate (FDR) correction (**Appendix 5**) (**Figure 5-20**).

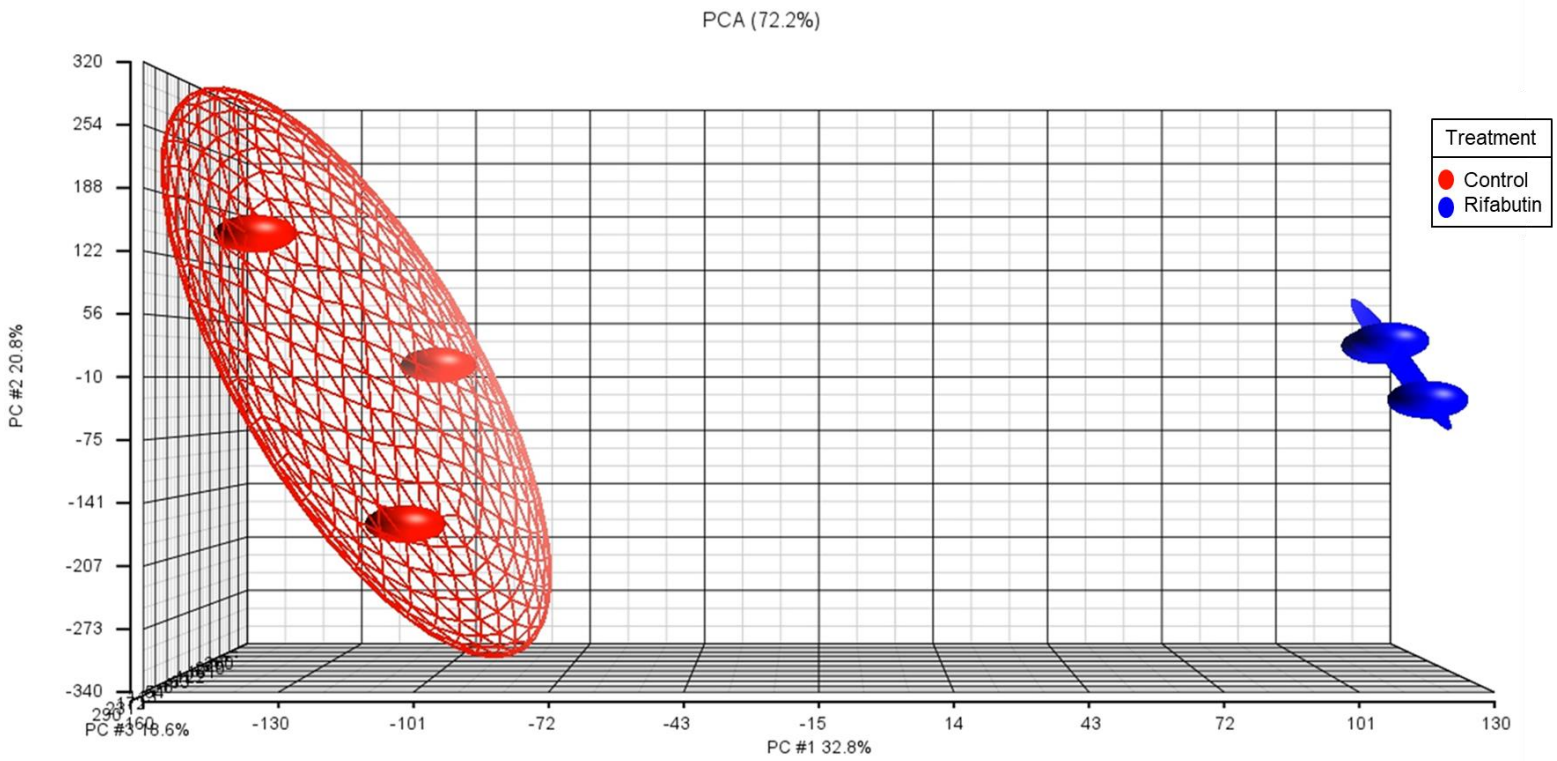


Figure 5-19: PCA analysis of variant genes for rifabutin treated and control (DMSO) colonospheres. The red circles correspond the control and blue circles represent rifabutin treatment. PCA analysis denoted a marked distinction between these two groups.

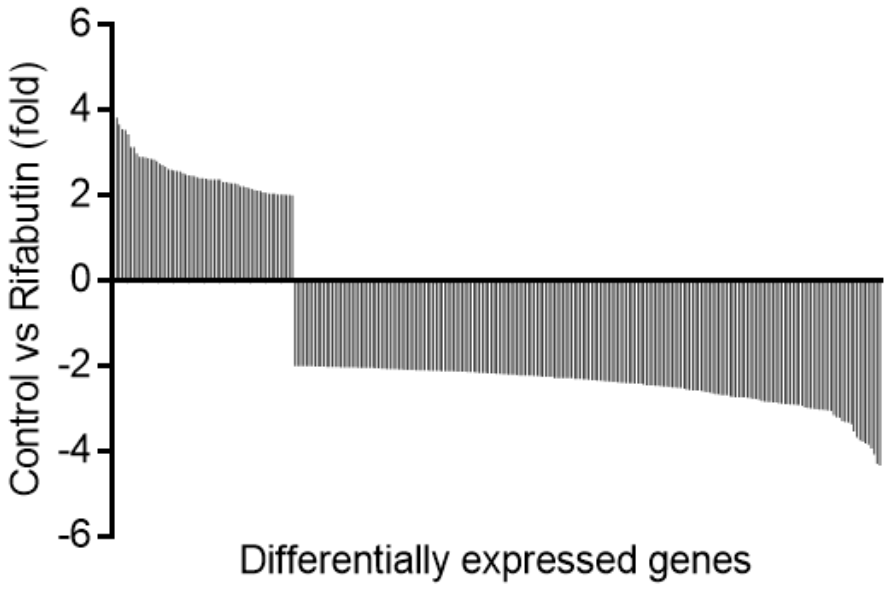


Figure 5-20: Differentially expressed genes on DLD-1 derived colonospheres treated with rifabutin. Each bar represents one gene that has a p-value of 0.001 or less and is 2 or higher fold increased or decreased on colonospheres following the drug treatments.

As predicted by the status of explants and organoids, the gene ontology (GO) pathways revealed the top genes that are differentially expressed by rifabutin treatment are associated with cell proliferation in CRC (**Figure 5-21**). Top 32 genes that were upregulated and downregulated upon rifabutin treatment were sorted by 3 or more-fold-changes, p value and FDR correction and were plotted in a heatmap (**Figure 5-22**). However, in reference to the 16 genes with 3 or more-fold changes associated with AM404 in **Chapter 4**, there were 9 genes, including FBXL5 upregulated and downregulated in the similar manner for both AM404 and rifabutin treated colonospheres. From the initial screening outlined in **Chapter 3**, both these compounds were found to induce

differentiation in colonospheres and therefore, these 9 common genes may suggest a potential scope for further investigation and may also represent an invaluable source of potential biomarkers in CRC. In consistent with the hypothesis in **Charter 4,** that AM404 targets FBXL5 to influence CRC-SC for differentiation, rifabutin shows a similar pattern in targeting FBXL5, and revealed FBXL5 as one of the top differentially expressed genes (**Figure 5-22**).

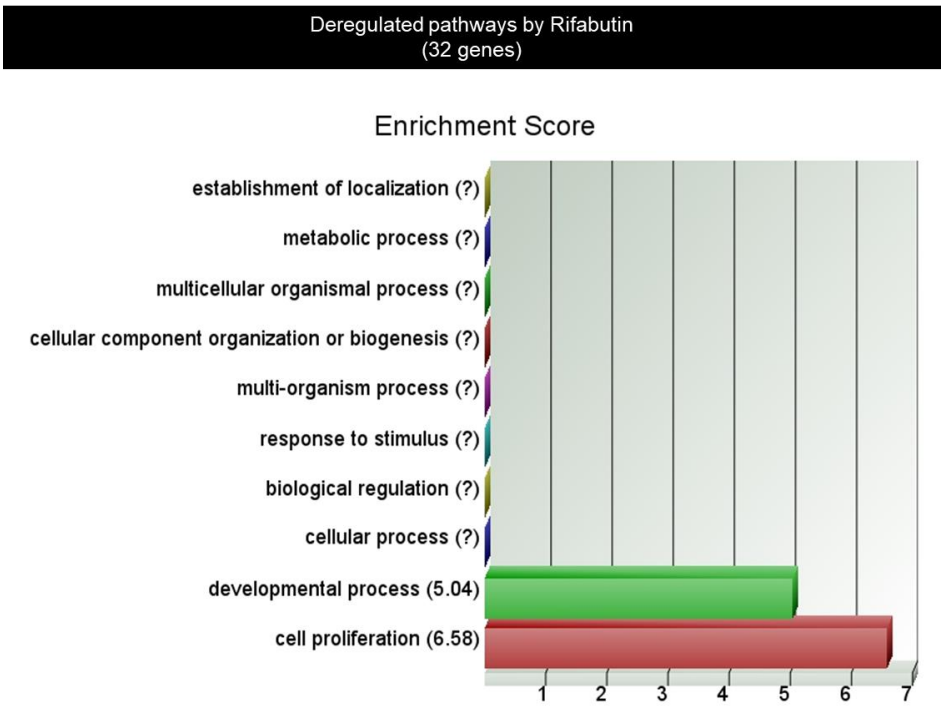


Figure 5-21: Gene ontology biological processes revealing the top biological processes affected by the top thirty-two differentially expressed genes. Functional annotation clustering with default settings was used; medium stringency and Benjamini–Hochberg correction was applied. Only the enriched GO terms with FDR <0.05 were selected and displayed in the bar chart.

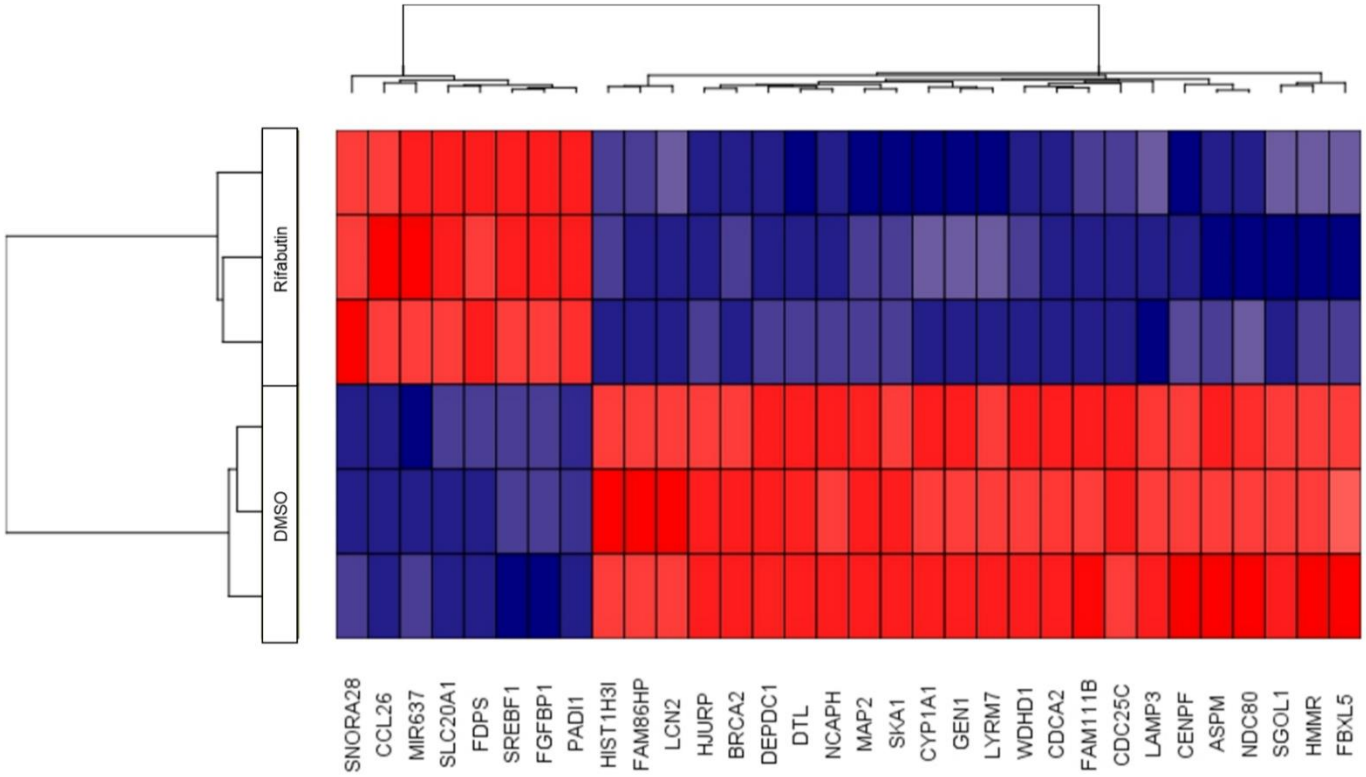


Figure 5-22: Heat-map representation of unsupervised clustering of the 32 differentially expressed genes (≥3-fold change) by rifabutin in DLD-1 derived colonospheres. Each column represents a single gene. Colour code within the graph represents: blue, downregulated; and red, upregulated. Horizontal and vertical clusters were created based in Euclidean distance.

As previously suggested for AM404 in **Chapter 4**, we next wanted to determine whether FBXL5 also works as a key target for rifabutin's effect in migration for CRC (Yao et al., 2018, Diaz and de Herreros, 2016, Dragoi et al., 2014). The CRISPR-Cas9 mediated *FBXL5*-knockout in DLD-1 cell line generated in our laboratory (**Chapter 4, Figure 4-24**) was used for evaluating rifabutin's effect in migration. The cytotoxicity assay on the *FBXL5*-knockout cell line was first carried out for rifabutin and the IC_{50} was measured as outlined in **Chapter 2;** Materials and Methods. The cytotoxicity assay confirmed that loss of FBXL5 induced sensitivity to rifabutin in DLD-1 cells, (26 μM vs 22 μM; $P<0.05$, $P<0.01$, $P<0.001$) (**Figure 5-23**), as it did for AM404 in **Chapter 4**.

As a first step in evaluating rifabutin's effect in CRC metastasis, a wound healing assay was conducted on DLD-1 cells as outlined in **Chapter 2;** Materials and Methods (**Figure 5-24**). Our result showed that, after 12 h, rifabutin made significant reduction in DLD-1 cell migration. This effect was consistent with 24, 48 and 72 h confirming Rifanutin's inhibitory effect in CRC migration (**Figure 5-24**). Of note, deletion of FBXL5 itself caused reduction on the migratory effect, suggesting FBXL5 as an important factor for migration (**Figures 5-24, 5-25**). This result was also shown in **Chapter 4**. Rifabutin, when treated on *FBXL5*-knockout cells, showed to mimic this effect and showed similar level of inhibition in cell migration. In both DLD-1 and *FBXL5*-knockout cells, rifabutin showed the same level of inhibition in CRC migration.

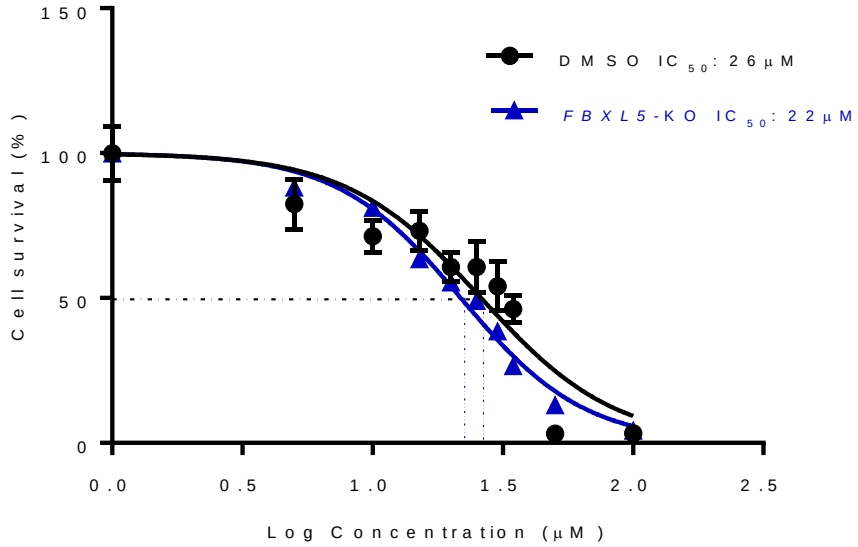


Figure 5-23: Cytotoxicity assay of rifabutin in DLD-1 and *FBXL5*-knockout DLD-1 cell line using sulforhodamine B (SRB). Survival curves were denoted by DLD-1 (black), and FBXL5-knockout DLD-1 (blue) treated with rifabutin. The dotted line represents half maximal inhibitory concentration (IC_{50}). Nonlinear regression was used to plot the data. Experiments were performed at least three independent occasions (n = 6). Error bars represent mean ± S.D. *, P < 0.05; **, P < 0.01; ***, P < 001.

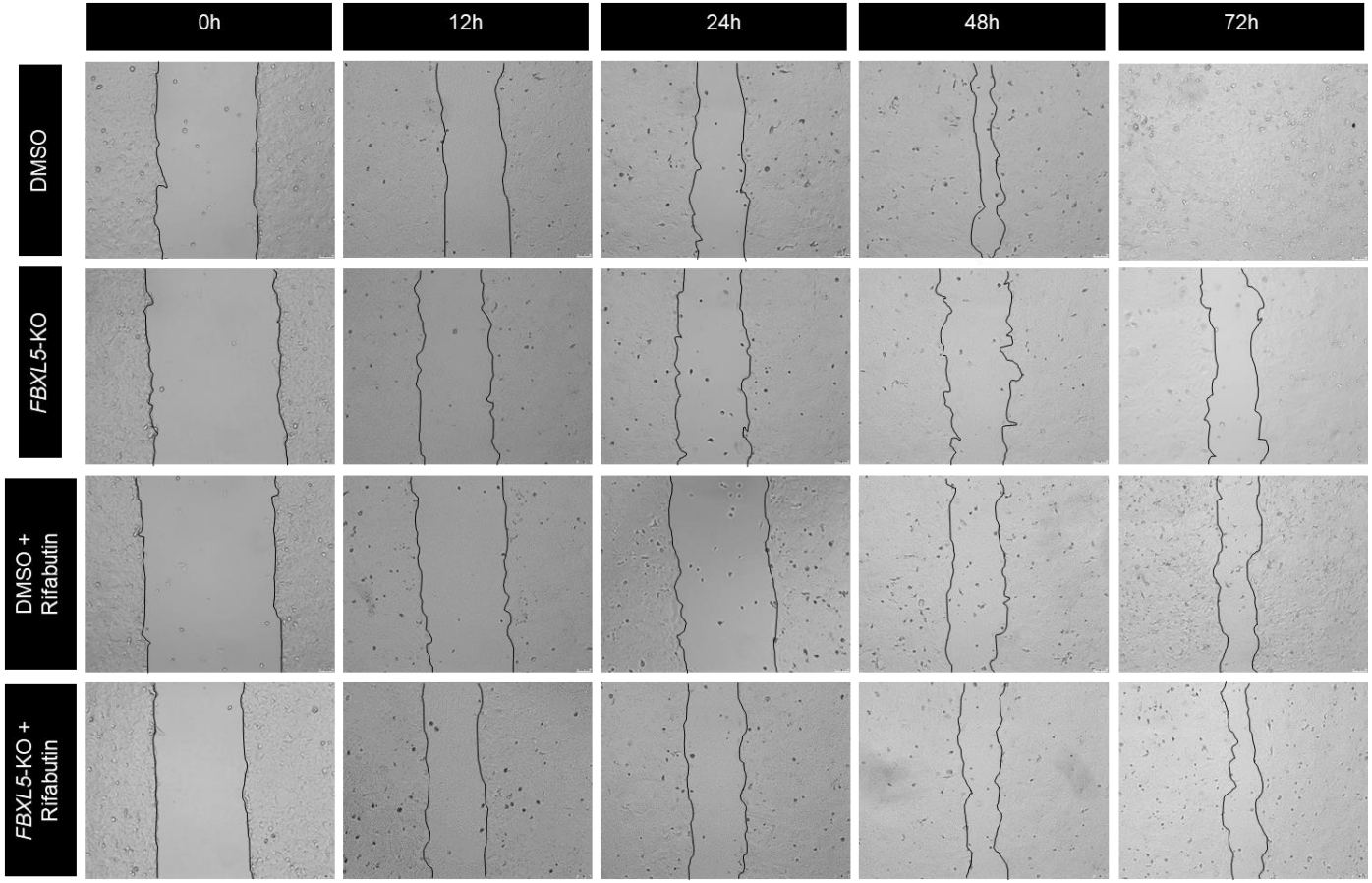


Figure 5-24: Rifabutin induced inhibition of migration in DLD-1 and *FBOXL5*-KO cells *in vitro*. Migration of DLD-1 and *FBOXL5*-KO cells was performed with scratch wound healing assay. Starved cells were scratch-wounded and wound width was measured to determine the healed distance at 0, 12, 24, 48 and 72 h.

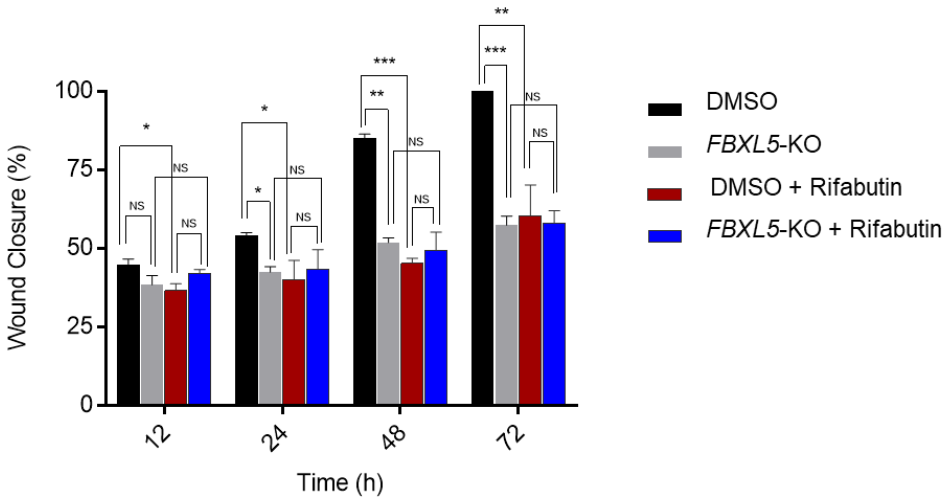


Figure 5-25: Significant inhibition of migration in DLD-1 and *FBOXL5*-KO cells by rifabutin. Significant reduction in cell migration was observed for both cell lines. Bars are expressed as mean ± S.D. (n = 10). *, $p < 0.05$; **, $p < 0.01$; and ***, $P < 0.001$.

5.3 Discussion

This study explores the potential antineoplastic effect of rifabutin on CRC, particularly to target CRC-SCs by reducing tumorigenic stem-like activity or inducing differentiation.

Rifabutin is an attractive candidate as it is already available in pharmaceutical market for clinical use in the treatment of tuberculosis, and therefore has a pharmacodynamic profile established for its medical use. In studying cancer, rifabutin was first reported in 2016 to have blunted the tumour progression in a non-small cell lung cancer patient presented with pulmonary tuberculosis (Li et al., 2016a). Since then, in recent years, rifabutin has been reported to reduce cell proliferation and self-renewal, and to induce apoptosis in lung and breast cancer (Kast et al., 2017, Li et al., 2016b, Siddiqui and Sonenberg, 2015, Lim et al., 2013).

It has been reported that rifabutin acts on lung cancer cells in an eIF4E-β-catenin-dependent manner (Li et al., 2016b, Siddiqui and Sonenberg, 2015, Lim et al., 2013). Eukaryotic translation initiation factor 4E (eIF4E) overexpression has been identified in 30% of human cancers, which regulates β-catenin activity by phosphorylation (Siddiqui and Sonenberg, 2015). Of note, in leukemia stem cells, self-renewal is regulated by eIF4E phosphorylation through activating Wnt/β-catenin signalling, whereas in breast cancer, its overexpression is correlated to the recurrence and metastasis (Kast et al., 2017, Lim et al., 2013). Rifabutin showed to suppress eIF4E phosphorylation, thereby decreased β-catenin phosphorylation and its subsequent transcriptional activities (Kast et al., 2017, Li et al., 2016b). Moreover, rifabutin also binds to BCL-6 and prevent its function in lymphoma and breast cancer.

In addition, rifabutin, showed remarkable inhibition in PD1–PDL1 protein–protein (programmed cell death protein 1- programmed cell death ligand 1) interaction. Overexpression of PDL1 is associated with tumours to escape the immune destruction system. Therefore, inhibiting PD1-PDL1 and its subsequent activation of the innate immune system is an important therapeutic approach in targeting various cancers that expresses PDL1, including CRC (Patil et al., 2018).

Based on the results from this study, we also report inhibition in cell proliferation, self-renewal characteristics, and induction of apoptosis by rifabutin in CRC. Moreover, we suggest FBXL5 as one of the potential targets associated in CRC, by which rifabutin might exert its anticancer effects on.

Our initial studies on 3 CRC cell lines exhibited cytotoxic effects in response to rifabutin with IC_{50} of 26-27 μM. Rifabutin suppressed the growth of CRC cells significantly, increasing the population doubling time (PDT) and causing distinct cell growth arrest. Additionally, it also caused significant reduction in the number and size of colonies. There were

distinct morphological differences between the control and rifabutin-treated colonies, with the treated colonies forming protrusions on their edges. In support, phalloidin staining of rifabutin treated colonies also showed a less dense cytoskeletal network, with filaments extending outwards, whereas, DAPI staining showed a relatively lower nuclear density. Together, this could be speculated that rifabutin might have induced differentiation in some extent or the caused induction of cell death or senescence. In parallel, colonosphere data supports this postulation by showing extensive morphology alteration upon rifabutin treatment accompanied by significantly increased expression in the relative fluorescence of differentiation marker MUC2 and reduced expression in stemness marker CD44. Therefore, it indicates a correlation between such changes in morphology with cellular differentiation.

Intriguingly, anti-tuberculosis drug rifabutin treatment on colonospheres showed significant increase in CDX2 and KRT20 expression, whilst showing significant reduction on CD44, LGR5, NANOG, and OCT4. These results were validated in two patient derived 3D *in vitro* organoid and *ex vivo* tissue explant models. The long-term culture of human adult intestinal cells remained difficult for a long time, but in recent years studies have identified and optimized culture conditions for long-term growth of organoids derived from neoplastic tissue. Our organoid data showed clear evidence of rifabutin induced growth impediment and altered morphology with more of branch-like enteroids and less of defined cyst structure. Of note, on day 15 of treatment, significant amount of cell death was observed in the treated group. Due to the technical difficulties in recovering organoids, there was a slight but not significant increase in PI staining indicating induction of cell death in the organoids. However, if used with large sample number, this could show a significant difference in the staining, as this result was clearly backed by the cell morphologies when looked under microscope. Of note,

rifabutin has also previously been reported to induce apoptosis in 3 different lung cancer cell lines (Lim et al., 2013). Additionally, the explant platform provides a patient-relevant model system for the preclinical evaluation of novel anticancer agents. When combined with tumour stratification approaches, the platform has the potential for personalizing drug treatment. Immunostaining on the tissue explants revealed reduction in proliferation and slight increase/no difference in apoptosis. Again, such effect was also observed in lung cancer with significant decrease in proliferating marker protein Ki67 and increase in pro-apoptotic protein active caspase-3 treated with rifabutin (Lim et al., 2013).

The gene array analysis uncovered 32 differentially expressed genes showing 3 or more-fold changes in their expression level, mostly associated to cell proliferation. Interestingly, FBXL5 was found to be one of them. Of note, this gene was also downregulated by another candidate drug AM404 in CRC, as outlined in Chapter 4. Gene array revealed that FBXL5 is downregulated in colonospheres upon rifabutin. Simultaneously, loss of FBXL5 conferred cells to be more sensitive to the therapy. Rifabutin associated reduced expression of FBXL5 caused reduction of CRC 'stemness' features, as shown in both 2D and 3D models, including cell proliferation, tumour growth, morphology, and induction of CRC differentiation and apoptosis. In addition, it has been markedly reported that, FBXL5 also showed negative correlation in EMT, particularly in gastric and cervical cancer and silencing FBXL5 showed decrease in metastasis with significant increase in expression of E-cadherin at posttranscriptional level (Yao et al., 2018, Diaz and de Herreros, 2016, Dragoi et al., 2014). In line with this, by mimicking the effect of FBXL5 deletion, rifabutin also significantly prevented metastasis in CRC cells. This postulation is also backed by the significant reduction in the N-cadherin and Vimentin expression level in rifabutin treated CRC-SC. This finding proposes FBXL5 as a potential target via which rifabutin

exerts its effects on CRC. However, being sensitive to *FBXL5*-knockout cells, rifabutin did not show any further additive inhibition in migration inhibition, which stresses on further studying of this gene in response to rifabutin to elucidate the underlying pathways. In particular, on functional level, CD44 has been reported to regulate the CSCs metastasis through the adhesion and EMT. It has been also suggested that CD44 might regulate self-renew through Nanog phosphorylation, Hedgehog and Notch pathway (Radwan et al., 2016). We showed reduced expression of both CD44 and NANOG by rifabutin, hence it is worth studying these genes further for their association in migration.

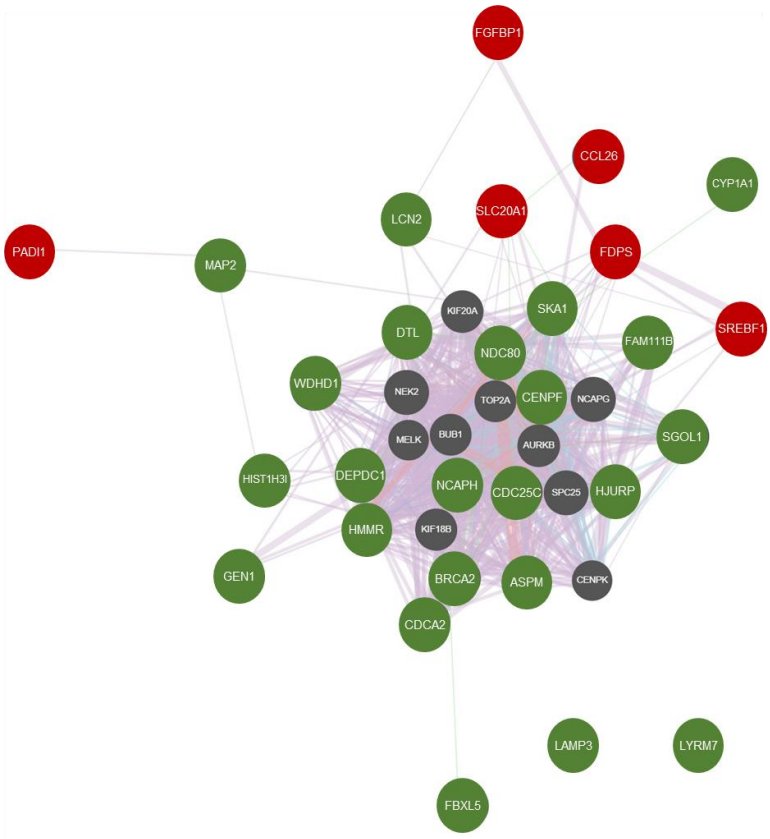


Figure 5-26: Gene array revealed potential pathways regulating rifabutin's effects in CRC. GeneMANIA was used to generate this pathway analysis. Genes that are presented in green circles represents 3 or higher

fold downregulation whereas red circles represent genes with 3 or more-fold upregulation upon rifabutin treatment of CRC-SC.

Due to the time limitation, exploring the required pathways as targeted by rifabutin induced FBXL5 downregulation was not completed. The signalling pathway analysis emphasises on the potential pathways involved in CRC upon rifabutin treatment. Amongst them, as outlined in **Figure 5-26**, FBXL5 association with BRCA2 can further be studied in addition to the 9 common genes differentially expressed in similar manner as of AM404. In conclusion, our results show interesting data of rifabutin as a new potential drug in CRC treatment, possibly by downregulating the *FBXL5* oncogene. Moreover, it has been widely reported that the combination therapy of the CSC-targeting drugs with conventional drugs presents a more effective approach. Therefore, it is also necessary to further evaluate rifabutin's effect in combination with other conventional CRC treatment regimens.

CHAPTER 6

Idarubicin Exhibits Antitumor Activity in CRC

6.1 Introduction

The role of CSCs in tumour recurrence after chemotherapy is now well-established. Subsequently, emerging reports also suggest that some chemotherapy can lead to propagation of CSCs and initiate secondary malignancies (Dracham et al., 2018, Gunduz et al., 2014b, Tanei et al., 2009).

Having evaluated two potential antibacterial drugs for their differentiation induction potential and overall anticancer effects in CRC, our experimental plan continued with the demonstration of a drug that has initially induced the stem-like characteristics in the compound library screening. Amongst the 11 compounds that have affected CRC-SC in similar manner, 3 of them was found to be increasing the 'stemness' as outlined in **Chapter 3**. Interestingly, all these compounds, including idarubicin, daunorubicin and epirubicin were anthracycline group of cytotoxic antibiotics, used in the treatment of different cancers. This phenomenon of anticancer drugs enriching CSCs is not necessarily a new concept and have been repeatedly reported till now, which stresses the importance of investigating anthracyclines for enriching CRC-SC and developing therapeutic strategies co-targeting both non-CSC and CSC populations.

Typically, anthracyclines are the cytotoxic antibiotics which is one of the most effective groups of anticancer drugs available for the treatment of haematological and various solid tumours. These compounds were found to have antitumor effect on the early 1950s with daunorubicin. Several analogues have been produced since then, but due to severe toxic effects, only a small number have been approved till now.

Idarubicin (4-demethoxy-daunorubicin) is a daunorubicin analogue with molecular formula of $C_{26}H_{28}ClNO_9$. Structurally, it differs from daunorubicin with no methoxy group at position 4 of the D ring of the aglycone (**Figure 6-1**) (Kolaric et al., 1988), which leads to high

lipophilicity, cellular uptake, and cytotoxicity (Fukushima et al., 1993, Boogerd et al., 1999).

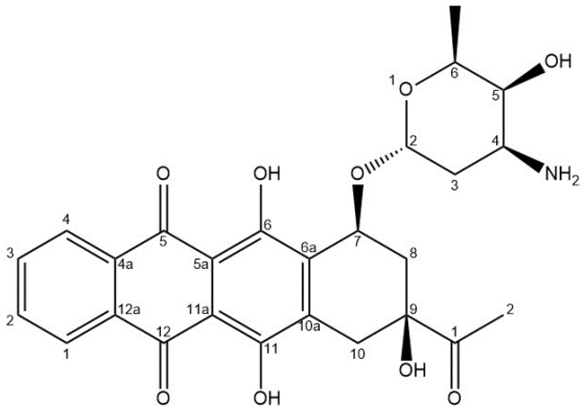


Figure 6-1: Schematic representation of the structural formula of idarubicin (PubChem CID: 42890).

Despite the advantages over other anthracyclines, idarubicin possesses numerous side effects including multiple drug resistance (MDR), and induction of secondary tumours (Gunduz et al., 2014b). Of note, secondary malignancy is one of the most common consequences associated with anthracyclines and alkylating agents, as well as, radiotherapy (Dracham et al., 2018, Vega-Stromberg, 2003). Interestingly, it has been reported that, different populations of CSCs may be responsible for developing secondary tumours (Shiozawa et al., 2013, Brower, 2013). Such effects have significant biological and clinical impact in tumour resistance, recurrence and metastasis.

Therefore, the objectives of this study were to:

(I) evaluate idarubicins' potential in inducing the de-differentiation and stemness properties of CRC stem-like cells

(II) evaluate idarubicins' effect on CRC cell death, proliferation and morphology alteration

6.2 Result

6.2.1 Validation of the candidate drugs determined the anti-cancer activity of idarubicin

Of the 707 NCC (NIH Clinical Collection) compounds screened (**Chapter 3**), idarubicin was characterised as one of the candidate compounds that induced the CDy1 fluorescence intensity in colonospheres (**Figure 6-2**). Thus, we investigated whether chemotherapeutic drug idarubicin could enrich CRC cells with stem-like characteristics while having potential anticancer activity in CRC.

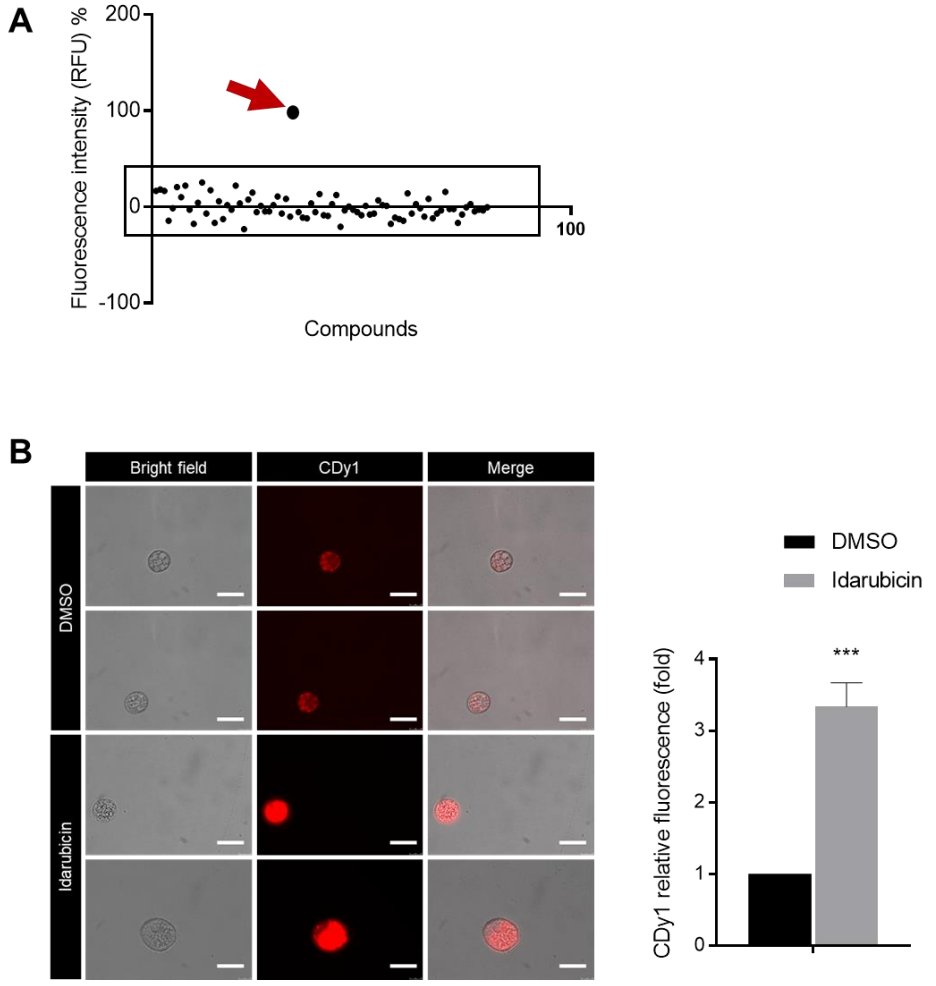


Figure 6-2: 3D drug screening revealed idarubicin inducing the stem-like characteristics in colonospheres. (A) Idarubicin induced the relative fluorescence presented by CDy1 Rosamine dye in colonosphres. CDy1 has been used as a measure of stem-like activity. Fluorescence intensity of DMSO-treated (control) colonosphere was set as 0. Intensities conferred by all compounds were presented as a percentage of their induction or reduction of stem-like activity. Idarubicin (arrowhead) showed to induce the fluorescence intensity. Image was reproduced from the primary screening of NIH clinical collection Plate 6 carried out on colonospheres derived from HCT116 cells (Figure 3-11). **(B)** Representative images of CDy1 stained DMSO-treated (control) and idarubicin treated colonospheres. Scale bar: 25 µm.

6.2.1.1 Cytotoxicity assay of idarubicin

To evaluate its effects on CRC, cytotoxicity assay of idarubicin was performed on HCT116, DLD-1 and SW480 cell lines (**Figure 6-3**). Ten increasing doses of idarubicin (from 1 to 80 nM) were administered to the experimental cell lines. After 72 hours of treatment, live cells were measured by Sulforhodamine B-based colorimetric assay and IC_{50} values were determined as described in **Chapter 2; 2.2.6**. The IC_{50} values obtained from CRC cell lines were 7.2 nM, 6.2 nM and 12 nM for HCT116, DLD-1 and SW480 cell lines, showing subsequent resistance towards SW480 cells (**Figure 6-3**).

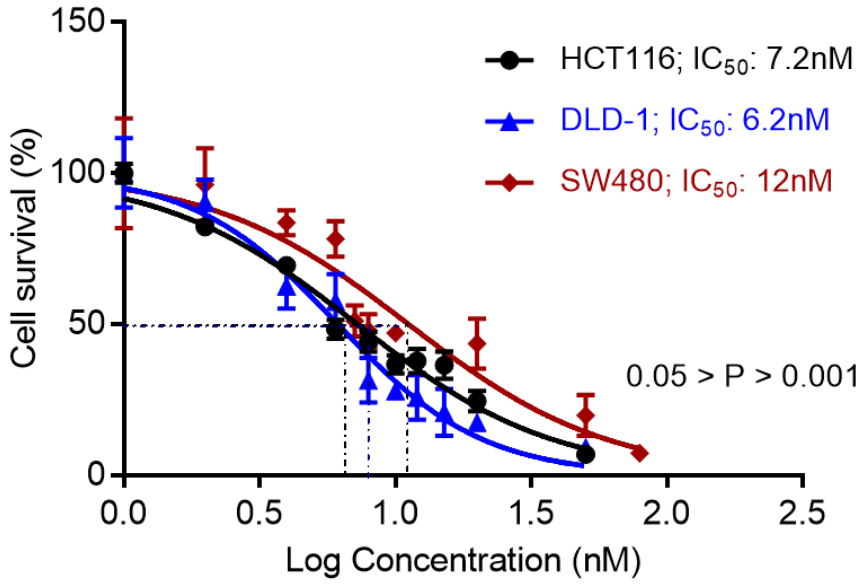


Figure 6-3: Cytotoxicity assay of idarubicin using sulforhodamine B (SRB) on human colorectal cancer cell lines. Survival curves were denoted by HCT116 (black), DLD-1 (blue) and SW480 cells (red) treated with idarubicin. The dotted line represents half maximal inhibitory concentration (IC_{50}). Nonlinear regression was used to plot the data. Error bars represent mean ± S.D. *, P < 0.05; **, P < 0.01; ***, P < 0.001. Experiments were performed in triplicate for each cell line on at least three independent occasions (n = 6).

6.2.1.2 Idarubicin reduces the tumorigenic ability in CRC cell lines

As the first step to investigate how idarubicin affects the tumorigenic ability in CRC, the *in vitro* clonogenic assay was carried out which often recapitulate *in vivo* tumour response (Kabakov and Gabai, 2018). Our data showed idarubicin has strong influence in reduction of colony formation efficiency **(Figure 6-4)**, morphological alteration (**Figure 6-5**), and therefore, subsequent reduction in colony size (**Figures 6-6** and **6-7**).

Next, colon formation assay was carried out as previously outlined in **Chapter 2; 2.2.7**. DLD-1 cells were allowed to grow into colonies for 6-7 days. On day 8, idarubicin was added to its IC_{50} and maintained in parallel with the vehicle-treated group (DMSO). Following the treatment, colonies were then stained with crystal violet and were manually counted (**Figure 6-4; A**). The number of colonies was significantly lower in the treatment group (54% vs 42%; P< 0.001) (**Figure 6-4; B**). However, in line with **Chapter 4** and **Chapter 5**, no colonies were formed in SW480 cell lines. Next, to evaluate any possible morphology alteration conferred by idarubicin, the colonies were stained with Phalloidin and DAPI as explained in **Chapter 2;** Materials and Methods. Idarubicin-treated colonies lacked the structural integrity and formed several dissociated projections. This effect was evident as seen with the more scattered nuclei throughout the colonies, not limited to only on the edges. Such disruption in stained nuclei might indicate that idarubicin induced cell death accompanied by certain level of cytotoxicity, or, induced the cells to undergo senescence or differentiation. In parallel with colony formation efficiency, reduction in colony size was also strongly evident upon idarubicin treatment (1192 ± 188 μm vs 343 ± 250 μm, P < 0.05) (**Figure 6-7**). Reduction in colony size can also be speculated by comparing the microscope photographs in F**igure 6-5** and **Figure 6-6**.

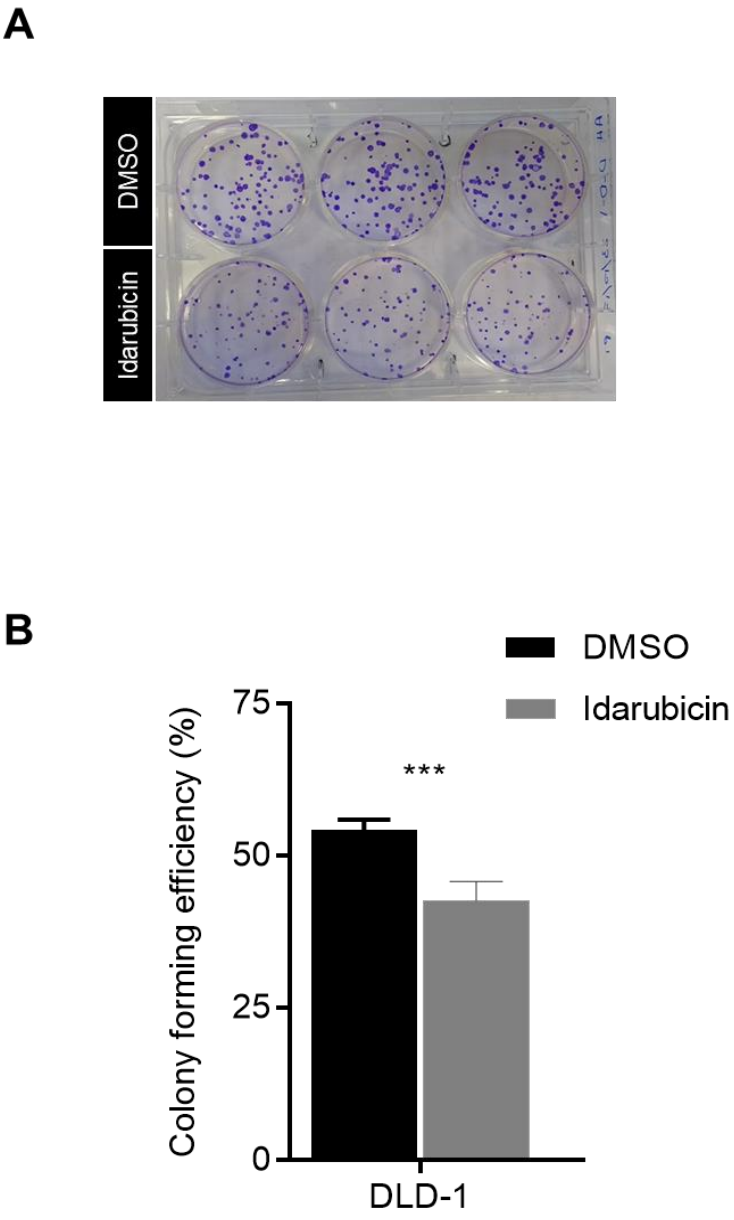


Figure 6-4: Reduction of colony formation efficiency by idarubicin in DLD-1 cells. (A) Representative images of colony formation assay on DLD-1 cells. **(B)** Idarubicin showing significant reduction in colony formation assay in DLD-1 cells. $P \leq 0.001$. Experiments were performed three independent occasions (n = 3).

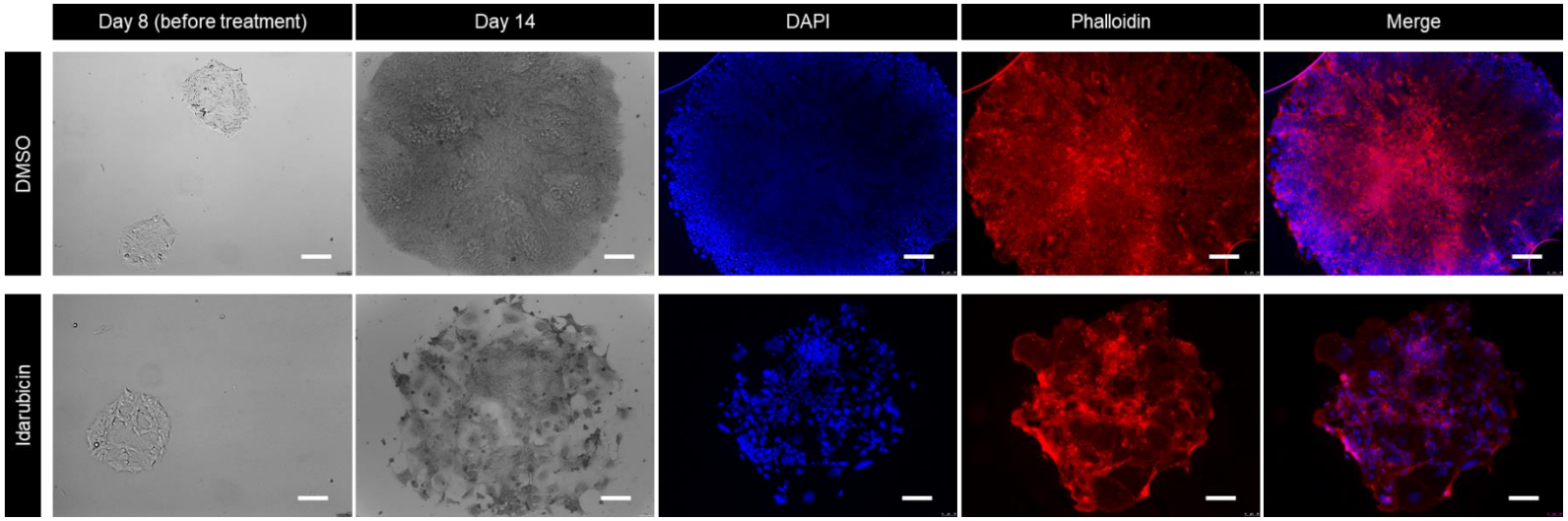


Figure 6-5: Idarubicin treatment on DLD-1 obtained cultured colonies and Phalloidin staining at the end of the treatment period. Nuclei were detected with DAPI-blue fluorescent stain. Scale bar: 75 μm.

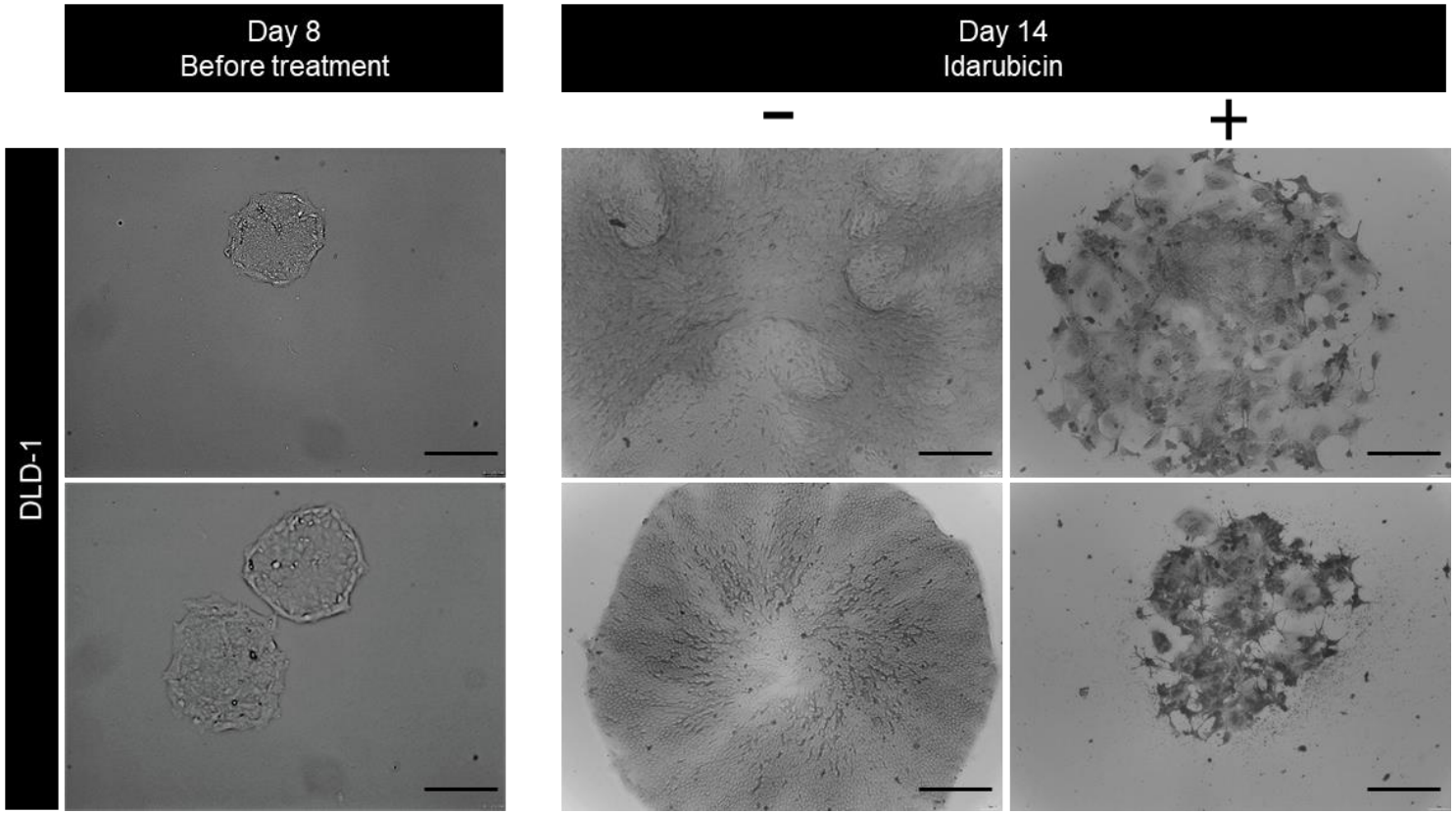


Figure 6-6: Idarubicin reduces the clonogenic activity of DLD-1 cells. Images were taken before idarubicin treatment on day 8, and on day 14. Day 14 control colonies show a denser network of cells while day 14 treated colonies show a less packed and smaller morphology with protruding edges. Scale bar: 75 µm.

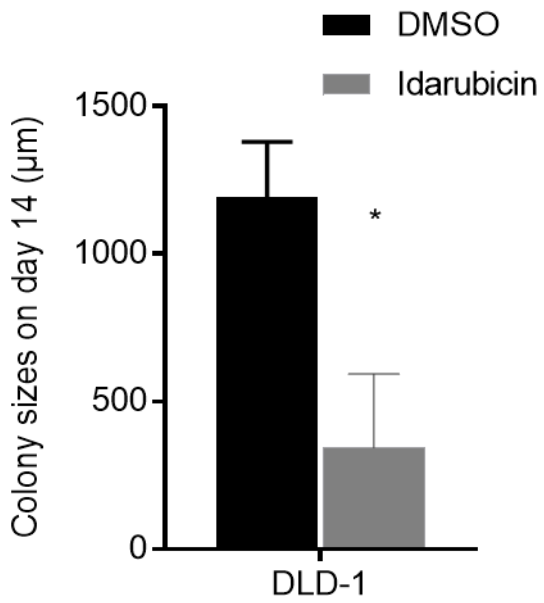


Figure 6-7: Idarubicin reduced the size of colonies in DLD-1 cells. Error bars represent mean ± S.D (n= 8). P < 0.05. Experiments were performed at least three independent occasions (n = 20); P < 0.05.

Additionally, reduction in cell growth and increase in doubling time was strongly evident in DLD-1 cell line upon idarubicin treatment. In contrast, idarubicin treated SW480 cells failed to reach their exponential phase and caused growth arrest. DLD-1 and SW480 cells were treated with the IC_{50} of idarubicin (**Figure 6-3**) on day 1 and were counted daily at the same time for a period of 8 days (**Figure 6-8**), and doubling time was measured as previously described in **Chapter 2; 2.2.8**. A distinct lag phase was absent between day 0-1 in both cell lines, while in log phase cell growth showed an exponential fashion reaching the plateau on day 6. Idarubicin treatment, on the other hand, caused the cells to reach the plateau by day 4 (DLD-1) and caused a shift in the population doubling time (PDT) from 28 h to 56 h. In SW480 cell line, however, idarubicin treatment caused a growth arrest

and no PDT was obtained due to the lack of distinct plateau and exponential phase as presented in the growth curve. These shifts suggested strong impedance in the exponential cell growth upon idarubicin treatment (**Figure 6-8**). To note, the numbers of cells in the treated groups were significantly lower throughout the experimental period (day 2-8).

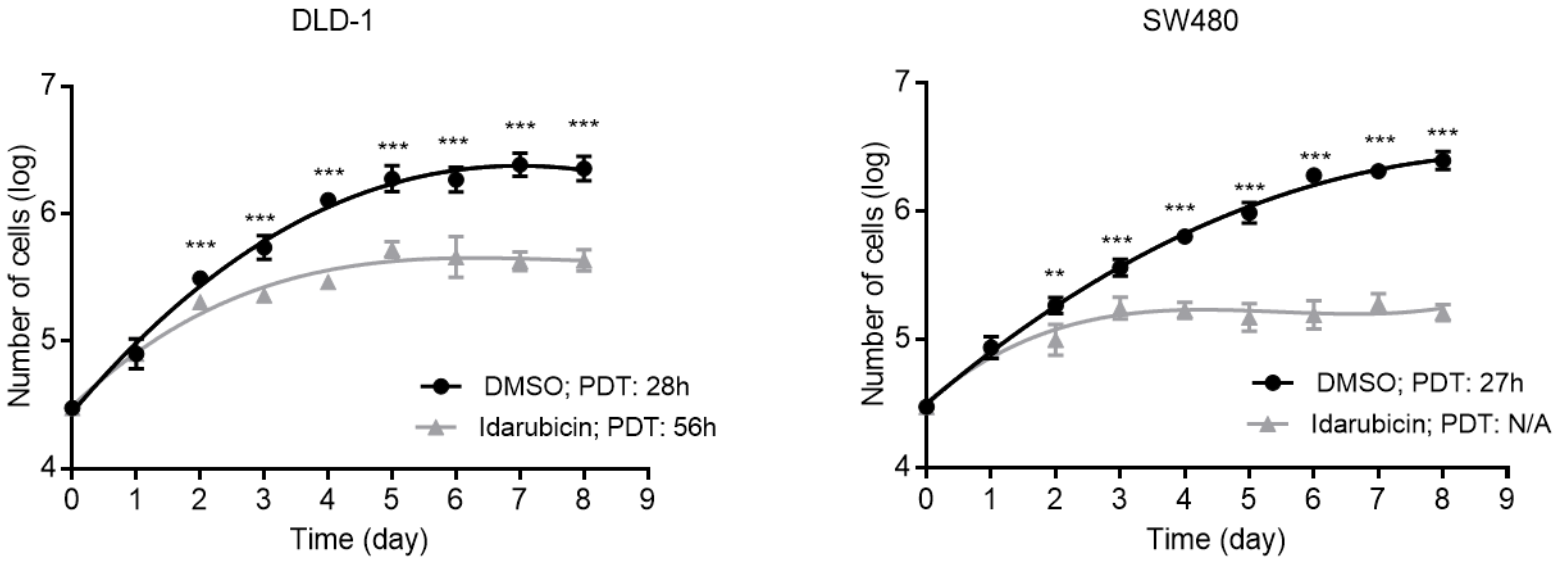


Figure 6-8: Growth curve of idarubicin treated and untreated colorectal cancer DLD-1 and SW480 cells. Idarubicin was added at its IC_{50} of 6.2 nM for DLD-1 and 12 nM for SW480 cells on day 1. Cells were cultured for a period of 8 days and were counted each day at the same time. Error bars represent mean ± S.D. (n = 6). **, P < 0.01; ***, P < 0.001.

6.2.2 Idarubicin induces acquisition of stem-like properties

To study the effect of idarubicin on CRC-SCs, three dimensional colonospheres representing CSC population were incorporated and assessed for their colonosphere formation ability, morphology changes as well as acquisition of stem-like properties.

3D colonospheres were cultured from CRC cell lines as described in **Chapter 2;** Materials and Methods (Shaheen et al., 2016c). On day 14, colonospheres were treated with idarubicin for 72 h. At the end of the treatment, colonospheres were counted under a microscope and their formation efficiency was quantified. In both DLD-1 and SW480 cell lines, as evidenced in the representative microscopic images in (**Figure 6-9**), idarubicin caused extensive irregularity and debris-like structure, particularly in DLD-1 cell derived colonospheres, making them difficult for manual counting. However, in SW480 cell derived colonospheres, our data showed significant reduction in colonosphere formation upon idarubicin treatment (**Figure 6-10**). Relative changes in colonospheres morphology were assessed by comparing the images of idarubicin treated and untreated colonospheres. The complete loss of spherical structure and integrity could be indication of cell death induced by idarubicin.

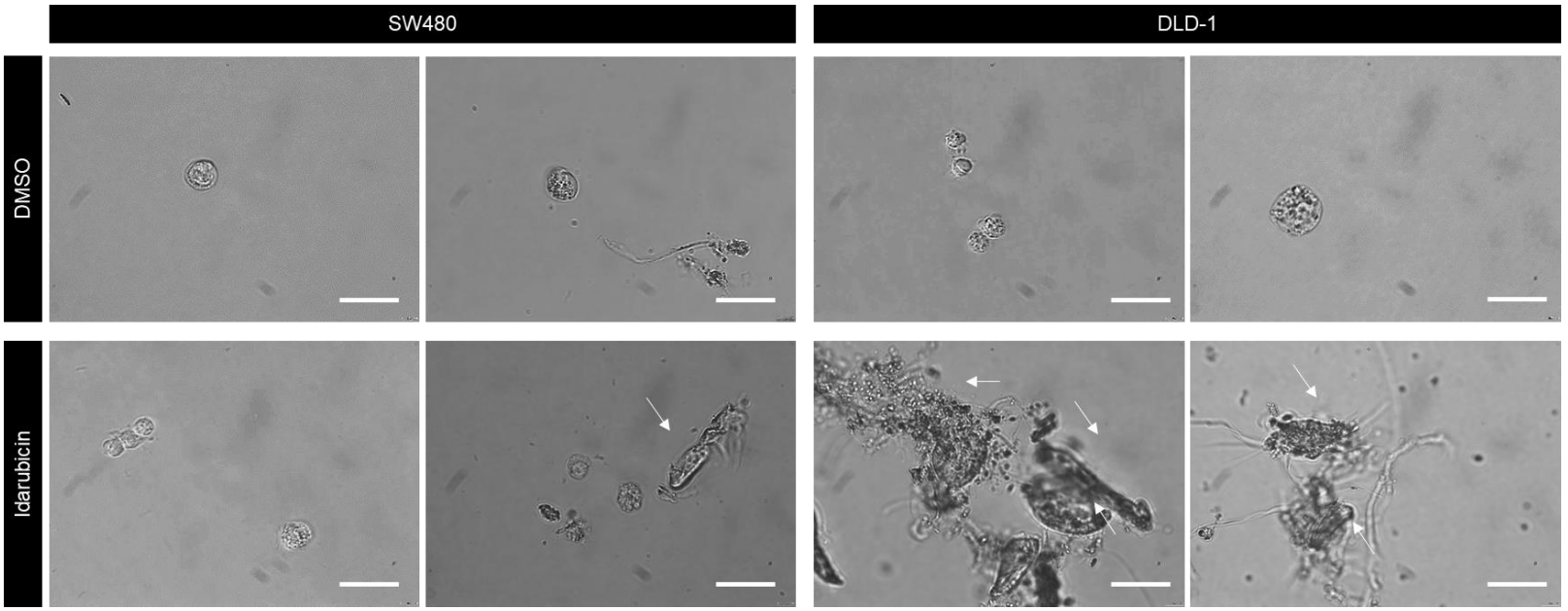


Figure 6-9: Idarubicin showing extensive irregular structures in colonosphere. Images were taken after idarubicin treatment. Untreated colonospheres maintained their distinct structural network of cells whereas the treated colonospheres showed discrete irregular debris-like structure and loss of their structural integrity. Scale bar: 25 μM.

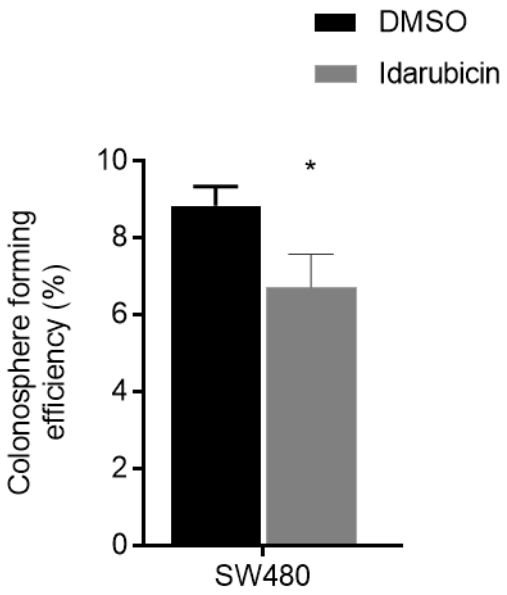


Figure 6-10: Idarubicin significantly reduced colonosphere formation efficiency in SW480 cells derived colonospheres. Colonospheres were derived from SW480 cells and were treated with idarubicin for 72 h. Significant reduction was observed for colonosphere formation in the treated group. Error bars represent mean ± S.D. (n = 25).

To depict the pathways associated with the mechanism of idarubicin on CRC, a gene expression analysis was performed from mRNA isolated from colonospheres using qPCR analysis. In contrast to **Chapter 4** and **Chapter 5**, our result showed significant increase in LGR5, CD44, NANOG and OCT-4 expression level upon idarubicin treatment, indicating induction of stem-like activity. This result was in line with the initial CDy1 based screening revealing high fluorescence intensity with idarubicin treatment.

In addition, differentiation markers KRT20, CDX2 and MUC2 were significantly decreased in the treated group indicating lack of differentiation with idarubicin treatment (**Figure 6-11; B**). Such results explain the stem-cell phenomena that is in favour of stemness associated to self-renewal over differentiation. Therefore, the extensive loss in

structural integrity in colonosphere as observed in **Figure 6-9**, indicates cell death or senescence rather than differentiation induction. In addition, idarubicin also increased both N-cadherin (NCAD) and Vimentin (VIM) expression (**Figure 6-11; C**) suggesting its affiliation on EMT (Li et al., 2019b). Due to the reduced level of tumour suppressor FBXW7, genes associated to the transcription factor for recurrence, poor survival, metastasis and tumour suppressors levels in general were also increased (**Figure 6-11; D**). Of note, deletion of FBXW7 itself is associated to high tumorigenic activity in CRC (**Chapter 3; 3.2.1**).

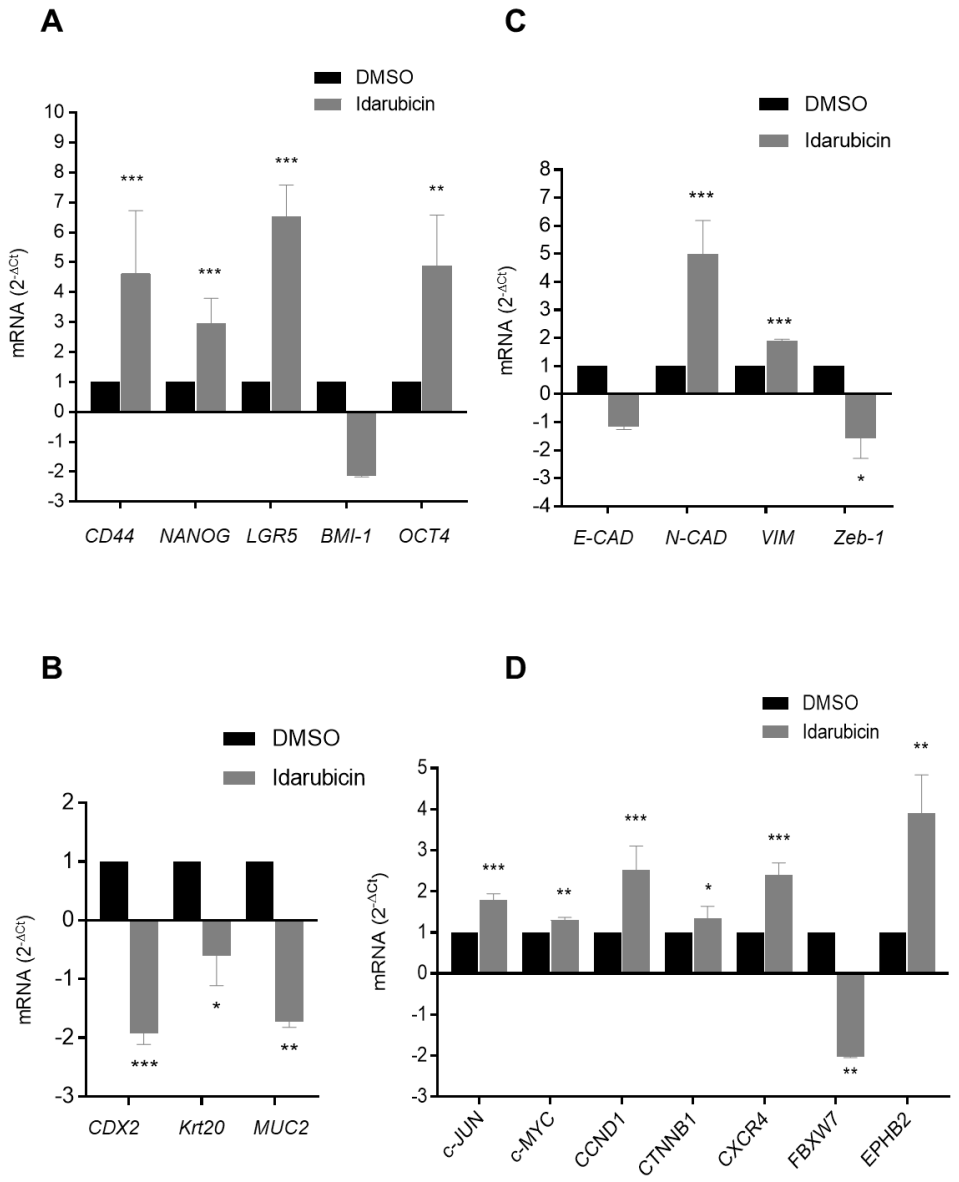


Figure 6-11: qPCR analysis of colonospheres upon idarubicin treatment. (A) Stemness, **(B)** differentiation, **(C)**, EMT, and **(D)** transcription factor for recurrence, poor survival, metastasis and tumour suppressor, in colonospheres obtained from DLD-1 cells. (n = 3; *, $P < 0.05$; **, $P \leq 0.01$; ***, $P \leq 0.001$).

6.2.3 Idarubicin induced apoptosis and growth arrest in patient derived *ex vivo* tumour organoids

Patient derived tumour organoids display selection of different morphologies that can be measured and assessed for any structural changes in response to drug treatment (Yip et al., 2018, Stelzner et al., 2012, Li et al., 2019b).

Patient derived organoids were cultured and for their treatment and subsequent analyses (Kashfi et al., 2018, Ahmed et al., 2019). Organoids were allowed to start budding for 5-6 days prior to treating them with idarubicin. In addition to growth, organoid morphology, survival and apoptosis were also evaluated in response to idarubicin. By analysing the complex phenotypical changes in organoid culture, idarubicin treatment exhibited reduced proliferative activity, extensive impediment on tumour growth, and induced apoptosis. Idarubicin treatment decelerated organoid growth caused cell death within the culture. Moreover, some level of morphology change was also observed. By looking at the morphologies of untreated tumour organoid, our data shows that at day three, most of the organoids in control group were formed by enterospheres (~70%). For over a period of fourteen days, these organoids tend to grow and eventually turned into defined round cystic organoids (>700 μm). In contrast, in the treatment group, at day three of idarubicin treatment, growth arrest was fully visible even though the majority of the organoids were still showing enterospheres phenotype. As treatment progressed, shrinkage in their size and eventually a densely packed dead-cell volume was thoroughly visible throughout the culture suggesting extensive growth arrest and cell death. (**Figures 6-12, 6-13**).

Idarubicin induced growth arrest was evident on day 3 of treatment, which continued to follow the same pattern throughout the treatment (1.99×10^8 μm^3 vs 0.12×10^8 μm^3; $P \leq 0.01$) (**Figure 6-14**). At the end of the treatment, almost all the treated organoids were considered to be

dead (**Figure 6-12**). However, amongst the living organoids, majority were in the size group of 100-300 μm, whereas, in untreated control organoids about 60% of organoids were within the range of 501-700 μm (**Figure 6-14**).

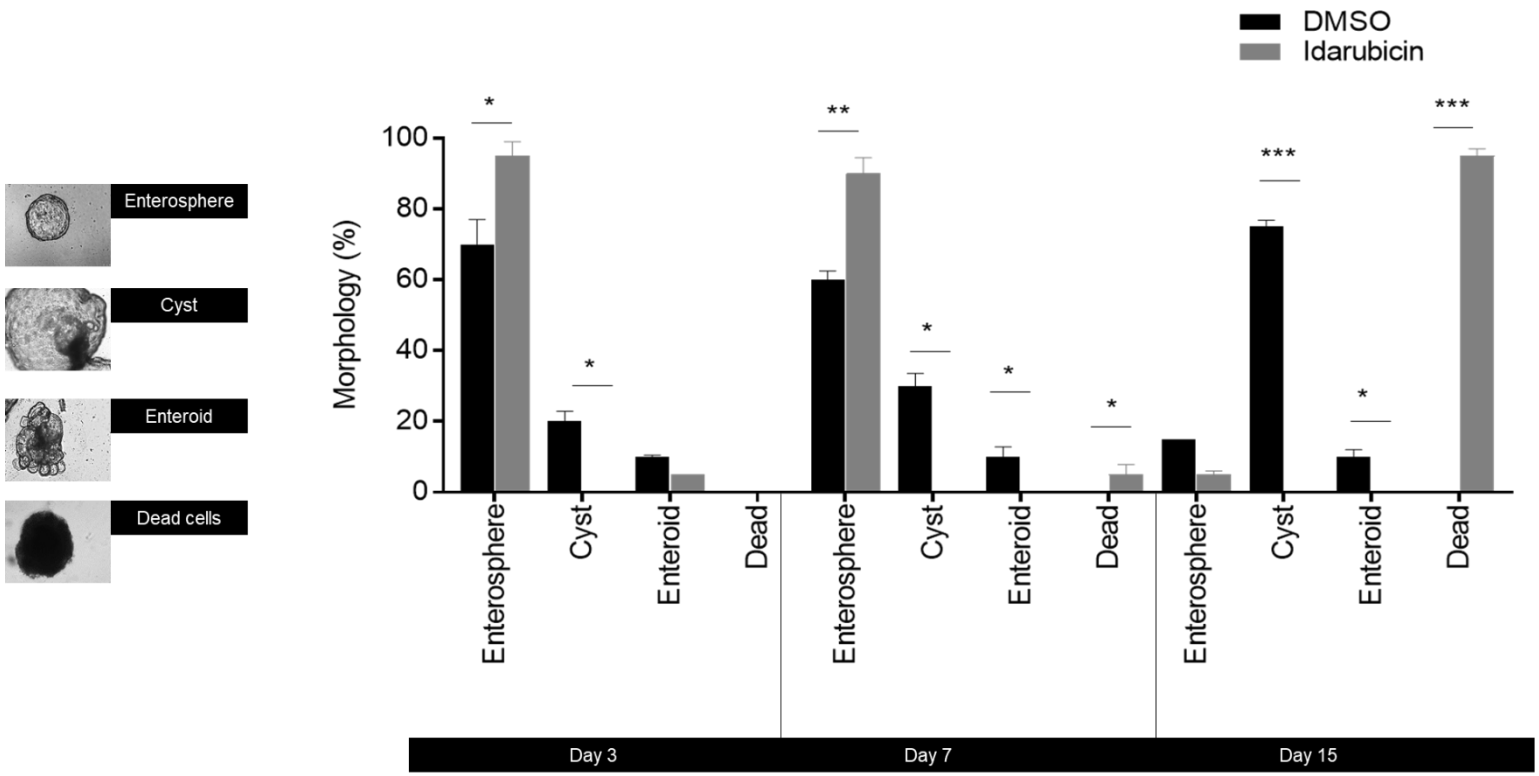


Figure 6-12: Idarubicin treatment induced cell death in tumour organoids. Percentage of enterospheres, cysts, enteroids and dead cells were measured at day 3, 7 and 15 days of treatment. Organoids were counted by microscopy. *, P < 0.05; **, P < 0.01; ***, P < 0.001.

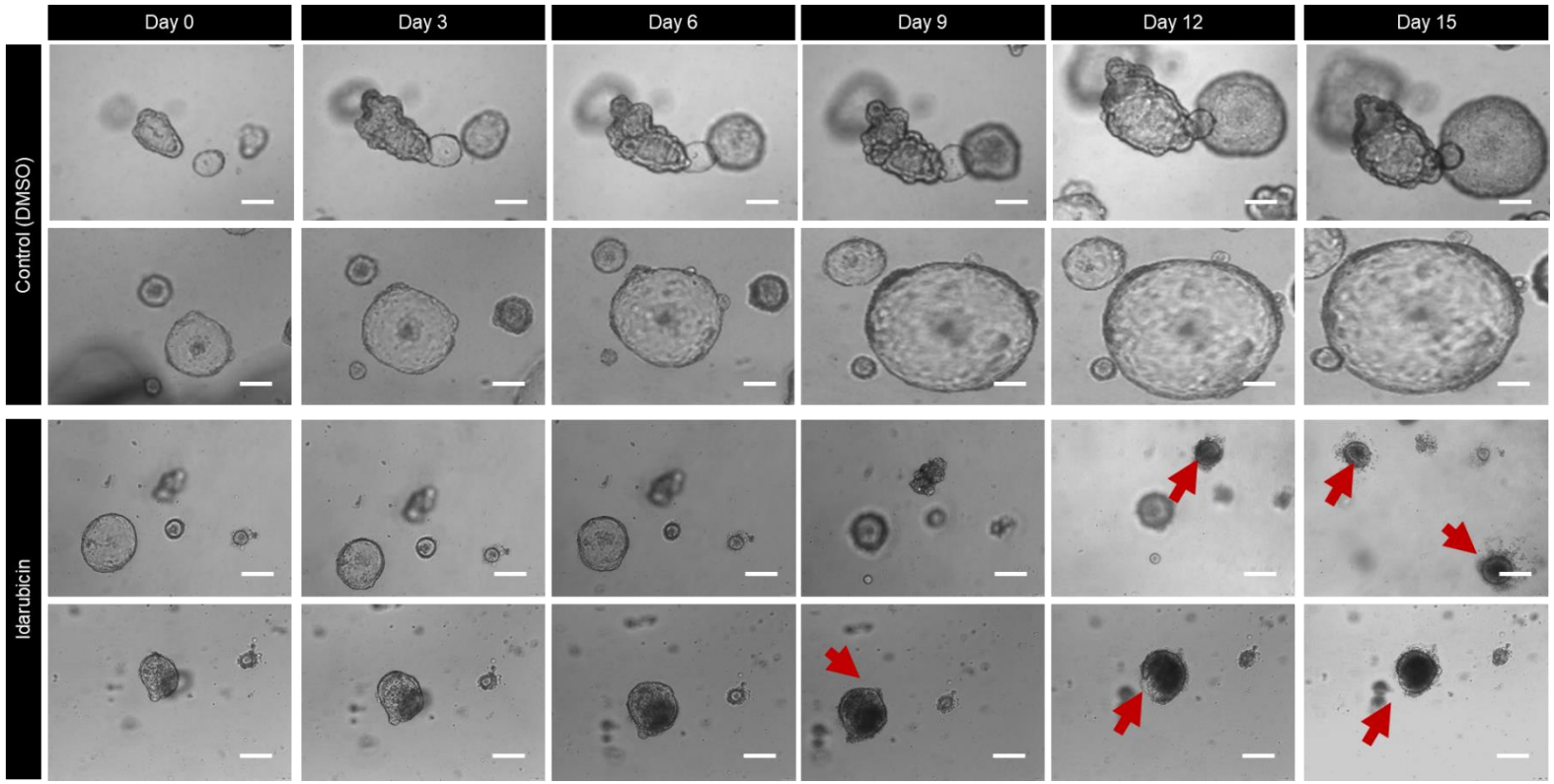


Figure 6-13: Organoid growth arrest and cell death induced by idarubicin. Representative images of tumour organoids treated with idarubicin for a period of 2 weeks. Cell death and variation in growth were observed throughout the treatment period (red arrowheads). Images were taken using Leica microscope. Scale bar: 75 µM.

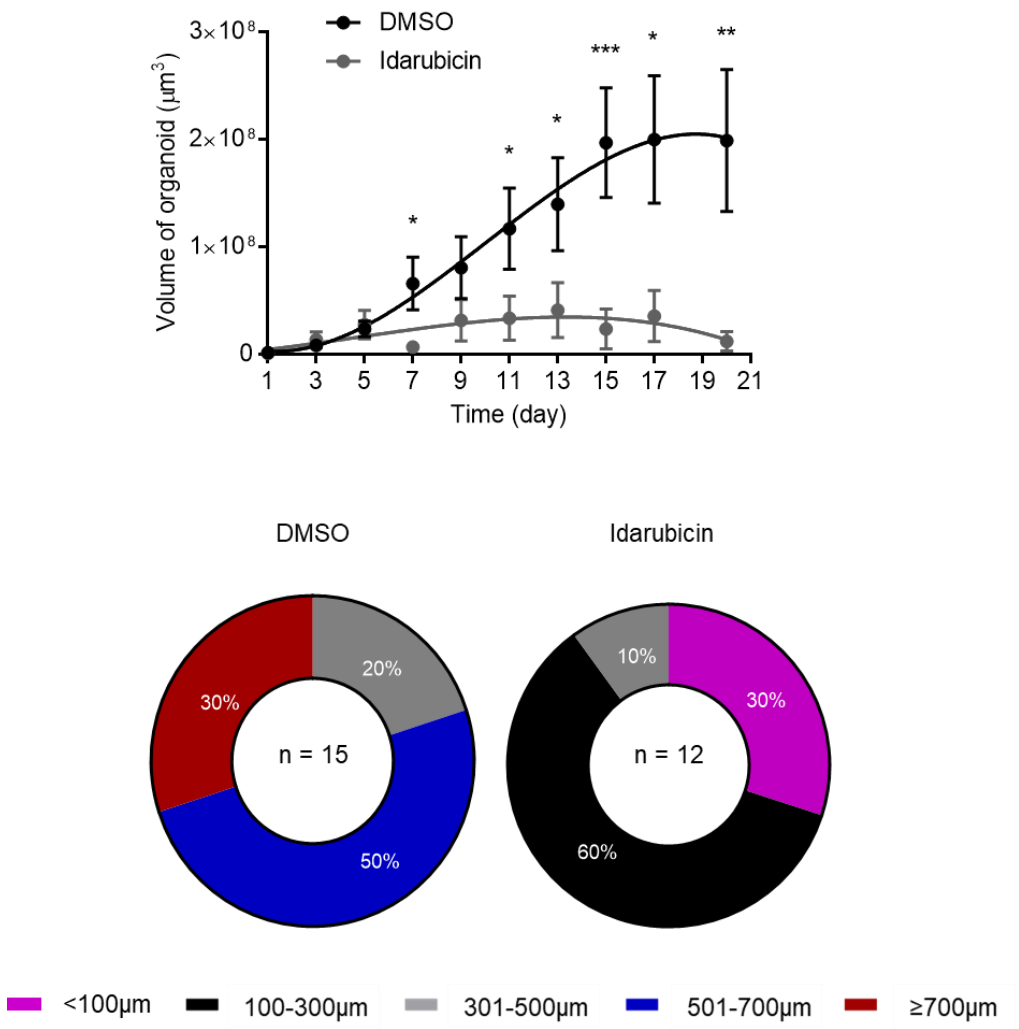


Figure 6-14: Idarubicin treatment hindered the growth in in tumour organoid. Volumes of organoids were measured every 2 days. Number of organoids in different size groups at the end of the treatment shows significant inhibition to the tumour growth in the treated group. Numbers in each size group are expressed as percentage of the total. Error bars represent mean ± S.D. (n = 15; control, n = 10, idarubicin).*, $P < 0.05$; **, $P < 0.01$; ***, $P < 0.001$.

This result shows that majority of idarubicin-treated organoids were dead and within smaller diameter range, suggesting its inhibitory effect on organoid growth and induction of apoptosis. In addition, cell dead/alive status was also identified by PI/Hoechst staining. At the end of the treatment period, organoids were collected carefully and processed for staining. Idarubicin treatment showed induction in PI

staining followed by a 2 weeks treatment period in tumour organoids (**Figure 6-15**). This result suggests idarubicin induced cell death on tumour organoids.

Therefore, based on the organoid data, this could potentially be hypothesised that idarubicin induces significant changes in tumour size and morphology and tumour growth, (**Figures 6-12, 6-13, 6-14**) and induced apoptosis (**Figures 6-12, 6-13, 6-15**) in organoid model.

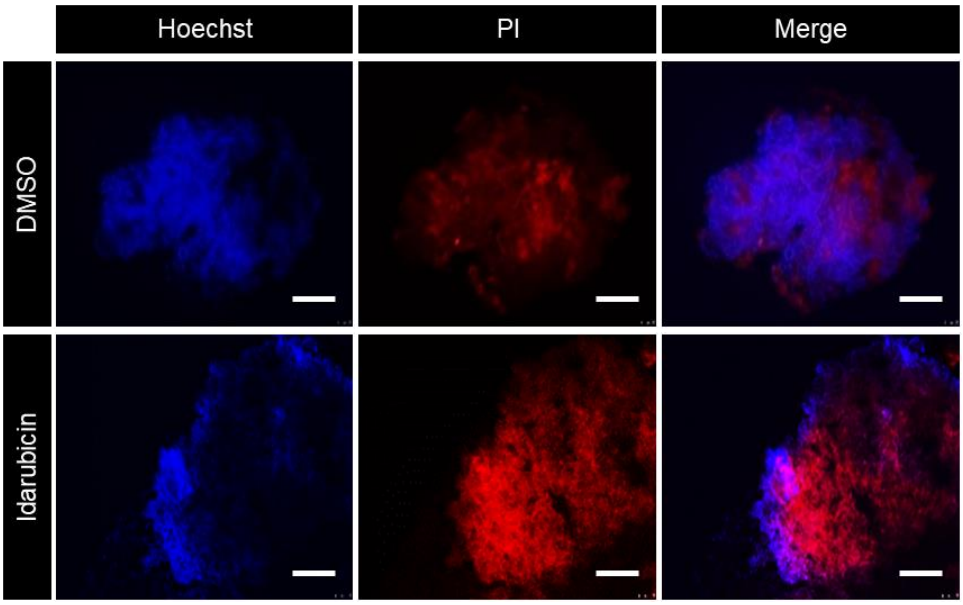


Figure 6-15: Hoechst/PI staining on idarubicin treated organoids. Increase in PI staining indicates induction of cell death in idarubicin treated group. (n = 10). Scale bar: 25 μM.

6.2.4. *Ex vivo* treatment of CRC patient biopsies evaluates idarubicin as an anticancer drug with capacity to enrich CSCs

In order to obtain patient relevant predictability of CRC response to idarubicin while maintaining the original tissue organization and architecture, we have utilised the *ex vivo* tumour explant model obtained from CRC patient tissues (Karekla et al., 2017a).

Tissue explants were cultured from 5 patients and treated with idarubicin as previously described in **Chapter 2;** Materials and Methods. Following the treatment, idarubicin's response was evaluated for subsequent stemness, differentiation, proliferation and apoptosis deliberated in tumour tissue (**Figure 6-16**). IHC analysis of idarubicin treated tumour explants showed a decreasing trend of cell proliferation and differentiation markers with increasing level of apoptosis and stemness marker (**Figure 6-16**). Levels of Ki-67 staining representing the proliferating cells were significantly decreased by idarubicin as compared to the control-treated group on explant model (**Figure 6-16; A**). In line with the organoid data suggesting induction of cell death, in the explant model, idarubicin treatment also showed a significant increase in pro-apoptotic protein Caspase-3 staining (**Figure 6-16; B**). This further confirms the organoid data exhibiting cell death by idarubicin treatment, however further investigation needs to be carried out whether idarubicin induces specific cell-cycle arrest or mechanisms for cell senescence is involved herewith. Next, to associate idarubicin with cellular differentiation and stem-like activity, CDX2 and MUC2 were also utilised as markers for differentiation and CD44 as 'stemness' marker in tumour explants (**Figure 6-16; C, D and E**). Our result showed a significant decrease in CDX2 expression in tumour explants suggesting significant reduction in differentiation as well as increase in tumorigenic activity. In addition, MUC2 expression is also extensively reduced with idarubicin treatment (H score: 120 vs 250) (**Figure 6-16; E**). Of note, MUC2 is a colonic mucin mostly usually by goblet cells (Betge et al.,

2016). In line with the proliferation pattern, CD44 also showed a similar trend in increasing the stemness level in cultured tumour explants treated with idarubicin (**Figure 6-16; D**). Therefore, the *ex vivo* tumour explant data suggests idarubicin to have antitumorigenic effect on CRC particularly for its inhibitory effect on tumour growth and proliferation. However, our data also reveals that idarubicin may also be capable of enriching CRC-SCs that express CD44.

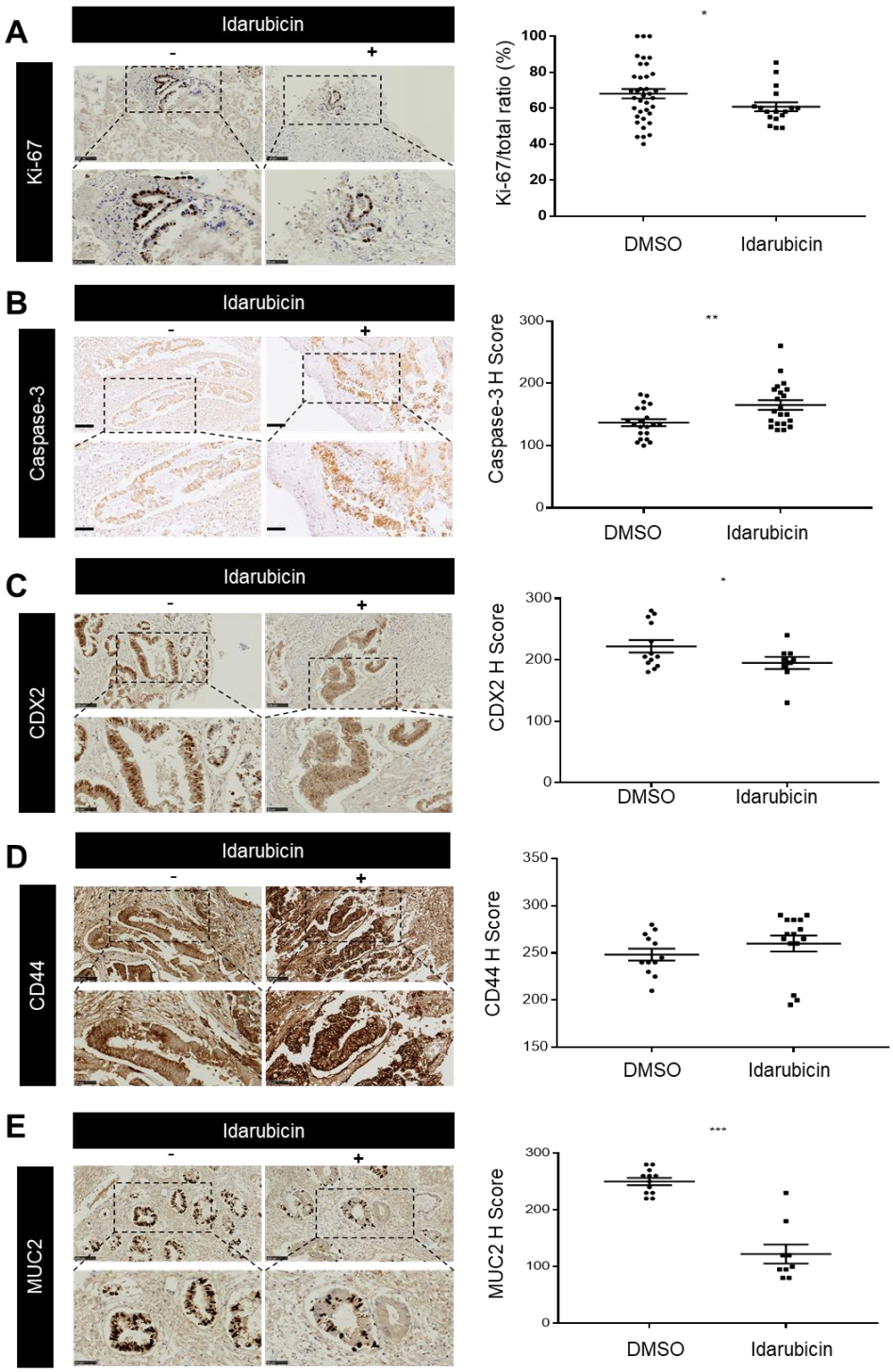


Figure 6-16: Effects of idarubicin on proliferation, apoptosis, stemness and differentiation level in the tissue explants obtained from CRC

patients. (A-E) Proliferation was assessed by quantitating Ki-67 **(A)** IHC staining, cell survival by caspase-3 **(B)**, whereas differentiation and stemness levels were assessed by CDX2 **(C)**, CD44 **(D)** and MUC2 **(E)** staining quantification respectively. IHC stains were counterstained with hematoxylin and eosin. Representative images (top panel) shows the images at 20x magnification with a scale bar of 100 μm. Bottom panel shows the selected parts in higher 40x magnification with scale bar 50 μm. Each dot (Right panels) represents an image used for quantification. Control treated groups represents the level of intrinsic proliferation, stemness and differentiation level in tumours. For the Ki-67 staining, Ki-67 +ve cells were counted and expressed as a percentage of the total cells. In case of CD44, MUC2, CDX2 and Caspase-3, H-scores were counted as a measure for the quantification. Tumour tissues were obtained from 5 different patients, and 4 segments of tissue were used for each patient. *, $P < 0.05$; **, $P < 0.01$; ***, $P < 0.001$.

6.3 Discussion

Our results suggest potential antitumor effect of idarubicin in CRC, with possible enrichment of stem-like characteristics. It has previously been reported that some chemotherapy drugs, including taxanes and anthracyclines, not only fail to eliminate CSCs, but selectively enrich CSCs possibly by inducing dedifferentiation or trans-differentiation (Larzabal et al., 2013, Zhou et al., 2009, Tanei et al., 2009, Yu et al., 2007b). This subsequently suggests an existing plasticity for both CSC and non-CSC populations. For example, combination therapy of Paclitaxel and anthracycline drug epirubicin has shown to increase the ALDH+ CSCs in human breast cancer cells *in vitro*. In lung cancer patients, both erlotinib and cisplatin-based chemotherapy has shown to selectively enrich CD133+ cells (Leon et al., 2016). In NSCLC, even a low dose of cisplatin treatment (IC_{20}) was sufficient to exert such effect and exhibit drug resistance and stem cell characteristics with high sphere formation and self-renewing capacity (Larzabal et al., 2013, Levina et al., 2008). All these reports suggest that certain conventional anticancer drugs have the potential to harbour the CSCs in addition to their antitumor activity.

Among the anthracyclines, idarubicin is more cytotoxic and effective, especially in its DNA binding capacity and apoptosis induction than the parent drug daunorubicin (Dragojew et al., 2008). Typically, it acts by intercalating into DNA and inhibiting topoisomerase II, thereby ultimately, inhibits DNA replication. Additionally, it also induces oxygen free radicals thereby causes destruction of DNA and cell membrane (Gunduz et al., 2014). However, one of the major disadvantages of anthracyclines is the irreversible cardiomyopathy which largely impacts patient quality of life for up to 30 years of post-anthracycline treatment (Silva Dos Santos et al., 2018, Raj et al., 2014). Idarubicin possesses reduced cardiac toxicity among the others, making it an important candidate to study in CRC.

A striking observation in this study was that treatment with idarubicin, although exhibiting antitumorigenic activity in CRC particularly by reducing tumour growth and volume, also increased the expression of

NANOG, LGR5, CD44, and OCT-4. In tumour explants, idarubicin reduced cell proliferation and induced apoptosis. Previously, a similar increase in Caspase-3 and subsequent intracellular calcium increase was reported to cause loss of mitochondrial membrane potential. Such idarubicin induced Caspase-3 activation occurred in the late stages of the apoptotic pathway (Gieseler et al., 2000).

Our results showed that idarubicin treated colonies have a scattered cytoskeletal network with relatively lower nuclear density. In organoid model, increase in cell death was evident from the PI staining. Our results were highly comparable with increase in transcription factors associated with recurrence, poor survival and metastasis with high expression of c-JUN, c-MYC, CCND1 and CXCR4 in idarubicin treated colonospheres. Accumulating data suggest that CXCR4 (CXC chemokine receptor-4) and SDF1 (Stromal derived factor-1) could regulate migration and metastasis and correlates to poor prognosis in a variety of cancer cells (Levina et al., 2008). For example, in lung CSCs, CXCR4 expression is reported to be higher than the non-CSC population (Larzabal et al., 2013). In line with this, our results showing such upregulations of CXCR4 could denote the enhanced tumorigenic and metastatic potentials influenced by idarubicin, which was also indicated by the wound healing assay.

In organoid model, idarubicin showed clear evidence of growth arrest and cell death. Such impairment of tumour growth could reflect on the increased progression free survival (PFS) in patients, which, while being initially advantageous, might be short lived and therefore not necessarily benefit in overall survival (OS), particularly due to the presence of CSCs (Pàez-Ribes et al., 2009). As such, bevacizumab and sunitinib, though inhibiting primary tumour growth, caused changes in microenvironment that especially allowed tumour extravasation, indicating the crucial influence of growth and angiogenic factors on their tumorigenic and metastatic potentials (Larzabal et al., 2013, Ebos et al., 2009, Levina et al., 2008).

Additionally, immunostaining of *ex vivo* tissue explants revealed reduction in proliferation and differentiation while inducing apoptosis and stemness activity with idarubicin treatment. Tumour cell proliferation has an important role in tumour progression and metastasis in a variety of human cancers. The chemokines and growth factors produced by the tumour can also help the tumour cells to eventually escape drug-mediated destruction (Levina et al., 2008). Realization of the vital question that how such therapy can offer patient benefit despite increasing metastasis and other CSC like properties, therefore, stresses on the fundamental strategies of targeting both CSC and non-CSC population. In future, it will be useful to carry out gene expression analysis to elucidate the target and potential pathways associated to idarubicin mediated anticancer effects in CRC.

CHAPTER 7

General Discussion

7.1 Overview

Tumorigenic subpopulation of undifferentiated cancer stem-like cells is of major therapeutic interest especially to devise novel diagnostic and therapeutic agents to meet the current challenges in cancer treatment. In this study, a colonosphere platform was utilised that selects a CSC-like population *in vitro* comprising only 2.5-5% of the total tumour population (Shaheen et al., 2016b, Weiswald et al., 2015a, Ricci-Vitiani et al., 2007) and incorporated it into a screening of NCC (NIH Clinical Collection) compound library. Three compounds with antibacterial/anti-inflammatory properties were characterised; AM404, rifabutin and cytotoxic antibiotic idarubicin for their ability to influence differentiation on CRC. Being one of the major hallmarks of cancer, inflammation itself can further contribute to multiple hallmark capabilities (angiogenesis, invasion and metastasis) by supplying several bioactive molecules (i.e. growth, survival and proangiogenic factors) to the tumour microenvironment (Hanahan and Weinberg, 2011, Greten and Grivennikov, 2019, Lasry et al., 2016). In this study, we showed that:

(I) the 3D colonosphere and CDy1 based platform can be utilised as a reproducible and reliable tool to conduct small-scale drug screening in order to identify compound(s) targeting CRC for differentiation.

(II) AM404 is a potent anticancer drug that acts via FBXL5-E3-ligase in CRC. FBXL5 (F-box and leucine-rich repeat protein 5) deleted cells, being sensitive to AM404, exhibits subsequent additional inhibition in the migration. In addition, AM404 causes differentiation in CRC cells, without necessarily inducing cell death.

(III) Rifabutin shows promising inhibitory effects in neoplastic cell growth and proliferation, possibly by suppressing FBXL5. Additionally, rifabutin exhibited apoptosis induction, and showed significant inhibition in migration independent of the FBXL5 status.

(IV) Idarubicin exhibits antitumor activity in CRC while enriching CRC-SCs.

(V) oncogenic FBXL5 plays a vital role in CRC metastasis, which can be reversed by FBXL5 deletion.

7.2 Anti-inflammatory drug AM404 targets FBXL5-E3 ligase in CRC

As mentioned earlier, we focused on the inflammatory aspect of cancer, which accounts for about 20% cases. Anti-inflammatory drugs including COX2 inhibitors have long been found to reduce tumour incidence, progression and mortality, particularly in the case of sporadic colon cancer (Grivennikov et al., 2010, Greten and Grivennikov, 2019). As an active metabolite of paracetamol, AM404 fundamentally acts as an inhibitor of both cyclooxygenase COX1 and COX2. Previously, in human T-cells, AM404 has been reported as a potent inhibitor for T-cell activation regulating NF-κB, NFAT, and AP-1 by inhibiting both IL-2 and TNF-α for transcription and protein synthesis (Saliba et al., 2017). Moreover, it has shown to decrease IL-1β and IL-6 production and thereby increase circulating TNF-α levels in murine model (Saliba et al., 2017).

Using the advent of colonospheres, organoids and tissue explant models, we are first to report its extensive anticancer effects on CRC (Ahmed et al., 2019). Our data suggests AM404 treatment causes significant reduction in tumour cell proliferation, metastasis, growth and volume, while increasing the expression of tumour suppressor *FBXW7*, which has recently been published from our lab to be affiliated in EMT (Li et al., 2019b). Of note, in both organoids and tissue explants, cell death was not affected by AM404 treatment, indicating AM404 mediated anticancer effects and induction of differentiation are independent of cell death. This postulation might follow the underlying principle of differentiation therapy, which forces the undifferentiated cancer stem-like cells toward

terminal differentiation. Such indication stresses the importance of investigating AM404 in combination with other conventional anticancer drugs targeted to eliminate the proliferating and differentiating cancer cells.

Furthermore, by suppressing *FBXL5* E3-ligase, AM404 mimics the effect of *FBXL5* deletion and prevents subsequent invasion in CRC cells. When used in *FBXL5*-deleted cells, AM404 showed sensitivity and further additive effect in preventing CRC invasion. This finding highlights AM404 as a new compound to target FBXL5 in blocking the invasiveness and metastasis associated with EMT (**Figure 7-1**).

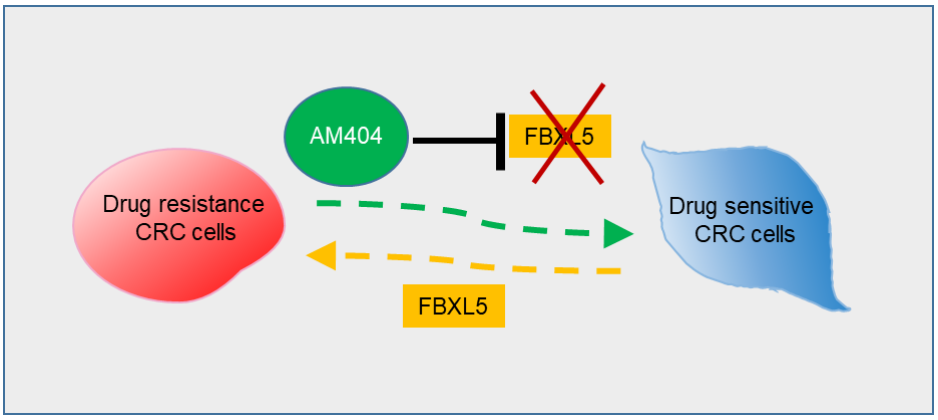


Figure 7-1: AM404 sensitivity demonstrating silencing of FBXL5. FBXL5 deletion confers to inhibition of migration, thereby re-sensitising the CRC cells to AM404 treatment.

7.3 Antimicrobial rifabutin confers antineoplastic activity in CRC

Rifabutin is a broad-spectrum antibiotic used in the treatment of tuberculosis and is currently being investigated for its anticancer effects in lung cancer. In this study, rifabutin showed significant anticancer effects on CRC by impeding neoplastic cell growth, inducing

differentiation, and inhibiting cell proliferation and metastasis, as similar to AM404.

However, unlike AM404, rifabutin showed slight induction of apoptosis in organoids. Induction of apoptosis with rifabutin has previously been reported for lung cancer (Li et al., 2016a). In both *in vitro* cultured lung cancer cells and *in vivo* xenograft mouse models, rifabutin effectively induced apoptosis by eIF4E-β-catenin-dependent manner (Lim et al., 2013, Siddiqui and Sonenberg, 2015, Li et al., 2016b). Additionally, antitumor agents have shown to inhibit Akt and Erk in colonospheres and xenografts leading to TRAIL-mediated cell death (Prabhu et al., 2015).

In addition, we showed that both rifabutin treatment and *FBXL5* deletion independently caused inhibition in CRC migration but combining them together did not cause any additional inhibitory effect. Given the observation from AM404, we speculated that the additive effect is due to the drug sensitivity mimicking *FBXL5* deletion. Interestingly, *FBXL5* deleted cells were also sensitive to rifabutin treatment and hence, combinatory additional inhibition was expected on *FBXL5* deleted cells upon rifabutin treatment. One possibility for such deviation could be explained by core pharmacokinetic point of view, considering receptor saturation. As such Paul Ehrlich's famous principle, "corpora non agunt nisi fixate"—a substance will not work unless it is bound (Yan, 2015), efficacy and binding of drugs to specific receptors highly depends on the availability of their receptors. The binding sites within a receptor are typically saturated at high ligand concentrations. When all binding sites are occupied, no further binding would occur, even with increasing ligand concentration. Of note, long term receptor saturation has previously been reported to result in severe side effects or toxicity, which might be indicative of rifabutin induced cell death (Fu et al., 2019). In parallel, once the pharmacological effects reach its maximum (Emax), further increase in the ligand concentration does not result in higher

response (Salahudeen and Nishtala, 2017). However, this phenomenon needs to be further investigated, possibly by incorporating receptor binding assays (Hulme and Trevethick, 2010) which would allow to determine the Kd (ligand concentration that binds to half the receptor sites at equilibrium) and Bmax (maximum number of binding sites). Furthermore, these observations could have clinical implications and potential for future research in respect to dose variation, treatment schedule and highlight the importance of combination drugs in adjuvant settings.

7.4 Possible CRC enrichment with idarubicin

Idarubicin belongs to anthracycline group of cytotoxic antibiotics and is used in the treatment of leukemia, lymphoma and advanced breast cancer. Our results suggest potential antitumor effect of idarubicin in CRC, though interestingly, while showing reduction in tumour growth and proliferation, idarubicin also showed possible enrichment of CRC-SCs. In general, anthracycline based chemotherapy confers high risk of initiating secondary carcinogenesis (Dracham et al., 2018, Vega-Stromberg, 2003), while the CSC population is well established for their capabilities in developing secondary tumours (Shiozawa et al., 2013, Brower, 2013).

However, harbouring CSCs with conventional anticancer drugs have been repeatedly reported including anthracycline and taxanes, for not only their failure to eliminate the CSCs population, but also for selectively enriching them (Zhou et al., 2009, Ahmed et al., 2017b, Tanei et al., 2009). For example, chemotherapy with Paclitaxel with and without anthracyclines has shown to select and expand the ALDH+ CSCs population in ovary cancer and breast cancer patients respectively (Li et al., 2008). In both Erlotinib and Cisplatin-based chemotherapy in lung cancer patients and Paclitaxel treatment in xenografts, CSC selection with enriched CD133+ cells and promoted lung metastasis was reported (Leon et al., 2016, Larzabal et al., 2013). In our study, idarubicin showed

increased expression of CD44, LGR5, and other well-established markers associated to stem cell signature, while showing reduction in E-cadherin and FBXW7 expression, indicating its negative regulation in EMT (Li et al., 2019b, Diaz and de Herreros, 2016). Moreover, it showed significant reduction in the differentiation level followed by significant induction of cell death in all the experimental models used. Previously, CD44 positive cells have been reported to have association with increased apoptosis. For example, such incident was reported with curcumin treatment by coupling to CD44 on the cell membrane and blocking glutamine transport into the cells, thereby decreasing its intracellular concentration (Huang et al., 2016). Nevertheless, having reduced the expression of tumour suppressor *FBXW7*, idarubicin further indicates higher CSC like activities. However, the interplay between *FBXW7* and stem-like activity in response to idarubicin needs further characterisation.

7.5 FBXL5 is associated in CRC metastasis

FBXL5 has previously been reported as an oncogene that is associated with colorectal cancer progression, cell proliferation, growth, and overall tumorigenesis (Yao et al., 2018, Dragoi et al., 2014). In line with this, our array revealed FBXL5 as one of the top differentially expressed genes that showed ≥ 3-fold suppression upon treatment with both AM404 and rifabutin. We further showed that deletion of *FBXL5* causes significant decrease in metastasis and by mimicking the effect of *FBXL5* deletion, both these drugs eventually prevented the migration in CRC cells. This postulation is backed by significant reduction in N-cadherin and Vimentin expression and increase in FBXW7 expression level. Of note, increased expression of FBXW7 caused subsequent reduction in Wnt target genes such as c-MYC, c-JUN and relevant prognostic factors for CRC. In this regard, FBXL5 has previously been reported for its negative correlation on EMT and EMT inducers (Li et al., 2019b, Yao et al., 2018, Diaz and de Herreros, 2016, Dragoi et al., 2014).

In CRC, FBXL5 acts through PTEN/PI3K/AKT signalling (Yao et al., 2018) and HIF-1 transcriptional activity (G et al., 2015) and its overexpression has resulted in high tumour formation ability in CRC (Yao et al., 2018, Dragoi et al., 2014). To note, PIK3CA/AKT/PTEN signalling have been postulated as one of the potential targets of NSAIDs for tumour associated inflammation (Diakos et al., 2014). In this study, AM404 and rifabutin treatment suppressed *FBXL5* expression, and in addition to inhibition of metastasis, we simultaneously showed that loss of FBXL5 also makes cells more sensitive to the therapy and therefore, we postulate FBXL5 as an associated key target gene in CRC. Moreover, ongoing works in our lab (data not shown) also suggests association of FBXL5 in targeting EMT in human colorectal cancer. Altogether, such findings also stress the importance to characterise other F-box proteins for their roles in cancer, which could be a key breakthrough for cancer therapy and offer new potential biomarker(s) for early detection of epithelial tumour progression.

7.6 Experimental limitations

Although a wide range of *in vitro* and *ex vivo* approaches were carried out for each finding yielded from this study and for ensuring effective evaluation of the anticancer effects of the selected compounds, several experimental limitations were also encountered. These mostly account for time limitations, for example:

(I) Due to time limitation, incorporating some additional important CSCs markers, including CD133, ASCL2, and SOX9 (Snippert et al., 2009, van der Flier et al., 2009b, Formeister et al., 2009) were not possible in this study. In addition to these CSC markers, we also could not investigate the self-renewal activity in response to the candidate drugs. Assessment of cells undergoing symmetrical cell division, indicative of CSC-enrichment would be important to justify our understanding for each compound differentiation (Lerner and Petritsch, 2014, Bu et al., 2013). This might

be of particular importance for evaluating idarubicin induced CSC enrichment.

(II) Characterisation and validation studies were also limited to using *FBXL5* deleted cells only. If time permitted, it would have been interesting to look into a few more differentially expressed genes and carry out their validation using WB and qPCR analysis.

(III) Due to time limitation, a limited number of studies were performed regarding cell migration and drug resistance analysis. Incorporating 5FU or Oxaliplatin resistant cell lines into the drug treatment could be beneficial for investigating the drugs induced chemosensitivity.

(IV) Again, for the time restriction, all the drugs were used as monotherapy. Employment of the candidate drugs into current chemotherapy regimens at different concentrations could essentially be helpful in designing new therapeutics with the ultimate objective of eliminating CSCs.

(V) Considering the fact that, the tumour tissues obtained following CRC patients' surgeries were limited and smaller in size, parallel experiments with multiple drugs at the same time made the sample size smaller for each group while studying the tumour explants.

(VI) All experiments were carried out using the IC_{50} obtained from monolayer cells. It is known that 3D models possess higher resistance to drugs compared to the monolayer cells (Langhans, 2018, Imamura et al., 2015, Huang and Hsu, 2014). While using this IC_{50} gave us an effective estimation, dose adjustment is required to minimize experimental technique errors and to obtain more accurate information in preclinical settings.

(VII) Absence of xenograft studies presents another limitation of this study. Future study to evaluate the candidate compounds on the invasive

and metastatic potential will be necessary to undertake using *in vivo* xenograft assay.

7.7 Concluding remarks and future perspectives

In conclusion, findings from this thesis highlight the antineoplastic prospective of three antibacterial/anti-inflammatory agents in colorectal cancer. In parallel, this study also unveils the potential involvement of FBXL5 in EMT-associated drug resistance, stem-like cells properties, invasion and metastasis, and thereby presents FBXL5 as a therapeutic target in CRC.

However, further research could be necessary to be followed-up in future:

(I) The cornerstone of governing molecular and cellular mechanisms of tumour-promoting inflammation needs to be defined in perspective of FBXL5 in cancer biology (Yao et al., 2018, Diakos et al., 2014).

(II) Examining the mode of cell division (symmetric vs. asymmetric) of FBXL5 knockout CRC cells by BrdU labelling and paired cell assays could provide better understanding of CSC homeostasis in response to the drugs.

(III) CRC patient derived *ex vivo* tissue explants can be obtained from normal adjacent tissues and compared to the drug responses obtained tumour explants. This would allow determining the specificity of drugs to selectively target cancer cells while sparing the healthy ones.

(IV) In addition, the gene expression data can be further interpreted using Gene Set Enrichment Analysis (GSEA) or Drug Set Enrichment Analysis (DSEA). Such methods utilise groups of genes that share common biological function, chromosomal location, and provide a pathway as a ranked list of drugs (Subramanian et al., 2005, Napolitano et al., 2016).

Using systems biology approaches, large-scale perturbation databases, including Connectivity Map (CMap) or Library of Integrated Network-based Cellular Signatures (LINCS) can be utilised on pathway and network level, where genes, drugs and disease states are connected by common gene expression signatures (Musa et al., 2018, Subramanian et al., 2017, Lamb et al., 2006). Such libraries could be used to predict the biochemical interactions of the characterised drugs as well as the top differentially expressed genes obtained from the gene array including FBXL5 in CRC (Musa et al., 2018, Lamb et al., 2006).

(V) Xenograft models using immunodeficient knock-out or transgenic mice, although expensive and difficult to uphold, should be the next step in research. This would allow to investigate the effect of drugs in a complex environment and estimate the side effects conferred by the drug. In addition, *in vivo* serial dilution assay can be used to determine the CRC initiating cell frequency of a primary tumour sample using immunocompromised murine xenograft models (Agro and O'Brien, 2015). Simultaneously, genetically engineered *FBXL5* deleted organoids and Patient-derived tumour organoids (PDTOs) could also be expanded for metastasis studies and investigating the drug associations with FBXL5 (Bleijs et al., 2019). This might replace and reduce the *in vivo* animal model use as well as reduce the experimental costs associated to such experiments.

References

AGRO, L. & O'BRIEN, C. 2015. In vitro and in vivo Limiting Dilution Assay for Colorectal Cancer. *Bio-protocol,* 5**,** 1-11.

AHMED, M., CHAUDHARI, K., BABAEI-JADIDI, R., DEKKER, L. V. & SHAMS NATERI, A. 2017a. Concise Review: Emerging Drugs Targeting Epithelial Cancer Stem-Like Cells. *Stem Cells,* 35**,** 839-850.

AHMED, M., CHAUDHARI, K., BABAEI-JADIDI, R., DEKKER, L. V. & SHAMS NATERI, A. 2017b. Concise Review: Emerging Drugs Targeting Epithelial Cancer Stem-Like Cells. 35**,** 839-850.

AHMED, M., JINKS, N., BABAEI-JADIDI, R., KASHFI, H., CASTELLANOS-URIBE, M., MAY, S. T., MUKHERJEE, A. & NATERI, A. S. 2019. Repurposing Antibacterial AM404 as a Potential Anticancer Drug for Targeting Colorectal Cancer Stem-Like Cells. *Cancers (Basel),* 12.

AL-EJEH, F., SMART, C. E., MORRISON, B. J., CHENEVIX-TRENCH, G., LÓPEZ, J. A., LAKHANI, S. R., BROWN, M. P. & KHANNA, K. K. 2011. Breast cancer stem cells: treatment resistance and therapeutic opportunities. *Carcinogenesis,* 32**,** 650-658.

ALCINDOR, T. & BEAUGER, N. 2011. Oxaliplatin: a review in the era of molecularly targeted therapy. *Current Oncology,* 18**,** 18-25.

ALFARISI, O., ALGHAMDI, W. A., AL-SHAER, M. H., DOOLEY, K. E. & PELOQUIN, C. A. 2017. Rifampin vs. rifapentine: what is the preferred rifamycin for tuberculosis? *Expert Rev Clin Pharmacol,* 10**,** 1027-1036.

AM, D., R, S., B, G. & H, A. 2014. - Novel strategies to enforce an epithelial phenotype in mesenchymal cells. *Cancer Res,* 74**,** 3659-72.

AMINI, S., FATHI, F., MOBALEGI, J., SOFIMAJIDPOUR, H. & GHADIMI, T. 2014. The expressions of stem cell markers: Oct4, Nanog, Sox2, nucleostemin, Bmi, Zfx, Tcl1, Tbx3, Dppa4, and Esrrb in bladder, colon, and prostate cancer, and certain cancer cell lines. *Anatomy & cell biology,* 47**,** 1-11.

ARFAOUI, A., RIOUALEN, C., AZZONI, V., PINNA, G., FINETTI, P., WICINSKI, J., JOSSELIN, E., MACARIO, M., CASTELLANO, R., LEONARD-STUMPF, C., BAL, A., GROS, A., LOSSY, S., KHARRAT, M., COLLETTE, Y., BERTUCCI, F., BIRNBAUM, D., DOUIK, H., BIDAUT, G., CHARAFE-JAUFFRET, E. & GINESTIER, C. 2019. A genome-wide RNAi screen reveals essential therapeutic targets of breast cancer stem cells. *EMBO Mol Med***,** e9930.

ARNOLD, M., SIERRA, M. S., LAVERSANNE, M., SOERJOMATARAM, I., JEMAL, A. & BRAY, F. 2017. Global patterns and trends in colorectal cancer incidence and mortality. *Gut,* 66**,** 683-691.

BABAEI-JADIDI, R., LI, N., SAADEDDIN, A., SPENCER-DENE, B., JANDKE, A., MUHAMMAD, B., IBRAHIM, E. E., MURALEEDHARAN, R., ABUZINADAH, M. & DAVIS, H. 2011a. FBXW7 influences murine intestinal homeostasis and cancer, targeting Notch, Jun, and DEK for degradation. *The Journal of experimental medicine,* 208**,** 295-312.

BABAEI-JADIDI, R., LI, N., SAADEDDIN, A., SPENCER-DENE, B., JANDKE, A., MUHAMMAD, B., IBRAHIM, E. E., MURALEEDHARAN, R., ABUZINADAH, M., DAVIS, H., LEWIS, A., WATSON, S., BEHRENS, A., TOMLINSON, I. & NATERI, A. S. 2011b. FBXW7 influences murine intestinal homeostasis and cancer, targeting Notch, Jun, and DEK for degradation. *J Exp Med,* 208**,** 295-312.

BAE, J. M., LEE, T. H., CHO, N.-Y., KIM, T.-Y. & KANG, G. H. J. W. J. O. G. W. 2015. Loss of CDX2 expression is associated with poor prognosis in colorectal cancer patients. 21**,** 1457.

BALBOUS, A., RENOUX, B., CORTES, U., MILIN, S., GUILLOTEAU, K., LEGIGAN, T., RIVET, P., BOISSONNADE, O., MARTIN, S., TRIPIANA, C., WAGER, M., BENSADOUN, R. J., PAPOT, S. & KARAYAN-TAPON, L. 2014. Selective release of a cyclopamine glucuronide prodrug toward stem-like cancer cell inhibition in glioblastoma. *Mol Cancer Ther,* 13**,** 2159-69.

BANO, N., YADAV, M. & DAS, B. C. 2018. Differential Inhibitory Effects of Curcumin Between HPV+ve and HPV-ve Oral Cancer Stem Cells. *Front Oncol,* 8**,** 412.

BAR, E. E., CHAUDHRY, A., LIN, A., FAN, X., SCHRECK, K., MATSUI, W., PICCIRILLO, S., VESCOVI, A. L., DIMECO, F. & OLIVI, A. 2007. Cyclopamine-Mediated Hedgehog Pathway Inhibition Depletes Stem-Like Cancer Cells in Glioblastoma. *Stem cells,* 25**,** 2524-2533.

BARBOSA, K., DESHPANDE, A., CHEN, B. R., GHOSH, A., SUN, Y., DUTTA, S., WEETALL, M., DIXON, J., ARMSTRONG, S. A., BOHLANDER, S. K. & DESHPANDE, A. J. 2019. Acute myeloid leukemia driven by the CALM-AF10 fusion gene is dependent on BMI1. *Exp Hematol,* 74**,** 42-51.e3.

BARKER, N. 2014. Adult intestinal stem cells: critical drivers of epithelial homeostasis and regeneration. *Nat Rev Mol Cell Biol,* 15**,** 19-33.

BARKER, N., RIDGWAY, R. A., VAN ES, J. H., VAN DE WETERING, M., BEGTHEL, H., VAN DEN BORN, M., DANENBERG, E., CLARKE, A. R., SANSOM, O. J. & CLEVERS, H. 2009. Crypt stem cells as the cells-of-origin of intestinal cancer. *Nature,* 457**,** 608-U119.

BARKER, N., VAN ES, J. H., KUIPERS, J., KUJALA, P., VAN DEN BORN, M., COZIJNSEN, M., HAEGEBARTH, A., KORVING, J., BEGTHEL, H., PETERS, P. J. & CLEVERS, H. 2007. Identification of stem cells in small intestine and colon by marker gene Lgr5. *Nature,* 449**,** 1003-U1.

BATLLE, E. & CLEVERS, H. 2017. Cancer stem cells revisited. *Nature Medicine,* 23**,** 1124.

BEDARD, P. L., CARDOSO, F. & PICCART-GEBHART, M. J. 2009. Stemming resistance to HER-2 targeted therapy. *Journal of mammary gland biology and neoplasia,* 14**,** 55-66.

BETGE, J., SCHNEIDER, N. I., HARBAUM, L., POLLHEIMER, M. J., LINDTNER, R. A., KORNPRAT, P., EBERT, M. P. & LANGNER, C. 2016. MUC1, MUC2, MUC5AC, and MUC6 in colorectal cancer: expression profiles and clinical significance. *Virchows Archiv : an international journal of pathology,* 469**,** 255-265.

BHATIA, R., HOLTZ, M., NIU, N., GRAY, R., SNYDER, D. S., SAWYERS, C. L., ARBER, D. A., SLOVAK, M. L. & FORMAN, S. J. 2003. Persistence of malignant hematopoietic progenitors in chronic myelogenous leukemia patients in complete cytogenetic remission following imatinib mesylate treatment. *Blood,* 101**,** 4701-4707.

BLEIJS, M., VAN DE WETERING, M., CLEVERS, H. & DROST, J. 2019. Xenograft and organoid model systems in cancer research. *The EMBO journal,* 38**,** e101654-e101654.

BOMAN, B. M. & WICHA, M. S. 2008. Cancer stem cells: a step toward the cure. *Journal of clinical oncology,* 26**,** 2795-2799.

BOOGERD, W., TJAHJA, I. S., VAN DE SANDT, M. M. & BEIJNEN, J. H. 1999. Penetration of idarubicin into malignant brain tumor tissue. *J Neurooncol,* 44**,** 65-9.

BOUWMAN, P. & JONKERS, J. 2012. The effects of deregulated DNA damage signalling on cancer chemotherapy response and resistance. *Nat Rev Cancer,* 12**,** 587-98.

BRAY, F., FERLAY, J., SOERJOMATARAM, I., SIEGEL, R. L., TORRE, L. A. & JEMAL, A. 2018. Global cancer statistics 2018: GLOBOCAN estimates of incidence and mortality worldwide for 36 cancers in 185 countries. *CA Cancer J Clin,* 68**,** 394-424.

BREITMAN, T. R., SELONICK, S. E. & COLLINS, S. J. 1980. Induction of differentiation of the human promyelocytic leukemia cell line (HL-60) by retinoic acid. *Proceedings of the National Academy of Sciences of the United States of America,* 77**,** 2936-2940.

BROWER, V. 2013. Tracking Chemotherapy's Effects on Secondary Cancers. *JNCI: Journal of the National Cancer Institute,* 105**,** 1421-1422.

BROWN, G. & HUGHES, P. 2012. Retinoid differentiation therapy for common types of acute myeloid leukemia. *Leukemia research and treatment,* 2012**,** 939021-939021.

BU, P., CHEN, K.-Y., LIPKIN, S. M. & SHEN, X. 2013. Asymmetric division: a marker for cancer stem cells in early stage tumors? *Oncotarget,* 4**,** 950-951.

BUBNA, A. K. 2015. Vorinostat-An Overview. *Indian journal of dermatology,* 60**,** 419-419.

BUCZACKI, S. J. A., POPOVA, S., BIGGS, E., KOUKORAVA, C., BUZZELLI, J., VERMEULEN, L., HAZELWOOD, L., FRANCIES, H., GARNETT, M. J. & WINTON, D. J. 2018. Itraconazole targets cell cycle heterogeneity in colorectal cancer. *J Exp Med,* 215**,** 1891-1912.

BUCZACKI, S. J. A., ZECCHINI, H. I., NICHOLSON, A. M., RUSSELL, R., VERMEULEN, L., KEMP, R. & WINTON, D. J. 2013. Intestinal label-retaining cells are secretory precursors expressing Lgr5. *Nature,* 495**,** 65-69.

CABALLERO, F. J., SOLER-TORRONTERAS, R., LARA-CHICA, M., GARCÍA, V., FIEBICH, B. L., MUÑOZ, E. & CALZADO, M. A. 2015. AM404 inhibits NFAT and NF-κB signaling pathways and impairs migration and invasiveness of neuroblastoma cells. *European Journal of Pharmacology,* 746**,** 221-232.

CAO, H., XU, E., LIU, H., WAN, L. & LAI, M. 2015a. Epithelial-mesenchymal transition in colorectal cancer metastasis: A system review. *Pathol Res Pract,* 211**,** 557-69.

CAO, J., FORREST, J. C. & ZHANG, X. 2015b. A screen of the NIH Clinical Collection small molecule library identifies potential anti-coronavirus drugs. *Antiviral Research,* 114**,** 1-10.

CASTRO, N. P., RANGEL, M. C., MERCHANT, A. S., MACKINNON, G., CUTTITTA, F., SALOMON, D. S. & KIM, Y. S. 2019. Sulforaphane Suppresses the Growth of Triple-negative Breast Cancer Stem-like Cells In vitro and In vivo. *Cancer Prev Res (Phila),* 12**,** 147-158.

CHAN, M. M., CHEN, R. & FONG, D. 2018. Targeting cancer stem cells with dietary phytochemical - Repositioned drug combinations. *Cancer Letters,* 433**,** 53-64.

CHANG, H.-T., HUANG, C.-C., CHENG, H.-H., WANG, J.-L., LIN, K.-L., HSU, P.-T., TSAI, J.-Y., LIAO, W.-C., LU, Y.-C., HUANG, J.-K. & JAN, C.-R. 2008. Mechanisms of AM404-induced [Ca2+]i rise and death in human osteosarcoma cells. *Toxicology Letters,* 179**,** 53-58.

CHAU, I. & CUNNINGHAM, D. 2009. Treatment in advanced colorectal cancer: what, when and how&quest. *British journal of cancer,* 100**,** 1704-1719.

CHEN, B., DODGE, M. E., TANG, W., LU, J., MA, Z., FAN, C.-W., WEI, S., HAO, W., KILGORE, J. & WILLIAMS, N. S. 2009. Small molecule–mediated disruption

of Wnt-dependent signaling in tissue regeneration and cancer. *Nature chemical biology,* 5**,** 100-107.

CHEN, J. K., TAIPALE, J., COOPER, M. K. & BEACHY, P. A. 2002. Inhibition of Hedgehog signaling by direct binding of cyclopamine to Smoothened. *Genes & development,* 16**,** 2743-2748.

CHEN, K., HUANG, Y.-H. & CHEN, J.-L. 2013a. Understanding and targeting cancer stem cells: therapeutic implications and challenges. *Acta Pharmacologica Sinica,* 34**,** 732-740.

CHEN, K., HUANG, Y.-H. & CHEN, J.-L. 2013b. Understanding and targeting cancer stem cells: therapeutic implications and challenges. *Acta Pharmacologica Sinica,* 34**,** 732.

CHEN, T., YOU, Y., JIANG, H. & WANG, Z. Z. 2017. Epithelial-mesenchymal transition (EMT): A biological process in the development, stem cell differentiation, and tumorigenesis. *Journal of cellular physiology,* 232**,** 3261-3272.

CHENG, H. & LEBLOND, C. P. 1974. ORIGIN, DIFFERENTIATION AND RENEWAL OF 4 MAIN EPITHELIAL-CELL TYPES IN MOUSE SMALL INTESTINE .1. COLUMNAR CELL. *American Journal of Anatomy,* 141**,** 461-&.

CHO, K., WANG, X., NIE, S. & SHIN, D. M. 2008. Therapeutic nanoparticles for drug delivery in cancer. *Clinical cancer research,* 14**,** 1310-1316.

CHOI, C.-H. R., AL BAKIR, I., DING, N.-S., LEE, G.-H., ASKARI, A., WARUSAVITARNE, J., MOORGHEN, M., HUMPHRIES, A., IGNJATOVIC-WILSON, A., THOMAS-GIBSON, S., SAUNDERS, B. P., RUTTER, M. D., GRAHAM, T. A. & HART, A. L. 2019. Cumulative burden of inflammation predicts colorectal neoplasia risk in ulcerative colitis: a large single-centre study. *Gut,* 68**,** 414.

CHOUDHARY, G. S., AL-HARBI, S. & ALMASAN, A. 2015. Caspase-3 activation is a critical determinant of genotoxic stress-induced apoptosis. *Methods Mol Biol,* 1219**,** 1-9.

CHUNG, S. S., DUTTA, P., CHARD, N., WU, Y., CHEN, Q. H., CHEN, G. & VADGAMA, J. 2019. A novel curcumin analog inhibits canonical and non-canonical functions of telomerase through STAT3 and NF-kappaB inactivation in colorectal cancer cells. *Oncotarget,* 10**,** 4516-4531.

CLEVERS, H. 2013. The intestinal crypt, a prototype stem cell compartment. *Cell,* 154**,** 274-84.

COLOTTA, F., ALLAVENA, P., SICA, A., GARLANDA, C. & MANTOVANI, A. 2009. Cancer-related inflammation, the seventh hallmark of cancer: links to genetic instability. *Carcinogenesis,* 30**,** 1073-1081.

CORRO, C., HEALY, M. E., ENGLER, S., BODENMILLER, B., LI, Z., SCHRAML, P., WEBER, A., FREW, I. J., RECHSTEINER, M. & MOCH, H. 2019. IL-8 and CXCR1 expression is associated with cancer stem cell-like properties of clear cell renal cancer. *J Pathol,* 248**,** 377-389.

COSTA, B., SINISCALCO, D., TROVATO, A. E., COMELLI, F., SOTGIU, M. L., COLLEONI, M., MAIONE, S., ROSSI, F. & GIAGNONI, G. 2006. AM404, an inhibitor of anandamide uptake, prevents pain behaviour and modulates cytokine and apoptotic pathways in a rat model of neuropathic pain. *British journal of pharmacology,* 148**,** 1022-1032.

COURTOIS, S., DURAN, R. V., GIRAUD, J., SIFRE, E., IZOTTE, J., MEGRAUD, F., LEHOURS, P., VARON, C. & BESSEDE, E. 2017. Metformin targets gastric cancer stem cells. *Eur J Cancer,* 84**,** 193-201.

CRABOL, Y., CATHERINOT, E., VEZIRIS, N., JULLIEN, V. & LORTHOLARY, O. 2016. Rifabutin: where do we stand in 2016? *Journal of Antimicrobial Chemotherapy,* 71**,** 1759-1771.

CUFÍ, S., COROMINAS-FAJA, B., VAZQUEZ-MARTIN, A., OLIVERAS-FERRAROS, C., DORCA, J., BOSCH-BARRERA, J., MARTIN-CASTILLO, B. & MENENDEZ, J. A. 2012. Metformin-induced preferential killing of breast cancer initiating CD44+ CD24−/low cells is sufficient to overcome primary resistance to trastuzumab in HER2+ human breast cancer xenografts. *Oncotarget,* 3**,** 395.

DALERBA, P., DYLLA, S. J., PARK, I. K., LIU, R., WANG, X., CHO, R. W., HOEY, T., GURNEY, A., HUANG, E. H., SIMEONE, D. M., SHELTON, A. A., PARMIANI, G., CASTELLI, C. & CLARKE, M. F. 2007. Phenotypic characterization of human colorectal cancer stem cells. *Proc Natl Acad Sci U S A,* 104**,** 10158-63.

DALERBA, P., SAHOO, D., PAIK, S., GUO, X., YOTHERS, G., SONG, N., WILCOX-FOGEL, N., FORGO, E., RAJENDRAN, P. S., MIRANDA, S. P., HISAMORI, S., HUTCHISON, J., KALISKY, T., QIAN, D., WOLMARK, N., FISHER, G. A., VAN DE RIJN, M. & CLARKE, M. F. 2016. CDX2 as a Prognostic Biomarker in Stage II and Stage III Colon Cancer. *N Engl J Med,* 374**,** 211-22.

DARZYNKIEWICZ, Z., ZHAO, H., ZHANG, S., LEE, M. Y. W. T., LEE, E. Y. C. & ZHANG, Z. 2015. Initiation and termination of DNA replication during S phase in relation to cyclins D1, E and A, p21WAF1, Cdt1 and the p12 subunit of DNA polymerase δ revealed in individual cells by cytometry. *Oncotarget,* 6**,** 11735-11750.

DB, L., HARKIN DP FAU - JOHNSTON, P. G. & PG, J. 2003. - 5-fluorouracil: mechanisms of action and clinical strategies. *Nat Rev Cancer,* 3**,** 330-8.

DE CRAENE, B. & BERX, G. 2013. Regulatory networks defining EMT during cancer initiation and progression. *Nature Reviews Cancer,* 13**,** 97-110.

DE FRANCESCO, E. M., ÓZSVÁRI, B., SOTGIA, F. & LISANTI, M. P. 2019. Dodecyl-TPP Targets Mitochondria and Potently Eradicates Cancer Stem Cells (CSCs): Synergy With FDA-Approved Drugs and Natural Compounds (Vitamin C and Berberine). *Frontiers in oncology,* 9**,** 615-615.

DE LAGO, E., GUSTAFSSON, S. B., FERNANDEZ-RUIZ, J., NILSSON, J., JACOBSSON, S. O. & FOWLER, C. J. 2006. Acyl-based anandamide uptake inhibitors cause rapid toxicity to C6 glioma cells at pharmacologically relevant concentrations. *J Neurochem,* 99**,** 677-88.

DE SOUSA E MELO, F., KURTOVA, A. V., HARNOSS, J. M., KLJAVIN, N., HOECK, J. D., HUNG, J., ANDERSON, J. E., STORM, E. E., MODRUSAN, Z., KOEPPEN, H., DIJKGRAAF, G. J. P., PISKOL, R. & DE SAUVAGE, F. J. 2017. A distinct role for Lgr5+ stem cells in primary and metastatic colon cancer. *Nature,* 543**,** 676.

DIAKOS, C. I., CHARLES, K. A., MCMILLAN, D. C. & CLARKE, S. J. 2014. Cancer-related inflammation and treatment effectiveness. *The Lancet Oncology,* 15**,** e493-e503.

DIAZ, V. M. & DE HERREROS, A. G. 2016. F-box proteins: Keeping the epithelial-to-mesenchymal transition (EMT) in check. *Semin Cancer Biol,* 36**,** 71-9.

DIENSTMANN, R., VERMEULEN, L., GUINNEY, J., KOPETZ, S., TEJPAR, S. & TABERNERO, J. 2017. Consensus molecular subtypes and the evolution of precision medicine in colorectal cancer. *Nat Rev Cancer,* 17**,** 79-92.

DOUGLAS, E. J., FIEGLER, H., ROWAN, A., HALFORD, S., BICKNELL, D. C., BODMER, W., TOMLINSON, I. P. M. & CARTER, N. P. 2004. Array comparative genomic hybridization analysis of colorectal cancer cell lines and primary carcinomas. *Cancer Research,* 64.

DOW, L. E., O'ROURKE, K. P., SIMON, J., TSCHAHARGANEH, D. F., VAN ES, J. H., CLEVERS, H. & LOWE, S. W. 2015. Apc Restoration Promotes Cellular Differentiation and Reestablishes Crypt Homeostasis in Colorectal Cancer. *Cell,* 161**,** 1539-1552.

DRACHAM, C. B., SHANKAR, A. & MADAN, R. 2018. Radiation induced secondary malignancies: a review article. *Radiation oncology journal,* 36**,** 85-94.

DRAGOI, A. M., SWISS, R., GAO, B. & AGAISSE, H. 2014. Novel strategies to enforce an epithelial phenotype in mesenchymal cells. *Cancer Res,* 74**,** 3659-72.

DRAGOJEW, S., MARCZAK, A., MASZEWSKI, J., ILNICKI, K. & JÓŹWIAK, Z. 2008. The induction of apoptosis by daunorubicin and idarubicin in human trisomic and diabetic fibroblasts. *Cellular & molecular biology letters,* 13**,** 182-194.

DROST, J., VAN JAARSVELD, R. H., PONSIOEN, B., ZIMBERLIN, C., VAN BOXTEL, R., BUIJS, A., SACHS, N., OVERMEER, R. M., OFFERHAUS, G. J., BEGTHEL, H., KORVING, J., VAN DE WETERING, M., SCHWANK, G., LOGTENBERG, M., CUPPEN, E., SNIPPERT, H. J., MEDEMA, J. P., KOPS, G. J. & CLEVERS, H. 2015. Sequential cancer mutations in cultured human intestinal stem cells. *Nature,* 521**,** 43-7.

EBOS, J. M. L., LEE, C. R., CRUZ-MUNOZ, W., BJARNASON, G. A., CHRISTENSEN, J. G. & KERBEL, R. S. 2009. Accelerated Metastasis after Short-Term Treatment with a Potent Inhibitor of Tumor Angiogenesis. *Cancer Cell,* 15**,** 232-239.

EDMONDSON, R., BROGLIE, J. J., ADCOCK, A. F. & YANG, L. 2014. Three-dimensional cell culture systems and their applications in drug discovery and cell-based biosensors. *Assay and drug development technologies,* 12**,** 207-218.

ELINAV, E., NOWARSKI, R., THAISS, C. A., HU, B., JIN, C. & FLAVELL, R. A. 2013. Inflammation-induced cancer: crosstalk between tumours, immune cells and microorganisms. *Nature Reviews Cancer,* 13**,** 759.

EMMINK, B. L., VAN HOUDT, W. J., VRIES, R. G., HOOGWATER, F. J., GOVAERT, K. M., VERHEEM, A., NIJKAMP, M. W., STELLER, E. J., JIMENEZ, C. R., CLEVERS, H., BOREL RINKES, I. H. & KRANENBURG, O. 2011a. Differentiated human colorectal cancer cells protect tumor-initiating cells from irinotecan. *Gastroenterology,* 141**,** 269-78.

EMMINK, B. L., VAN HOUDT, W. J., VRIES, R. G., HOOGWATER, F. J. H., GOVAERT, K. M., VERHEEM, A., NIJKAMP, M. W., STELLER, E. J. A., JIMENEZ, C. R., CLEVERS, H., BOREL RINKES, I. H. M. & KRANENBURG, O. 2011b. Differentiated Human Colorectal Cancer Cells Protect Tumor-Initiating Cells From Irinotecan. *Gastroenterology,* 141**,** 269-278.

EZEH, U. I., TUREK, P. J., REIJO, R. A. & CLARK, A. T. 2005. Human embryonic stem cell genes OCT4, NANOG, STELLAR, and GDF3 are expressed in both seminoma and breast carcinoma. *Cancer,* 104**,** 2255-65.

FEARON, E. R. 2011. Molecular genetics of colorectal cancer. *Annu Rev Pathol,* 6**,** 479-507.

FEARON, E. R. & VOGELSTEIN, B. 1990. A genetic model for colorectal tumorigenesis. *Cell,* 61**,** 759-767.

FINNIN, M. S., DONIGIAN, J. R., COHEN, A., RICHON, V. M., RIFKIND, R. A., MARKS, P. A., BRESLOW, R. & PAVLETICH, N. P. 1999. Structures of a histone deacetylase homologue bound to the TSA and SAHA inhibitors. *Nature,* 401**,** 188-193.

FORMEISTER, E. J., SIONAS, A. L., LORANCE, D. K., BARKLEY, C. L., LEE, G. H. & MAGNESS, S. T. 2009. Distinct SOX9 levels differentially mark stem/progenitor populations and enteroendocrine cells of the small

intestine epithelium. *Am J Physiol Gastrointest Liver Physiol,* 296**,** G1108-18.

FRANKEN, N. A. P., RODERMOND, H. M., STAP, J., HAVEMAN, J. & VAN BREE, C. 2006. Clonogenic assay of cells in vitro. *Nature Protocols,* 1**,** 2315-2319.

FREEMAN, A. E. & HOFFMAN, R. M. 1986. In vivo-like growth of human tumors in vitro. 83**,** 2694-2698.

FREEMAN, H. J. 2013. Early stage colon cancer. *World journal of gastroenterology,* 19**,** 8468-8473.

FU, J., WANG, F., DONG, L.-H., XING, M.-J., CHENG, X., WEI, S., XU, J.-Z., HAN, M., DONG, K. & SONG, H.-F. 2019. Receptor occupancy measurement of anti-PD-1 antibody drugs in support of clinical trials. 11**,** 1347-1358.

FUJII, N., YOU, L., XU, Z., UEMATSU, K., SHAN, J., HE, B., MIKAMI, I., EDMONDSON, L. R., NEALE, G. & ZHENG, J. 2007. An Antagonist of Dishevelled Protein-Protein Interaction Suppresses β-Catenin–Dependent Tumor Cell Growth. *Cancer research,* 67**,** 573-579.

FUJIKI, H., SUEOKA, E., RAWANGKAN, A. & SUGANUMA, M. 2017. Human cancer stem cells are a target for cancer prevention using (-)-epigallocatechin gallate. *J Cancer Res Clin Oncol,* 143**,** 2401-2412.

FUJITA, K., KUBOTA, Y., ISHIDA, H. & SASAKI, Y. 2015. Irinotecan, a key chemotherapeutic drug for metastatic colorectal cancer. *World J Gastroenterol,* 21**,** 12234-48.

FUKUSHIMA, T., UEDA, T., UCHIDA, M. & NAKAMURA, T. 1993. Action mechanism of idarubicin (4-demethoxydaunorubicin) as compared with daunorubicin in leukemic cells. *Int J Hematol,* 57**,** 121-30.

G, M.-O., E, G., AC, M., J, F.-O., I, P.-L. & J, B. 2015. - FBXL5 modulates HIF-1alpha transcriptional activity by degradation of CITED2. *Arch Biochem Biophys,* 576**,** 61-72.

GALLUZZI, L., KEPP, O. & KROEMER, G. 2011. Caspase-3 and prostaglandins signal for tumor regrowth in cancer therapy. *Oncogene,* 31**,** 2805.

GARZA-TREVIÑO, E. N., SAID-FERNÁNDEZ, S. L. & MARTÍNEZ-RODRÍGUEZ, H. G. 2015. Understanding the colon cancer stem cells and perspectives on treatment. *Cancer Cell International,* 15**,** 1-9.

GERITS, E., SPINCEMAILLE, P., DE CREMER, K., DE BRUCKER, K., BEULLENS, S., THEVISSEN, K., CAMMUE, B. P. A., VANDAMME, K., FAUVART, M., VERSTRAETEN, N. & MICHIELS, J. 2017. Repurposing AM404 for the treatment of oral infections by Porphyromonas gingivalis. *Clinical and experimental dental research,* 3**,** 69-76.

GIESELER, F., CLARK, M., STIEBELING, K., PUSCHMANN, M. & VALSAMAS, S. 2000. Induction of apoptosis by idarubicin: how important is the plasma peak? *Int J Clin Pharmacol Ther,* 38**,** 217-21.

GIGUERE, V., ONG, E. S., SEGUI, P. & EVANS, R. M. 1987. Identification of a receptor for the morphogen retinoic acid. *Nature,* 330**,** 624-9.

GLINSKY, G. V., BEREZOVSKA, O. & GLINSKII, A. B. 2005. Microarray analysis identifies a death-from-cancer signature predicting therapy failure in patients with multiple types of cancer. *Journal of Clinical Investigation,* 115**,** 1503.

GOLOVKO, D., KEDRIN, D., YILMAZ, Ö. H. & ROPER, J. 2015. Colorectal cancer models for novel drug discovery. *Expert opinion on drug discovery,* 10**,** 1217-1229.

GÓMEZ-LÓPEZ, S., LERNER, R. G. & PETRITSCH, C. 2014. Asymmetric cell division of stem and progenitor cells during homeostasis and cancer. *Cellular and molecular life sciences : CMLS,* 71**,** 575-597.

GONZÁLEZ, M. M., JOA, J. A. G., CABRALES, L. E. B., PUPO, A. E. B., SCHNEIDER, B., KONDAKCI, S., CIRIA, H. M. C., REYES, J. B., JARQUE, M. V., MATEUS, M. A. O. F., GONZÁLEZ, T. R., BROOKS, S. C. A., CÁCERES, J. L. H. & GONZÁLEZ, G. V. S. 2017. Is cancer a pure growth curve or does it follow a kinetics of dynamical structural transformation? *BMC cancer,* 17**,** 174-174.

GOTTESMAN, M. M. 2002. Mechanisms of Cancer Drug Resistance. *Annual Review of Medicine,* 53**,** 615-627.

GRADY, W. M. & CARETHERS, J. M. 2008. Genomic and epigenetic instability in colorectal cancer pathogenesis. *Gastroenterology,* 135.

GRAULE, J., UTH, K., FISCHER, E., CENTENO, I., GALVÁN, J. A., EICHMANN, M., RAU, T. T., LANGER, R., DAWSON, H., NITSCHE, U., TRAEGER, P., BERGER, M. D., SCHNÜRIGER, B., HÄDRICH, M., STUDER, P., INDERBITZIN, D., LUGLI, A., TSCHAN, M. P. & ZLOBEC, I. 2018. CDX2 in colorectal cancer is an independent prognostic factor and regulated by promoter methylation and histone deacetylation in tumors of the serrated pathway. *Clinical epigenetics,* 10**,** 120-120.

GREENBURG, G. & HAY, E. D. 1982. Epithelia suspended in collagen gels can lose polarity and express characteristics of migrating mesenchymal cells. *J Cell Biol,* 95**,** 333-9.

GRETEN, F. R. & GRIVENNIKOV, S. I. 2019. Inflammation and Cancer: Triggers, Mechanisms, and Consequences. *Immunity,* 51**,** 27-41.

GRIVENNIKOV, S. I., GRETEN, F. R. & KARIN, M. 2010. Immunity, inflammation, and cancer. *Cell,* 140**,** 883-99.

GUGNONI, M., SANCISI, V., GANDOLFI, G., MANZOTTI, G., RAGAZZI, M., GIORDANO, D., TAMAGNINI, I., TIGANO, M., FRASOLDATI, A., PIANA, S. & CIARROCCHI, A. 2016. Cadherin-6 promotes EMT and cancer metastasis by restraining autophagy. *Oncogene,* 36**,** 667.

GUINNEY, J., DIENSTMANN, R., WANG, X., DE REYNIES, A., SCHLICKER, A., SONESON, C., MARISA, L., ROEPMAN, P., NYAMUNDANDA, G., ANGELINO, P., BOT, B. M., MORRIS, J. S., SIMON, I. M., GERSTER, S., FESSLER, E., DE SOUSA, E. M. F., MISSIAGLIA, E., RAMAY, H., BARRAS, D., HOMICSKO, K., MARU, D., MANYAM, G. C., BROOM, B., BOIGE, V., PEREZ-VILLAMIL, B., LADERAS, T., SALAZAR, R., GRAY, J. W., HANAHAN, D., TABERNERO, J., BERNARDS, R., FRIEND, S. H., LAURENT-PUIG, P., MEDEMA, J. P., SADANANDAM, A., WESSELS, L., DELORENZI, M., KOPETZ, S., VERMEULEN, L. & TEJPAR, S. 2015. The consensus molecular subtypes of colorectal cancer. *Nat Med,* 21**,** 1350-6.

GUNDUZ, U., KESKIN, T., TANSIK, G., MUTLU, P., YALCIN, S., UNSOY, G., YAKAR, A., KHODADUST, R. & GUNDUZ, G. 2014a. Idarubicin-loaded folic acid conjugated magnetic nanoparticles as a targetable drug delivery system for breast cancer. *Biomed Pharmacother,* 68**,** 729-36.

GUNDUZ, U., KESKIN, T., TANSıK, G., MUTLU, P., YALCıN, S., UNSOY, G., YAKAR, A., KHODADUST, R. & GUNDUZ, G. 2014b. Idarubicin-loaded folic acid conjugated magnetic nanoparticles as a targetable drug delivery system for breast cancer. *Biomedicine & Pharmacotherapy,* 68**,** 729-736.

GUZMAN, C., BAGGA, M., KAUR, A., WESTERMARCK, J. & ABANKWA, D. 2014. ColonyArea: an ImageJ plugin to automatically quantify colony formation in clonogenic assays. *PLoS One,* 9**,** e92444.

H, Y., S, S., D, X., M, W., Z, L., W, C., L, R. & L, X. 2018. - F-box and leucine-rich repeat protein 5 promotes colon cancer progression by modulating PTEN/PI3K/AKT signaling pathway. *Biomed Pharmacother,* 107**,** 1712-1719.

HAN, Z., YANG, Q., LIU, B., WU, J., LI, Y., YANG, C. & JIANG, Y. 2012. MicroRNA-622 functions as a tumor suppressor by targeting K-Ras and enhancing the anticarcinogenic effect of resveratrol. *Carcinogenesis,* 33**,** 131-139.

HANAHAN, D. & WEINBERG, R. A. 2000. The hallmarks of cancer. *Cell,* 100**,** 57-70.

HANAHAN, D. & WEINBERG, R. A. 2011. Hallmarks of cancer: the next generation. *Cell,* 144**,** 646-74.

HAWLEY, T. S., RIZ, I., YANG, W., WAKABAYASHI, Y., DEPALMA, L., CHANG, Y. T., PENG, W., ZHU, J. & HAWLEY, R. G. 2013. Identification of an ABCB1 (P-glycoprotein)-positive carfilzomib-resistant myeloma subpopulation by the pluripotent stem cell fluorescent dye CDy1. *Am J Hematol,* 88**,** 265-72.

HE, B., REGUART, N., YOU, L., MAZIERES, J., XU, Z., LEE, A. Y., MIKAMI, I., MCCORMICK, F. & JABLONS, D. M. 2005. Blockade of Wnt-1 signaling induces apoptosis in human colorectal cancer cells containing downstream mutations. *Oncogene,* 24**,** 3054-3058.

HERMSEN, M., POSTMA, C., BAAK, J., WEISS, M., RAPALLO, A., SCIUTTO, A., ROEMEN, G., ARENDS, J. W., WILLIAMS, R., GIARETTI, W., DE GOEIJ, A. & MEIJER, G. 2002. Colorectal adenoma to carcinoma progression follows multiple pathways of chromosomal instability. *Gastroenterology,* 123.

HIDALGO, M., BRUCKHEIMER, E., RAJESHKUMAR, N. V., GARRIDO-LAGUNA, I., DE OLIVEIRA, E., RUBIO-VIQUEIRA, B., STRAWN, S., WICK, M. J., MARTELL, J. & SIDRANSKY, D. 2011. A pilot clinical study of treatment guided by personalized tumorgrafts in patients with advanced cancer. *Molecular cancer therapeutics,* 10**,** 1311-1316.

HIRSCH, H. A., ILIOPOULOS, D., TSICHLIS, P. N. & STRUHL, K. 2009. Metformin selectively targets cancer stem cells, and acts together with chemotherapy to block tumor growth and prolong remission. *Cancer research,* 69**,** 7507-7511.

HOEY, T., YEN, W.-C., AXELROD, F., BASI, J., DONIGIAN, L., DYLLA, S., FITCH-BRUHNS, M., LAZETIC, S., PARK, I.-K. & SATO, A. 2009. DLL4 blockade inhibits tumor growth and reduces tumor-initiating cell frequency. *Cell stem cell,* 5**,** 168-177.

HOLOHAN, C., VAN SCHAEYBROECK, S., LONGLEY, D. B. & JOHNSTON, P. G. 2013. Cancer drug resistance: an evolving paradigm. *Nature Reviews Cancer,* 13**,** 714.

HOUTGRAAF, J. H., VERSMISSEN, J. & VAN DER GIESSEN, W. J. 2006. A concise review of DNA damage checkpoints and repair in mammalian cells. *Cardiovascular revascularization medicine : including molecular interventions,* 7**,** 165-72.

HOWELLS, L. M., IWUJI, C. O. O., IRVING, G. R. B., BARBER, S., WALTER, H., SIDAT, Z., GRIFFIN-TEALL, N., SINGH, R., FOREMAN, N., PATEL, S. R., MORGAN, B., STEWARD, W. P., GESCHER, A., THOMAS, A. L. & BROWN, K. 2019. Curcumin Combined with FOLFOX Chemotherapy Is Safe and Tolerable in Patients with Metastatic Colorectal Cancer in a Randomized Phase IIa Trial. *The Journal of Nutrition,* 149**,** 1133-1139.

HSU, H.-P., LAI, M.-D., LEE, J.-C., YEN, M.-C., WENG, T.-Y., CHEN, W.-C., FANG, J.-H. & CHEN, Y.-L. 2017. Mucin 2 silencing promotes colon cancer metastasis through interleukin-6 signaling. *Scientific Reports,* 7**,** 5823.

HUANG, Y.-J. & HSU, S.-H. 2014. Acquisition of epithelial–mesenchymal transition and cancer stem-like phenotypes within chitosan-hyaluronan membrane-derived 3D tumor spheroids. *Biomaterials,* 35**,** 10070-10079.

HUANG, Y. T., LIN, Y. W., CHIU, H. M. & CHIANG, B. H. 2016. Curcumin Induces Apoptosis of Colorectal Cancer Stem Cells by Coupling with CD44 Marker. *J Agric Food Chem,* 64**,** 2247-53.

HULME, E. C. & TREVETHICK, M. A. 2010. Ligand binding assays at equilibrium: validation and interpretation. *British journal of pharmacology,* 161**,** 1219-1237.

HUMPHRIES, H. N., WICKREMESEKERA, S. K., MARSH, R. W., BRASCH, H. D., MEHROTRA, S., TAN, S. T. & ITINTEANG, T. 2018. Characterization of Cancer Stem Cells in Colon Adenocarcinoma Metastasis to the Liver. *Frontiers in surgery,* 4**,** 76-76.

HUO, Y., CHEN, W. S., LEE, J., FENG, G. S. & NEWTON, I. G. 2019. Stress Conditions Induced by Locoregional Therapies Stimulate Enrichment and Proliferation of Liver Cancer Stem Cells. *J Vasc Interv Radiol*.

HWANG, W. L., JIANG, J. K., YANG, S. H., HUANG, T. S., LAN, H. Y., TENG, H. W., YANG, C. Y., TSAI, Y. P., LIN, C. H., WANG, H. W. & YANG, M. H. 2014. MicroRNA-146a directs the symmetric division of Snail-dominant colorectal cancer stem cells. *Nat Cell Biol,* 16**,** 268-80.

IM, C. N., KANG, N. Y., HA, H. H., BI, X., LEE, J. J., PARK, S. J., LEE, S. Y., VENDRELL, M., KIM, Y. K. & LEE, J. S. J. A. C. 2010. A fluorescent rosamine compound selectively stains pluripotent stem cells. 122**,** 7659-7662.

IMAMURA, Y., MUKOHARA, T., SHIMONO, Y., FUNAKOSHI, Y., CHAYAHARA, N., TOYODA, M., KIYOTA, N., TAKAO, S., KONO, S., NAKATSURA, T. & MINAMI, H. 2015. Comparison of 2D- and 3D-culture models as drug-testing platforms in breast cancer. *Oncol Rep,* 33**,** 1837-43.

ISHIGURO, T., OHATA, H., SATO, A., YAMAWAKI, K., ENOMOTO, T. & OKAMOTO, K. 2017. Tumor-derived spheroids: Relevance to cancer stem cells and clinical applications. *Cancer science,* 108**,** 283-289.

IZUMI, D., ISHIMOTO, T., MIYAKE, K., ETO, T., ARIMA, K., KIYOZUMI, Y., UCHIHARA, T., KURASHIGE, J., IWATSUKI, M., BABA, Y., SAKAMOTO, Y., MIYAMOTO, Y., YOSHIDA, N., WATANABE, M., GOEL, A., TAN, P. & BABA, H. 2017. Colorectal Cancer Stem Cells Acquire Chemoresistance Through the Upregulation of F-Box/WD Repeat-Containing Protein 7 and the Consequent Degradation of c-Myc. *Stem Cells,* 35**,** 2027-2036.

JACKSON, S. P. & BARTEK, J. 2009. The DNA-damage response in human biology and disease. *Nature,* 461**,** 1071-1078.

JACKSTADT, R., VAN HOOFF, S. R., LEACH, J. D., CORTES-LAVAUD, X., LOHUIS, J. O., RIDGWAY, R. A., WOUTERS, V. M., ROPER, J., KENDALL, T. J., ROXBURGH, C. S., HORGAN, P. G., NIXON, C., NOURSE, C., GUNZER, M., CLARK, W., HEDLEY, A., YILMAZ, O. H., RASHID, M., BAILEY, P., BIANKIN, A. V., CAMPBELL, A. D., ADAMS, D. J., BARRY, S. T., STEELE, C. W., MEDEMA, J. P. & SANSOM, O. J. 2019. Epithelial NOTCH Signaling Rewires the Tumor Microenvironment of Colorectal Cancer to Drive Poor-Prognosis Subtypes and Metastasis. *Cancer Cell,* 36**,** 319-336.e7.

JANZER, A., GERMAN, N. J., GONZALEZ-HERRERA, K. N., ASARA, J. M., HAIGIS, M. C. & STRUHL, K. 2014. Metformin and phenformin deplete tricarboxylic acid cycle and glycolytic intermediates during cell transformation and NTPs in cancer stem cells. *Proceedings of the National Academy of Sciences,* 111**,** 10574-10579.

JEMAL, A., SIEGEL, R., XU, J. & WARD, E. 2010. Cancer statistics, 2010. *CA: a cancer journal for clinicians,* 60**,** 277-300.

JING, Y., ZHOU, Q., ZHU, H., ZHANG, Y., SONG, Y., ZHANG, X., HUANG, X., YANG, Y., NI, Y. & HU, Q. 2019. Ki-67 is an independent prognostic marker for the recurrence and relapse of oral squamous cell carcinoma. *Oncology letters,* 17**,** 974-980.

JONSSON, K. O., ANDERSSON, A., JACOBSSON, S. O., VANDEVOORDE, S., LAMBERT, D. M. & FOWLER, C. J. 2003. AM404 and VDM 11 non-specifically inhibit C6 glioma cell proliferation at concentrations used to block the cellular accumulation of the endocannabinoid anandamide. *Arch Toxicol,* 77**,** 201-7.

KABAKOV, A. E. & GABAI, V. L. 2018. Cell Death and Survival Assays. *Methods Mol Biol,* 1709**,** 107-127.

KALLIFATIDIS, G., RAUSCH, V., BAUMANN, B., APEL, A., BECKERMANN, B. M., GROTH, A., MATTERN, J., LI, Z., KOLB, A. & MOLDENHAUER, G. 2009. Sulforaphane targets pancreatic tumour-initiating cells by NF-κB-induced antiapoptotic signalling. *Gut,* 58**,** 949-963.

KANG, N.-Y., YUN, S.-W., HA, H.-H., PARK, S.-J. & CHANG, Y.-T. 2011a. Embryonic and induced pluripotent stem cell staining and sorting with the live-cell fluorescence imaging probe CDy1. *Nature Protocols,* 6**,** 1044.

KANG, N.-Y., YUN, S.-W., HA, H.-H., PARK, S.-J. & CHANG, Y.-T. 2011b. Embryonic and induced pluripotent stem cell staining and sorting with the live-cell fluorescence imaging probe CDy1. *Nature Protocols,* 6**,** 1044-1052.

KAREKLA, E., LIAO, W.-J., SHARP, B., PUGH, J., REID, H., QUESNE, J. L., MOORE, D., PRITCHARD, C., MACFARLANE, M. & PRINGLE, J. H. 2017a. Ex Vivo Explant Cultures of Non–Small Cell Lung Carcinoma Enable Evaluation of Primary Tumor Responses to Anticancer Therapy. 77**,** 2029-2039.

KAREKLA, E., LIAO, W. J., SHARP, B., PUGH, J., REID, H., QUESNE, J. L., MOORE, D., PRITCHARD, C., MACFARLANE, M. & PRINGLE, J. H. 2017b. Ex Vivo Explant Cultures of Non-Small Cell Lung Carcinoma Enable Evaluation of Primary Tumor Responses to Anticancer Therapy. *Cancer Res,* 77**,** 2029-2039.

KASHFI, S. M. H., ALMOZYAN, S., JINKS, N., KOO, B.-K. & NATERI, A. S. 2018. Morphological alterations of cultured human colorectal matched tumour and healthy organoids. *Oncotarget,* 9**,** 10572-10584.

KAST, R. E., SKULI, N., COS, S., KARPEL-MASSLER, G., SHIOZAWA, Y., GOSHEN, R. & HALATSCH, M.-E. 2017. The ABC7 regimen: a new approach to metastatic breast cancer using seven common drugs to inhibit epithelial-to-mesenchymal transition and augment capecitabine efficacy. *Breast cancer (Dove Medical Press),* 9**,** 495-514.

KEMPER, K., PRASETYANTI, P. R., DE LAU, W., RODERMOND, H., CLEVERS, H. & MEDEMA, J. P. 2012a. Monoclonal antibodies against Lgr5 identify human colorectal cancer stem cells. *Stem Cells,* 30**,** 2378-86.

KEMPER, K., RODERMOND, H., COLAK, S., GRANDELA, C. & MEDEMA, J. P. 2012b. Targeting colorectal cancer stem cells with inducible caspase-9. *Apoptosis,* 17**,** 528-537.

KHALEK, F. J. A., GALLICANO, G. I. & MISHRA, L. 2010. Colon Cancer Stem Cells. *Gastrointestinal Cancer Research : GCR***,** S16-S23.

KIM, J. B., KO, E., HAN, W., SHIN, I., PARK, S. Y. & NOH, D.-Y. 2008. Berberine diminishes the side population and ABCG2 transporter expression in MCF-7 breast cancer cells. *Planta medica,* 74**,** 1693-1700.

KIM, J. H., RHEE, Y. Y., BAE, J. M., CHO, N. Y. & KANG, G. H. 2013. Loss of CDX2/CK20 expression is associated with poorly differentiated carcinoma, the CpG island methylator phenotype, and adverse prognosis in microsatellite-unstable colorectal cancer. *Am J Surg Pathol,* 37**,** 1532-41.

KINZLER, K. W. & VOGELSTEIN, B. 1996. Lessons from hereditary colorectal cancer. *Cell,* 87**,** 159-70.

KNUDSON, A. G., JR. 1971. Mutation and cancer: statistical study of retinoblastoma. *Proc Natl Acad Sci U S A,* 68**,** 820-3.

KOLARIC, K., POTREBICA, V., VUKAS, D., MECHL, Z. & SOPKOVA, B. 1988. Combination chemotherapy with 5-fluorouracil, oral Idarubicin, and cyclophosphamide (FIC) in metastatic breast cancer--an open phase II study. *J Cancer Res Clin Oncol,* 114**,** 301-5.

KOO, B. K., SPIT, M., JORDENS, I., LOW, T. Y., STANGE, D. E., VAN DE WETERING, M., VAN ES, J. H., MOHAMMED, S., HECK, A. J., MAURICE, M. M. & CLEVERS, H. 2012. Tumour suppressor RNF43 is a stem-cell E3 ligase that induces endocytosis of Wnt receptors. *Nature,* 488**,** 665-9.

KRESO, A., VAN GALEN, P., PEDLEY, N. M., LIMA-FERNANDES, E., FRELIN, C., DAVIS, T., CAO, L., BAIAZITOV, R., DU, W. & SYDORENKO, N. 2014. Self-renewal as a therapeutic target in human colorectal cancer. *Nature medicine,* 20**,** 29-36.

KRESO, A., VAN GALEN, P., PEDLEY, N. M., LIMA-FERNANDES, E., FRELIN, C., DAVIS, T., CAO, L., BAIAZITOV, R., DU, W., SYDORENKO, N., MOON, Y.-C., GIBSON, L., WANG, Y., LEUNG, C., ISCOVE, N. N., ARROWSMITH, C. H., SZENTGYORGYI, E., GALLINGER, S., DICK, J. E. & O'BRIEN, C. A. 2013. Self-renewal as a therapeutic target in human colorectal cancer. *Nature Medicine,* 20**,** 29.

KRUG, U., GANSER, A. & KOEFFLER, H. P. 2002. Tumor suppressor genes in normal and malignant hematopoiesis. *Oncogene,* 21**,** 3475-3495.

KUIPERS, E. J., GRADY, W. M., LIEBERMAN, D., SEUFFERLEIN, T., SUNG, J. J., BOELENS, P. G., VAN DE VELDE, C. J. & WATANABE, T. 2015. Colorectal cancer. *Nat Rev Dis Primers,* 1**,** 15065.

LAMB, J., CRAWFORD, E. D., PECK, D., MODELL, J. W., BLAT, I. C., WROBEL, M. J., LERNER, J., BRUNET, J. P., SUBRAMANIAN, A., ROSS, K. N., REICH, M., HIERONYMUS, H., WEI, G., ARMSTRONG, S. A., HAGGARTY, S. J., CLEMONS, P. A., WEI, R., CARR, S. A., LANDER, E. S. & GOLUB, T. R. 2006. The Connectivity Map: using gene-expression signatures to connect small molecules, genes, and disease. *Science,* 313**,** 1929-35.

LAMOUILLE, S., XU, J. & DERYNCK, R. 2014. Molecular mechanisms of epithelial-mesenchymal transition. *Nat Rev Mol Cell Biol,* 15**,** 178-96.

LANGHANS, S. A. 2018. Three-Dimensional in Vitro Cell Culture Models in Drug Discovery and Drug Repositioning. *Frontiers in pharmacology,* 9**,** 6-6.

LAPIDOT, T., SIRARD, C., VORMOOR, J., MURDOCH, B., HOANG, T., CACERES-CORTES, J., MINDEN, M., PATERSON, B., CALIGIURI, M. A. & DICK, J. E. 1994. A cell initiating human acute myeloid leukaemia after transplantation into SCID mice. *Nature,* 367**,** 645-648.

LARZABAL, L., EL-NIKHELY, N., REDRADO, M., SEEGER, W., SAVAI, R. & CALVO, A. 2013. Differential Effects of Drugs Targeting Cancer Stem Cell (CSC) and Non-CSC Populations on Lung Primary Tumors and Metastasis. *PLOS ONE,* 8**,** e79798.

LASRY, A., ZINGER, A. & BEN-NERIAH, Y. 2016. Inflammatory networks underlying colorectal cancer. *Nature Immunology,* 17**,** 230.

LAU, T., CHAN, E., CALLOW, M., WAALER, J., BOGGS, J., BLAKE, R. A., MAGNUSON, S., SAMBRONE, A., SCHUTTEN, M., FIRESTEIN, R., MACHON, O., KORINEK, V., CHOO, E., DIAZ, D., MERCHANT, M., POLAKIS, P., HOLSWORTH, D. D., KRAUSS, S. & COSTA, M. 2013. A novel tankyrase small-molecule inhibitor suppresses APC mutation-driven colorectal tumor growth. *Cancer Res,* 73**,** 3132-44.

LEON, G., MACDONAGH, L., FINN, S. P., CUFFE, S. & BARR, M. P. 2015. Cancer stem cells in drug resistant lung cancer: Targeting cell surface markers and signaling pathways. *Pharmacology & therapeutics*.

LEON, G., MACDONAGH, L., FINN, S. P., CUFFE, S. & BARR, M. P. 2016. Cancer stem cells in drug resistant lung cancer: Targeting cell surface markers and signaling pathways. *Pharmacol Ther,* 158**,** 71-90.

LERNER, R. G. & PETRITSCH, C. 2014. A microRNA-operated switch of asymmetric-to-symmetric cancer stem cell divisions. *Nature cell biology,* 16**,** 212-214.

LESZCZYNIECKA, M., ROBERTS, T., DENT, P., GRANT, S. & FISHER, P. B. 2001. Differentiation therapy of human cancer: basic science and clinical applications. *Pharmacology & Therapeutics,* 90**,** 105-156.

LEVINA, V., MARRANGONI, A. M., DEMARCO, R., GORELIK, E. & LOKSHIN, A. E. 2008. Drug-Selected Human Lung Cancer Stem Cells: Cytokine Network, Tumorigenic and Metastatic Properties. *PLOS ONE,* 3**,** e3077.

LI, E., ZHANG, T., SUN, X., LI, Y., GENG, H., YU, D. & ZHONG, C. 2019a. Sonic hedgehog pathway mediates genistein inhibition of renal cancer stem cells. *Oncol Lett,* 18**,** 3081-3091.

LI, J., HUANG, Y., GAO, Y., WU, H., DONG, W. & LIU, L. 2016a. Antibiotic drug rifabutin is effective against lung cancer cells by targeting the eIF4E-beta-catenin axis. *Biochem Biophys Res Commun,* 472**,** 299-305.

LI, J., HUANG, Y., GAO, Y., WU, H., DONG, W. & LIU, L. 2016b. Antibiotic drug rifabutin is effective against lung cancer cells by targeting the eIF4E-β-catenin axis. *Biochemical and Biophysical Research Communications,* 472**,** 299-305.

LI, N., BABAEI-JADIDI, R., LORENZI, F., SPENCER-DENE, B., CLARKE, P., DOMINGO, E., TULCHINSKY, E., VRIES, R. G. J., KERR, D., PAN, Y., HE, Y., BATES, D. O., TOMLINSON, I., CLEVERS, H. & NATERI, A. S. 2019b. An FBXW7-ZEB2 axis links EMT and tumour microenvironment to promote colorectal cancer stem cells and chemoresistance. *Oncogenesis,* 8**,** 13.

LI, X., LEWIS, M. T., HUANG, J., GUTIERREZ, C., OSBORNE, C. K., WU, M. F., HILSENBECK, S. G., PAVLICK, A., ZHANG, X., CHAMNESS, G. C., WONG, H., ROSEN, J. & CHANG, J. C. 2008. Intrinsic resistance of tumorigenic breast cancer cells to chemotherapy. *J Natl Cancer Inst,* 100**,** 672-9.

LI, Y., ROGOFF, H. A., KEATES, S., GAO, Y., MURIKIPUDI, S., MIKULE, K., LEGGETT, D., LI, W., PARDEE, A. B. & LI, C. J. 2015. Suppression of cancer relapse and metastasis by inhibiting cancer stemness. *Proceedings of the National Academy of Sciences of the United States of America,* 112**,** 1839-1844.

LIANG, C.-C., PARK, A. Y. & GUAN, J.-L. 2007. In vitro scratch assay: a convenient and inexpensive method for analysis of cell migration in vitro. *Nature Protocols,* 2**,** 329.

LIM, S., SAW, T. Y., ZHANG, M., JANES, M. R., NACRO, K., HILL, J., LIM, A. Q., CHANG, C.-T., FRUMAN, D. A., RIZZIERI, D. A., TAN, S. Y., FAN, H., CHUAH, C. T. H. & ONG, S. T. 2013. Targeting of the MNK–eIF4E axis in blast crisis chronic myeloid leukemia inhibits leukemia stem cell function. 110**,** E2298-E2307.

LIN, C.-Y., HSIEH, P.-L., LIAO, Y.-W., PENG, C.-Y., LU, M.-Y., YANG, C.-H., YU, C.-C. & LIU, C.-M. 2017. Berberine-targeted miR-21 chemosensitizes oral carcinomas stem cells. *Oncotarget,* 8**,** 80900-80908.

LINNEKAMP, J. F., HOOFF, S. R. V., PRASETYANTI, P. R., KANDIMALLA, R., BUIKHUISEN, J. Y., FESSLER, E., RAMESH, P., LEE, K., BOCHOVE, G. G. W., DE JONG, J. H., CAMERON, K., LEERSUM, R. V., RODERMOND, H. M., FRANITZA, M., NURNBERG, P., MANGIAPANE, L. R., WANG, X., CLEVERS, H., VERMEULEN, L., STASSI, G. & MEDEMA, J. P. 2018. Consensus molecular subtypes of colorectal cancer are recapitulated in in vitro and in vivo models. *Cell Death Differ,* 25**,** 616-633.

LIU, H., LV, L. & YANG, K. 2015. Chemotherapy targeting cancer stem cells. *American Journal of Cancer Research,* 5.

LIU, J., KOPECKOVÁ, P., BÜHLER, P., WOLF, P., PAN, H., BAUER, H., ELSÄSSER-BEILE, U. & KOPECEK, J. 2009. Biorecognition and Subcellular Trafficking of HPMA Copolymer− Anti-PSMA Antibody Conjugates by Prostate Cancer Cells. *Molecular pharmaceutics,* 6**,** 959-970.

LONGLEY, D. B., HARKIN, D. P. & JOHNSTON, P. G. 2003. 5-Fluorouracil: Mechanisms of action and clinical strategies. *Nature Reviews Cancer,* 3**,** 330-338.

LORENZI, F., BABAEI-JADIDI, R., SHEARD, J., SPENCER-DENE, B. & NATERI, A. S. 2016a. Fbxw7-associated drug resistance is reversed by induction of terminal differentiation in murine intestinal organoid culture. *Molecular Therapy - Methods & Clinical Development,* 3**,** 16024.

LORENZI, F., BABAEI-JADIDI, R., SHEARD, J., SPENCER-DENE, B. & NATERI, A. S. 2016b. Fbxw7-associated drug resistance is reversed by induction of terminal differentiation in murine intestinal organoid culture. *Molecular Therapy — Methods & Clinical Development,* 3**,** 16024.

LYTLE, N. K., BARBER, A. G. & REYA, T. 2018. Stem cell fate in cancer growth, progression and therapy resistance. *Nature Reviews Cancer,* 18**,** 669-680.

M, A., MS, S., M, L., I, S., A, J. & F, B. 2017. - Global patterns and trends in colorectal cancer incidence and mortality. *Gut,* 66**,** 683-691.

MA, Z., GINSBERG, A. M. & SPIGELMAN, M. 2007. 7.24 - Antimycobacterium Agents. *In:* TAYLOR, J. B. & TRIGGLE, D. J. (eds.) *Comprehensive Medicinal Chemistry II.* Oxford: Elsevier.

MACDONAGH, L., GRAY, S. G., BREEN, E., CUFFE, S., FINN, S. P., O'BYRNE, K. J. & BARR, M. P. 2018. BBI608 inhibits cancer stemness and reverses cisplatin resistance in NSCLC. *Cancer Lett,* 428**,** 117-126.

MACHADO-OLIVEIRA, G., GUERREIRO, E., MATIAS, A. C., FACUCHO-OLIVEIRA, J., PACHECO-LEYVA, I. & BRAGANCA, J. 2015. FBXL5 modulates HIF-1alpha

transcriptional activity by degradation of CITED2. *Arch Biochem Biophys,* 576**,** 61-72.

MAJUMDER, B., BARANEEDHARAN, U., THIYAGARAJAN, S., RADHAKRISHNAN, P., NARASIMHAN, H., DHANDAPANI, M., BRIJWANI, N., PINTO, D. D., PRASATH, A., SHANTHAPPA, B. U., THAYAKUMAR, A., SURENDRAN, R., BABU, G. K., SHENOY, A. M., KURIAKOSE, M. A., BERGTHOLD, G., HOROWITZ, P., LODA, M., BEROUKHIM, R., AGARWAL, S., SENGUPTA, S., SUNDARAM, M. & MAJUMDER, P. K. 2015. Predicting clinical response to anticancer drugs using an ex vivo platform that captures tumour heterogeneity. *Nature Communications,* 6**,** 6169.

MANI, S. A., GUO, W., LIAO, M. J., EATON, E. N., AYYANAN, A., ZHOU, A. Y., BROOKS, M., REINHARD, F., ZHANG, C. C., SHIPITSIN, M., CAMPBELL, L. L., POLYAK, K., BRISKEN, C., YANG, J. & WEINBERG, R. A. 2008. The epithelial-mesenchymal transition generates cells with properties of stem cells. *Cell,* 133**,** 704-15.

MANTOVANI, A. 2009. Inflaming metastasis. *Nature,* 457**,** 36-37.

MARQUARDT, S., SOLANKI, M., SPITSCHAK, A., VERA, J. & PUTZER, B. M. 2018. Emerging functional markers for cancer stem cell-based therapies: Understanding signaling networks for targeting metastasis. *Semin Cancer Biol,* 53**,** 90-109.

MARTIN, E. S., TONON, G., SINHA, R., XIAO, Y., FENG, B., KIMMELMAN, A. C., PROTOPOPOV, A., IVANOVA, E., BRENNAN, C., MONTGOMERY, K., KUCHERLAPATI, R., BAILEY, G., REDSTON, M., CHIN, L. & DEPINHO, R. A. 2007. Common and distinct genomic events in sporadic colorectal cancer and diverse cancer types. *Cancer Research,* 67.

MARTINS-NEVES, S. R., PAIVA-OLIVEIRA, D. I., FONTES-RIBEIRO, C., BOVÉE, J. V. M. G., CLETON-JANSEN, A.-M. & GOMES, C. M. F. 2018. IWR-1, a tankyrase inhibitor, attenuates Wnt/β-catenin signaling in cancer stem-like cells and inhibits in vivo the growth of a subcutaneous human osteosarcoma xenograft. *Cancer Letters,* 414**,** 1-15.

MASUDA, M., SAWA, M. & YAMADA, T. 2015. Therapeutic targets in the Wnt signaling pathway: Feasibility of targeting TNIK in colorectal cancer. *Pharmacology & therapeutics,* 156**,** 1-9.

MAZALEUSKAYA, L. L., SANGKUHL, K., THORN, C. F., FITZGERALD, G. A., ALTMAN, R. B. & KLEIN, T. E. 2015. PharmGKB summary: pathways of acetaminophen metabolism at the therapeutic versus toxic doses. *Pharmacogenetics and genomics,* 25**,** 416-426.

MEACHAM, C. E. & MORRISON, S. J. 2013. Tumour heterogeneity and cancer cell plasticity. *Nature,* 501**,** 328.

MEDEMA, J. P. & VERMEULEN, L. 2011. Microenvironmental regulation of stem cells in intestinal homeostasis and cancer. *Nature,* 474**,** 318-26.

MERLOS-SUÁREZ, A., BARRIGA, FRANCISCO M., JUNG, P., IGLESIAS, M., CÉSPEDES, MARÍA V., ROSSELL, D., SEVILLANO, M., HERNANDO-MOMBLONA, X., DA SILVA-DIZ, V., MUÑOZ, P., CLEVERS, H., SANCHO, E., MANGUES, R. & BATLLE, E. 2011. The Intestinal Stem Cell Signature Identifies Colorectal Cancer Stem Cells and Predicts Disease Relapse. *Cell Stem Cell,* 8**,** 511-524.

MHAIDAT, N. M., BOUKLIHACENE, M. & THORNE, R. F. 2014. 5-Fluorouracil-induced apoptosis in colorectal cancer cells is caspase-9-dependent and mediated by activation of protein kinase C-δ. *Oncology letters,* 8**,** 699-704.

MIN, H. J., CHO, I. R., SRISUTTEE, R., PARK, E. H., CHO, D. H., AHN, J. H., LEE, I. S., JOHNSTON, R. N., OH, S. & CHUNG, Y. H. 2009. Hexachlorophene suppresses beta-catenin expression by up-regulation of Siah-1 in EBV-infected B lymphoma cells. *Cancer Lett,* 276**,** 136-42.

MOHELNIKOVA-DUCHONOVA, B., MELICHAR, B. & SOUCEK, P. 2014. FOLFOX/FOLFIRI pharmacogenetics: the call for a personalized approach in colorectal cancer therapy. *World journal of gastroenterology,* 20**,** 10316-10330.

MONTGOMERY, R. K., CARLONE, D. L., RICHMOND, C. A., FARILLA, L., KRANENDONK, M. E., HENDERSON, D. E., BAFFOUR-AWUAH, N. Y., AMBRUZS, D. M., FOGLI, L. K., ALGRA, S. & BREAULT, D. T. 2011. Mouse telomerase reverse transcriptase (mTert) expression marks slowly cycling intestinal stem cells. *Proc Natl Acad Sci U S A,* 108**,** 179-84.

MORATH, I., HARTMANN, T. N. & ORIAN-ROUSSEAU, V. 2016. CD44: More than a mere stem cell marker. *Int J Biochem Cell Biol,* 81**,** 166-173.

MOTTAMAL, M., ZHENG, S., HUANG, T. L. & WANG, G. 2015. Histone deacetylase inhibitors in clinical studies as templates for new anticancer agents. *Molecules,* 20**,** 3898-3941.

MUNKHOLM, P. 2003. Review article: the incidence and prevalence of colorectal cancer in inflammatory bowel disease. *Aliment Pharmacol Ther,* 18 Suppl 2**,** 1-5.

MURAMATSU, S., SHIRAISHI, S., MIYANO, K., SUDO, Y., TODA, A., MOGI, M., HARA, M., YOKOYAMA, A., KAWASAKI, Y., TANIGUCHI, M. & UEZONO, Y. 2016. Metabolism of AM404 From Acetaminophen at Human Therapeutic Dosages in the Rat Brain. *Anesthesiology and pain medicine,* 6**,** e32873-e32873.

MUSA, A., GHORAIE, L. S., ZHANG, S.-D., GLAZKO, G., YLI-HARJA, O., DEHMER, M., HAIBE-KAINS, B. & EMMERT-STREIB, F. 2018. A review of connectivity map and computational approaches in pharmacogenomics. *Briefings in bioinformatics,* 19**,** 506-523.

MUTO, Y., NISHIYAMA, M., NITA, A., MOROISHI, T. & NAKAYAMA, K. I. 2017. Essential role of FBXL5-mediated cellular iron homeostasis in maintenance of hematopoietic stem cells. *Nature Communications,* 8**,** 16114.

NAPOLITANO, F., SIRCI, F., CARRELLA, D. & DI BERNARDO, D. 2016. Drug-set enrichment analysis: a novel tool to investigate drug mode of action. *Bioinformatics (Oxford, England),* 32**,** 235-241.

NATERI, A. S., RIERA-SANS, L., DA COSTA, C. & BEHRENS, A. 2004. The ubiquitin ligase SCFFbw7 antagonizes apoptotic JNK signaling. *Science,* 303**,** 1374-8.

NAUJOKAT, C. & STEINHART, R. 2012. Salinomycin as a drug for targeting human cancer stem cells. *BioMed Research International,* 2012.

NAUTIYAL, J., KANWAR, S. S., YU, Y. & MAJUMDAR, A. P. 2011. Combination of dasatinib and curcumin eliminates chemo-resistant colon cancer cells. *Journal of molecular signaling,* 6**,** 7.

NING, X., SHU, J., DU, Y., BEN, Q. & LI, Z. 2013. Therapeutic strategies targeting cancer stem cells. *Cancer biology & therapy,* 14**,** 295-303.

NISHIDA, Y., MAEDA, A., CHACHAD, D., ISHIZAWA, J., QIU, Y. H., KORNBLAU, S. M., KIMURA, S., ANDREEFF, M. & KOJIMA, K. 2015. Preclinical activity of the novel B-cell-specific Moloney murine leukemia virus integration site 1 inhibitor PTC-209 in acute myeloid leukemia: Implications for leukemia therapy. *Cancer Science,* 106**,** 1705-1713.

O'ROURKE, K. P., LOIZOU, E., LIVSHITS, G., SCHATOFF, E. M., BASLAN, T., MANCHADO, E., SIMON, J., ROMESSER, P. B., LEACH, B., HAN, T., PAULI, C., BELTRAN, H., RUBIN, M. A., DOW, L. E. & LOWE, S. W. 2017. Transplantation of engineered organoids enables rapid generation of metastatic mouse models of colorectal cancer. *Nature biotechnology,* 35**,** 577-582.

ONUMA, K., OCHIAI, M., ORIHASHI, K., TAKAHASHI, M., IMAI, T., NAKAGAMA, H. & HIPPO, Y. 2013. Genetic reconstitution of tumorigenesis in primary intestinal cells. *Proceedings of the National Academy of Sciences of the United States of America,* 110**,** 11127-11132.

PÀEZ-RIBES, M., ALLEN, E., HUDOCK, J., TAKEDA, T., OKUYAMA, H., VIÑALS, F., INOUE, M., BERGERS, G., HANAHAN, D. & CASANOVAS, O. 2009. Antiangiogenic Therapy Elicits Malignant Progression of Tumors to Increased Local Invasion and Distant Metastasis. *Cancer Cell,* 15**,** 220-231.

PAN, J., LEE, Y., ZHANG, Q., XIONG, D., WAN, T. C., WANG, Y. & YOU, M. 2017a. Honokiol Decreases Lung Cancer Metastasis through Inhibition of the STAT3 Signaling Pathway. *Cancer Prev Res (Phila),* 10**,** 133-141.

PAN, Q., MENG, L., YE, J., WEI, X., SHANG, Y., TIAN, Y., HE, Y., PENG, Z., CHEN, L., CHEN, W., BIAN, X. & WANG, R. 2017b. Transcriptional repression of miR-200 family members by Nanog in colon cancer cells induces epithelial–mesenchymal transition (EMT). *Cancer Letters,* 392**,** 26-38.

PANCIONE, M., REMO, A. & COLANTUONI, V. 2012. Genetic and epigenetic events generate multiple pathways in colorectal cancer progression. *Patholog Res Int,* 2012**,** 509348.

PARMAR, A., MARZ, S., RUSHTON, S., HOLZWARTH, C., LIND, K., KAYSER, S., DÖHNER, K., PESCHEL, C., OOSTENDORP, R. A. & GÖTZE, K. S. 2011. Stromal niche cells protect early leukemic FLT3-ITD+ progenitor cells against first-generation FLT3 tyrosine kinase inhibitors. *Cancer research,* 71**,** 4696-4706.

PARVEZ, M. M., JUNG, J. A., SHIN, H. J., KIM, D. H. & SHIN, J. G. 2016. Characterization of 22 Antituberculosis Drugs for Inhibitory Interaction Potential on Organic Anionic Transporter Polypeptide (OATP)-Mediated Uptake. *Antimicrob Agents Chemother,* 60**,** 3096-105.

PATIL, S. P., YOON, S. C., ARADHYA, A. G., HOFER, J., FINK, M. A., ENLEY, E. S., FISHER, J. E., HERB, M. C., KLINGOS, A., PROULX, J. T. & FEDORKY, M. T. 2018. Macrocyclic Compounds from Ansamycin Antibiotic Class as Inhibitors of PD1-PDL1 Protein-Protein Interaction. *Chem Pharm Bull (Tokyo),* 66**,** 773-778.

PINO, M. S. & CHUNG, D. C. 2010. The Chromosomal Instability Pathway in Colon Cancer. *Gastroenterology,* 138**,** 2059-2072.

PISTOLLATO, F., CALDERON IGLESIAS, R., RUIZ, R., APARICIO, S., CRESPO, J., DZUL LOPEZ, L., GIAMPIERI, F. & BATTINO, M. 2017. The use of natural compounds for the targeting and chemoprevention of ovarian cancer. *Cancer Lett,* 411**,** 191-200.

POTTEN, C. S. 1977. EXTREME SENSITIVITY OF SOME INTESTINAL CRYPT CELLS TO X AND GAMMA-IRRADIATION. *Nature,* 269**,** 518-521.

POTTEN, C. S., KOVACS, L. & HAMILTON, E. 1974. CONTINUOUS LABELING STUDIES ON MOUSE SKIN AND INTESTINE. *Cell and Tissue Kinetics,* 7**,** 271-283.

POWELL, A. E., WANG, Y., LI, Y., POULIN, E. J., MEANS, A. L., WASHINGTON, M. K., HIGGINBOTHAM, J. N., JUCHHEIM, A., PRASAD, N., LEVY, S. E., GUO, Y., SHYR, Y., ARONOW, B. J., HAIGIS, K. M., FRANKLIN, J. L. & COFFEY, R. J. 2012.

The pan-ErbB negative regulator Lrig1 is an intestinal stem cell marker that functions as a tumor suppressor. *Cell,* 149**,** 146-58.

PRABHU, V. V., ALLEN, J. E., DICKER, D. T. & EL-DEIRY, W. S. 2015. Small-Molecule ONC201/TIC10 Targets Chemotherapy-Resistant Colorectal Cancer Stem-like Cells in an Akt/Foxo3a/TRAIL-Dependent Manner. *Cancer Res,* 75**,** 1423-32.

QUAIL, D. F. & JOYCE, J. A. 2013. Microenvironmental regulation of tumor progression and metastasis. *Nat Med,* 19**,** 1423-37.

QUALTROUGH, D., HINOI, T., FEARON, E. & PARASKEVA, C. J. G. 2002. Expression of CDX2 in normal and neoplastic human colon tissue and during differentiation of an in vitro model system. 51**,** 184-190.

RADWAN, A. A., AL-MOHANNA, F., ALANAZI, F. K., MANOGARAN, P. S. & AL-DHFYAN, A. 2016. Target β-catenin/CD44/Nanog axis in colon cancer cells by certain N′-(2-oxoindolin-3-ylidene)-2-(benzyloxy)benzohydrazides. *Bioorganic & Medicinal Chemistry Letters,* 26**,** 1664-1670.

RAJ, S., FRANCO, V. I. & LIPSHULTZ, S. E. J. C. T. O. I. C. M. 2014. Anthracycline-Induced Cardiotoxicity: A Review of Pathophysiology, Diagnosis, and Treatment. 16**,** 315.

RAJAGOPALAN, H., NOWAK, M. A., VOGELSTEIN, B. & LENGAUER, C. 2003. The significance of unstable chromosomes in colorectal cancer. *Nat Rev Cancer,* 3**,** 695-701.

RAMASAMY, T. S., AYOB, A. Z., MYINT, H. H. L., THIAGARAJAH, S. & AMINI, F. 2015. Targeting colorectal cancer stem cells using curcumin and curcumin analogues: insights into the mechanism of the therapeutic efficacy. *Cancer cell international,* 15**,** 1.

REYA, T., MORRISON, S. J., CLARKE, M. F. & WEISSMAN, I. L. 2001. Stem cells, cancer, and cancer stem cells. *nature,* 414**,** 105-111.

RICCI-VITIANI, L., LOMBARDI, D. G., PILOZZI, E., BIFFONI, M., TODARO, M., PESCHLE, C. & DE MARIA, R. 2007. Identification and expansion of human colon-cancer-initiating cells. *Nature,* 445**,** 111-5.

RICHON, V. M. 2006. Cancer biology: mechanism of antitumour action of vorinostat (suberoylanilide hydroxamic acid), a novel histone deacetylase inhibitor. *British Journal Of Cancer,* 95**,** S2.

RICHON, V. M., EMILIANI, S., VERDIN, E., WEBB, Y., BRESLOW, R., RIFKIND, R. A. & MARKS, P. A. 1998. A class of hybrid polar inducers of transformed cell differentiation inhibits histone deacetylases. *Proceedings of the National Academy of Sciences of the United States of America,* 95**,** 3003-3007.

SACHLOS, E., RISUEÑO, R. M., LARONDE, S., SHAPOVALOVA, Z., LEE, J.-H., RUSSELL, J., MALIG, M., MCNICOL, J. D., FIEBIG-COMYN, A. & GRAHAM, M. 2012a. Identification of drugs including a dopamine receptor antagonist that selectively target cancer stem cells. *Cell,* 149**,** 1284-1297.

SACHLOS, E., RISUEÑO, RUTH M., LARONDE, S., SHAPOVALOVA, Z., LEE, J.-H., RUSSELL, J., MALIG, M., MCNICOL, JAMIE D., FIEBIG-COMYN, A., GRAHAM, M., LEVADOUX-MARTIN, M., LEE, JUNG B., GIACOMELLI, ANDREW O., HASSELL, JOHN A., FISCHER-RUSSELL, D., TRUS, MICHAEL R., FOLEY, R., LEBER, B., XENOCOSTAS, A., BROWN, ERIC D., COLLINS, TONY J. & BHATIA, M. 2012b. Identification of Drugs Including a Dopamine Receptor Antagonist that Selectively Target Cancer Stem Cells. *Cell,* 149**,** 1284-1297.

SAILAJA, B. S., HE, X. C. & LI, L. 2016. The regulatory niche of intestinal stem cells. *J Physiol,* 594**,** 4827-36.

SALAHUDEEN, M. S. & NISHTALA, P. S. 2017. An overview of pharmacodynamic modelling, ligand-binding approach and its application in clinical practice. *Saudi pharmaceutical journal : SPJ : the official publication of the Saudi Pharmaceutical Society,* 25**,** 165-175.

SALIBA, S. W., MARCOTEGUI, A. R., FORTWÄNGLER, E., DITRICH, J., PERAZZO, J. C., MUÑOZ, E., DE OLIVEIRA, A. C. P. & FIEBICH, B. L. J. J. O. N. 2017. AM404, paracetamol metabolite, prevents prostaglandin synthesis in activated microglia by inhibiting COX activity. 14**,** 246.

SAMPIERI, K. & FODDE, R. Cancer stem cells and metastasis. Seminars in cancer biology, 2012. Elsevier, 187-193.

SANCHEZ-TILLO, E., LIU, Y., DE BARRIOS, O., SILES, L., FANLO, L., CUATRECASAS, M., DARLING, D. S., DEAN, D. C., CASTELLS, A. & POSTIGO, A. 2012. EMT-activating transcription factors in cancer: beyond EMT and tumor invasiveness. *Cell Mol Life Sci,* 69**,** 3429-56.

SANCHO, E., BATLLE, E. & CLEVERS, H. 2003. Live and let die in the intestinal epithelium. *Curr Opin Cell Biol,* 15**,** 763-70.

SANCHO, E., BATLLE, E. & CLEVERS, H. 2004. Signaling pathways in intestinal development and cancer. *Annu. Rev. Cell Dev. Biol.,* 20**,** 695-723.

SANCHO, R., JANDKE, A., DAVIS, H., DIEFENBACHER, M. E., TOMLINSON, I. & BEHRENS, A. 2010. F-box and WD repeat domain-containing 7 regulates intestinal cell lineage commitment and is a haploinsufficient tumor suppressor. *Gastroenterology,* 139**,** 929-41.

SANGIORGI, E. & CAPECCHI, M. R. 2008. Bmi1 is expressed in vivo in intestinal stem cells. *Nature Genetics,* 40**,** 915-920.

SANSOM, O. J., REED, K. R., HAYES, A. J., IRELAND, H., BRINKMANN, H., NEWTON, I. P., BATLLE, E., SIMON-ASSMANN, P., CLEVERS, H., NATHKE, I. S., CLARKE, A. R. & WINTON, D. J. 2004. Loss of Apc in vivo immediately perturbs Wnt signaling, differentiation, and migration. *Genes Dev,* 18**,** 1385-90.

SANTOS, A. J. M., LO, Y.-H., MAH, A. T. & KUO, C. J. 2018. The Intestinal Stem Cell Niche: Homeostasis and Adaptations. *Trends in Cell Biology,* 28**,** 1062-1078.

SATO, R., SEMBA, T., SAYA, H. & ARIMA, Y. 2016. Concise Review: Stem Cells and Epithelial-Mesenchymal Transition in Cancer: Biological Implications and Therapeutic Targets. *Stem Cells,* 34**,** 1997-2007.

SATO, T., STANGE, D. E., FERRANTE, M., VRIES, R. G. J., VAN ES, J. H., VAN DEN BRINK, S., VAN HOUDT, W. J., PRONK, A., VAN GORP, J., SIERSEMA, P. D. & CLEVERS, H. 2011. Long-term Expansion of Epithelial Organoids From Human Colon, Adenoma, Adenocarcinoma, and Barrett's Epithelium. *Gastroenterology,* 141**,** 1762-1772.

SATO, T., VRIES, R. G., SNIPPERT, H. J., VAN DE WETERING, M., BARKER, N., STANGE, D. E., VAN ES, J. H., ABO, A., KUJALA, P., PETERS, P. J. & CLEVERS, H. 2009a. Single Lgr5 stem cells build crypt-villus structures in vitro without a mesenchymal niche. *Nature,* 459**,** 262-5.

SATO, T., VRIES, R. G., SNIPPERT, H. J., VAN DE WETERING, M., BARKER, N., STANGE, D. E., VAN ES, J. H., ABO, A., KUJALA, P., PETERS, P. J. & CLEVERS, H. 2009b. Single Lgr5 stem cells build crypt-villus structures in vitro without a mesenchymal niche. *Nature,* 459**,** 262-265.

SCHEEL, C. & WEINBERG, R. A. 2012. Cancer stem cells and epithelial-mesenchymal transition: Concepts and molecular links. *Seminars in Cancer Biology,* 22**,** 396-403.

SEBIO, A., KAHN, M. & LENZ, H.-J. 2014. The potential of targeting Wnt/β-catenin in colon cancer. *Expert opinion on therapeutic targets,* 18**,** 611-615.

SENBANJO, L. T. & CHELLAIAH, M. A. 2017. CD44: A Multifunctional Cell Surface Adhesion Receptor Is a Regulator of Progression and Metastasis of Cancer Cells. *Frontiers in cell and developmental biology,* 5**,** 18-18.

SHAFFER, S. M., DUNAGIN, M. C., TORBORG, S. R., TORRE, E. A., EMERT, B., KREPLER, C., BEQIRI, M., SPROESSER, K., BRAFFORD, P. A., XIAO, M., EGGAN, E., ANASTOPOULOS, I. N., VARGAS-GARCIA, C. A., SINGH, A., NATHANSON, K. L., HERLYN, M. & RAJ, A. 2018. Correction: Corrigendum: Rare cell variability and drug-induced reprogramming as a mode of cancer drug resistance. *Nature,* 555**,** 274-274.

SHAHEEN, S., AHMED, M., LORENZI, F. & NATERI, A. S. 2016a. Spheroid-Formation (Colonosphere) Assay for in Vitro Assessment and Expansion of Stem Cells in Colon Cancer. *Stem Cell Rev,* 12**,** 492-9.

SHAHEEN, S., AHMED, M., LORENZI, F. & NATERI, A. S. 2016b. Spheroid-Formation (Colonosphere) Assay for in Vitro Assessment and Expansion of Stem Cells in Colon Cancer. *Stem Cell Rev Rep,* 12**,** 492-9.

SHAHEEN, S., AHMED, M., LORENZI, F., NATERI, A. S. J. S. C. R. & REPORTS 2016c. Spheroid-Formation (Colonosphere) Assay for in Vitro Assessment and Expansion of Stem Cells in Colon Cancer. 12**,** 492-499.

SHANG, D., SONG, B. & LIU, Y. 2018. Epirubicin suppresses proliferative and metastatic potential by downregulating transforming growth factor-beta-induced expression in urothelial carcinoma. *Cancer Sci,* 109**,** 980-987.

SHERR, C. J. 2004. Principles of tumor suppression. *Cell,* 116**,** 235-46.

SHIBATA, H., YAMAKOSHI, H., SATO, A., OHORI, H., KAKUDO, Y., KUDO, C., TAKAHASHI, Y., WATANABE, M., TAKANO, H. & ISHIOKA, C. 2009. Newly synthesized curcumin analog has improved potential to prevent colorectal carcinogenesis in vivo. *Cancer science,* 100**,** 956-960.

SHICHIRI, M. & TANAKA, Y. 2010. Inhibition of cancer progression by rifampicin: involvement of antiangiogenic and anti-tumor effects. *Cell Cycle,* 9**,** 64-68.

SHIMOKAWA, M., OHTA, Y., NISHIKORI, S., MATANO, M., TAKANO, A., FUJII, M., DATE, S., SUGIMOTO, S., KANAI, T. & SATO, T. 2017. Visualization and targeting of LGR5+ human colon cancer stem cells. *Nature,* 545**,** 187.

SHIOZAWA, Y., NIE, B., PIENTA, K. J., MORGAN, T. M. & TAICHMAN, R. S. 2013. Cancer stem cells and their role in metastasis. *Pharmacology & therapeutics,* 138**,** 285-293.

SIDDIQUI, N. & SONENBERG, N. 2015. Signalling to eIF4E in cancer. *Biochemical Society transactions,* 43**,** 763-772.

SIEGEL, R. L., MILLER, K. D., FEDEWA, S. A., AHNEN, D. J., MEESTER, R. G. S., BARZI, A. & JEMAL, A. 2017. Colorectal cancer statistics, 2017. *CA Cancer J Clin,* 67**,** 177-193.

SILVA DOS SANTOS, D., BRASIL, G. V., RAMOS, I. P. R., MESQUITA, F. C. P., KASAI-BRUNSWICK, T. H., CHRISTIE, M. L. A., CAHLI, G. M., BARBOSA, R. A. Q., DA CUNHA, S. T., PEREIRA, J. X., MEDEI, E., CAMPOS DE CARVALHO, A. C., CARVALHO, A. B. & GOLDENBERG, R. C. D. S. 2018. Embryonic stem cell-derived cardiomyocytes for the treatment of doxorubicin-induced cardiomyopathy. *Stem cell research & therapy,* 9**,** 30-30.

SINGH, A. & SETTLEMAN, J. 2010. EMT, cancer stem cells and drug resistance: an emerging axis of evil in the war on cancer. *Oncogene,* 29**,** 4741-4751.

SINGH, B. N., FU, J., SRIVASTAVA, R. K. & SHANKAR, S. 2011. Hedgehog signaling antagonist GDC-0449 (Vismodegib) inhibits pancreatic cancer stem cell characteristics: molecular mechanisms. *PloS one,* 6**,** e27306.

SJOEBLOM, T., JONES, S., WOOD, L. D., PARSONS, D. W., LIN, J., BARBER, T. D., MANDELKER, D., LEARY, R. J., PTAK, J., SILLIMAN, N., SZABO, S., BUCKHAULTS, P., FARRELL, C., MEEH, P., MARKOWITZ, S. D., WILLIS, J., DAWSON, D., WILLSON, J. K. V., GAZDAR, A. F., HARTIGAN, J., WU, L., LIU, C., PARMIGIANI, G., PARK, B. H., BACHMAN, K. E., PAPADOPOULOS, N., VOGELSTEIN, B., KINZLER, K. W. & VELCULESCU, V. E. 2006. The consensus coding sequences of human breast and colorectal cancers. *Science,* 314.

SMITH, D. C., EISENBERG, P. D., MANIKHAS, G., CHUGH, R., GUBENS, M. A., STAGG, R. J., KAPOUN, A. M., XU, L., DUPONT, J. & SIKIC, B. 2014. A phase I dose escalation and expansion study of the anticancer stem cell agent demcizumab (anti-DLL4) in patients with previously treated solid tumors. *Clin Cancer Res,* 20**,** 6295-303.

SNIPPERT, H. J., VAN ES, J. H., VAN DEN BORN, M., BEGTHEL, H., STANGE, D. E., BARKER, N. & CLEVERS, H. 2009. Prominin-1/CD133 marks stem cells and early progenitors in mouse small intestine. *Gastroenterology,* 136**,** 2187-2194.e1.

STELZNER, M., HELMRATH, M., DUNN, J. C. Y., HENNING, S. J., HOUCHEN, C. W., KUO, C., LYNCH, J., LI, L., MAGNESS, S. T., MARTIN, M. G., WONG, M. H., YU, J. & CONSORTIUM, N. I. H. I. S. C. 2012. A nomenclature for intestinal in vitro cultures. *American journal of physiology. Gastrointestinal and liver physiology,* 302**,** G1359-G1363.

SUAREZ-CARMONA, M., LESAGE, J., CATALDO, D. & GILLES, C. 2017. EMT and inflammation: inseparable actors of cancer progression. *Molecular oncology,* 11**,** 805-823.

SUBRAMANIAN, A., NARAYAN, R., CORSELLO, S. M., PECK, D. D., NATOLI, T. E., LU, X., GOULD, J., DAVIS, J. F., TUBELLI, A. A., ASIEDU, J. K., LAHR, D. L., HIRSCHMAN, J. E., LIU, Z., DONAHUE, M., JULIAN, B., KHAN, M., WADDEN, D., SMITH, I. C., LAM, D., LIBERZON, A., TODER, C., BAGUL, M., ORZECHOWSKI, M., ENACHE, O. M., PICCIONI, F., JOHNSON, S. A., LYONS, N. J., BERGER, A. H., SHAMJI, A. F., BROOKS, A. N., VRCIC, A., FLYNN, C., ROSAINS, J., TAKEDA, D. Y., HU, R., DAVISON, D., LAMB, J., ARDLIE, K., HOGSTROM, L., GREENSIDE, P., GRAY, N. S., CLEMONS, P. A., SILVER, S., WU, X., ZHAO, W.-N., READ-BUTTON, W., WU, X., HAGGARTY, S. J., RONCO, L. V., BOEHM, J. S., SCHREIBER, S. L., DOENCH, J. G., BITTKER, J. A., ROOT, D. E., WONG, B. & GOLUB, T. R. 2017. A Next Generation Connectivity Map: L1000 Platform and the First 1,000,000 Profiles. *Cell,* 171**,** 1437-1452.e17.

SUBRAMANIAN, A., TAMAYO, P., MOOTHA, V. K., MUKHERJEE, S., EBERT, B. L., GILLETTE, M. A., PAULOVICH, A., POMEROY, S. L., GOLUB, T. R., LANDER, E. S. & MESIROV, J. P. 2005. Gene set enrichment analysis: a knowledge-based approach for interpreting genome-wide expression profiles. *Proceedings of the National Academy of Sciences of the United States of America,* 102**,** 15545-15550.

TAKEDA, N., JAIN, R., LEBOEUF, M. R., WANG, Q., LU, M. M. & EPSTEIN, J. A. 2011. Interconversion between intestinal stem cell populations in distinct niches. *Science,* 334**,** 1420-4.

TANEI, T., MORIMOTO, K., SHIMAZU, K., KIM, S. J., TANJI, Y., TAGUCHI, T., TAMAKI, Y. & NOGUCHI, S. 2009. Association of breast cancer stem cells identified

by aldehyde dehydrogenase 1 expression with resistance to sequential Paclitaxel and epirubicin-based chemotherapy for breast cancers. *Clin Cancer Res,* 15**,** 4234-41.

TARPGAARD, L. S., QVORTRUP, C., NYGÅRD, S. B., NIELSEN, S. L., ANDERSEN, D. R., JENSEN, N. F., STENVANG, J., DETLEFSEN, S., BRÜNNER, N. & PFEIFFER, P. 2016. A phase II study of Epirubicin in oxaliplatin-resistant patients with metastatic colorectal cancer and TOP2A gene amplification. *BMC Cancer,* 16**,** 91.

TAURIELLO, D. V. F., PALOMO-PONCE, S., STORK, D., BERENGUER-LLERGO, A., BADIA-RAMENTOL, J., IGLESIAS, M., SEVILLANO, M., IBIZA, S., CAÑELLAS, A., HERNANDO-MOMBLONA, X., BYROM, D., MATARIN, J. A., CALON, A., RIVAS, E. I., NEBREDA, A. R., RIERA, A., ATTOLINI, C. S.-O. & BATLLE, E. 2018. TGFβ drives immune evasion in genetically reconstituted colon cancer metastasis. *Nature,* 554**,** 538.

TESTA, U., PELOSI, E. & CASTELLI, G. 2018. Colorectal cancer: genetic abnormalities, tumor progression, tumor heterogeneity, clonal evolution and tumor-initiating cells. *Medical sciences (Basel, Switzerland),* 6**,** 31.

THANKI, K., NICHOLLS, M. E., GAJJAR, A., SENAGORE, A. J., QIU, S., SZABO, C., HELLMICH, M. R. & CHAO, C. 2017. Consensus Molecular Subtypes of Colorectal Cancer and their Clinical Implications. *International biological and biomedical journal,* 3**,** 105-111.

THIERY, J. P., ACLOQUE, H., HUANG, R. Y. & NIETO, M. A. 2009. Epithelial-mesenchymal transitions in development and disease. *Cell,* 139**,** 871-90.

TIAN, F., MYSLIWIETZ, J., ELLWART, J., GAMARRA, F., HUBER, R. M. & BERGNER, A. 2012. Effects of the Hedgehog pathway inhibitor GDC-0449 on lung cancer cell lines are mediated by side populations. *Clinical and experimental medicine,* 12**,** 25-30.

TIGNANELLI, C. J., HERRERA LOEZA, S. G. & YEH, J. J. 2014. KRAS and PIK3CA mutation frequencies in patient-derived xenograft models of pancreatic and colorectal cancer are reflective of patient tumors and stable across passages. *Am Surg,* 80**,** 873-7.

TODARO, M., GAGGIANESI, M., CATALANO, V., BENFANTE, A., IOVINO, F., BIFFONI, M., APUZZO, T., SPERDUTI, I., VOLPE, S., COCORULLO, G., GULOTTA, G., DIELI, F., DE MARIA, R. & STASSI, G. 2014. CD44v6 is a marker of constitutive and reprogrammed cancer stem cells driving colon cancer metastasis. *Cell Stem Cell,* 14**,** 342-56.

TODEN, S., TRAN, H. M., TOVAR-CAMARGO, O. A., OKUGAWA, Y. & GOEL, A. 2016. Epigallocatechin-3-gallate targets cancer stem-like cells and enhances 5-fluorouracil chemosensitivity in colorectal cancer. *Oncotarget,* 7**,** 16158-71.

TOLEDO-GUZMÁN, M. E., BIGONI-ORDÓÑEZ, G. D., IBÁÑEZ HERNÁNDEZ, M. & ORTIZ-SÁNCHEZ, E. 2018. Cancer stem cell impact on clinical oncology. *World journal of stem cells,* 10**,** 183-195.

TOMLINSON, I., SASIENI, P. & BODMER, W. 2002. How many mutations in a cancer? *The American journal of pathology,* 160**,** 755-758.

TONG, K., PELLÓN-CÁRDENAS, O., SIRIHORACHAI, V. R., WARDER, B. N., KOTHARI, O. A., PEREKATT, A. O., FOKAS, E. E., FULLEM, R. L., ZHOU, A., THACKRAY, J. K., TRAN, H., ZHANG, L., XING, J. & VERZI, M. P. 2017. Degree of Tissue Differentiation Dictates Susceptibility to BRAF-Driven Colorectal Cancer. *Cell reports,* 21**,** 3833-3845.

VALENTI, G., QUINN, H. M., HEYNEN, G., LAN, L., HOLLAND, J. D., VOGEL, R., WULF-GOLDENBERG, A. & BIRCHMEIER, W. 2017. Cancer Stem Cells Regulate Cancer-Associated Fibroblasts via Activation of Hedgehog Signaling in Mammary Gland Tumors. *Cancer Res,* 77**,** 2134-2147.

VAN DE WETERING, M., FRANCIES, H. E., FRANCIS, J. M., BOUNOVA, G., IORIO, F., PRONK, A., VAN HOUDT, W., VAN GORP, J., TAYLOR-WEINER, A., KESTER, L., MCLAREN-DOUGLAS, A., BLOKKER, J., JAKSANI, S., BARTFELD, S., VOLCKMAN, R., VAN SLUIS, P., LI, V. S. W., SEEPO, S., SEKHAR PEDAMALLU, C., CIBULSKIS, K., CARTER, S. L., MCKENNA, A., LAWRENCE, M. S., LICHTENSTEIN, L., STEWART, C., KOSTER, J., VERSTEEG, R., VAN OUDENAARDEN, A., SAEZ-RODRIGUEZ, J., VRIES, R. G. J., GETZ, G., WESSELS, L., STRATTON, M. R., MCDERMOTT, U., MEYERSON, M., GARNETT, M. J. & CLEVERS, H. 2015. Prospective derivation of a living organoid biobank of colorectal cancer patients. *Cell,* 161**,** 933-945.

VAN DER FLIER, L. G., HAEGEBARTH, A., STANGE, D. E., VAN DE WETERING, M. & CLEVERS, H. 2009a. OLFM4 is a robust marker for stem cells in human intestine and marks a subset of colorectal cancer cells. *Gastroenterology,* 137**,** 15-7.

VAN DER FLIER, L. G., VAN GIJN, M. E., HATZIS, P., KUJALA, P., HAEGEBARTH, A., STANGE, D. E., BEGTHEL, H., VAN DEN BORN, M., GURYEV, V., OVING, I., VAN ES, J. H., BARKER, N., PETERS, P. J., VAN DE WETERING, M. & CLEVERS, H. 2009b. Transcription factor achaete scute-like 2 controls intestinal stem cell fate. *Cell,* 136**,** 903-12.

VAN ES, J. H., SATO, T., VAN DE WETERING, M., LYUBIMOVA, A., NEE, A. N. Y., GREGORIEFF, A., SASAKI, N., ZEINSTRA, L., VAN DEN BORN, M., KORVING, J., MARTENS, A. C. M., BARKER, N., VAN OUDENAARDEN, A. & CLEVERS, H. 2012. Dll1(+) secretory progenitor cells revert to stem cells upon crypt damage. *Nature Cell Biology,* 14**,** 1099-+.

VEGA-STROMBERG, T. 2003. Chemotherapy-induced secondary malignancies. *J Infus Nurs,* 26**,** 353-61.

VERMEULEN, L., DE SOUSA, E. M. F., VAN DER HEIJDEN, M., CAMERON, K., DE JONG, J. H., BOROVSKI, T., TUYNMAN, J. B., TODARO, M., MERZ, C., RODERMOND, H., SPRICK, M. R., KEMPER, K., RICHEL, D. J., STASSI, G. & MEDEMA, J. P. 2010. Wnt activity defines colon cancer stem cells and is regulated by the microenvironment. *Nat Cell Biol,* 12**,** 468-76.

VERMEULEN, L. & SNIPPERT, H. J. 2014. Stem cell dynamics in homeostasis and cancer of the intestine. *Nat Rev Cancer,* 14**,** 468-80.

VERMEULEN, L., TODARO, M., DE SOUSA MELLO, F., SPRICK, M. R., KEMPER, K., PEREZ ALEA, M., RICHEL, D. J., STASSI, G. & MEDEMA, J. P. 2008. Single-cell cloning of colon cancer stem cells reveals a multi-lineage differentiation capacity. *Proc Natl Acad Sci U S A,* 105**,** 13427-32.

VICHAI, V. & KIRTIKARA, K. 2006. Sulforhodamine B colorimetric assay for cytotoxicity screening. *Nat Protoc,* 1**,** 1112-6.

VISVADER, J. E. 2011. Cells of origin in cancer. *Nature,* 469**,** 314-322.

VLACHOGIANNIS, G., HEDAYAT, S., VATSIOU, A., JAMIN, Y., FERNÁNDEZ-MATEOS, J., KHAN, K., LAMPIS, A., EASON, K., HUNTINGFORD, I., BURKE, R., RATA, M., KOH, D.-M., TUNARIU, N., COLLINS, D., HULKKI-WILSON, S., RAGULAN, C., SPITERI, I., MOORCRAFT, S. Y., CHAU, I., RAO, S., WATKINS, D., FOTIADIS, N., BALI, M., DARVISH-DAMAVANDI, M., LOTE, H., ELTAHIR, Z., SMYTH, E. C., BEGUM, R., CLARKE, P. A., HAHNE, J. C., DOWSETT, M., DE BONO, J.,

WORKMAN, P., SADANANDAM, A., FASSAN, M., SANSOM, O. J., ECCLES, S., STARLING, N., BRACONI, C., SOTTORIVA, A., ROBINSON, S. P., CUNNINGHAM, D. & VALERI, N. 2018. Patient-derived organoids model treatment response of metastatic gastrointestinal cancers. *Science (New York, N.Y.),* 359**,** 920-926.

VOSKOGLOU-NOMIKOS, T., PATER, J. L. & SEYMOUR, L. 2003. Clinical predictive value of the in vitro cell line, human xenograft, and mouse allograft preclinical cancer models. *Clin Cancer Res,* 9**,** 4227-39.

WALTHER, A., JOHNSTONE, E., SWANTON, C., MIDGLEY, R., TOMLINSON, I. & KERR, D. 2009. Genetic prognostic and predictive markers in colorectal cancer. *Nature Reviews Cancer,* 9**,** 489-499.

WANG, Q., ZHOU, Y., RYCHAHOU, P., FAN, T. W., LANE, A. N., WEISS, H. L. & EVERS, B. M. 2017a. Ketogenesis contributes to intestinal cell differentiation. *Cell Death Differ,* 24**,** 458-468.

WANG, Y., FU, M., LIU, J., YANG, Y., YU, Y., LI, J., PAN, W., FAN, L., LI, G., LI, X. & WANG, X. 2019a. Inhibition of tumor metastasis by targeted daunorubicin and dioscin codelivery liposomes modified with PFV for the treatment of non-small-cell lung cancer. *Int J Nanomedicine,* 14**,** 4071-4090.

WANG, Y., GAO, W., SHI, X., DING, J., LIU, W., HE, H., WANG, K. & SHAO, F. 2017b. Chemotherapy drugs induce pyroptosis through caspase-3 cleavage of a gasdermin. *Nature,* 547**,** 99.

WANG, Z., INUZUKA, H., ZHONG, J., WAN, L., FUKUSHIMA, H., SARKAR, F. H. & WEI, W. 2012. Tumor suppressor functions of FBW7 in cancer development and progression. *FEBS letters,* 586**,** 1409-1418.

WANG, Z., LI, Y., AHMAD, A., AZMI, A. S., KONG, D., BANERJEE, S. & SARKAR, F. H. 2010. Targeting miRNAs involved in cancer stem cell and EMT regulation: An emerging concept in overcoming drug resistance. *Drug resistance updates,* 13**,** 109-118.

WANG, Z., ZHOU, L., XIONG, Y., YU, S., LI, H., FAN, J., LI, F., SU, Z., SONG, J., SUN, Q., LIU, S.-S., XIA, Y., ZHAO, L., LI, S., GUO, F., HUANG, P., CARSON, D. A. & LU, D. 2019b. Salinomycin exerts anti-colorectal cancer activity by targeting the β-catenin/T-cell factor complex. *British journal of pharmacology,* 176**,** 3390-3406.

WEISWALD, L.-B., BELLET, D. & DANGLES-MARIE, V. 2015a. Spherical cancer models in tumor biology. *Neoplasia (New York, N.Y.),* 17**,** 1-15.

WEISWALD, L. B., BELLET, D. & DANGLES-MARIE, V. 2015b. Spherical cancer models in tumor biology. *Neoplasia,* 17**,** 1-15.

WELCKER, M. & CLURMAN, B. E. 2008. FBW7 ubiquitin ligase: a tumour suppressor at the crossroads of cell division, growth and differentiation. *Nat Rev Cancer,* 8**,** 83-93.

WOOD, L. D., PARSONS, D. W., JONES, S., LIN, J., SJOBLOM, T., LEARY, R. J., SHEN, D., BOCA, S. M., BARBER, T., PTAK, J., SILLIMAN, N., SZABO, S., DEZSO, Z., USTYANKSKY, V., NIKOLSKAYA, T., NIKOLSKY, Y., KARCHIN, R., WILSON, P. A., KAMINKER, J. S., ZHANG, Z., CROSHAW, R., WILLIS, J., DAWSON, D., SHIPITSIN, M., WILLSON, J. K. V., SUKUMAR, S., POLYAK, K., PARK, B. H., PETHIYAGODA, C. L., PANT, P. V. K., BALLINGER, D. G., SPARKS, A. B., HARTIGAN, J., SMITH, D. R., SUH, E., PAPADOPOULOS, N., BUCKHAULTS, P., MARKOWITZ, S. D., PARMIGIANI, G., KINZLER, K. W., VELCULESCU, V. E. & VOGELSTEIN, B. 2007. The genomic landscapes of human breast and colorectal cancers. *Science,* 318.

WU, X., LUO, F., LI, J., ZHONG, X. & LIU, K. 2016. Tankyrase 1 inhibitior XAV939 increases chemosensitivity in colon cancer cell lines via inhibition of the Wnt signaling pathway. *International journal of oncology,* 48**,** 1333-1340.

XU, H., JIAO, Y., QIN, S., ZHAO, W., CHU, Q. & WU, K. 2018. Organoid technology in disease modelling, drug development, personalized treatment and regeneration medicine. *Experimental hematology & oncology,* 7**,** 30-30.

YAMADA, K. M. & CUKIERMAN, E. 2007. Modeling Tissue Morphogenesis and Cancer in 3D. *Cell,* 130**,** 601-610.

YAN, H., CHEN, X., ZHANG, Q., QIN, J., LI, H., LIU, C., CALHOUN-DAVIS, T., COLETTA, L. D., KLOSTERGAARD, J. & FOKT, I. 2011. Drug-tolerant cancer cells show reduced tumor-initiating capacity: depletion of CD44 cells and evidence for epigenetic mechanisms. *PloS one,* 6**,** e24397.

YAN, K. S., CHIA, L. A., LI, X., OOTANI, A., SU, J., LEE, J. Y., SU, N., LUO, Y., HEILSHORN, S. C., AMIEVA, M. R., SANGIORGI, E., CAPECCHI, M. R. & KUO, C. J. 2012. The intestinal stem cell markers Bmi1 and Lgr5 identify two functionally distinct populations. *Proc Natl Acad Sci U S A,* 109**,** 466-71.

YAN, W. 2015. Binding time—not just affinity—gains stature in drug design. *Nature Medicine,* 21**,** 545.

YAN, Y., ZUO, X. & WEI, D. 2015. Concise Review: Emerging Role of CD44 in Cancer Stem Cells: A Promising Biomarker and Therapeutic Target. *Stem Cells Transl Med,* 4**,** 1033-43.

YANG, A. D., FAN, F., CAMP, E. R., VAN BUREN, G., LIU, W., SOMCIO, R., GRAY, M. J., CHENG, H., HOFF, P. M. & ELLIS, L. M. 2006. Chronic oxaliplatin resistance induces epithelial-to-mesenchymal transition in colorectal cancer cell lines. *Clin Cancer Res,* 12**,** 4147-53.

YANG, T. & RYCAJ, K. 2015a. Targeted therapy against cancer stem cells (Review). *Oncology Letters,* 10**,** 27-33.

YANG, T. & RYCAJ, K. J. O. L. 2015b. Targeted therapy against cancer stem cells. 10**,** 27-33.

YAO, C., SU, L., SHAN, J., ZHU, C., LIU, L., LIU, C., XU, Y., YANG, Z., BIAN, X., SHAO, J., LI, J., LAI, M., SHEN, J. & QIAN, C. 2016. IGF/STAT3/NANOG/Slug Signaling Axis Simultaneously Controls Epithelial-Mesenchymal Transition and Stemness Maintenance in Colorectal Cancer. *Stem Cells,* 34**,** 820-31.

YAO, H., SU, S., XIA, D., WANG, M., LI, Z., CHEN, W., REN, L. & XU, L. 2018. F-box and leucine-rich repeat protein 5 promotes colon cancer progression by modulating PTEN/PI3K/AKT signaling pathway. *Biomedicine & Pharmacotherapy,* 107**,** 1712-1719.

YEUNG, T. M., GANDHI, S. C., WILDING, J. L., MUSCHEL, R. & BODMER, W. F. 2010. Cancer stem cells from colorectal cancer-derived cell lines. 107**,** 3722-3727.

YIP, H. Y. K., TAN, C. W., HIROKAWA, Y. & BURGESS, A. W. 2018. Colon organoid formation and cryptogenesis are stimulated by growth factors secreted from myofibroblasts. *PloS one,* 13**,** e0199412-e0199412.

YOU, L., HE, B., XU, Z., UEMATSU, K., MAZIERES, J., FUJII, N., MIKAMI, I., REGUART, N., MCINTOSH, J. K. & KASHANI-SABET, M. 2004. An anti-Wnt-2 monoclonal antibody induces apoptosis in malignant melanoma cells and inhibits tumor growth. *Cancer Research,* 64**,** 5385-5389.

YU, F., YAO, H., ZHU, P., ZHANG, X., PAN, Q., GONG, C., HUANG, Y., HU, X., SU, F. & LIEBERMAN, J. 2007a. let-7 regulates self renewal and tumorigenicity of breast cancer cells. *Cell,* 131**,** 1109-1123.

YU, F., YAO, H., ZHU, P., ZHANG, X., PAN, Q., GONG, C., HUANG, Y., HU, X., SU, F., LIEBERMAN, J. & SONG, E. 2007b. let-7 regulates self renewal and tumorigenicity of breast cancer cells. *Cell,* 131**,** 1109-23.

YU, J., LIU, D., SUN, X., YANG, K., YAO, J., CHENG, C., WANG, C. & ZHENG, J. 2019. CDX2 inhibits the proliferation and tumor formation of colon cancer cells by suppressing Wnt/β-catenin signaling via transactivation of GSK-3β and Axin2 expression. *Cell Death & Disease,* 10**,** 26.

YU, Y., KANWAR, S. S., PATEL, B. B., NAUTIYAL, J., SARKAR, F. H. & MAJUMDAR, A. P. 2009. Elimination of colon cancer stem-like cells by the combination of curcumin and FOLFOX. *Translational oncology,* 2**,** 321-328.

ZEILSTRA, J., JOOSTEN, S. P. J., VERMEULEN, L., KOSTER, J., MEDEMA, J. P., VERSTEEG, R., SPAARGAREN, M. & PALS, S. T. 2013. CD44 expression in intestinal epithelium and colorectal cancer is independent of p53 status. *PloS one,* 8**,** e72849-e72849.

ZHANG, G., ZHANG, S., REN, J., YAO, C., ZHAO, Z., QI, X., ZHANG, X., WANG, S. & LI, L. 2018. Salinomycin may inhibit the cancer stem-like populations with increased chemoradioresistance that nasopharyngeal cancer tumorspheres contain. *Oncology letters,* 16**,** 2495-2500.

ZHOU, B. B., ZHANG, H., DAMELIN, M., GELES, K. G., GRINDLEY, J. C. & DIRKS, P. B. 2009. Tumour-initiating cells: challenges and opportunities for anticancer drug discovery. *Nat Rev Drug Discov,* 8**,** 806-23.

ZHOU, C., QIAN, W., MA, J., CHENG, L., JIANG, Z., YAN, B., LI, J., DUAN, W., SUN, L., CAO, J., WANG, F., WU, E., WU, Z., MA, Q. & LI, X. 2019. Resveratrol enhances the chemotherapeutic response and reverses the stemness induced by gemcitabine in pancreatic cancer cells via targeting SREBP1. *Cell Prolif,* 52**,** e12514.

ZHOU, Q., PENG, C., DU, F., ZHOU, L., SHI, Y., DU, Y., LIU, D., SUN, W., ZHANG, M. & CHEN, G. 2018. Design, synthesis and activity of BBI608 derivatives targeting on stem cells. *European Journal of Medicinal Chemistry,* 151**,** 39-50.

ZHOU, Y., RYCHAHOU, P., WANG, Q., WEISS, H. L. & EVERS, B. M. 2015. TSC2/mTORC1 signaling controls Paneth and goblet cell differentiation in the intestinal epithelium. *Cell death & disease,* 6**,** e1631-e1631.

ZHU, P., ZHU, X., WU, J., HE, L., LU, T., WANG, Y., LIU, B., YE, B., SUN, L., FAN, D., WANG, J., YANG, L., QIN, X., DU, Y., LI, C., HE, L., REN, W., WU, X., TIAN, Y. & FAN, Z. 2019. IL-13 secreted by ILC2s promotes the self-renewal of intestinal stem cells through circular RNA circPan3. *Nature Immunology,* 20**,** 183-194.

ZOLLER, M. 2011. CD44: can a cancer-initiating cell profit from an abundantly expressed molecule? *Nat Rev Cancer,* 11**,** 254-67.

Appendices

Appendix 1

List of compounds in the NCC library.

NCC Compound Name	Compound Formula	Pubchem_ SID
Primaquine diphosphate	$C_{15}H_{21}N_{3O}.2H_3P0_4$	104170105
Chloroxine	$C_9H_5Cl_2NO$	104170003
Dehydrocholic acid	$C_{24}H_{34}O_5$	46386890
Bendrofluazide	$C_{15}H_{14}F_3N_3O_4S_2$	104170162
Triamterene	$C_{12}H_{11}N_7$	104170042
Homoveratrylamine	$C_{10}H_{15}NO_2$	46386943
Dolasetron mesylate	$C_{19}H_{20}N_2O_3.CH_4O_3S$	46386881
Ganciclovir	$C_9H_{13}N_5O_4$	104170145
Sulfacetamide	$C_8H_{10}N_2O_3S$	104170036
Cefoxitin sodium	$C_{16}H_{16}N_3NaO_7S_2$	104170054
Nicotinic acid	$C_6H_5NO_2$	104170022
Sulfinpyrazone	$C_{23}H_{20}N_2O_3S$	104170037
SB 205607 dihydrobromide	$C_{23}H_{28}Br_2N_2O_2$	46387006
Chlorpromazine hydrochloride	$C_{17}H_{20}Cl_2N_2S$	104170050
Chlorpropamide	$C_{10}H_{13}ClN_2O_3S$	104170001
Tolbutamide	$C_{12}H_{18}N_2O_3S$	104170041
Zardaverine	$C_{12}H_{10}F_2N_2O_3$	46386923
6-Azauridine	$C_8H_{11}N_3O_6$	46386950
Lomifylline	$C_{13}H_{18}N_4O_3$	46386754
Benztropine mesylate	$C_{21}H_{25}NO.CH_4O_3S$	104170144
Rufloxacin hydrochloride	$C_{17}H_{19}ClFN_3O_3S$	46386706
Fluocinolone acetonide	$C_{24}H_{30}F_2O_6$	104170060
Torasemide	$C_{16}H_{20}N_4O_3S$	46386585
Secnidazole	$C_7H_{11}N_3O_3$	46386696

Clobenpropit	$C_{14}H_{17}ClN_4S$	46387016
Ormetoprim	$C_{14}H_{18}N_4O_2$	46386708
Levonorgestrel	$C_{21}H_{28}O_2$	46386677
Loxapine succinate	$C_{22}H_{24}ClN_3O_5$	46386931
Dipyridamole	$C_{24}H_{40}N_8O_4$	104169946
Mexiletine hydrochloride	$C_{11}H_{18}ClNO$	104170180
Beclomethasone dipropionate	$C_{28}H_{37}ClO_7$	104170108
Nafcillin sodium	$C_{21}H_{21}N_2NaO_5S$	104170104
Bestatin	$C_{16}H_{24}N_2O_4$	46386830
Tranilast	$C_{18}H_{17}NO_5$	46386750
Chloramphenicol	$C_{11}H_{12}Cl2N_2O_5$	104170151
Azelastine hydrochloride	$C_{22}H_{25}Cl_2N_3O$	46386661
Lofexidine hydrochloride	$C_{11}H_{13}Cl_3N_2O$	46386875
Levosulpiride	$C_{15}H_{23}N_3O_4S$	46386685
Amcinonide	$C_{28}H_{35}FO_7$	104170128
Montelukast sodium	$C_{35}H_{35}ClNNaO_3S$	46386714
Mupirocin	$C_{26}H_{44}O_9$	104170118
Diazepam	$C_{16}H_{13}ClN_2O$	46386554
Stiripentol	$C_{14}H_{18}O_3$	46386912
Bumetanide	$C_{17}H_{20}N_2O_5S$	104170048
Phenothiazine	$C_{12}H_9NS$	46386888
5-Nonyloxytryptamine hydrochloride	$C_{19}H_{31}ClN_2O$	46387012
Prostaglandin E1	$C_{20}H_{34}O_5$	46386879
Benproperine phosphate	$C_{21}H_{27}NO.H_3PO_4$	46386752
Disulfiram	$C_{10}H_{20}N_2S_4$	46386898
Zalcitabine	$C_9H_{13}N_3O_3$	46386814
Methylandrostenediol	$C_{20}H_{32}O_2$	46386580
Diphenhydramine hydrochloride	$C_{17}H_{22}ClNO$	46386874
Carvedilol	$C_{24}H_{26}N_2O_4$	46386749
Trazodone hydrochloride	$C_{19}H_{23}Cl_2N_5O$	46386915

trans-Retinoic acid	$C_{20}H_{28}O_2$	104169979
Ribavirin	$C_8H_{12}N_4O_5$	104170186
Cisapride hydrate	$C_{23}H_{31}ClFN_3O_5$	46386802
Ethambutol	$C_{10}H_{24}N_2O_2$	104170193
Riluzole hydrochloride	$C_8H_6ClF_3N_2OS$	46386847
Glipizide	$C_{21}H_{27}N_5O_4S$	104170062
Trihexyphenidyl hydrochloride	$C_{20}H_{32}ClNO$	104169984
Busulfan	$C_6H_{14}O_6S_2$	104169996
Trimethoprim	$C_{14}H_{18}N_4O_3$	104169981
Flumadine hydrochloride	$C_{12}H_{22}ClN$	104170172
Cytarabine	$C_9H_{13}N_3O_5$	46386862
(-)-Cotinine	$C_{10}H_{12}N_2O$	46386857
Sotalol hydrochloride	$C_{12}H_{21}ClN_2O_3S$	46386705
3,5,3'-Triiodothyronine	$C_{15}H_{12}I_3NO_4$	104169993
Lorazepam	$C_{15}H_{10}Cl_2N_2O_2$	46386878
Goserelin acetate	$C_{59}H_{82}N_{18}O_{14}.C_2H_4O_2$	310263966
Famotidine	$C_8H_{15}N_7O_2S_3$	46386903
Glycopyrronium bromide	$C_{19}H_{28}BrNO_3$	46386646
Mesoridazine besylate	$C_{27}H_{32}N_2O_4S_3$	46386921
Diphenylcyclopropenone	$C_{15}H_{10}O$	46386897
Tramadol hydrochloride	$C_{16}H_{26}ClNO_2$	46386884
Calcitriol	$C_{27}H_{44}O_3$	46386784
Gatifloxacin	$C_{19}H_{22}FN_3O_4$	104170200
Tibolone	$C_{21}H_{28}O_2$	46386825
Metronidazole	$C_6H_9N_3O_3$	46386860
Oligomycin A	$C_{45}H_{74}O_{11}$	310263965
Ebselen	$C_{13}H_9NOSe$	46386980
Taxifolin-(+/-)	$C_{15}H_{12}O_7$	46386773
Naphazoline hydrochloride	$C_{14}H_{15}ClN_2$	104170021
Chlordiazepoxide	$C_{16}H_{14}ClN_3O$	46386831

Lobeline hydrochloride	$C_{22}H_{28}ClNO_2$	46386920
Felbamate	$C_{11}H_{16}N_2O_5$	46386855
Digoxin	$C_{41}H_{64}O_{14}$	104170057
Pinacidil monohydrate	$C_{13}H_{21}N_5O$	46387019
Rutin	$C_{27}H_{30}O_{16}$	46386546
Naftopidil	$C_{24}H_{28}N_2O_3$	46386715
CCPA	$C_{15}H_{22}ClN_5O_5$	46386935
Oxaprozin	$C_{18}H_{15}NO_3$	46386783
Corticosterone	$C_{21}H_{30}O_4$	46386953
CGS 12066B dimaleate	$C_{25}H_{25}F_3N_4O_8$	46386975
Edrophonium chloride	$C_{10}H_{16}ClNO$	104170059
Etoposide	$C_{29}H_{32}O_{13}$	46386954
Letrozole	$C_{17}H_{11}N_5$	46386665
Atracurium besylate	$C_{53}H_{72}N_2O_{12}.2C_6H_5O_3S$	46386822
Repaglinide	$C_{27}H_{36}N_2O_4$	46386564
Clomifene citrate	$C_{32}H_{36}ClNO_8$	104170129
Fluphenazine dihydrochloride	$C_{22}H_{28}Cl_2F_3N_3OS$	46386937
Nimetazepam	$C_{16}H_{13}N_3O_3$	46386768
3-Pyridinemethanol	C_6H_7NO	46386968
Ursodeoxycholic acid	$C_{24}H_{40}O_4$	104169985
Tetracycline	$C_{22}H_{24}N_2O_8$	104170039
Cefixime trihydrate	$C_{16}H_{21}N_5O_{10}S_2$	46386832
RU-486	$C_{29}H_{35}NO_2$	46386955
3'-Deoxydenosine	$C_{10}H_{15}N_5O_4$	46386791
Ibuprofen	$C_{13}H_{18}O_2$	104169956
Estrone 3-sulfate sodium salt	$C_{18}H_{21}NaO_5S$	46386974
Mestranol	$C_{21}H_{26}O_2$	46386940
Zucapsaicin	$C_{18}H_{27}NO_3$	46386797
Zacopride hydrochloride hydrate	$C_{15}H_{23}Cl_2N_3O_3$	46386978
Deferiprone	$C_7H_9NO_2$	46386865

Bicalutamide	$C_{18}H_{14}F_4N_2O_4S$	46386630
Crotamiton	$C_{13}H_{17}NO$	46386684
Aminolevulinic acid	$C_5H_9NO_3$	104170099
Ethynylestradiol	$C_{20}H_{24}O_2$	46386858
Lomerizine dihydrochloride	$C_{27}H_{32}Cl_2F_2N_2O_3$	46386707
Cladribine	$C_{10}H_{12}ClN_5O_3$	46386544
Flumazenil	$C_{15}H_{14}FN_3O_3$	46386776
Nortriptyline hydrochloride	$C_{19}H_{22}ClN$	104170020
Levofloxacin	$C_{18}H_{20}FN_3O_4$	46386771
Docetaxel	$C_{43}H_{53}NO_{14}$	46386672
Mecillinam	$C_{15}H_{23}N_3O_3S$	46386744
Nitrendipine	$C_{18}H_{20}N_2O_6$	46386549
Racecadotril	$C_{21}H_{23}NO_4S$	46386930
Sulfisoxazole	$C_{11}H_{13}N_3O_3S$	104170034
Doxylamine succinate	$C_{21}H_{28}N_2O_5$	46386900
Vincristine sulfate	$C_{46}H_{56}N_4O_{10}.H_2O4_S$	46386588
Doxapram hydrochloride	$C_{24}H_{31}ClN_2O_2$	46386821
Piroxicam	$C_{15}H_{15}N_3O_5S$	46386918
Azithromycin	$C_{38}H_{72}N_2O_{12}$	104170210
Halometasone monohydrate	$C_{22}H_{27}ClF_2O_5$	46386633
Tizanidine hydrochloride	$C_9H_9Cl_2N_5S$	104170152
Medrysone	$C_{22}H_{32}O_3$	104170097
Ethacrynic acid	$C_{13}H_{12}Cl_2O_4$	104169948
Verapamil hydrochloride	$C_{27}H_{41}ClN_2O_5$	46386795
Idebenone	$C_{19}H_{30}O_5$	46386682
Anastrozole	$C_{17}H_{19}N_5$	46386543
Methazolamide	$C_5H_8N_4O_3S_2$	104170116
Prednisolone	$C_{21}H_{28}O_5$	104169971
Prednisone	$C_{21}H_{26}O_5$	104169973
L-Thyroxine	$C_{15}H_{11}I_4NO_4$	104169983

Mevastatin	$C_{23}H_{34}O_5$	46386660
Fluvastatin	$C_{24}H_{26}FNO_4$	104170157
Zonisamide	$C_8H_8N_2O_3S$	104170135
Ipratropium bromide	$C_{20}H_{30}BrNO_3$	104170067
Carbidopa	$C_{10}H_{16}N_2O_5$	104170225
Azathioprine	$C_9H_7N_7O_2S$	104170112
Methylprednisolone	$C_{22}H_{30}O_5$	104170189
Raloxifene hydrochloride	$C_{28}H_{28}ClNO_4S$	104170163
Medroxyprogesterone 17-acetate	$C_{24}H_{34}O_4$	104170072
Ethionamide	$C_8H_{10}N_2S$	104170006
Cyproheptadine hydrochloride	$C_{21}H_{22}ClN$	46386957
Thiabendazole	$C_{10}H_7N_3S$	104170091
Methylprednisolone acetate	$C_{24}H_{32}O_6$	104170126
Miglitol	$C_8H_{17}NO_5$	46386758
Prilocaine hydrochloride	$C_{13}H_{21}ClN_2O$	104169972
Minocycline hydrochloride	$C_{23}H_{28}ClN_3O_7$	104169958
Enrofloxacin	$C_{19}H_{22}FN_3O_3$	46386889
Dilantin	$C_{15}H_{11}N_2NaO_2$	104170140
Propranolol hydrochloride	$C_{16}H_{22}ClNO_2$	104170185
Nitazoxanide	$C_{12}H_9N_3O_5S$	46386689
Acarbose	$C_{25}H_{43}NO_{18}$	46386746
Chlorambucil	$C_{14}H_{19}Cl_2NO_2$	104170053
Nicotinamide	$C_6H_6N_2O$	46386893
Oxiconazole nitrate	$C_{18}H_{14}Cl_4N_4O_4$	46386704
Isoproterenol hydrochloride	$C_{11}H_{18}ClNO_3$	104170013
Carbamazepine	$C_{15}H_{12}N_2O$	104170177
Ketoprofen	$C_{16}H_{14}O_3$	104169957
Clomipramine hydrochloride	$C_{19}H_{24}Cl_2N_2$	104170176
Buspirone hydrochloride	$C_{21}H_{32}ClN_5O_2$	104170171
Tamoxifen	$C_{26}H_{29}NO$	104170047

Doxepin hydrochloride	$C_{19}H_{22}ClNO$	104169945
Rifabutin	$C_{46}H_{62}N_4O_{11}$	104170218
Dapsone	$C_{12}H_{12}N_2O_2S$	104169986
Enalapril maleate	$C_{24}H_{32}N_2O_9$	104170123
Dantrolene sodium	$C_{14}H_9N_4NaO_5$	104170142
Piperacillin sodium	$C_{23}H_{26}N_5NaO_7S$	104169975
Naloxone hydrochloride	$C_{19}H_{22}ClNO_4$	104170085
Cyclophosphamide hydrate	$C_7H_{17}Cl_2N_2O_3P$	104170160
Bethanechol chloride	$C_7H_{17}ClN_2O_2$	104170158
Quinidine	$C_{20}H_{24}N_2O_2$	104169976
Atropine	$C_{17}H_{23}NO_3$	104169991
Eszopiclone	$C_{17}H_{17}ClN_6O_3$	104170161
Terbutaline sulfate	$C_{12}H_{19}NO_3.H_2O_4S$	104170117
Metyrapone	$C_{14}H_{14}N_2O$	104169960
Daunorubicin hydrochloride	$C_{27}H_{29}NO_{10}.HCl$	104170197
Penicillin V	$C_{16}H_{18}N_2O_5S$	104170199
Fluorometholone	$C_{22}H_{29}FO_4$	104170223
Rifapentine	$C_{47}H_{64}N_4O_{12}$	104170198
Hexachlorophene	$C_{13}H_6Cl_6O_2$	104170010
Thiothixene	$C_{23}H_{29}N_3O_2S_2$	104170208
Ofloxacin	$C_{18}H_{20}FN_3O_4$	104169964
Doxazosin	$C_{23}H_{25}N_5O_5$	104170183
Pindolol	$C_{14}H_{20}N_2O_2$	104169965
Meloxicam	$C_{14}H_{13}N_3O_4S_2$	104170196
Oxacillin sodium	$C_{19}H_{18}N_3NaO_5S$	104170106
Cetirizine	$C_{21}H_{25}ClN_2O_3$	104170194
Probenecid	$C_{13}H_{19}NO_4S$	104170028
Aminoglutethimide	$C_{13}H_{16}N_2O_2$	104170212
Promethazine hydrochloride	$C_{17}H_{21}ClN_2S$	104169969
Nadolol	$C_{17}H_{27}NO_4$	104169962

Hydroxyzine pamoate	$C_{44}H_{42}ClN_2O_8$	104170009
Acitretin	$C_{21}H_{26}O_3$	104170221
Fexofenadine hydrochloride	$C_{32}H_{40}ClNO_4$	104170222
Minoxidil	$C_9H_{15}N_5O$	104170184
Fluoxetine hydrochloride	$C_{17}H_{19}ClF_3NO$	104170213
Acyclovir	$C_8H_{11}N_5O_3$	104170215
Felodipine	$C_{18}H_{19}Cl_2NO_4$	104170219
Cortisol 21-acetate	$C_{23}H_{32}O_6$	104169955
Hydrochlorothiazide	$C_7H_8ClN_3O_4S_2$	104170008
Orphenadrine hydrochloride	$C_{18}H_{24}ClNO$	104169963
Lovastatin	$C_{24}H_{36}O_5$	104170211
Priscoline hydrochloride	$C_{10}H_{13}ClN_2$	104170110
Mafenide acetate	$C_9H_{14}N_2O_4S$	104170207
Folic acid	$C_{19}H_{19}N_7O_6$	104169953
Furosemide	$C_{12}H_{11}ClN_2O_5S$	104169951
Methocarbamol	$C_{11}H_{15}NO_5$	104170007
Hydrocortisone	$C_{21}H_{30}O_5$	104169954
Oxybutynin hydrochloride	$C_{22}H_{32}ClNO_3$	104170078
19-Norethindrone acetate	$C_{22}H_{28}O_3$	104170073
Midodrine hydrochloride	$C_{12}H_{19}ClN_2O_4$	104170071
Clopidogrel	$C_{16}H_{16}ClNO_2S$	104170201
Valproic acid	$C_8H_{16}O_2$	104170082
Phenoxybenzamine hydrochloride	$C_{18}H_{23}Cl_2NO$	104170096
Diflunisal	$C_{13}H_8F_2O_3$	104170004
Altretamine	$C_9H_{18}N_6$	104170093
Nabumetone	$C_{15}H_{16}O_2$	104170077
Penicillin G potassium	$C_{16}H_{17}KN_2O_4S$	104170081
Labetalol hydrochloride	$C_{19}H_{25}ClN_2O_3$	104170069
Tropicamide	$C_{17}H_{20}N_2O_2$	104170087
Triamcinolone acetonide	$C_{24}H_{31}FO_6$	104170089

Eryped	$C_{43}H_{75}NO_{16}$	104170095
Pyridostigmine bromide	$C_9H_{13}BrN_2O_2$	104170079
Nicardipine hydrochloride	$C_{26}H_{29}N_3O_6.HCl$	104170076
Loperamide hydrochloride	$C_{29}H_{34}Cl_2N_2O_2$	104170070
Fludarabine	$C_{10}H_{12}FN_5O_4$	104170131
Dexamethasone	$C_{22}H_{29}FO_5$	104170143
Epigallocatechin gallate	$C_{22}H_{18}O_{11}$	46386901
Pemolide	$C_9H_8N_2O_2$	46386687
4-Phenylbutyric acid	$C_{10}H_{12}O_2$	104169967
Telmisartan	$C_{33}H_{30}N_4O_2$	46386620
Pentoxifylline	$C_{13}H_{18}N_4O_3$	46386861
Bisoprolol fumarate	$C_{22}H_{35}NO_8$	46386635
Moclobemide	$C_{13}H_{17}ClN_2O_2$	46386631
Sumatriptan succinate	$C_{18}H_{27}N_3O_6S$	46386597
Quetiapine fumarate	$C_{25}H_{29}N_3O_6S$	46386812
CGS 15943	$C_{13}H_8ClN_5O$	46386800
Tripelennamine hydrochloride	$C_{16}H_{22}ClN_3$	46386917
D-Cycloserine	$C_3H_6N_2O_2$	46386864
Tacrolimus	$C_{44}H_{69}NO_{12}$	46386734
Didanosine	$C_{10}H_{12}N_4O_3$	46386730
MK 886	$C_{27}H_{34}ClNO_2S$	46386984
Linopirdine dihydrochloride	$C_{26}H_{25}Cl_2N_3O_2$	46386985
Clotrimazole	$C_{22}H_{17}ClN_2$	46386926
Flecainide hydrochloride	$C_{17}H_{20}F_6N_2O_3.HCl$	310263964
Rimcazole dihydrochloride	$C_{21}H_{31}Cl_2N_3O$	46387003
Spectinomycin	$C_{14}H_{24}N_2O_7.5H_2O._2HCl$	104170086
Hexamethylenebisacetamide	$C_{10}H_{20}N_2O_2$	46386869
Pirenperone	$C_{23}H_{24}FN_3O_2$	46386967
Cerivastatin sodium	$C_{26}H_{33}FNNaO_5$	46386572
Argatroban	$C_{23}H_{36}N_6O_5S$	46386718

PD 81723	$C_{14}H_{12}F_3NOS$	46386976
Indomethacin hydrate	$C_{19}H_{18}ClNO_5$	46386809
Prochlorperazine maleate	$C_{28}H_{32}ClN_3O_8S$	46386924
Lidocaine	$C_{14}H_{22}N_2O$	46386868
Balsalazide	$C_{17}H_{15}N_3O_6$	46386828
Actarit	$C_{10}H_{11}NO_3$	46386663
Cilastatin sodium	$C_{16}H_{25}N_2NaO_5S$	46386570
Clarithromycin	$C_{38}H_{69}NO_{13}$	46386761
Phenelzine sulfate	$C_8H_{12}N_2.H_2O_4S$	46386907
6-Aminoindazole	$C_7H_7N_3$	46386887
19-Nortestosterone	$C_{18}H_{26}O_2$	46386764
Methylperone hydrochloride	$C_{16}H_{23}ClFNO$	46387011
Pidotimod	$C_9H_{12}N_2O_4S$	46386775
Aripiprazole	$C_{23}H_{27}Cl_2N_3O_2$	46386763
Alprazolam	$C_{17}H_{13}ClN_4$	46386679
Medroxyprogesterone	$C_{22}H_{32}O_3$	46387018
(+/-)-Vesamicol hydrochloride	$C_{17}H_{26}ClNO$	46386799
Pergolide mesylate	$C_{19}H_{26}N_2S.CH_4O_3S$	46386979
Diazoxide	$C_8H_7ClN_2O_2S$	46386946
E-4031 dihydrochloride	$C_{21}H_{29}Cl_2N_3O_3S$	46387000
Midazolam hydrochloride	$C_{18}H_{14}Cl_2FN_3$	46386603
Raltitrexed	$C_{21}H_{22}N_4O_6S$	46386823
Azasetron hydrochloride	$C_{17}H_{21}Cl_2N_3O_3$	46386991
Exemestane	$C_{20}H_{24}O_2$	46386592
Nifedipine	$C_{17}H_{18}N_2O_6$	46386790
Proxymetacaine	$C_{16}H_{27}ClN_2O_3$	104170084
Benactyzine hydrochloride	$C_{20}H_{26}ClNO_3$	46386942
Altanserin hydrochloride	$C_{22}H_{22}FN_3O_2S.1H2O.HCl$	46386989
Tryptoline	$C_{11}H_{12}N_2$	46386936

Omeprazole	$C_{17}H_{19}N_3O_3S$	46386973
Procyclidine hydrochloride	$C_{19}H_{30}ClNO$	104170083
Clofazimine	$C_{27}H_{22}Cl_2N_4$	46386952
Tegafur	$C_8H_9FN_2O_3$	46386579
Desoximetasone	$C_{22}H_{29}FO_4$	46386959
Stanozolol	$C_{21}H_{32}N_2O$	46386608
Diphenoxylate hydrochloride	$C_{30}H_{33}ClN_2O_2$	46386550
Itraconazole	$C_{35}H_{38}Cl_2N_8O_4$	46386736
Olanzapine	$C_{17}H_{20}N_4S$	46386668
Tolazamide	$C_{14}H_{21}N_3O_3S$	104170088
Ifenprodil hemitartrate	$C_{21}H_{27}NO_2.0.5H_2O.0.5$ $C_4H_6O_6$	46386807
Dichloroacetic acid	$C_2H_2Cl_2O_2$	46386944
Megestrol acetate	$C_{24}H_{32}O_4$	46386702
Lacidipine	$C_{26}H_{33}NO_6$	46386664
GR 89696 fumarate	$C_{23}H_{29}Cl_2N_3O_7$	46386996
Vindesine sulfate	$C_{43}H_{55}N_5O_7.H_2O_4S$	46386586
Tremulacin	$C_{27}H_{28}O_{11}$	46386886
Amlodipine	$C_{20}H_{25}ClN_2O_5$	46386686
Nevirapine	$C_{15}H_{14}N_4O$	46386569
Rolipram	$C_{16}H_{21}NO_3$	46386779
Pramipexole	$C_{10}H_{17}N_3S$	46386856
S(-)-Timolol maleate	$C_{17}H_{28}N_4O_7S$	104170090
Propafenone	$C_{21}H_{27}NO_3$	104170080
Parecoxib sodium	$C_{19}H_{17}N_2NaO_4S$	46386785
Saquinavir mesylate	$C_{38}H_{50}N_6O_5.CH_4O_3S$	46386596
Isradipine	$C_{19}H_{21}N_3O_5$	46386602
Amlexanox	$C_{16}H_{14}N_2O_4$	46386726
Pralidoxime chloride	$C_7H_9ClN_2O$	104170029
Indapamide	$C_{16}H_{16}ClN_3O_3S$	104170066

Mesalamine	$C_7H_7NO_3$	46386870
Etodolac	$C_{17}H_{21}NO_3$	104170216
Fluocinolone acetonide 21-acetate	$C_{26}H_{32}F_2O_7$	104170119
Chlorzoxazone	$C_7H_4ClNO_2$	104169997
Cefuroxime	$C_{16}H_{16}N_4O_8S$	104170159
Oxytetracycline hydrochloride	$C_{22}H_{25}ClN_2O_9$	104170024
Toremifene citrate	$C_{32}H_{36}ClNO_8$	46386786
Griseofulvin	$C_{17}H_{17}ClO_6$	104170114
Cefotaxime sodium	$C_{16}H_{16}N_5NaO_7S_2$	104170202
Cromolyn sodium	$C_{23}H_{14}O_{11}.2Na+$	104170109
Primidone	$C_{12}H_{14}N_2O_2$	104170030
Naltrexone hydrochloride	$C_{20}H_{24}ClNO_4$	104170191
Desipramine hydrochloride	$C_{18}H_{23}ClN_2$	104170179
Floxuridine	$C_9H_{11}FN_2O_5$	104170121
Zidovudine	$C_{10}H_{13}N_5O_4$	104170164
N-Methylparoxetine	$C_{20}H_{22}FNO_3$	46386650
Erythromycin	$C_{37}H_{67}NO_{13}$	310263951
N-Fmoc-D-leucine	$C_{21}H_{23}NO_4$	46386836
L-Carnitine inner salt	$C_7H_{15}NO_3$	310263880
Dexamethasone sodium phosphate	$C_{22}H_{28}FO_8P.2Na+$	310263943
Cilostazol	$C_{20}H_{27}N_5O_2$	46386994
Natamycin	$C_{33}H_{47}NO_{13}$	46386740
Ziprasidone	$C_{21}H_{21}ClN_4OS$	46386625
Gemcitabine hydrochloride	$C_9H_{12}ClF_2N_3O_4$	46386568
Doxycycline	$C_{22}H_{24}N_2O_8$	104170107
Pyrazinamide	$C_5H_5N_3O$	104170032
Dopamine hydrochloride	$C_8H_{12}ClNO_2$	104170043
5-Azacytidine	$C_8H_{12}N_4O_5$	104170170
Propofol	$C_{12}H_{18}O$	104169947
Amoxicillin	$C_{16}H_{19}N_3O_5S$	104170168

5-Fluorouracil	$C_4H_3FN_2O_2$	104169952
Ampicillin sodium	$C_{16}H_{18}N_3NaO_4S$	104170166
DL-Penicillamine	$C_5H_{11}NO_2S$	104169974
Phylloquinone	$C_{31}H_{46}O_2$	104170094
Nicotine	$C_{10}H_{14}N_2$	104170075
Mesna	$C_2H_5NaO_3S_2$	104170146
Captopril	$C_9H_{15}NO_3S$	104170052
Demeclocycline	$C_{21}H_{21}ClN_2O_8$	104170101
Quinacrine hydrochloride hydrate	$C_{23}H_{30}ClN_3O.2H_2O.2HCl$	46386910
Zanamivir hydrate	$C_{12}H_{20}N_4O_7.H_2O$	46386819
alpha-Methyl-L-tyrosine	$C_{10}H_{13}NO_3$	46386969
Olmesartan medoxomil	$C_{29}H_{30}N_6O_6$	46386651
Fenpiverinium bromide	$C_{22}H_{29}BrN_2O$	46386658
Amisulpride	$C_{17}H_{27}N_3O_4S$	46386656
Ketorolac tromethamine	$C_{19}H_{24}N_2O_6$	46386614
Ethylestrenol	$C_{20}H_{32}O$	46386573
5-Methoxytryptamine	$C_{11}H_{14}N_2O$	46387021
Tadalafil	$C_{22}H_{19}N_3O_4$	46386604
Citalopram hydrobromide	$C_{20}H_{22}BrFN_2O$	46386617
Nimodipine	$C_{21}H_{26}N_2O_7$	46386964
Topiramate	$C_{12}H_{21}NO_8S$	46386619
Artesunate	$C_{19}H_{28}O_8$	46386645
Isoquercitrin	$C_{21}H_{20}O_{12}$	46386780
Rizatriptan benzoate	$C_{22}H_{25}N_5O_2$	46386632
Levetiracetam	$C_8H_{14}N_2O_2$	46386557
Flurbiprofen	$C_{15}H_{13}FO_2$	46386788
Xanthinol nicotinate	$C_{19}H_{26}N_6O_6$	46387024
Finasteride	$C_{23}H_{36}N_2O_2$	46386559
Pantoprazole sodium	$C_{16}H_{14}F_2N_3NaO_4S$	46386609

Oxcarbazepine	$C_{15}H_{12}N_2O_2$	46386767
Icariin	$C_{33}H_{40}O_{15}$	46386578
Zeranol	$C_{18}H_{26}O_5$	46386627
Tiagabine hydrochloride	$C_{20}H_{26}ClNO_2S_2$	46386642
Zafirlukast	$C_{31}H_{33}N_3O_6S$	46386595
Ezetimibe	$C_{24}H_{21}F_2NO_3$	46386640
Pterostilbene	$C_{16}H_{16}O_3$	46386623
Ramipril	$C_{23}H_{32}N_2O_5$	46386770
Risperidone	$C_{23}H_{27}FN4O_2$	46386613
Temozolomide	$C_6H_6N_6O_2$	46386653
Alfuzosin	$C_{19}H_{27}N_5O_4$	46386655
Latanoprost	$C_{26}H_{40}O_5$	46386728
Zaleplon	$C_{17}H_{15}N_5O$	46386657
Benzbromarone	$C_{17}H_{12}Br_2O_3$	46386951
Olopatadine hydrochloride	$C_{21}H_{24}ClNO_3$	46386826
Triclabendazole	$C_{14}H_9Cl_3N_2OS$	46386738
Desloratadine	$C_{19}H_{19}ClN_2$	46386563
Rofecoxib	$C_{17}H_{14}O_4S$	46386634
Linezolid	$C_{16}H_{20}FN_3O_4$	46386641
Lamotrigine	$C_9H_7Cl_2N_5$	46386680
Diclofenac sodium	$C_{14}H_{10}Cl_2NNaO_2$	46386927
Bupropion hydrochloride	$C_{13}H_{19}Cl_2NO$	46386703
Rifaximin	$C_{43}H_{51}N_3O_{11}$	46386615
Dofetilide	$C_{19}H_{27}N_3O_5S_2$	46386638
Famciclovir	$C_{14}H_{19}N_5O_4$	46386745
Cefaclor	$C_{15}H_{14}ClN_3O_4S$	46386958
Brucine	$C_{23}H_{26}N_2O_4$	46386939
Cefpodoxime proxetil	$C_{21}H_{27}N_5O_9S_2$	46386731
Irsogladine maleate	$C_{13}H_{11}Cl_2N_5O_4$	46386698
L-694,247	$C_{20}H_{25}N_5O_5S$	46386999

Amiodarone hydrochloride	$C_{25}H_{30}ClI_2NO_3$	46386662
Tocainide	$C_{11}H_{16}N_2O$	46386772
Cefdinir	$C_{14}H_{13}N_5O_5S_2$	46386833
Sibutramine	$C_{17}H_{26}ClN$	46387014
Ornidazole	$C_7H_{10}ClN_3O_3$	46386947
Nizatidine	$C_{12}H_{21}N_5O_2S_2$	46386765
Pazufloxacin	$C_{16}H_{15}FN_2O_4$	46386755
Voriconazole	$C_{16}H_{14}F_3N_5O$	46386721
Methyltestosterone	$C_{20}H_{30}O_2$	46386739
Benazepril hydrochloride	$C_{24}H_{29}ClN_2O_5$	46386692
Honokiol	$C_{18}H_{18}O_2$	46386673
Topotecan hydrochloride	$C_{23}H_{24}ClN_3O_5$	46386667
Beclomethasone	$C_{22}H_{29}ClO_5$	46386972
Palonosetron hydrochloride	$C_{19}H_{25}ClN_2O$	46386820
Nialamide	$C_{16}H_{18}N_4O_2$	46386894
Vecuronium bromide	$C_{34}H_{57}BrN_2O_4$	46386876
Nobiletin	$C_{21}H_{22}O_8$	46386719
Pravastatin sodium	$C_{23}H_{35}NaO_7$	46386713
Maltol	$C_6H_6O_3$	46386945
Salmeterol	$C_{25}H_{37}NO_4$	46387005
Naproxen sodium	$C_{14}H_{13}NaO_3$	46386948
Mepirizole	$C_{11}H_{14}N_4O_2$	46386965
Idarubicin hydrochloride	$C_{26}H_{28}ClNO_9$	46386733
Irbesartan	$C_{25}H_{28}N_6O$	46386566
SDM25N hydrochloride	$C_{26}H_{29}ClN_2O_4$	46387008
Levocetirizine	$C_{21}H_{25}ClN_2O_3$	46386593
Valdecoxib	$C_{16}H_{14}N_2O_3S$	46386621
Etomoxir	$C_{17}H_{23}ClO_4$	46386895
Etomidate	$C_{14}H_{16}N_2O_2$	46386983
Chlorthalidone	$C_{14}H_{11}ClN_2O_4S$	104170188

Lincomycin hydrochloride	$C_{18}H_{35}ClN_2O_6S$	104170115
Propantheline bromide	$C_{23}H_{30}BrNO_3$	104170027
Tetrahydrozoline hydrochloride	$C_{13}H_{17}ClN_2$	104169982
Symmetrel	$C_{10}H_{18}ClN$	104169987
Quinapril hydrochloride	$C_{25}H_{31}ClN_2O_5$	104170220
Miconazole nitrate	$C_{18}H_{15}Cl_4N_3O_4$	104169959
Sulfasalazine	$C_{18}H_{14}N_4O_5S$	46386548
Stavudine	$C_{10}H_{12}N_2O_4$	104170182
Ipriflavone	$C_{18}H_{16}O_3$	46386694
Allopurinol	$C_5H_4N_4O$	104169990
Acetazolamide	$C_4H_6N_4O_3S_2$	104169989
Perphenazine	$C_{21}H_{26}ClN_3OS$	104169970
Sulfamethoxazole	$C_{10}H_{11}N_3O3S$	104170035
Mercaptopurine	$C_5H_4N_4S$	104170111
Propylthiouracil	$C_7H_{10}N_2OS$	104170031
(+/-)-Norepinephrine hydrochloride	$C_8H_{12}ClNO_3$	104170127
Norfloxacin	$C_{16}H_{18}FN_3O_3$	104169961
Ondansetron	$C_{18}H_{19}N_3O$	104170204
Kitasamycin	$C_{42}H_{69}NO_{15}$	46386711
Duvadilan	$C_{18}H_{24}ClNO_3$	104170012
Econazole nitrate	$C_{18}H_{16}Cl_3N_3O_4$	104170005
Ru 24969 hemisuccinate	$C_{18}H_{22}N_2O_5$	46387004
Nateglinide	$C_{19}H_{27}NO_3$	46386701
Isoniazid	$C_6H_7N_3O$	104170011
Zileuton	$C_{11}H_{12}N_2O_2S$	46386751
Pyrimethamine	$C_{12}H_{13}ClN_4$	104170026
Flucytosine	$C_4H_4FN_3O$	46386766
Podofilox	$C_{22}H_{22}O_8$	104170173
Amitriptyline hydrochloride	$C_{20}H_{24}ClN$	104169995
Dicloxacillin sodium	$C_{19}H_{16}Cl_2N_3NaO_5S$	104170195

Thioridazine hydrochloride	$C_{21}H_{27}ClN_2S_2$	104170092
Albendazole	$C_{12}H_{15}N_3O_2S$	104170113
Mepivacaine hydrochloride	$C_{15}H_{23}ClN_2O$	46386949
Hydroflumethiazide	$C_8H_8F_3N_3O_4S_2$	104169994
Phentolamine mono-hydrochloride	$C_{17}H_{19}N_3O$	104170130
Procaine hydrochloride	$C_{13}H_{21}ClN_2O_2$	104170025
19-Norethindrone	$C_{20}H_{26}O_2$	104170074
Simvastatin	$C_{25}H_{38}O_5$	104170217
Terazosin	$C1_9H_{25}N_5O_4$	104170187
Acebutolol hydrochloride	$C_{18}H_{29}ClN_2O_4$	104170167
Acetylcholine chloride	$C_7H_{16}ClNO_2$	104170141
Clozapine	$C_{18}H_{19}ClN_4$	104170165
Imipramine hydrochloride	$C_{19}H_{25}ClN_2$	104170068
Fenofibrate	$C_{20}H_{21}ClO_4$	104169950
Carisoprodol	$C_{12}H_{24}N_2O_4$	104170000
Racepinephrine	$C_9H_{13}NO_3$	104170169
Methoxsalen	$C_{12}H_8O_4$	104170150
Praziquantel	$C_{19}H_{24}N_2O_2$	104169966
Warfarin sodium	$C_{19}H_{15}NaO_4$	104169988
Homoharringtonine	$C_{29}H_{39}NO_9$	46386877
Triclosan	$C_{12}H_7Cl_3O_2$	104170014
Ranitidine hydrochloride	$C_{13}H_{23}ClN_4O_3S$	104169977
Cimetidine	$C_{10}H_{16}N_6S$	104169999
LY 171883	$C_{16}H_{22}N_4O_3$	46386838
Meclofenamic acid sodium salt	$C_{14}H_{10}Cl_2NNaO_2$	104170147
Metoclopramide hydrochloride	$C_{14}H_{23}Cl_2N_3O_2$	104170017
Gemfibrozil	$C_{15}H_{22}O_3$	104170063
SR 57227A	$C_{10}H_{15}Cl_2N_3$	46386849
Memantine hydrochloride	$C_{12}H_{22}ClN$	104170178
Mefenamic acid	$C_{15}H_{15}NO_2$	104170015

Rifampicin	$C_{43}H_{58}N_4O_{12}$	104169978
Mepenzolate bromide	$C_{21}H_{26}BrNO_3$	104170016
Thalidomide	$C_{13}H_{10}N_2O_4$	104170098
Dicyclomine hydrochloride	$C_{19}H_{36}ClNO_2$	104170002
(+)-cis-Diltiazem hydrochloride	$C_{22}H_{27}ClN_2O_4S$	104170056
Flutamide	$C_{11}H_{11}F_3N_2O_3$	104169949
Vidarabine	$C_{10}H_{13}N_5O_4$	104170045
Disopyramide phosphate	$C_{21}H_{29}N_{3O}.H_3PO_4$	104170181
Amoxapine	$C_{17}H_{16}ClN_3O$	104170044
Methyldopa	$C_{10}H_{13}NO_4$	104170018
Fluconazole	$C_{13}H_{12}F_2N_6O$	104170148
Mefloquine hydrochloride	$C_{17}H_{17}ClF_6N_2O$	104170120
Brimonidine	$C_{11}H_{10}BrN_5$	104170136
Sulindac	$C_{20}H_{17}FO_3S$	104170038
Theophylline	$C_7H_8N_4O_2$	104170040
Zolpidem tartrate	$C_{19}H_{21}N_3O.0.5C_4H_6O_6$	46386567
Zolmitriptan	$C_{16}H_{21}N_3O_2$	46386880
Estradiol valerate	$C_{23}H_{32}O_3$	104170058
Spironolactone	$C_{24}H_{32}O_4S$	104169980
Hydrocortisone hemisuccinate	$C_{25}H_{34}O_8$	104170065
Hydrocortisone 17-valerate	$C_{26}H_{38}O_6$	104170102
Nitrazepam	$C_{15}H_{11}N_3O_3$	46386691
Nitrofurantoin	$C_8H_6N_4O_5$	104170019
Chlorothiazide	$C_7H_6ClN_3O_4S_2$	104169998
Carbinoxamine maleate	$C_{20}H_{23}ClN_2O_5$	104170100
Cortisone acetate	$C_{23}H_{30}O_6$	104170175
Mebendazole	$C_{16}H_{13}N_3O_3$	104170137
Molindone hydrochloride	$C_{16}H_{25}ClN_2O_2$	104170156
Atenolol	$C_{14}H_{22}N_2O_3$	104170046
Flubendazole	$C_{16}H_{12}FN_3O_3$	46386742

Oxymetholone	$C_{21}H_{32}O_3$	46386778
Cefazolin sodium	$C_{14}H_{13}N_8NaO_4S_3$	104170051
Methimazole	$C_4H_6N_2S$	104170134
Danazol	$C_{22}H_{27}NO_2$	104170055
Nalidixic acid	$C_{12}H_{12}N_2O_3$	104169992
Prednisolone acetate	$C_{23}H_{30}O_6$	104169968
Meclizine hydrochloride	$C_{25}H_{29}Cl_3N_2$	104170138
Mitoxantrone hydrochloride	$C_{22}H_{29}ClN_4O_6$	104170122
Clobetasol propionate	$C_{25}H_{32}ClFO_5$	104170049
Isotretinoin	$C_{20}H_{28}O_2$	104170133
Prednisolone sodium succinate	$C_{25}H_{31}NaO_8$	46386971
Testosterone	$C_{19}H_{28}O_2$	46501387
Glyburide	$C_{23}H_{28}ClN_3O_5S$	104170064
Metaproterenol	$C_{11}H_{17}NO_3$	104170149
Procainamide hydrochloride	$C_{13}H_{22}ClN_3O$	104170033
Secoisolariciresinol	$C_{20}H_{26}O_6$	46386735
Resveratrol	$C_{14}H_{12}O_3$	46386962
Troxipide	$C_{15}H_{22}N_2O_4$	46386769
Cortisone	$C_{21}H_{28}O_5$	46386956
11-Deoxycortisol	$C_{21}H_{30}O_4$	46386963
Taxifolin-(+)	$C_{15}H_{12}O_7$	46386813
Dehydroepiandrosterone	$C_{19}H_{28}O_2$	46387028
Benzylimidazole	$C_{10}H_{10}N_2$	46386891
MDL 73005EF hydrochloride	$C_{20}H_{28}Br_2N_2O_4$	46387017
GR 79236	$C_{15}H_{24}ClN_5O_6$	46387015
Dactinomycin	$C_{62}H_{86}N_{12}O_{16}$	46386883
Methotrexate trihydrate	$C_{20}H_{28}N_8O_8$	46386835
Piceid	$C_{20}H_{22}O_8$	46386700
Budesonide	$C_{25}H_{34}O_6$	104170124
Raclopride	$C_{15}H2_0Cl_2N_2O_3$	46386981

Modafinil	$C_{15}H_{15}NO_2S$	46386605
HTMT dimaleate	$C_{27}H_{33}F_3N_4O_9$	46386998
Mestanolone	$C_{20}H_{32}O_2$	46386759
Oxyphenonium bromide	$C_{21}H_{34}BrNO_3$	46386961
Pilocarpine hydrochloride	$C_{11}H_{17}ClN_2O_2$	46386789
Tinidazole	$C_8H_{13}N_3O_4S$	46387025
Dihydrexidine hydrochloride	$C_{17}H_{17}NO_2.1H_2O.HCl$	46386992
AM-251	$C_{22}H_{21}Cl_2IN_4O$	46386990
Milrinone	$C_{12}H_9N_3O$	46386629
Valsartan	$C_{24}H_{29}N_5O_3$	46386599
2-Pyridylethylamine	$C_7H_{10}N_2$	46386941
Triptolide	$C_{20}H_{24}O_6$	46386571
Mirtazapine	$C_{17}H_{19}N_3$	46386716
P1075	$C_{12}H_{17}N_5$	46386997
Dextrorphan D-tartrate	$C_{17}H_{23}NO.C_4H_6O_6$	46386873
Gabexate mesilate	$C_{16}H_{23}N_3O_4.CH_4O_3S$	46386710
Dextromethorphan hydrobromide, monohydrate	$C_{18}H_{28}BrNO_2$	46386932
Tosufloxacin tosilate	$C_{26}H_{23}F_3N_4O_6S$	46386743
Ritonavir	$C_{37}H_{48}N_6O_5S_2$	46386817
Galanthamine hydrobromide	$C_{17}H_{22}BrNO_3$	46386805
Tegaserod maleate	$C_{20}H_{27}N_5O_5$	46386624
Procysteine	$C_4H_5NO_3S$	46386866
Nicorandil	$C_8H_9N_3O_4$	46386683
Pioglitazone hydrochloride	$C_{19}H_{21}ClN_2O_3S$	46386618
Nefazodone hydrochloride	$C_{25}H_{33}Cl_2N_5O_2$	46386669
Loxoprofen sodium	$C_{15}H_{17}NaO_3$	46386612
Penciclovir	$C_{10}H_{15}N_5O_3$	46386598
7-Nitroindazole	$C_7H_5N_3O_2$	46387020
Glimepiride	$C_{24}H_{34}N_4O_5S$	46386690

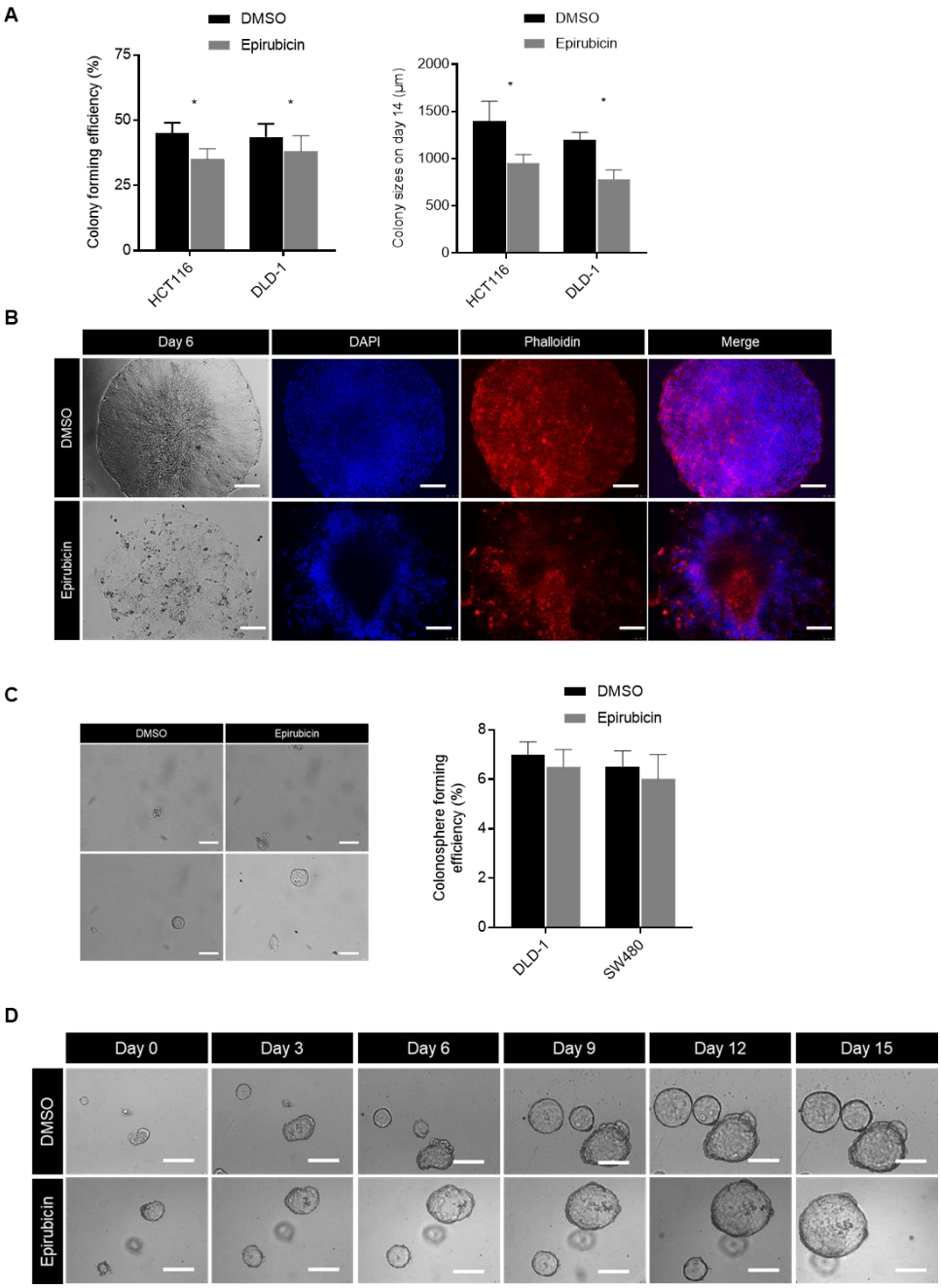
Carmofur	$C_{11}H_{16}FN_3O_3$	46386675
Phenprobamate	$C_{10}H_{13}NO_2$	46386753
Vinorelbine tartrate	$C_{45}H_{54}N_4O_8.2C_4H_6O_6$	46386815
Ampiroxicam	$C_{20}H_{21}N_3O_7S$	46386688
Remacemide hydrochloride	$C_{17}H_{21}ClN_2O$	46386987
Betaxolol hydrochloride	$C_{18}H_{30}ClNO_3$	46386993
Artemether	$C_{16}H_{26}O_5$	46386824
Synephrine	$C_9H_{13}NO_2$	46386970
R(+)-SCH-23390 hydrochloride	$C_{17}H_{19}Cl_2NO$	46387007
Nalbuphine hydrochloride	$C_{21}H_{28}ClNO_4$	46386933
Cephalexin hydrate	$C_{16}H_{19}N_3O_5S$	46386774
Lofepramine	$C_{26}H_{27}ClN_2O$	46386649
Meropenem	$C_{17}H_{25}N_3O_5S$	46386666
Orlistat	$C_{29}H_{53}NO_5$	46386654
Lansoprazole	$C_{16}H_{14}F_3N_3O_2S$	46386562
DuP 697	$C_{17}H_{12}BrFO_2S_2$	46387010
Procarbazine hydrochloride	$C_{12}H_{20}ClN_3O$	46386582
Nornicotine	$C_9H_{12}N_2$	46386896
Enalaprilat	$C_{18}H_{24}N_2O_5$	46386741
Rabeprazole	$C_{18}H_{21}N_3O_3S$	46386636
Nisoldipine	$C_{20}H_{24}N_2O_6$	46386699
Calcipotriol	$C_{27}H_{40}O_3$	46386727
Rolitetracycline	$C_{27}H_{33}N_3O_8$	46386966
Vardenafil citrate	$C_{29}H_{40}N_6O_{11}S$	46386591
2-Chloroadenosine	$C_{10}H_{12}ClN_5O_4$	46386960
Milnacipran hydrochloride	$C_{15}H_{23}ClN_2O$	46386905
Tacrine hydrochloride	$C_{13}H_{15}ClN_2$	46386852
Amiloride hydrochloride hydrate	$C_6H_8ClN_7O.2H_2O.HCl$	46386846
Moxifloxacin hydrochloride	$C_{21}H_{25}ClFN_3O_4$	46386670
Roxatidine acetate hydrochloride	$C_{19}H_{29}ClN_2O_4$	46386565

Formoterol fumarate dihydrate	$C_{19}H_{24}N_2O_4.2H_2O.C_4H_4O_4$	46386732
Venlafaxine hydrochloride	$C_{17}H_{28}ClNO_2$	46386590
Huperzine A	$C_{15}H_{18}N_2O$	46386885
Granisetron hydrochloride	$C_{18}H_{25}ClN_4O$	46386545
Nifekalant hydrochloride	$C_{19}H_{28}ClN_5O_5$	46386697
Escitalopram oxalate	$C_{22}H_{23}FN_2O_5$	46386725
Fenoldopam mesylate	$C_{16}H_{16}ClNO_3.CH_4O_3S$	46386722
Ticlopidine hydrochloride	$C_{14}H_{15}Cl_2NS$	46386576
Cefatrizine propylene glycol	$C_{21}H_{26}N_6O_7S_2$	46386659
Mosapride citrate	$C_{27}H_{33}ClFN_3O_{10}$	46386693
Moxonidine hydrochloride	$C_9H_{13}Cl_2N_5O$	46386777
Esomeprazole magnesium	$C_{17}H_{18}N_3O_3S.0.5Mg+2$	46386556
Ketotifen fumarate	$C_{23}H_{23}NO_5S$	46386834
Anagrelide hydrochloride	$C_{10}H_8Cl_3N_3O$	46386622
Indirubin	$C_{16}H_{10}N_2O_2$	46386581
Ranolazine dihydrochloride	$C_{24}H_{35}Cl_2N_3O_4$	46386552
Sertraline hydrochloride	$C_{17}H_{18}Cl_3N$	46386723
Terbinafine hydrochloride	$C_{21}H_{26}ClN$	46386583
Nelfinavir mesylate	$C_{32}H_{45}N_3O_4S.CH_4O_3S$	46386712
Itopride hydrochloride	$C_{20}H_{27}ClN_2O_4$	46386560
Epirubicin hydrochloride	$C_{27}H_{30}ClNO_{11}$	46386577
Indatraline hydrochloride	$C_{16}H_{16}Cl_3N$	46386808
Haloperidol hydrochloride	$C_{21}H_{24}Cl_2FNO_2$	46386806
Picrotin - Picrotoxinin	$C_{30}H_{34}O_{13}$	46386843
Fluperlapine	$C_{19}H_{20}FN_3$	46386904
Pizotyline maleate	$C_{23}H_{25}NO_4S$	46386908
Clonidine hydrochloride	$C_9H_{10}Cl_3N_3$	46386982
Physostigmine hemisulfate	$C_{15}H_{21}N_3O_2.0.5H_2O_4S$	46386842
Otenzepad	$C_{24}H_{31}N_5O_2$	46386986

Ipidacrine	$C_{12}H_{16}N_2$	46386925
Ketoconazole	$C_{26}H_{28}Cl_2N_4O_4$	46386810
Beta-estradiol	$C_{18}H_{24}O_2$	46386902
AM 404	$C_{26}H_{37}NO_2$	46386792
Loratadine	$C_{22}H_{23}ClN_2O_2$	46386837
Fluticasone propionate	$C_{25}H_{31}F_3O_5S$	46386601
Urapidil hydrochloride	$C_{20}H_{30}ClN_5O_3$	46386851
Ozagrel hydrochloride	$C_{13}H_{13}ClN_2O_2$	46386611
Selegiline hydrochloride	$C_{13}H_{18}ClN$	46386796
Nafadotride	$C_{22}H_{27}N_3O_2$	46387001
Trifluoperazine hydrochloride	$C_{21}H_{26}Cl_2F_3N_3S$	46386916
Prazosin hydrochloride hydrate	$C_{19}H_{24}ClN_5O_5$	46386845
5-Fluoro-2-pyrimidone	$C_4H_3FN_2O$	46386867
Doxorubicin hydrochloride	$C_{27}H_{30}ClNO_{11}$	46386781
Indinavir sulfate	$C_{36}H_{47}N_5O_4.H_2O_4S$	46386606
Alosetron monohydrochloride	$C_{17}H_{19}ClN_4O$	46386816
Bifemelane hydrochloride	$C_{18}H_{24}ClNO$	46386922
TFMPP hydrochloride	$C_{11}H_{14}ClF_3N_2$	46386913
Imatinib mesylate	$C_{29}H_{31}N_7O.CH_4O_3S$	46386639
Cinanserin	$C_{20}H_{27}ClN_2O_2S$	46386801
Cetraxate hydrochloride	$C_{17}H_{24}ClNO_4$	46386678
Fluvoxamine maleate	$C_{19}H_{25}F_3N_2O_6$	46386804
Salbutamol sulfate	$C_{13}H_{21}NO_3.0.5H_2O_4S$	46386798
L-NMMA acetate	$C_9H_{20}N_4O_4$	46386919
Progesterone	$C_{21}H_{30}O_2$	46386909
Hyperoside	$C_{21}H_{20}O_{12}$	46386811
Tolterodine tartrate	$C_{22}H_{31}NO.C_4H_6O_6$	46386674
Trimebutine maleate	$C_{26}H_{33}NO_9$	46386760
Lamivudine	$C_8H_{11}N_3O_3S$	46386600
Losartan potassium	$C_{22}H_{22}ClKN_6O$	46386652

Paroxetine maleate	$C_{23}H_{24}FNO_7$	46386841
Benidipine hydrochloride	$C_{28}H_{32}ClN_3O_6$	46386729
Naltrindole hydrochloride hydrate	$C_{26}H_{26}N_2O_3.1H_2O.HCl$	46386854
Perospirone hydrochloride	$C_{23}H_{31}ClN_4O_2S$	46386671
Bifonazole	$C_{22}H_{18}N_2$	46386787
Chlorpheniramine maleate	$C_{20}H_{23}ClN_2O_4$	46386872
SKF 83566 hydrobromide	$C_{17}H_{19}Br_2NO$	46386977
Scopolamine hydrobromide	$C_{17}H_{21}NO_4.3H_2O.HBr$	46386794
Atomoxetine hydrochloride	$C_{17}H_{22}ClNO$	46386643
Dexchlorpheniramine maleate	$C_{20}H_{23}ClN_2O_4$	46386575
Efavirenz	$C_{14}H_9ClF_3NO_2$	46386724
Esmolol hydrochloride	$C_{16}H_{26}ClNO_4$	46386551
Pancuronium dibromide	$C_{35}H_{60}N_2O_4.2Br$-	46386853
Duloxetine hydrochloride	$C_{18}H_{20}ClNOS$	46386541
1,1-Dimethyl-4-phenylpiperazinium iodide	$C_{12}H_{19}IN_2$	46387026
Ropivacaine hydrochloride	$C_{17}H_{27}ClN_2O$	46386542
Donepezil hydrochloride	$C_{24}H_{30}ClNO_3$	46386644
Pefloxacin mesylate	$C_{17}H_{20}FN_3O_3.CH_4O_3S$	46386589
Itavastatin calcium	$C_{25}H_{23}FNO_4.0.5Ca+2$	46386827
Buflomedil hydrochloride	$C_{17}H_{26}ClNO_4$	46386737
Valaciclovir hydrochloride	$C_{13}H_{21}ClN_6O_4$	46386762
Rosiglitazone maleate	$C_{22}H_{23}N_3O_7S$	46386628
Dexbrompheniramine maleate	$C_{20}H_{23}BrN_2O_4$	46386574
Irinotecan hydrochloride	$C_{33}H_{38}N_4O_6.3H_2O.HCl$	46386616
Tropisetron hydrochloride	$C_{17}H_{21}ClN_2O_2$	46386594
Piribedil hydrochloride	$C_{16}H_{21}ClN_4O_3$	46386844
Maprotiline hydrochloride	$C_{20}H_{24}ClN$	46386839
Droperidol	$C_{22}H_{22}FN_3O_2$	46386863

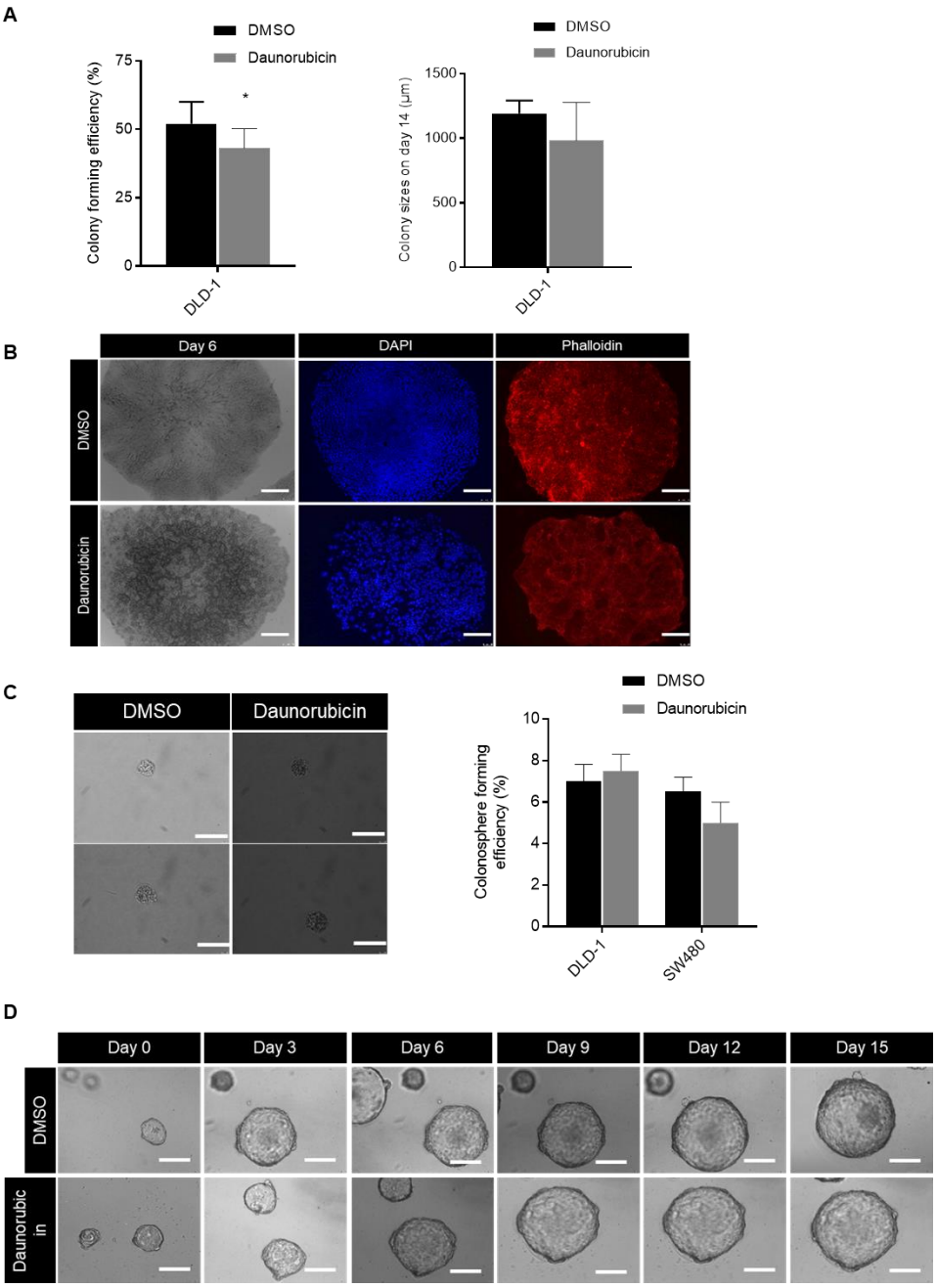
Appendix 2



Appendix 2: Effect of epirubicin on colony formation, colonosphere formation and organoid growth. Experiments were performed three

independent occasions (n=3). **(A)** Epirubicin showed reduction in colony formation, while retaining the similar size and morphology in DLD-1 cell derived colonies. **(B)** Phalloidin staining of epirubicin treated colonies. Nuclei were detected with DAPI-blue fluorescent stain. Scale bar: 75 µm. **(C)** No significant change in colonosphere formation as well as their size and morphology. **(A), (B)** and **(C)** were carried out as part of BMedSci project. **(D)** No distinct change observed for organoid growth and morphology upon epirubicin treatment. Scale bar: 75 µm.

Appendix 3



Appendix 3: Effect of daunorubicin on colony formation, colonosphere formation and organoid growth. Experiments were performed three

independent occasions (n=3). **(A)** Daunorubicin showed significant reduction in colony formation efficiency as well as changes the size and morphology of the treated colonies derived from DLD-1 cells. **(B)** Phalloidin staining of daunorubicin treated colonies. Nuclei were detected with DAPI-blue fluorescent stain. Scale bar: 75 µm. **(C)** No significant change in colonosphere formation efficiency. **(D)** No distinct change observed for organoid growth and morphology upon daunorubicin treatment. Scale bar: 75 µm.

Appendix 4

List of genes differentially expressed upon AM404 treatment. Red colour represents the upregulated genes.

Gene Symbol (≥2 F; p ≤ 0.001)	Gene Symbol (≥2.5 F; p ≤ 0.001)
SLC20A1	SLC20A1
SNORA31	SNORA31
SNORA28	SNORA28
MIR3115	MIR3115
HIST1H2BJ	HIST1H2BJ
MIR637	MIR637
SPDYA	SPDYA
TNFSF9	TNFSF9
CHORDC1	CHORDC1
SNORD59B	SNORD59B
TPT1	TPT1
OTTHUMG00000165727	OTTHUMG00000165727
BRD2	BRD2
GLUD1	GLUD1
MIR3662	MIR3662
HSPA1B	HSPA1B
HSPA1B	HSPA1B

HIST2H2BE	CYP2R1
BHLHE40	LDLRAD1
FDPS	SLC2A10
HSPA1B	SHCBP1
SNORA10	MGAT2
HSPA1B	CDC7
MPZL3	NEIL3
IL8	BRCA1
HSPA1A	KIAA1279
SNORD51	FAM72D
CTGF	FAM86HP
HSPA1B	NCAPH
KLF6	MIF4GD
HMGCS1	WDHD1
LOC100129785	SGOL1
TSC22D3	GOPC
LOC100506766	PARS2
OTTHUMG00000171211	BLM
PPP1R2	FAM208A
HSPA1A	F8A1
HSPA1A	SNORD121A
HSPA1A	CYP1A1
HSPA1A	RAD51
LOC554174	SLC46A3

ZBTB40-IT1	CHTF8
TMEM55B	ESCO2
MAFG	DZIP3
PRPF39	SPTLC3
PER1	IRAK4
INSIG1	DTD2
ZBTB34	SNORD90
ECM1	OTTHUMG00000163993
MIR3143	SNORD63
ADM	DTL
GRHL1	CDCA2
JUN	HIST1H4L
MVD	LINC00858
CLK1	HIST2H2AB
HIST1H4B	DEPDC1
SNORD58A	INTS5
RNF39	ULBP1
YOD1	F8A3
ARL14	F8A3
NR4A2	BRIP1
CDKN1C	FBXL5
LRCH4	FAM111B
RPLP1	HMMR
OTTHUMG00000154962	NOX1

FANCD2	PDIA3
ACADM	FAM86B2
OMA1	F8A3
IRAK1BP1	MIR1184-1
FASTKD3	MIR1184-1
CCP110	C1orf116
NCAPG	ASPM
LAMP3	SKA1
SEPHS2	NDC80
MLF1IP	PUS7L
CCDC71	SNORA2A
KIF20A	GEN1
HENMT1	HIST1H3I
SNORD72	
H2AFY2	
ADAT1	
SULT1C2	
TIRAP	
C12orf66	
MINA	
UBLCP1	
ZNF594	
RFC5	
DSCC1	
UEVLD	
KLK10	
CEP19	
ID3	
DHODH	
FECH	

SELRC1
YEATS4
TTC26
SFXN2
TRIM32
DLAT
FAM114A2
DSTNP2
GPR1
FJX1
BUB1
LOC100129502
SKAP1
GSG2
KIAA0586
USP13
POLI
KIAA1107
DCLRE1A
HCG15
HCG15
HCG15
HCG15
HCG15
HCG15
HCG15
ERAL1
PLK4
CABYR
AASDHPPT
LOC100507449
KLHL4
CCDC113
RBL1
ASF1B
SKA3
TICRR

WDR92
FXYD3
SYK
TBCK
RPGRIP1L
HAUS1
TRMT61B
CENPK
DNAJC11
TRMT1L
CASP6
SNORD111
OSGEPL1
TMEM9B-AS1
SNORD100
CDK1
FAM173B
THEM4
ASCL2
SIRT5
ZMYND11
MBLAC2
IGFL4
MRPL15
KLHDC1
FARSB
NMRK1
DYNC2LI1
PIGV
ZNF280B
SLC25A10
C2orf43
PRSS35
ERCC4
MOCOS
CPT2
PNPO

SLC16A13
ANKEF1
GTF2H3
TRIP11
KIF23
TST
ZFP69
COX10-AS1
PLK1
C6orf70
C5orf63
ZNF266
RRS1
C4orf32
KIAA1524
DET1
RMI1
CDX2
SCRN3
PLA2G7
PRMT3
LOC100506963
SBSPON
SNORD9
C6orf203
POLQ
ZNF554
PPIL1
KRCC1
MRM1
NARG2
LCN2
THAP10
CETN3
MCM10
HJURP
OBSCN

HSD17B1
LOC202181
PMS2
SRBD1
KIF11
XRCC2
RBM45
ZBED3
CCDC125
SLC9A8
TMEM52B
CKAP2L
GTF2IRD2
LOC100507516
KIAA1377
FAM83D
MARS2
NCOA5
TSEN2
KIF20B
FKTN
SDAD1
SNORD126
STRADA
IFT80
FAM86DP
LYRM7
CHAF1B
OTTHUMG00000059903
PRIM1
PSMD5-AS1
SNORD69
CSRP2BP
BRCA2
CFTR
GEMIN4
CENPF

ZFP90
RWDD2B
MGME1
SYCE2
C12orf4
OTTHUMG00000037424
FLJ14186
ZNF252P
ACER2
CDC25C
PTCD2
ABO
GINS1
ZNF23
CES2
CLUAP1
USP40
RNF170
WDR76
CYP2R1
LDLRAD1
SLC2A10
SHCBP1
MGAT2
CDC7
NEIL3
BRCA1
KIAA1279
FAM72D
FAM86HP
NCAPH
MIF4GD
WDHD1
SGOL1
GOPC
PARS2
BLM

FAM208A
F8A1
SNORD121A
CYP1A1
RAD51
SLC46A3
CHTF8
ESCO2
DZIP3
SPTLC3
IRAK4
DTD2
SNORD90
OTTHUMG00000163993
SNORD63
DTL
CDCA2
HIST1H4L
LINC00858
HIST2H2AB
DEPDC1
INTS5
ULBP1
F8A3
F8A3
BRIP1
FBXL5
FAM111B
HMMR
NOX1
PDIA3
FAM86B2
F8A3
MIR1184-1
MIR1184-1
C1orf116
ASPM

SKA1
NDC80
PUS7L
SNORA2A
GEN1
HIST1H3I

Appendix 5

List of genes differentially expressed upon rifabutin treatment.

Gene Symbol (≥2 FC; p ≤ 0.001)	
Upregulated genes	**Downregulated genes**
RPS6KA5	PADI1
DCLRE1B	SLC20A1
QTRTD1	MIR637
FBXL4	SREBF1
CCDC53	FDPS
ABCB1	FGFBP1
ID3	CCL26
SLC9A8	SNORA28
PLA2G7	HMGCS1
MKI67	MIR23A
CEP55	CEACAM1
ZNF658B	TNFSF9
FZD1	TSC22D3
ZNF318	HSPA1B
TTF2	HSPA1B
KIAA0922	ACSS2
HCP5	CHORDC1
NCAPD3	HSPA1B
CDKN3	CHRNA1
TRIM32	HSPA1B
ZNF629	ACAT2
PEX12	INSIG1
KLHL20	HSPA1A
ZSCAN32	METTL7A
ENOX2	OTTHUMG00000154962

SP8	BHLHE40
SNORD20	HSPA1B
MOCS3	BRD2
MCM4	MVD
POC1A	LSS
TLR3	HSPA1A
POLD3	SNORD59B
AURKA	KLF6
KNSTRN	CEACAM5
PRR11	HSPA1A
MOCOS	HSPA1A
ANGEL1	HSPA1A
ZMYM1	SNORD13P2
MELK	IL2RG
LMLN	FASN
RMI2	ADM
CHAF1B	YOD1
ELP3	H19
LCMT2	PCSK9
NUDT1	SQLE
DIRC2	EBP
ERI2	JUN
TTPAL	TMPRSS4
C6orf70	TPT1
RFC5	TMEM55B
KIF14	ECM1
ANKEF1	ZBTB40-IT1
CWF19L1	SLC30A1
DLGAP5	MPZL3
PPP3CA	CAPN8

ZNF786	SNHG15
CCDC125	MICB
DCBLD2	PHKG2
ORC5	MICB
MTM1	MICB
TCEANC2	STARD4
CDCA3	MICB
FAM84A	CLK1
TSEN2	
ALKBH3	
SLX4IP	
WDR76	
CIRH1A	
ZNF311	
FAM129A	
AASDHPPT	
LANCL1	
OTTHUMG00000183534	
PAAF1	
RRP7B	
OR2A20P	
LOC100507449	
GTF2IRD2	
ZCRB1	
RSPH3	
NCOA5	
TSTD3	
GLTSCR1L	
CCNA2	
ZNF362	

DYNC2LI1
SLC46A3
THEM4
FAM114A2
LOC81691
SRBD1
F8A1
RTKN2
BIRC5
ZC2HC1A
TRMT1L
E2F7
SPC24
ZBED3
CDCA8
FANCD2
CROT
C2orf43
PPAPDC2
C12orf66
STYXL1
PRIM1
NCAPG
DIAPH3
ZKSCAN3
AIMP2
SNORA72
TRMT61B
PLK1
KIAA1107

AP3M2
TMEM9B-AS1
TAF9B
TRMT12
MGME1
KIF20A
OSGEPL1
EXO1
ZMYND11
UST
KIF15
VIPAS39
SEPHS2
MARS2
KLHDC1
RMI1
HSD17B1
UBLCP1
ETS1
CES2
CLUAP1
KIF11
CCNB1
GSG2
FAM173B
PLK4
KCTD18
OIP5
KIAA1279
ASF1B

C5orf63
ZNF441
XRCC2
FARSB
FAM208A
KIF23
CYP2R1
CASC5
CSRP2BP
MBLAC2
BUB1
SDAD1
LOC100506963
KIAA1524
GINS1
CHTF8
HIST1H4L
CDK1
STRADA
ZNF23
IRAK4
F8A3
F8A3
SNORD9
SKA3
MIF4GD
CCDC113
THAP10
C1orf116
GPR1

DET1
FAM86B2
SHCBP1
CKAP2L
GOPC
FBXL5
HMMR
LYRM7
WDHD1
HJURP
LAMP3
MAP2
CENPF
CDC25C
LCN2
DTL
NCAPH
HIST1H3I
BRCA2
GEN1
FAM86HP
SGOL1
FAM111B
CDCA2
DEPDC1
ASPM
SKA1
NDC80
CYP1A1

Publications

Resulted from this study,

Ahmed M., Jinks N., Babaei-Jadidi R., Kashfi H., Castellanos-Uribe M., May S.T., Mukherjee, A., and Nateri, A.S. Repurposing antibacterial drug AM404 as a potential anticancer agent for targeting oncogenic FBXL5 in colorectal cancer. *Cancers*, 12, 106; doi:10.3390/cancers12010106 (2020).

Ahmed M., Chaudhari K., Babaei-Jadidi R., Dekker L.V. and Nateri A.S. Concise Review: Emerging drugs targeting epithelial cancer stem-like cells. *Stem Cells,* 35, 839-850 (2017).

Shaheen S., **Ahmed M.**, Lorenzi F., and Nateri A.S. Spheroid-formation (Colonosphere) assay for in vitro assessment and expansion of stem cells in colon cancer. *Stem Cell Reviews and Reports*, 1-8 (2016).